



RAM

● ROBOTICS
AND
MECHATRONICS

MULTI-FREQUENCY ELECTRICAL IMPEDANCE MYOGRAPHY AS AN ALTERNATIVE TO ELECTRO-MYOGRAPHY

C.E. (Ewout) Baars

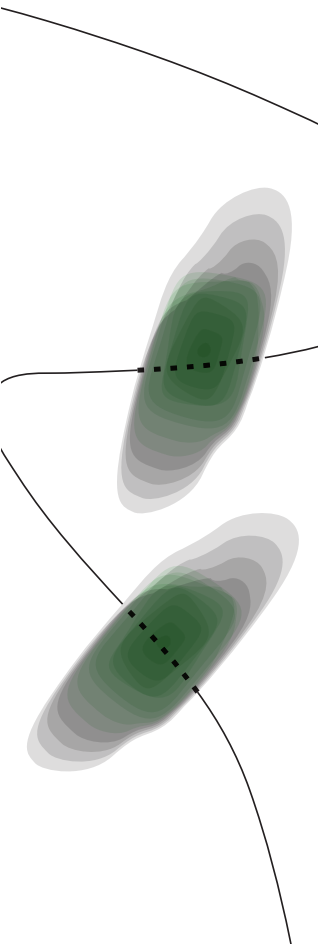
MSC ASSIGNMENT

Committee:

prof. dr. ir. G.J.M. Krijnen
ir. M. Schouten
dr. S.U. Yavuz

October, 2021

068RaM2021
Robotics and Mechatronics
EEMCS
University of Twente
P.O. Box 217
7500 AE Enschede
The Netherlands



Summary

In this study a contribution is made to the research on the use of Electrical Impedance myography (EIM) as an alternative to EMG, with potential application in the control of a robotic prosthetic hand.

Previous studies have found that bio-impedances change as a result of muscle contraction. Increasing amounts of delivered force resulted in increasing amounts of change in the measured bio-impedance. Not only has it been found to be a result of contraction but also a result of change in arm position. The usage of multi-frequency (mf) EIT and high-frequency (hf) EIT has been researched in static cases as well, without contraction or movement.

During this study it is attempted to relate the muscle contraction and change in arm position to the bio-impedance measurements. Multiple movement patterns have been introduced. These included various contractions and movements to enforce bio-impedance change.

The optimal measurement parameters have been found and the measurements have been conducted. A Neural Network is introduced to relate the EIM measurements to the contractions and movements, as well as to the various levels of contraction.

A Neural Network (NN) has been used to predict the muscle contraction and arm position. Furthermore the different levels of these muscle contractions are predicted. Finally the time delay of the change in the bio-impedance has been determined.

Contents

1	Introduction	1
1.1	Context	1
1.2	Research questions	3
1.3	Approach	3
1.4	Report structure	3
2	Literature review	4
2.1	Bio-impedance	5
2.2	Tomography	6
2.3	Single bio-impedance measurements	7
2.4	EMG and force	9
2.5	High and multi frequency	9
2.6	Aplications	9
2.7	Conclusion	10
3	Measurement method	11
3.1	Introduction	11
3.2	Measurement system	11
3.3	Parameter analysis	18
3.4	Measurements	21
3.5	Conclusion	25
4	Data processing	26
4.1	Introduction	26
4.2	Data Grouping	26
4.3	Cole's model	28
4.4	Filtering	30
4.5	Neural network	30
4.6	Down sampling	35
4.7	Conclusion	36
5	Results	37
5.1	Introduction	37
5.2	Amplitude selection	37
5.3	Frequency selection	39
5.4	Cole Model	40
5.5	Movement	42

5.6 Force	46
5.7 Time delay	49
5.8 Conclusion	50
6 Conclusion and Discussion	52
Bibliography	55
A Amplitude selection data	60
B Isometric data	64
C Isotonic data	79
D Cole fit parameters	92
D.1 Fmincon	92
D.2 Lsqnonlin	94
D.3 Pattern search	96
E Movement pattern 3 data	98
F Movement pattern 4 data	126
G Muscle contraction and movement data	137
H Force measurements	148
I Time delay	159
J System validation	163

1 Introduction

This work describes the research done by Ewout Baars for his final assignment of his master. The goal is to examine the suitability of multi-frequency electrical impedance tomography (mfEIT) and high-frequency electrical impedance tomography (hfEIT) to be used as an alternative to electromyography (EMG) for the control of a robotic prosthetic hand. This research is a step towards this goal, where electrical impedance myography (EIM) is used to predict muscle activation.

1.1 Context

At this moment multiple robotic prosthetic hands are already produced and used. Their prices range from less than \$ 10,000.- up to \$ 50,000.- [1]. Most of these prosthetic hands make use of myoelectric control systems in combination with pre-configured hand positions [1]. The use of pre-configured hand positions makes it impossible for the prosthetic hand to make every move a human hand can make. The solution towards a prosthetic hand without pre-configured hand positions lays in the reconstruction of the real desired movement of the user. This can be achieved if a relation can be found between muscle force, movement and a measurable signal such as Electromyography or Electrical Impedance Tomography (EIT).

1.1.1 Electromyography

Relations have been found between EMG and the amount of muscle force exerted [2–4]. This relation makes it possible to use EMG as an intuitive way of controlling a prosthetic hand. The user would essentially control the prosthetic hand as if it were a real hand. Besides being intuitive EMG is faster than control executed via buttons. The electromechanical delay present in EMG signals has been found to be around 30 ms to 100 ms with some measurements indicating even smaller delays around 8.5 ms while others found much larger delays around maximum 312 ms [5,6]. The measured signals lay in the frequency spectrum from 0 Hz up to 500 Hz. Most of the robotic hands use surface electrodes attached to the skin to measure the EMG signals [1]. Most of the power of a surface EMG (sEMG) signal is present between 50 Hz and 200 Hz [7]. Generally these signals are processed as follows [8]. First a high pass filter with a cut off frequency between 10 Hz and 20 Hz is applied. The goal of this filter is to remove any slow variations in the signal due to movement artifacts and instability of the electrode-skin interface [8]. The amplitude of the EMG signal is estimated by rectifying the signal after which a low-pass filter is applied. This results in a moving average of the rectified EMG signal also called the Average Rectified Value (ARV). The ARV can also be calculated by applying an averaging filter over a specified window with length N as formulated in Equation 1.1.

$$\text{ARV} = \frac{1}{N} \sum_{i=1}^N |x_i| \quad (1.1)$$

The low pass filter or averaging window introduces a delay based on the cut-off frequency and the type of filter [8]. A lower cut-off frequency corresponds to a bigger averaging window and an increase in the time delay. An advantage of a low cut off frequency is a bigger reliability of the estimated amplitude of a static activation [8]. Which cut off frequency is used is case dependent. Therefore it is up to the researcher to decide what the cut off frequency will be and why. An example is given in the SENIAM project [8] a motor task with a cyclic character is performed at 1 Hz the used cut off frequency is 2 Hz.

When EMG is used as control signal the desired movement of the user is based on the processed EMG signals. For most currently used robotic prosthetic hands these measurements are mapped to one of the pre-configured hand movements [1]. If mapped correctly the user sees

the hand make the movement as he/she desires. However when the user tries to make a movement which is not configured, the hand will move to one of the configured movements. Which hand position it will be depends on the EMG signals and the map of the signals to the hand positions. To overcome this problem more EMG measurements can be done simultaneously such that more different hand positions can be distinguished and thus can be configured. When every pool of motor units can be uniquely distinguished every unique hand position which a human hand can make can be distinguished as well. Therefore the map between EMG measurements and hand positions changes from a discrete map to a continuous map. The cocktail party problem shows [9] that in order to uniquely distinguish a number of "x" sources at least a number of "x" signal measurements are needed. Therefore to uniquely distinguish the signals coming from all motor unit pools at least as many EMG measurements have to be done. Research has been done on the estimation of the number of motor units in different hand muscles. A research on the amount of motor units in the hypothenar and thenar muscle is performed by R.E.P. SICA [10]. Two muscle groups at the base of the little finger and thumb respectively. The research shows a mean of 380 hypothenar motor units and 340 thenar motor units. Therefore many electrodes are required to identify the activity of all muscles such that every desired hand movement can be made. This introduces multiple problems. One of the problems involves the size and/or placement of the electrodes. The amount of measurement space is limited to the size of the surface of the skin. This leads to the requirement to use smaller electrodes. Smaller electrodes have a higher contact impedance compared to larger electrodes. Smaller electrodes also have a lower signal to noise ratio (SNR), which is not beneficial for the signal processing. A second problem is the amount of processing which has to be done. When more EMG signals are measured simultaneously more signal processing has to be done. This implies more or bigger processing units have to be used which both take up space and consume power. The increase in power consumption results in the demand for a bigger battery. Therefore more EMG processing may result in a bigger and/or heavier prosthetic.

1.1.2 Electrical impedance myography

Electrical impedance myography is a non-invasive measurement method focused on the electrical impedance of a muscle or muscle group. A small alternating current is imposed between two skin-surface electrodes. By measuring the voltage drop between two electrodes the bio-impedance can be calculated using Equation 1.2, where \mathbf{Z} is the complex impedance, \mathbf{V} the measured complex voltage, \mathbf{I} the complex current and the asterisk (*) denotes complex conjugation. The (bio-)impedance is denoted in the form given in Equation 1.3, where X is the resistance, Y the reactance and i is defined by $i^2 = -1$.

$$\mathbf{Z} = \frac{\mathbf{V}}{\mathbf{I}} = \frac{\mathbf{V}\mathbf{I}^*}{\mathbf{I}\mathbf{I}^*} \quad (1.2)$$

$$\mathbf{Z} = X + iY \quad (1.3)$$

The electrodes used for imposing the current and the electrodes used for measuring the voltage drop can be the same. This way only two electrodes are needed. However using 2 pair of electrodes, one pair for the voltage measurement and one pair for imposing the current, benefits the precision of the measurement since this makes the measurement independent of the electrode impedance [11].

Using multiple EIM measurements around a certain part of the body a cross-sectional image can be created of the impedance distribution. This technique is called electrical impedance tomography (EIT) and will be used in the following steps beyond this research. This technique is further explained in Section 2.2.

The low-pass filter as described in section 1.1.1 is a disadvantage of EMG since it introduces a time delay. With the use of EIT it might be possible that the used low-pass filter has a much higher cut off frequency making it more suitable as a control signal. This would be an advantage of using EIT.

Instead of inducing a sinusoidal current at one frequency it is possible to induce a current consisting of multiple frequencies. This way with only one measurement more information can be deducted from the state of the muscle. This technique is called multi-frequency Electrical Impedance Tomography (mfEIT). Besides making use of multiple frequencies with the available equipment it is possible to measure up to 3.125 MHz. Using High-frequency EIT (hfEIT) the influence of muscle contraction and movement can be determined for a broader frequency range.

1.2 Research questions

The goal of this project is to study the possibility of detecting muscle activity using mfEIT and hf-EIT as an alternative to EMG for the control of a prosthetic arm. Four main research questions arise within this goal;

- To what extent is it possible to predict muscle activation in various arm positions using mfEIT and/or hfEIT?
- How precise and accurate can different levels of muscle contraction be distinguished?
- What is the time delay between muscle activation and bio-impedance changes?
- To what extent is it possible to distinguish muscle contraction and arm movement?

1.3 Approach

The first challenge is to determine the desired bio-impedance measurement settings, such as the frequency and amplitude of the induced current. These are found by performing multiple measurements using different parameters. The measurement settings are optimized to detect muscle activity and arm movement. Next, multiple movement patterns are created. Each movement pattern is focused on a different aspects, such as time delay and level of contraction. The movement patterns will be performed and the bio-impedance and EMG signals will be measured using the determined settings. Each movement pattern is processed in its own way such that the research question can be answered.

1.4 Report structure

Chapter 2 describes research done on bio-impedance measurements and different applications of this technique. The used hardware and software are given in Chapter 3, besides are the movement patterns described in this chapter. Chapter 4 discusses the different data processing methods used for the measurements. The results of the measurements are given in Chapter 5. The report is concluded in Chapter 6.

2 Literature review

In 1936 Dubuisson studied the behavior of bio-impedance changes during muscle contraction [12]. The study was performed on (Hungarian and Belgian) frog legs, that were stimulated by a small stimulation current. The impedance was measured using a sinusoidal signal with a frequency of 2 kHz and two circular silver chloride electrodes. Dubuisson concluded that an increase in impedance is measured in a perfect isometric contraction. This impedance increase suggests a relation between the bio-impedance and the chemical processes which occur in a muscle [12]. However in an imperfect isometric contraction the fibers shorten and the impedance decreases [12]. These effects interfere in any muscle contraction. Since then similar results were found in multiple different settings [13, 14].

The change in impedance is mostly assigned to two phenomena. When a bio-electrical impedance measurement is done with surface electrodes the electrodes are attached to the skin when the muscle is in a relaxed state. However when the muscle is contracted the muscle shape differs from the relaxed state. This influences the bio-impedance directly. As stated before it was found that shortening of the muscle fibers results in a lowering of the impedance [12]. The change in muscle shape also results in displacement of e.g. fat, skin and veins within the body, influencing the measured impedance [13]. In this work these influences are regarded as morphological effects.

The second category which influences the measured bio-impedance consist of the physiological changes when a muscle contracts. These include the change of blood flow and the depolarisation of axon's within and around the muscle [15, 16]. How big the influence of both effects is depends among other things on the type of muscle contraction. In general there are two types of contractions, isometric and isotonic. Isotonic contraction means the subject is actually moving and thus, since work is the product of force and displacement, work is done. Isometric contraction on the other hand is a contraction without movement, such as trying to push a bar which is fixed in position as is shown in Figure 2.1.

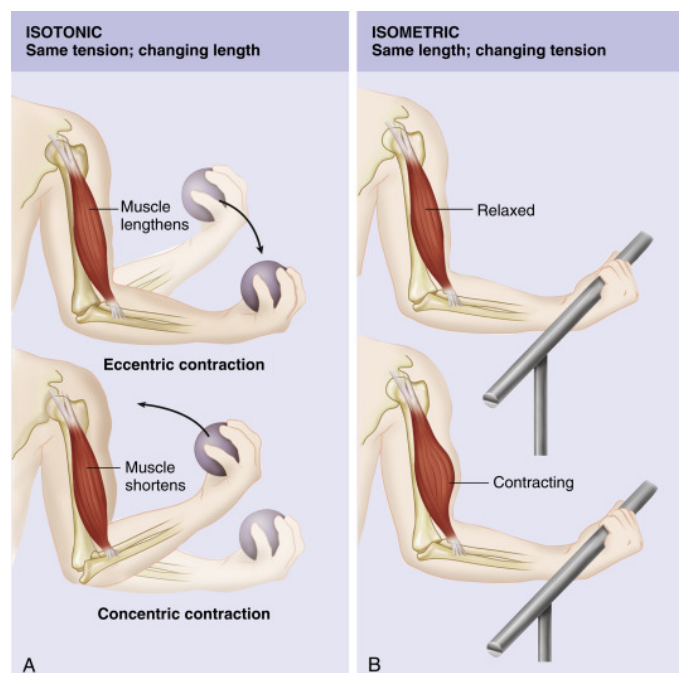


Figure 2.1: The difference between isotonic and isometric contraction. [17]

2.1 Bio-impedance

In 1940 K.S. Cole proposed a model to represent bio-impedances. The model consist of two electrical resistors and a constant phase element, and is given in Figure 2.2 [18]. The Cole model is better known as the Cole-Cole model, as it was used again in 1941 by K.S. Cole and R.H. Cole [19]. The constant phase element (CPE) introduces a phase shift which is constant over all frequencies. A constant phase element can have any arbitrary phase shift between 0° and 90° based on the value of n , with $0 \leq n \leq 1$. The impedance of the CPE is given in Equation 2.1, the corresponding plot of the impedance at different frequencies is given in Figure 2.3. This plot shows that, indeed, the phase is constant over all frequencies even though the impedance amplitude is not.

$$Z_{\text{CPE}} = \frac{1}{Q(i\omega)^n} \quad (2.1)$$

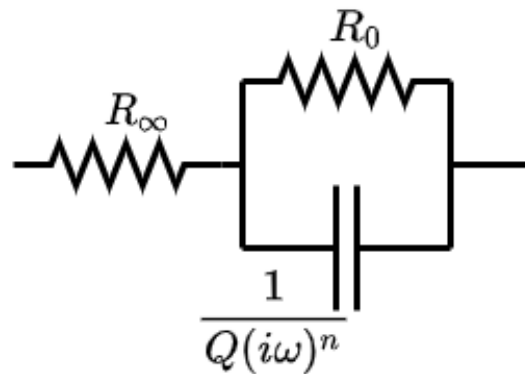


Figure 2.2: The Cole-Cole model represented by electrical components. The electrical resistance at high frequencies is given by R_∞ and the resistance at lower frequencies is given by $R_\infty + R_0$.

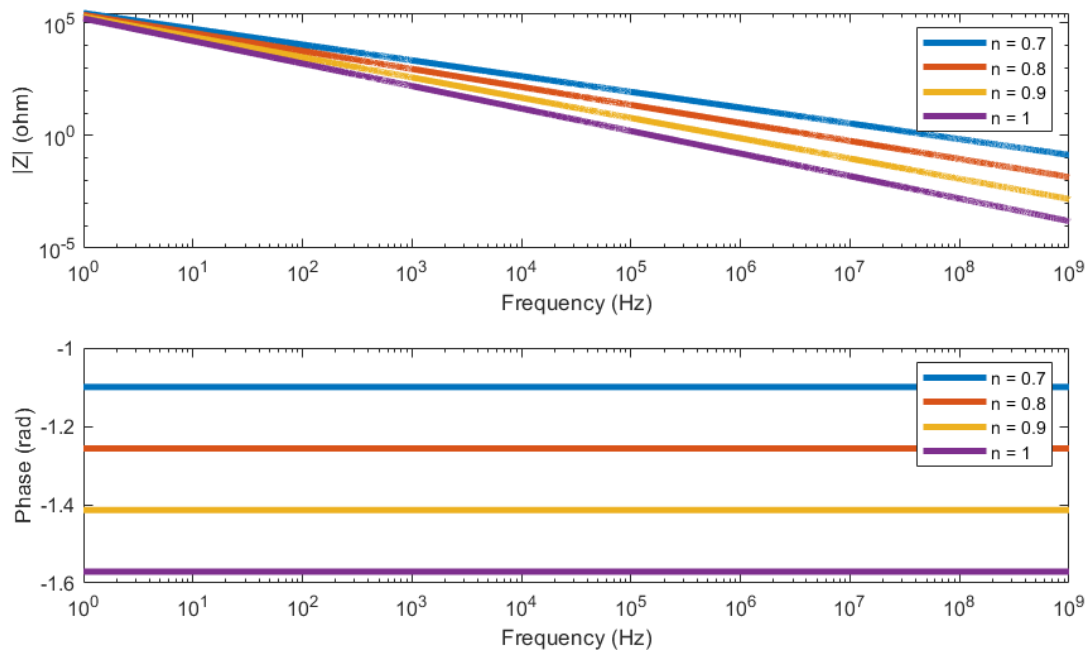


Figure 2.3: The impedance of a constant phase element for different frequencies, $Q = 1 \mu\text{F}/\text{s}^{(1-n)}$ [20]

The model is widely used to analyze bio-impedance within the body and in many cases the model fits measured data rather well [15, 21, 22]. The Cole-Cole model is based on the knowl-

edge that the intra- and extracellular space works as a resistor when it comes to electrical current. Adjacent cells on the other hand act as a trans-membrane capacitor [23]. The electrical characteristics of cells is depicted in Figure 2.4. When the circuit of Figure 2.4 is placed in series and parallel to itself many times, it represents a small segment of the human body. The Cole-Cole model simplifies this network of circuits into three components. The resistance coming from the extracellular space, represented by R_e in Figure 2.4 is represented in the Cole-Cole model by the combination of R_0 and R_∞ as in Figure 2.2. The intracellular resistance and trans-membrane capacitance represented by R_m , C_m and R_i in Figure 2.4 are represented by R_∞ and the CPE of the Cole-Cole model, Figure 2.2. The Cole-Cole model has four unknown parameters. The values of these parameters, R_∞ , R_0 , Q and n , depend on the substance (cell) structure. The total impedance of this circuit is equal to:

$$Z_{CC}(\omega) = R_\infty + \frac{R_0}{1 + (j\omega)^n QR_0} \quad (2.2)$$

For low frequencies this impedance is equal to:

$$\lim_{\omega \rightarrow 0} Z_{CC}(\omega) = R_\infty + R_0 \quad (2.3)$$

Since R_0 is of great influence at the lower frequencies down to 0 Hz the resistor has the subscript 0. For high frequencies this impedance is equal to:

$$\lim_{\omega \rightarrow \infty} Z_{CC}(\omega) = R_\infty \quad (2.4)$$

Since R_∞ is of great influence at the higher frequencies, the resistor has the subscript ∞ .

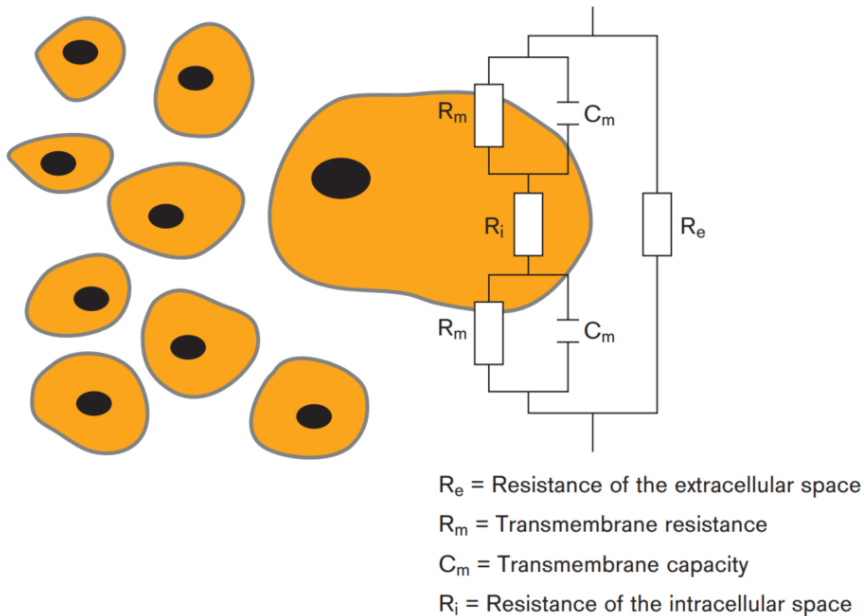


Figure 2.4: The electrical behaviour of a single cell v [23].

2.2 Tomography

With a single point measurement using four electrodes an impedance change can be recorded when the muscle changes from a relaxed to a contracted state or the other way around. However when more electrodes are used and placed around a cross-section of the body multiple

measurements can be combined to measure an impedance distribution of the cross section of the body. An image can be created of this impedance distribution. This way of imaging is called electrical impedance tomography (EIT). This way insight can be gained in the condition of a patient, internal hemorrhage can be spotted or it can be used to recognize various positions of a hand while the measurement is performed on the lower arm. [23–25]

EIT has already been proven useful for different applications. The company Dräger uses EIT to regionally monitor the ventilation inside the lungs of patients [23]. A band including 16 electrodes is placed around the chest of a patient. Between two adjacent electrodes a current is imposed. The other 14 electrodes each measure their voltage with respect to their neighbor electrode, resulting in 13 voltage measurements, as is depicted in Figure 2.5. After one measurement is done the current is imposed on the next two electrodes (2,3) and a new measurement is done. Therefore this method can be used to do 16 measurements each consisting of 13 voltage measurements. The image is created based on all measurements of a full circle.

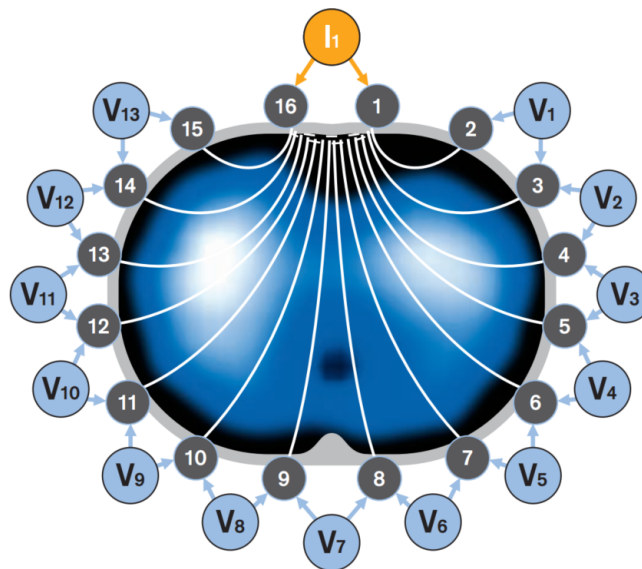


Figure 2.5: The electrodes used to impose a current (1,16) and used to measure the resulting voltage (2-15) for a lung EIT measurement [23].

Besides patient monitoring, is it possible to use EIT images to train a neural network to distinguish different hand positions. Both at the Carnegie Mellon University and University College London a wearable EIT system was build. Their goals, almost identical, were to recognize different hand positions based on the measurements from the wearable EIT system placed on the lower arm, see Figure 2.6. Finally the systems were able to distinguish 11 to 15 different hand signs with accuracies varying from 60 % to 98 %.

2.3 Single bio-impedance measurements

Where EIT always uses multiple measurements, in order to create the image, much knowledge can be gained from a single or just a few measurements as well. Even with one or a few measurement points the muscle activation can be detected [26, 27]. Liao reported the impedance change of skeletal muscle during contraction as well as the latency of the impedance change with respect to the time of contraction [27]. A high correlation was found between these impedance changes and simultaneously recorded EMG signals by L.T.L. Fiuza [15]. This corre-

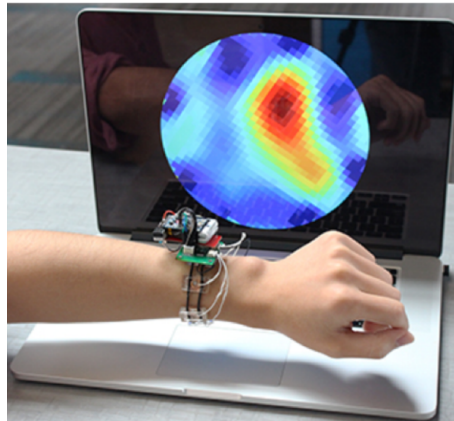


Figure 2.6: The wearable lower arm EIT system (Tommo), designed by Yang Zhang, Carnegie Mellon University, Human-Computer Interaction Institute. [25]

lation implies that bio-impedance measurements could be used for comparable applications as EMG is used for nowadays, e.g. the control of a robotic arm. This suggests EIT as an alternative to EMG, although the two techniques could also complement each other, as is suggested by R. Kusche and M. Ryschk [28]. Kusche and Ryschk performed a comparable research as presented earlier in Section 2.2, where hand positions were recognized based on EIT images of the lower arm. Now four bio-impedance measurements were combined with 4 EMG measurements and again used to distinguish different hand positions.

The relation between levels of muscle contraction and bio-impedance changes is researched in various ways. A comparison between the bio-impedance changes when a subject relaxes its bicep, contracts it for 25 %, 50 % and 100 % is made by T.D. Orth [14]. By holding different weights during the measurements the different levels of contraction are created. The highest impedance measured corresponded to the relaxed state. A decrease in impedance is measured for each next step in level of contraction (25 %, 50 % and 100 %) [14]. Comparable results were found by Shiffman et al, where subjects pushed onto a dynamometer [13]. Each subject created multiple ramp functions by slowly increasing the exerted muscle force and multiple pulses by quickly increasing the exerted force to a certain level. Both studies discussed the influence of morphological and physiological changes during contraction. However since both studies used isometric contractions the comparison with an isotonic contraction is lacking. Besides the change in bio-impedance as result of change in exerted force both study the influence of fatigue as well [13, 14]. Both concluded a significant change in bio-impedance due to fatigue. T. Orth reported an increase in the resistance and a decrease in the reactance during muscle fatigue. However when the amount of delivered force increased an decrease in both the resistance and reactance was found [14].

A.B.B. Coutinho measured the bicep bio-impedance while contracting under different elbow angles [29]. It was found that under the different angles the bio-impedance differed. This was assigned to not only physiological but also morphological changes which arose due to the change in elbow angle. T. Zagar did a comparable study, where they contracted and relaxed the muscle in many different positions [30]. The measured impedance's were fed to a Principal Component Analysis (PCA) algorithm. Based on the first and second component a soft independent modeling of class analogy (SIMCA) classifier could classify 80 % of the time correctly if the muscle was relaxed or contracted. This means that even though there are morphological

changes it is still possible to distinguish a contracted muscle from a relaxed muscle.

2.4 EMG and force

EMG has been studied broadly and as a result of this different researchers have found a relation between EMG or surface EMG (sEMG) measurements and the force exerted by the muscles. In 1997 A.L. Hof published his work on the relation between EMG and produced muscle force [31]. A linear relation between the smoothed rectified EMG (SRE) signal and the extruded force by the muscle was shown. Not only A.L. Hof came to this conclusion, G.C. Ray and S.K. Guha strengthened it with a broader theoretical approach [32]. G.C. Ray and S.K. Guha stated that most of the theoretical studies suggest an increase in the EMG amplitude which relates to the square root of the muscle tension. Experiments show however a linear relationship [32]. G.C. Ray and S.K. Guha show that the reason for the difference between the theoretical studies and the experiments are a set of oversimplified assumptions. These assumptions include; the assumption that all motor units are of the same size and the assumption that all action potentials have the same magnitude and fire with the same frequency [32].

The linear relation is however influenced by the placement of the electrodes as is shown by N.U. Ahamed [2]. When placed incorrectly the goodness of the linear fit on the relation between EMG and extruded muscle force decreases [2]. Nevertheless in 2 of the 3 electrode placements in this study [2] a linear relation is visible.

2.5 High and multi frequency

Typical EIT systems insert current at one frequency around 50 kHz [33]. Shiffman did research on the effect of using higher frequencies, up to 2 MHz [34]. In this research a major rise in the reactance was found for frequencies above 500 kHz as well as a gradual decrease in the resistance [34]. This was reported for muscles in a relaxed state. The effect of movement and/or contraction might influence the impedance at higher frequencies differently compared to lower frequencies.

Multi-frequency EIT has already been used in stroke patients to differentiate between an ischaemic and haemorrhagic stroke [35,36]. The use of multiple frequencies opens up the possibility to distinguish different muscle states based on more data, which could make it more reliable. Research showed that the difference in reactance between a contracted and relaxed muscle differs at varying measurement frequencies [14].

2.6 Applications

Currently EIT is already used in various applications. As mentioned in Section 2.5 mfEIT has been used for patients with acute stroke. Using mfEIT it is possible to image changes in the brain due to acute stroke. Using these images it can potentially distinguish between haemorrhagic and ischemic brain stroke. Something that was not possible using conventional techniques such as CT and MRI. It permits the use of thrombolytic drugs more rapidly benefiting the patient [35,36].

For lung ventilation monitoring Dräger makes use of an EIT band around the chest [23]. Section 2.2 showed their image, Figure 2.5, used to explain how the creation of such an EIT image works. The advantage of using EIT in this case is that it can be performed while the patient lays in its own bed. There is no need to move the patient to a different room, which is the case with the usually used CT scan. An other advantage of EIT over CT in this case is that EIT can be used for continuous monitoring without harming the patient. Something which is not the case with CT.

Research has been done on the monitoring of slow internal hemorrhaging [24]. Patients with delayed traumatic intracranial hemorrhage often get a negative result from a CT brain scan

which is done shortly after a trauma. Often the condition of these patients falls back in the time laps of 24 to 72 hours after the traumatic event [24]. Continuous monitoring could be key for these patients. Software is developed which can detect internal hemorrhage by using EIT measurements. Again, continuously monitoring is possible with EIT while it is not with CT, fitting the requirements for the treatment of these patients.

The detection of various obesity and heart diseases using EIT is also researched [37]. Cardiovascular atherosclerosis is *the buildup of fats, cholesterol and other substances in and on artery walls* [38] and is still the leading cause of mortality [37]. Using EIT a fatty liver can be detected in an early stage.

Some research has been done on the detection of breast cancer using Electrical Impedance Spectroscopy (EIS). The electrical properties of cancerous tissue differ from healthy tissue. This difference is utilized to detect cancerous tissue. The same advantages as for the other applications apply. EIS is noninvasive and comfortable for the patient. Other advantages are that a scan can be made in about 15 minutes and the equipment is cheaper than the equipment currently in use, such as ultrasound machines [39]. Therefore, EIS would be a promising candidate for the future to detect breast cancer.

2.7 Conclusion

It can be concluded that the measured bio-impedance does change when a muscle contracts both in an isometric as and isotonic situation. The measured reactance difference between contracted and relaxed state differs per frequency. The measured reactance above 2 MHz showed a major rise compared to the lower frequencies for a relaxed muscle state. The resistance and reactance can be and are used to detect and/or distinguish different body tissues. EIT has already several applications and it is expected more will come.

3 Measurement method

3.1 Introduction

This chapter consist of three parts, each with a different aspect related to the performed measurements. First the technical setup, used to measure the bio-impedance, is described in Section 3.2. This includes the different parts of the hardware and software. Secondly two experiments are discussed in Section 3.3. Both give insight in the optimal choice for the settings of the induced alternating current. When the desired measurement parameters are found the focus shifts towards the characteristics of the bio-impedance signals. Three different measurements are done, each focused on a different aspect of the bio-impedance, such as time delay, contraction level and distinguishing contraction from movement.

3.2 Measurement system

The used measurement system consist of a hardware and a software part. The hardware is used to induce the current, measure the voltages and measure the current. The purpose of the software is to control the different hardware settings, collect the measurement data through the hardware and subsequently perform the processing of the data.

3.2.1 Hardware

The used measurement hardware consist of three pieces, a TiePie Handyscope HS5 USB oscilloscope (TiePie), a custom PCB [40] and a computer. The TiePie, the custom PCB, the connection wires and the electrodes are shown in Figure 3.1. The computer is connected to the TiePie via a USB connection. A powerful GPU is required since the FFT calculations employed in the algorithm are handled by the GPU. The software makes use of NVIDIA CUDA [41] which means the GPU is required to be an NVIDIA GPU. The TiePie can be powered over the USB as well as by using a separate power adapter. Most computer USB ports have a maximum current supply of 0.5 A for USB 2.0 or up to 0.9 A for USB 3.0 [42]. The TiePie current demand can go up to 2 A. Therefore the external power supply might be needed.

TiePie oscilloscope

The TiePie Handyscope HS5 is an oscilloscope including two measurement channels and an arbitrary waveform generator. The TiePie has an input impedance of 1 M Ω , an input capacitance of 25 pF, a programmable resolution of 8, 12, 14 or 16 bits and at 16 bits it still has a streaming speed of 6.25 MSa s⁻¹ [43]. The integrated waveform generator will be used in combination with a guarded and improved Howland current source to create the injected current. The waveform generator has a frequency reach from 1 μ Hz up to 40 MHz [43] for sinusoidal signals. The integrated sample memory of 64 MSa makes it possible to create a multi-sine signal with a broad band of different frequencies.

Electrodes

Electrodes are used to connect the skin with the custom PCB. Two types of electrodes have been used.

The first used electrode consist of conductive and adhesive hydro-gel such that it sticks to the skin well and let current pass through it [44]. The used electrode is a silver/silver chloride electrode (AgAgCl). It is commonly used because it is easy to manufacture and provides a low skin-electrode impedance [45]. It has a round shape with a diameter of 24 mm, the conductive inner part has a diameter of 16 mm [44].

The second electrode type is a Unipolar Micro electrode (microcoax) made by TMSI [46]. These are applied together with double sided adhesives and Electrode gel [47]. The electrodes are a



Figure 3.1: The TiePie oscilloscope, top black box, connected with three coax connections to the custom PCB (bottom black box). Two measurement connections and one connects to the waveform generator. The used coax cables connect the electrodes with the four PCB outputs, $H_{\text{cur,I}}$, H_{pot} , L_{pot} and L_{cur} .

lot smaller with a diameter of 1.5 mm. The contact resistance increases as the electrode size decreases [48]. The bio-impedance measurement will not be influenced by the increase in contact resistance because a four point measurement is performed. The EMG signal is amplified by a differential amplifier, this means the impedance of the skin electrode interface is not of great importance as long as the different electrodes have similar impedance and the impedance of the electrodes is small compared to the input impedance of the amplifier [49]. The smaller electrodes make it possible to measure with a higher spatial resolution [46]. The electrodes are placed as indicated in Figure 3.2. From top to bottom are the electrodes connected to; $H_{\text{cur,I}}$, H_{pot} , L_{pot} and L_{cur} as given in Figure 3.3.

Custom PCB

The custom PCB (TiePieLCR) makes an LCR measurement system from the oscilloscope and makes it possible to simultaneously measure the bio-impedance and the EMG signals [40]. In Figure 3.3 an overview of the schematic of the TiePieLCR is given. The TiePieLCR is powered by batteries in order to prevent introduction of 50 Hz noise coming from the power grid. Besides it is safer for the subject since the battery can only drain that much power in a specified amount of time.

The TiePieLCR is directly connected to the TiePie at three points, all given in Figure 3.3. The first input, V_{in} , is used as input for all sources. The TiePieLCR offers 4 different sources; 2 voltage controlled current sources and 2 voltage sources. One of the voltage sources equals V_{in} while the other has as output $-V_{\text{in}}$. The current sources have a comparable relation. As can be deduced from Figure 3.3 the lower current source ($\overline{H_{\text{cur,I}}}$) generates the reverse current of the top one. Only the first current source is used in these measurements, indicated by $H_{\text{cur,I}}$ in Figure 3.3. The current sources are based on a improved Howland current pump [50]. An



Figure 3.2: The electrodes as they are placed on the arm. The smaller electrodes are used in this picture. The electrodes are connected to the PCB as follows, from high to low: $H_{\text{cur},I}$, H_{pot} , L_{pot} and L_{cur} .

Howland current pump is a voltage controlled current source. It is especially use full in the bio-impedance measurement since it can have a high output impedance as well as an high frequency bandwidth [51]. The gain of the current source is set to $370 \mu\text{A}\text{V}^{-1}$. In order to protect the circuitry from electrostatic discharge TVS diode's are placed between the guards and the ground and between the guards and the signal input. Between both the shield and the output a $2.7 \text{ k}\Omega$ resistor is placed to prevent high currents flowing through the user.

The voltage measurement is performed using an instrumentation amplifier. This makes it possible to measure the voltage differential. It is created using LTC6268 opamps which have an input impedance higher than $1 \text{ T}\Omega$ with a bias current of 3 fA . This input impedance will in practice be lower because of the current leakage of the PCB. The cables between the skin contact and the TiePieLCR are 1.5 m long. The capacitance of these cables is typically about 100 pF which is a lot higher than the PCB capacitance (1 pF up to 20 pF) and the input capacitance of the opamps of 450 fF . The cable capacitance is decreased by applying the buffered input to the shield of the cables. The voltage difference between the shield and the core of the cable decreases and thus the current in the cable decrease as well. The instrumentation amplifier can be used with two different gains, $1\times$ and $50\times$. A relay is used to connect and disconnect a resistor to make the gain switch happen. Between the output of the instrumentation amplifier and the input of the TiePie a first order anti-aliasing filter is placed with a cut-off at 9.6 MHz . The output of this filter is fed to the TiePie and is indicated by V_{out} in Figure 3.3. The input capacitance of the TiePie is parallel to the capacitor of this low-pass filter. Therefore will the real cut-off frequency be around 9 MHz instead of 9.6 MHz .

The current measurement is required because of the undesired current flow from the core of the electrode wires into the shielding of the wires. However the TiePie is only able to measure voltages. To measure the current a trans-impedance amplifier (TIA) is used to convert the current to a voltage. Multiple trans impedance amplifiers are used each with their own gain and thus operating range. The inputs and outputs of all TIA's can be connected and disconnected using relays. Between the output of every TIA and the input of the TiePie a 50Ω resistor is placed to prevent the opamps from overheating in the case multiple relays are accidentally enabled. Capacitors are placed in parallel to all resistors from $R_{\text{sens},1}$ to $R_{\text{sens},2}$ in Figure 3.3 in order to keep the circuit stable. Again a $2.7 \text{ k}\Omega$ resistor is placed in series to limit the currents

going into the trans-impedance amplifier to 1 mA when the load is below 2.7 k Ω . The output indicated by I_{out} Figure 3.3 is thus a voltage representing the current.

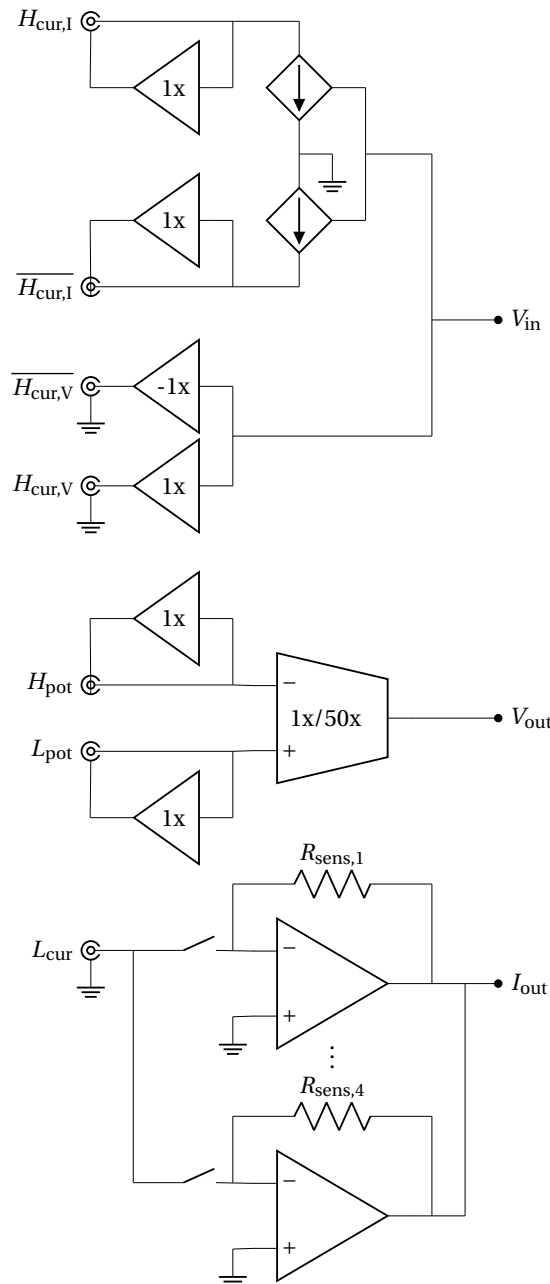


Figure 3.3: Simplified circuit of the TiePieLCR. [40]. The TiePie is connected on the right side of this circuit, the subject on the left. Only the first current source is used indicated by $H_{cur,I}$.

3.2.2 Software

The software is a custom python program created by M.Schouten [40]. The TiePie driver as well as the NVIDIA CUDA driver are required to be installed on the used computer [41, 52]. A GUI is created to let the user change various measurement parameters and to display the real time measurement results. In Figure 3.4 a picture of the GUI is given, different pieces are indicated with colored boxes. In the orange box on the top left all parameters with respect to the current and voltage measurements are given. All input frequencies and the amplitude of the induced current can be set in the red box. Notice that each frequency gets a weight factor which should all add up to one. This weight factor is a percentage of the maximum current

to be used at this frequency. The blue box on the top right includes some parameters used for the generated plots. The green box includes all demodulation and measurement settings. The measurement settings apply to the TiePie settings while the demodulation applies to the filtering. The purple box shows two plots including the measured current and voltage against the time and frequency. The two plots below show the output in a desired format which will in this research be the resistance and reactance.

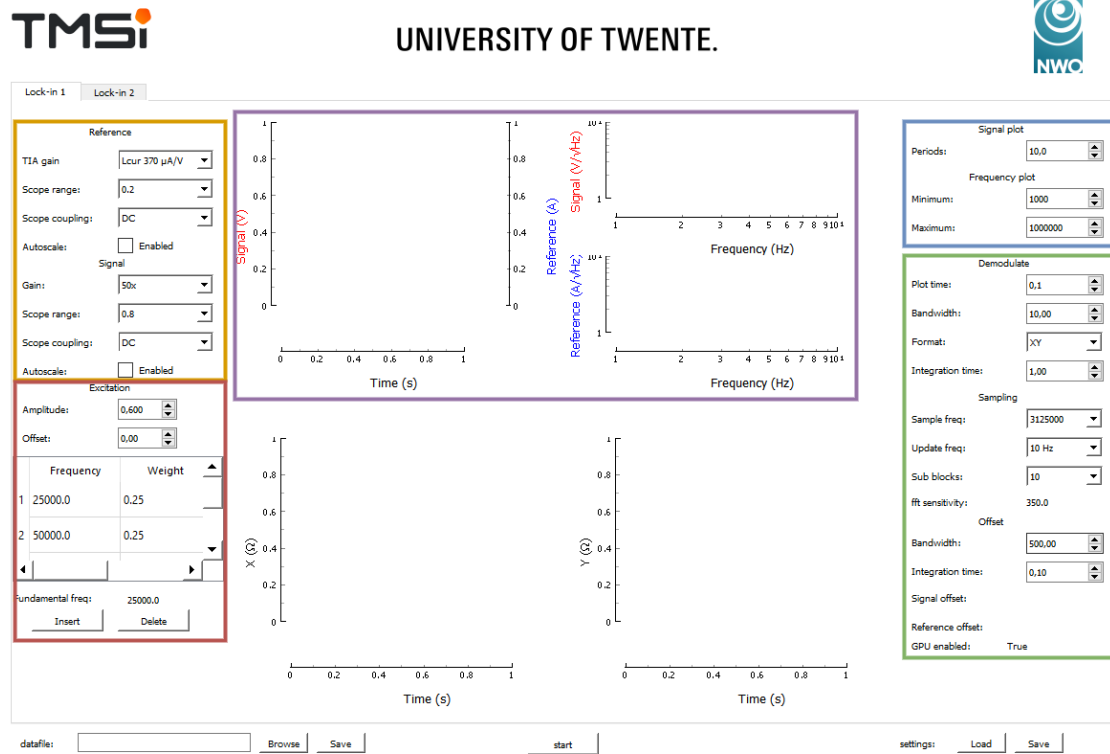


Figure 3.4: The software GUI including different hardware and software settings. Top two graphs show the measured current and voltage versus the time and frequency respectively. The bottom two graphs show the resistance and reactance versus time. [40]

Filtering

The measurements of the TiePie are digitally filtered before the data is saved, all filtering steps described in the following section are shown in Figure 3.5 [40]. The filtering is done in the frequency domain, since it is computational faster than filtering in the time domain. The inverse FFT (iFFT) will be performed as one of the final steps. The envelope returned by the iFFT has a sample frequency which is way higher than the update frequency of the computer. The update frequency of the computer is in the range of 1 Hz to 20 Hz while the sample frequency of the envelope is about 7 to 140 times higher depending on the settings of the amount of sub-blocks. Therefore even though the iFFT takes up more computational power it's usage is justified by the fact it does increase the sample frequency of the bio-impedance.

The bin size in the frequency domain Δf depends on the length of the signal in the time domain. Since the processing is done real time it depends on the update frequency f_u of the TiePie data and the number of sub-blocks n_b per TiePie update. Every FFT is calculated using two data packages, this halves the bin size of the FFT as given in Equation 3.1.

$$\Delta f = \frac{f_u n_b}{2} \quad (3.1)$$

The current and previous data package are used to calculate the real sided Fast Fourier Transform (rFFT). An rFFT only computes the positive frequencies. For a real signal, such as the voltage and the current in this case, the FFT of the positive frequencies equals the complex conjugate of the negative frequencies. The Blackman-Harris window is applied before the rFFT. The Blackman-Harris window has more than 120 dB rejection for frequencies that are more than 20 bins away from the center frequency. [40]. When an NVIDIA GPU including cupy [41] is available the rFFTs are calculated on the GPU. By doing so the rFFTs are calculated faster and the CPU has time for other tasks increasing the overall speed even further.

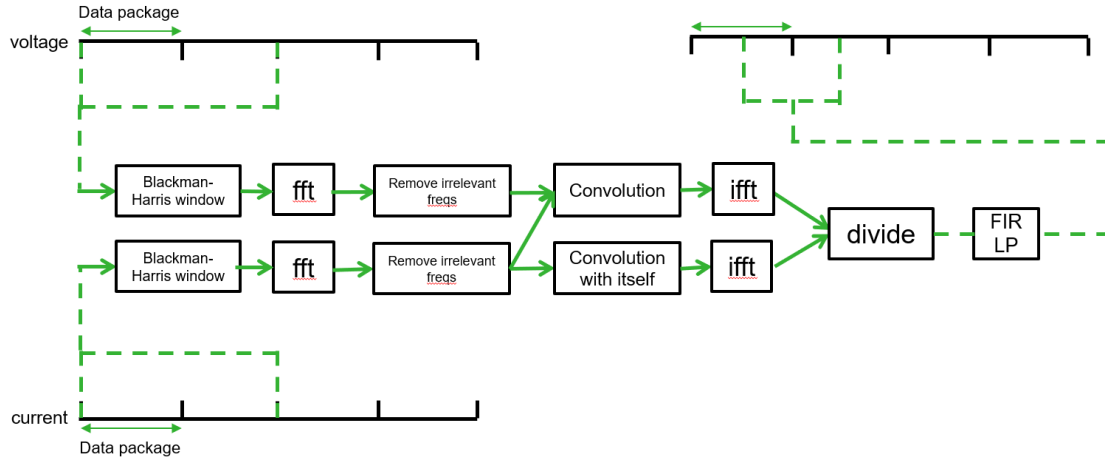


Figure 3.5: Data flow of the digital filtering used for the bio-impedance calculations. [40]

The desired bandwidth B_w used to calculate the impedance is determined by the user. The number of bins L which represent this bandwidth is calculated using Equation 3.2. If this calculation is lower than 7 it is discarded and $L = 7$ will be used. The used window spreads out the power of the desired harmonic, which will be lost if the used bandwidth is too small.

$$L = \text{int} \left(2 \frac{B_w}{\Delta f} \right) \quad (3.2)$$

The numbers of the bins used for the impedance calculation n_{use} depends on the desired impedance measurement frequency f the number of bins representing the bandwidth L and the frequency resolution Δf . The range of numbers of used bins n_{use} is determined using Equation 3.3.

$$n_{\text{use}} = \text{floor} \left(\frac{f}{\Delta f} \right) - L \dots \text{ceil} \left(\frac{f}{\Delta f} \right) + L \quad (3.3)$$

In the impedance calculation as given in Equation 1.2 both the voltage and the current are multiplied by the complex conjugate of the current. A multiplication in the time domain equals a convolution in the frequency domain [53]. This relation is described as:

$$\mathcal{F}\{g \cdot h\} = \mathcal{F}\{g\} * \mathcal{F}\{h\} \quad (3.4)$$

where $\mathcal{F}\{x\}$ indicates the Fourier transform of x . The discrete time domain convolution is calculated by:

$$\mathfrak{F}\{g \cdot h\}[n] = \sum_{m=-M}^M \mathfrak{F}\{g[n-m]h[m]\} \quad (3.5)$$

where \mathfrak{F} indicates the discrete time Fourier transform.

In the previous step the bins corresponding to the frequencies of interest and the surrounding bandwidths were found. These bins are the only ones used for the impedance calculations, leaving the FFTs zero for all bins which are not indicated by n_{use} . The interval of $-M \leq m \leq M$ reduces effectively to $m = \pm n_{\text{use}}$. The resulting convolution is performed over the real frequency bins of g and h indicated by G and H in equation Equation 3.6.

$$\begin{aligned} \mathfrak{F}\{g \cdot h\}[n] = & \sum_{m=n_{\text{use}}} G[n-m]H[m] \\ & + \sum_{m=n_{\text{use}}} G[n-m]H^*[-m] \\ & + \sum_{m=n_{\text{use}}} G^*[n+m]H[m] \\ & + \sum_{m=n_{\text{use}}} G^*[n+m]H^*[-m] \end{aligned} \quad (3.6)$$

The first and fourth term have a non-zero result for frequencies around $n = 0$. The second and third term are non-zero when n is around two times the frequency of interest $n = 2\frac{f}{\Delta f}$. The impedance is calculated using the envelope of the current and voltage signals convoluted with the complex conjugate of the current. The envelope can be obtained by removing the high frequency signals, which is accomplished by removing the second and third term of Equation 3.6. An inverse FFT (iFFT) is applied which results in the envelope of the current and voltage signals both multiplied with the complex conjugate of the current. As described earlier (Equation 1.2) the impedance can be calculated by a division of these signals. Since both represent the envelope of respectively the voltage multiplied by the complex current and the current multiplied by the complex current the result is not the instantaneous impedance but an averaged impedance.

3.2.3 System validation

The measurement system will be validated on three main points, the precision and accuracy, the drift and the time delay. The precision and accuracy can be determined by measuring resistors and capacitors with known values. Therefore the measurement circuit consist of a resistor placed in parallel with a capacitor, Figure 3.6.

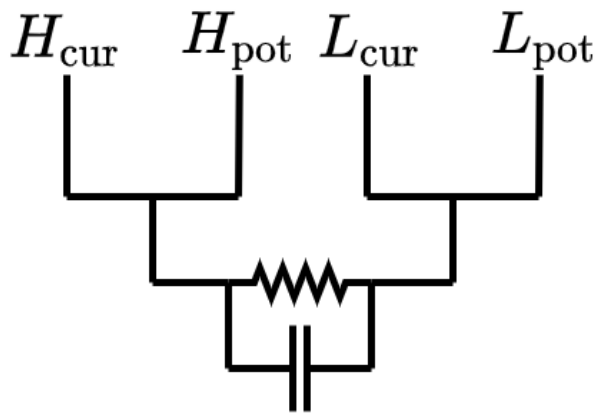


Figure 3.6: The circuit used for system validation of the precision, accuracy and drift.

This choice was made because the software is able to directly calculate the resistance and capacitance of this circuit and it matches the cole-cole model at a specific frequency, Section 2.1.

For both the resistor and the capacitor multiple measurements shall be done, each time using different resistance and capacitance values. All of these shall be in the range of the expected impedance of the human arm. T.J. Freeborn and S. Critcher reported a range of values for all three Cole-circuit elements for the right arm [54]. The first resistor, R_∞ in Figure 2.4, can be expected to have a value of $100\ \Omega$ up to $300\ \Omega$. The second resistor, R_0 , lays between $60\ \Omega$ and $125\ \Omega$. The capacitance is between $1\ \mu\text{F}$ and $6\ \mu\text{F}$. Since the used circuit matches the Cole-Cole model at a specific frequency it gives confidence that these ranges are applicable. The measurement will be done using multiple frequencies simultaneously, spread over the spectrum from $0\ \text{Hz}$ to $3\ \text{MHz}$. Each measurement will take $60\ \text{s}$, the mean and standard deviation over these $60\ \text{s}$ are calculated.

In order to measure the drift of the system one measurement per combination of capacitance and resistance value will be done for a longer period of time, $10\ \text{min}$. The resistance and capacitance as measured by the system are plotted against the time. Any drift should show up as a slow but consistent increase or decrease in the impedance. The drift is determined for only ten minutes since no measurement is expected to be longer.

The last validation measurement is done to gain insight in the time delay between the measured EMG and bio-impedance signals. The circuit is given in Figure 3.7 and consists of one resistor more than the previously described validation circuit given in Figure 3.6. The connection to this extra resistor will be disconnected and reconnected from time to time at the point indicated with the letter "A" in Figure 3.7. This way the EMG and bio-impedance values will likely almost instantly change their values. These rapid changes can be used to correlate the two signals such that the time delay between them can be determined.

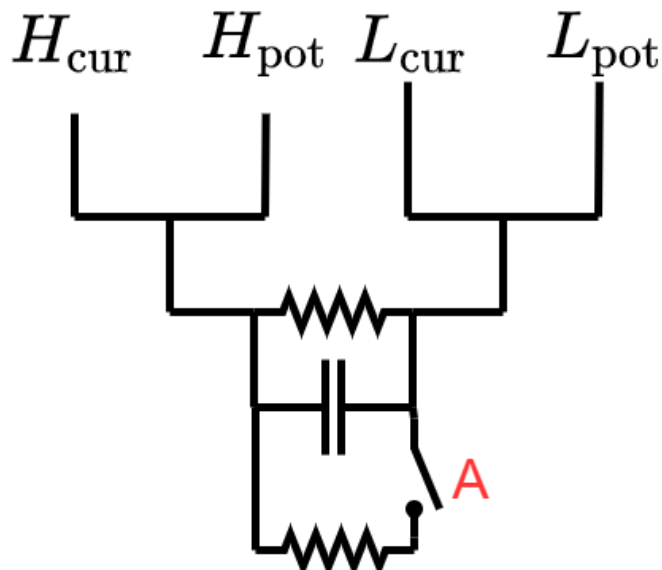


Figure 3.7: The circuit used for system validation of the time delay. The connection is disconnected and reconnected from time to time at point "A".

3.3 Parameter analysis

As described in section 3.2.1 multiple frequencies can be used simultaneously to measure the bio-impedance. Besides it is possible to vary the amplitude of the induced current. All measurements will be done on the biceps brachii, however no research was found on the bio-impedance of the biceps brachii under different circumstances (e.g. contracting and relaxing) at various frequencies or current amplitudes. Therefore two movement patterns are described

in Section 3.3.1. These patterns will be used in the amplitude analysis, Section 3.3.2, and the frequency analysis, Section 3.3.3.

3.3.1 Isotonic and isometric patterns

The two movement patterns have one important difference. The isotonic movement is a movement with minimum effort, while the isometric movement is maximum effort with minimum movement. The importance of this is that in the end it should be possible to distinguish arm movement from arm contraction as stated in the last research question in Section 1.2.

The first pattern is performed to examine the impedance difference between a muscle contraction and relaxation. It starts with a subject sitting in a chair with the lower arm, from elbow to wrist, on an arm rest. The chair is placed such that the hand is beneath a table top, see Figure 3.8. The biceps brachii is in a relaxed state. The subject switches between relaxing its bicep and contracting it and the other way around, situation A and B of Figure 3.8. When contracted the hand pushes against the table top, creating an isometric contraction.

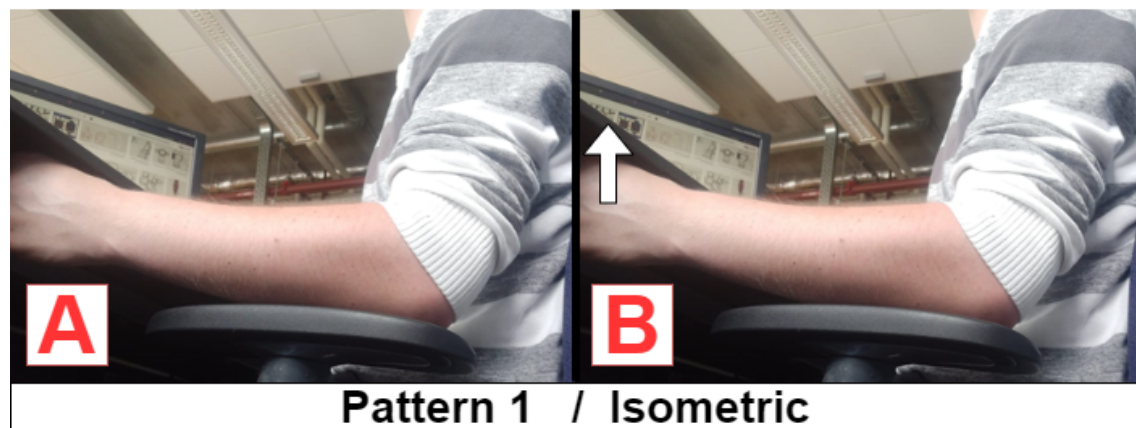


Figure 3.8: The two different arm positions of movement pattern 1. A: arm resting on armrest, bicep is relaxed. B: Arm still on armrest, bicep is contracted such that hand pushes against downside of table top.

The second movement pattern is performed to examine the impedance difference between two different arm positions. For this movement pattern the user is standing. This time the subject starts with a horizontally stretched arm (elbow 180°), with the hand palm facing upwards. When contracting the subject changes the angle of the elbow from about 180° to 90° , position A and B of Figure 3.9. When relaxing the elbow angle changes back from 90° to 180° . The bicep contracts when the switch from state “A” to “B” is made. However once in state “B” the bicep is almost fully relaxed. It is expected that most of the measured bio-impedance change is therefore due to the change in arm position instead of muscle contraction.

3.3.2 Amplitude analysis

Multiple measurements at frequencies spread over the frequency band from 125 Hz to 3 MHz are done. Since it is a broad bandwidth it is split into two. The lower part of the bandwidth reaches from 125 Hz up to and including 100 kHz, the higher part of the bandwidth includes frequencies from 100 kHz to 3 MHz. The used frequencies are given in Table 3.1.

The voltage output of the TiePie is set at 0.1 V and is increased with 0.1 V with every new measurement up to 0.8 V. As described in Section 3.2.1 the gain of the current pump is equal to $370 \mu\text{A V}^{-1}$. This means that the alternating current amplitude is set to 37 μA and each step it

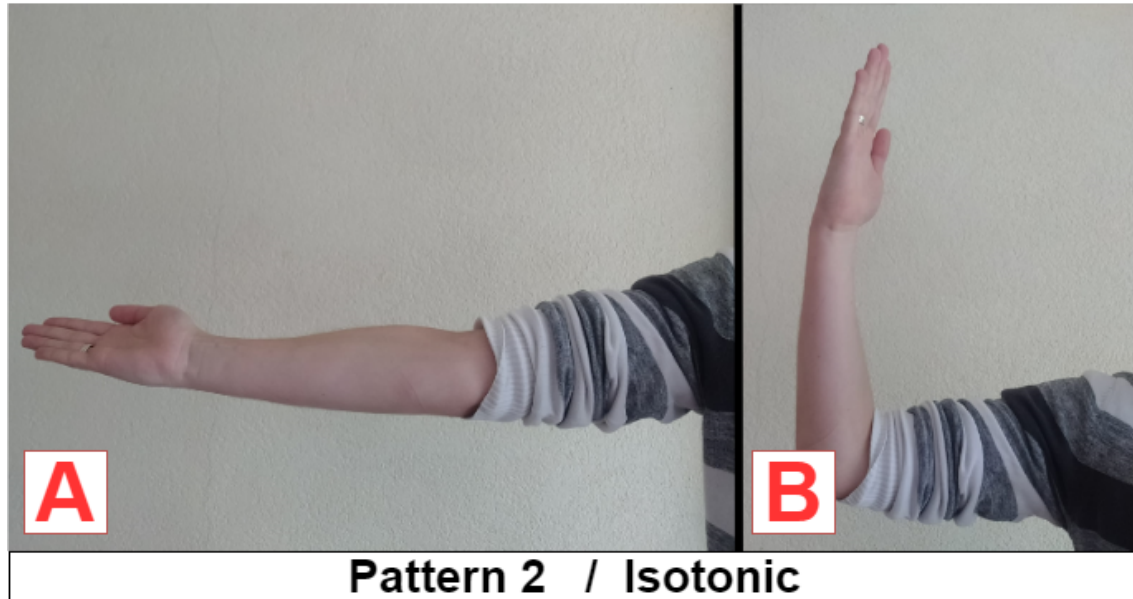


Figure 3.9: The two different arm positions of movement pattern 2. A: arm stretched, elbow about 180°. B: hand upwards, elbow about 90°.

Low frequencies	High frequencies
125 Hz	100 kHz
250 Hz	250 kHz
500 Hz	500 kHz
1 kHz	1 MHz
2.5 kHz	1.25 MHz
5 kHz	1.5 MHz
10 kHz	2 MHz
25 kHz	2.25 MHz
50 kHz	2.5 MHz
100 kHz	3 MHz

Table 3.1: The measurement frequencies are divided into two groups, the low frequencies group and the high frequencies group.

is increased by $37\mu\text{A}$ up to $296\mu\text{A}$, which is still way below the maximum allowed current of $500\mu\text{A}$. The measurements are done using the isometric movement pattern. Each measurement starts in the relaxed state. Each 5 seconds the user switches between the relaxed and contracted state. From state A to B or from state B to A as depicted in Figure 3.8. This is done for 60 seconds. The amplitude selection is based on the difference between the contracted and relaxed state for the resistance and for the reactance. The resistance and reactance difference can both be calculated for each frequency by subtracting the mean of the contracted state from the mean of the relaxed state and taking the absolute value of it, $|\bar{R}_{\text{relax}}(f) - \bar{R}_{\text{contract}}(f)|$. Summing all these differences gives the total resistance/reactance difference over all frequencies for a certain current amplitude. This idea is described in Equation 3.7. This difference should be as high as possible for both the resistance and the reactance in order to make the distinction between these states as clear as possible.

$$\Delta R = \sum_{f=125\text{ Hz}}^{3\text{ MHz}} |\bar{R}_{\text{relax}}(f) - \bar{R}_{\text{contract}}(f)| \quad (3.7)$$

3.3.3 Frequency analysis

For the frequency analysis the same frequencies are used as for the amplitude analysis (Section 3.3.2) given in Table 3.1. Two movement patterns are used, one with an isometric and one with an isotonic contraction, both described in Section 3.3.1 given in Figure 3.8 and Figure 3.9. Again each measurement starts in the relaxed state. Each 5 seconds the user switches between the relaxed and contracted state, from state A to B or from state B to A as depicted in Figure 3.8 for the isometric and in Figure 3.9 for the isotonic movement pattern. Each measurement takes in total 60 seconds.

The impedance's for both contracted and relaxed states will be plotted against the frequency. From these data the frequencies which will be used later on will be deducted, based on the criteria below. There is no specific order in these criteria, each one is equally important. This means it is most likely that a compromise shall be necessary between the criteria.

- The standard deviation over multiple measurements is low.
- The difference in impedance between the two states of Figure 3.8, contracted and relaxed muscle, is high.
- The difference in impedance between the two states of Figure 3.9, elbow 90° and 180°, is high.
- A distinction can be made between the (difference in impedance) of the isometric and the isotonic movement pattern.

3.4 Measurements

Three measurements are discussed each focuses on a different aspect, these are movement/contraction, time delay and contraction level. The first section, Section 3.4.1, is focused on bio-impedance changes between different arm positions and impedance changes due to contraction in different situations. Section 3.4.2 focuses on bio-impedance during various levels of contraction. The last measurement is dedicated to the time delay of the bio-impedance measurement, Section 3.4.3.

3.4.1 Movement measurements

In order to get insight in contraction in different situations and the influence of movement on the measurements two different movement patterns are introduced. These movement patterns include both isotonic and isometric contractions. Both movement patterns are performed while sitting in a chair, such that other movements of the body can be limited as much as possible. The numbering of the movement patterns is consecutive to prevent confusion.

The first new movement pattern includes three different arm configurations. During each configuration the muscle is kept in both a relaxed and a contracted state. All states are given in Figure 3.10, where the white arrows indicate the direction of delivered force. This means for state "A" the arm is relaxing on the arm rest while state "B" indicates that the hand is pushing upwards against the table top. In situation "C" the hand is resting on the table top while holding a bottle and in "D" the hand is squeezing the bottle. Finally situation "E" and "F" represent resting against the shoulder using a bottle and pushing the bottle towards the shoulder respectively. One measurement starts at "A" and ends at "F", the movements are not repeated within one measurement.

The fourth movement pattern is similar to the third one, however state "C" and "D" of the third movement pattern are left out. This is done since the least amount of bicep contraction is expected in state "D" and thus adding the least new information to the measurement. This way four states remain starting again with state "A" where the arm is resting on the arm rest, as given in Figure 3.11. Next in state "B" the hand is pushed upwards against the downside of the table

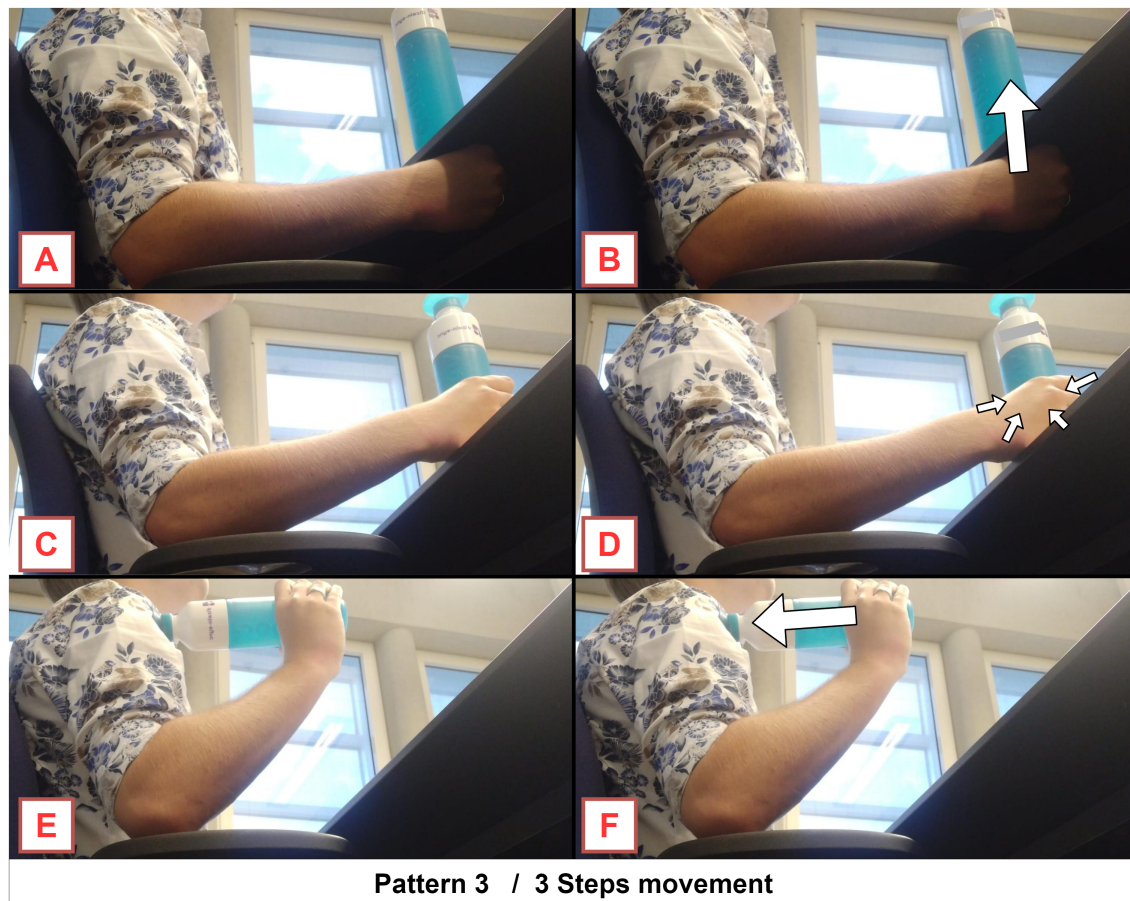


Figure 3.10: The six different arm positions for the third movement pattern, including three different arm configurations. The white arrows indicate the direction of the force of the hand. A: Arm resting on armrest. B: Arm on armrest, contracting the bicep by pushing upwards against downside of table top. C: Hand resting on table holding a bottle. D: squeezing the bottle E: Hand upwards. F: pushing bottle onto shoulder.

top, creating an isometric contraction. Then the hand is brought towards the shoulder holding a bottle. This creates an isotonic contraction from state “B” to state “C” in Figure 3.11. Finally the bottle is strongly pressed against the shoulder again creating an isometric contraction. One measurement starts at “A” and ends at “D”, again there is no repetition of the movement.

3.4.2 Force measurement

The relation between change in bio-impedance and the amount of delivered force can be analysed if the delivered muscle force is simultaneously measured with the bio-impedance signals. This is done using a weighting scale. The Subject sits in a chair with the upper arm resting on the arm rest. A scale is placed between the hand of the subject and the bottom of the table top, as shown in Figure 3.13. By contracting the biceps the hand is pushed upwards such that the scale is pressed. The amount of delivered force can be varied which will result in the weighting scale indicating different weights.

Weighting scale

The weighting scale used is an OHAUS Scout Pro 6001 (SP6001). It can measure up to a maximum of 6 kg with a resolution of 0.1 g [55]. The whole scale is 19.2 cm x 5.4 cm x 21.0 cm while the surface of the weighting platform is 16.5 cm x 14.2 cm. This means the scale is compact

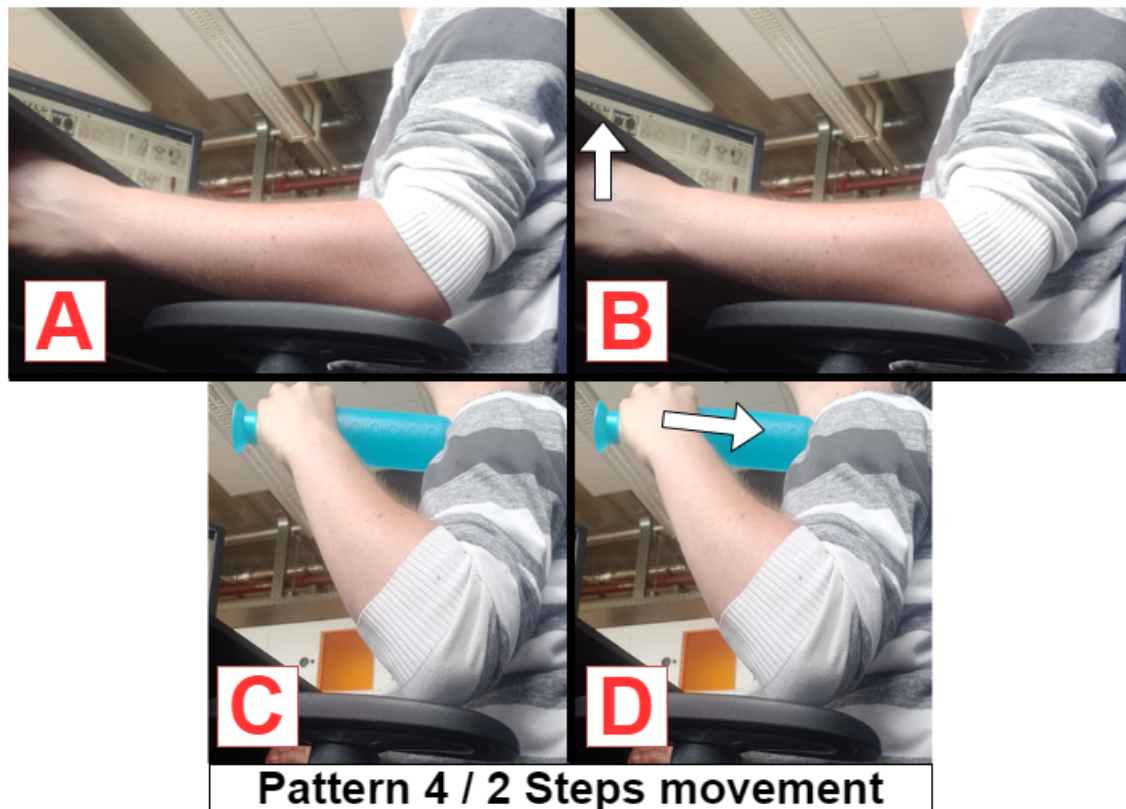


Figure 3.11: The four different arm positions of the fourth movement pattern. The white arrows indicate the direction of the force of the hand, delivered by the biceps brachii. A: Arm resting on armrest. B: Arm on armrest, contracting the bicep by pushing upwards against downside of the table top. C: Hand upwards holding a bottle, relaxing as much as possible. D: Hand upwards, pushing bottle onto the shoulder.

enough to place it between the hand and the table while the contact surface of the scale is still larger than the hand. Which makes it easier to press on it. The scale weighs about 1.8 kg and is therefore not too heavy to lift. A screen shows the current weight which will be used as feedback to the subject. The scale has an optional USB connection which makes it possible to transfer the weight information to the computer. A python program timestamps and logs the data from the scale. The timestamps can be used to relate the weighting data to the bio-impedance data.

Force movement

The subject starts in a relaxed state such that the scale is at about 0 kg. In each next state the subject is asked to push harder at the weighting scale such that the indicated weight is increased by 1 kg. The maximum desired weight is 5 kg. The weighting scale can go higher, with a maximum of 6 kg, however the subject will never reach the desired value perfectly. If the desired value is 6 kg and the subject pushes a little too hard an error is returned by the weighting scale, deeming the measurement useless. The subject is asked to try to maintain the delivered force for a period of time such that the weighting scale indicates the same weight for a short period of time. It is expected that the subject will never perfectly reach and maintain the steps of 1 kg. The current value as measured by the weighting scale is directly shown to the subject. This visual feedback should help the subject to maintain the desired weight value as good as possible. Since the bio-impedance should fluctuate in the same manner as the weight fluctuates around the desired value they can still be correlated to each other as long as there is no time delay introduced between these signals.



Figure 3.12: The used weighting scale, Ohaus Scout Pro 6001. The maximum weight is 6 kg with a resolution of 0.1 g.



Figure 3.13: Movement pattern 5. The weighting scale is placed on top of the hand beneath a table top.

3.4.3 Time delay measurement

The time delay of the bio-impedance will be based on the EMG signal. The real time delay of the bio-impedance compared to delivered muscle force remains unknown. The measurements done regarding the time delay of the bio-impedance include many switching moments from muscle contraction to relaxation and the other way around. This is done since the time delay is based on a cross correlation between the bio-impedance signal and the EMG signal. Multiple switching moments in one measurement will average out any fluctuating time delay. Measurement pattern 1 of Section 3.3.1, as depicted in Figure 3.8, is used. The user is sitting in a chair with a hand under a table relaxing and switches to contraction by trying to push the ta-

ble top upwards. To further increase the reliability of the measurement the contraction should be a maximum contraction. This might result in fatigue of the muscle. Therefore short measurements should be done. Each measurement should thus be short but also include many transitions. This automatically means the switching should be done rather fast, e.g. switching every second. The switching moments will be indicated using a metronome set at 60 beats per minute. [56].

3.5 Conclusion

By using a combination of a current source, instrumentation amplifier and transimpedance amplifier it is expected that it will be possible to do an accurate 4 points measurement of the bio-impedance. Besides it is expected that the FFT filtering and impedance calculation can be done real time using the GPU. The first and second movement pattern are used to determine the desired combination of settings. These are optimized to distinguish muscle contraction and arm movement. The other movement patterns are created to support the various research questions. Pattern 3 and 4 both include a contraction in different arm positions. It should be possible to answer research question 1, about predicting the contraction, and question 4, about distinguishing movement from contraction. When performing movement pattern 1 with many switching moments it is possible to determine the time delay corresponding to research question 2. Using movement pattern 5 it is possible to relate the bio-impedance measurement to the amount of delivered force. This can aid in distinguishing contraction levels based on the bio-impedance measurements. Therefore it is expected that this set of movements is sufficient to answer all research questions.

4 Data processing

4.1 Introduction

Various data processing methods are required and introduced. In order to compare different states of one movement pattern with each other the data of a measurement has to be cut into pieces. This is especially needed for the data of movement pattern 1 and 2 which will be used for the frequency and amplitude selection. These are the isometric movement pattern, Figure 3.8 and the isotonic movement pattern Figure 3.9. The data is grouped per state as is described in Section 4.2. The grouped data is not only useful for the selection of the parameters but can also be used to extract the Cole parameters of different states. Section 4.3 describes how the bio-impedance of Cole's model is plotted and a fit is made to extract the Cole parameters.

The measurements regarding the separation of movement and contraction as well as for different levels of delivered force of Section 3.4.1 and Section 3.4.2 are processed using a Neural network. By using a neural network it might be possible to find relate the contraction and the bio-impedance measurements as described in Section 4.5.

All signal processing is done in Mathworks MATLAB R2020a [57].

4.2 Data Grouping

Movement pattern 1 and 2 are performed and measured multiple times. The data of all measurement is grouped based on the state. Such that each group includes all data belonging to one state. This is needed to compare the bio-impedance of different states with each other. The separation of the data within these states has to be done for both the resistance and the reactance. The first and last 0.29 s of data of each measurement are thrown away. The subject had some undesired movements at the beginning and at the end of each measurement since the start and stop button had to be pressed.

The switching moments between two states of each movement pattern are found by the MATLAB function `findchangepts` [58]. The index of the sample in the middle of the switching moment is returned. Since every switch is not instantaneously a short period of time (0.14 s) before and after the switching moment is added which indicate the cut points. The data between these cut points is thrown away, since it only includes data of a switching moment between two states. In Figure 4.1 and Figure 4.2 one of the low frequency and one of the high frequency measurements are given, both having movement pattern 2 of Section 3.3.1. The red shaded area is data which is thrown away since it is either the start or end of the measurement or around a switching point. The switching points are clearly visible in the red areas, the bio-impedance values increase or decrease rapidly in those segments compared to the blue and yellow area's. The yellow area indicates the time when the bicep was in state A of the movement pattern. In the blue area the user was performing state B of the movement pattern. The data in these segments is grouped. One group includes all data of state A and the other all data of state B. Within those groups are the resistance and reactance kept separated such that four different data groups can be assigned, resistance of A, reactance of A, resistance of B and reactance of B. The mean and standard deviation per data group are calculated. These can be plotted per frequency to give insight in the frequency response of the bio-impedance.

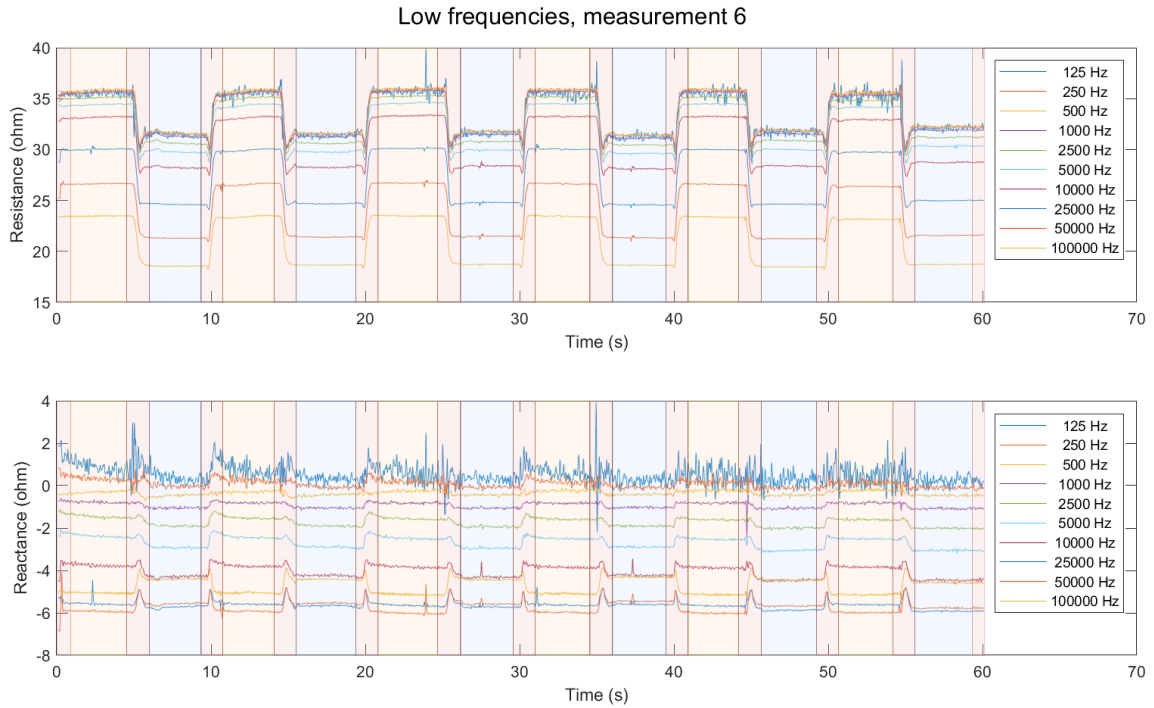


Figure 4.1: The resistance and reactance measured at low frequencies during an isotonic movement , the second pattern as described in section 3.3.3. Red shaded area: this part of the signal is thrown away since it is either start/stop of the signal or around a switching point. Yellow shaded area: the bicep was in a relaxed state. Blue shaded area: the bicep was in a contracted state.

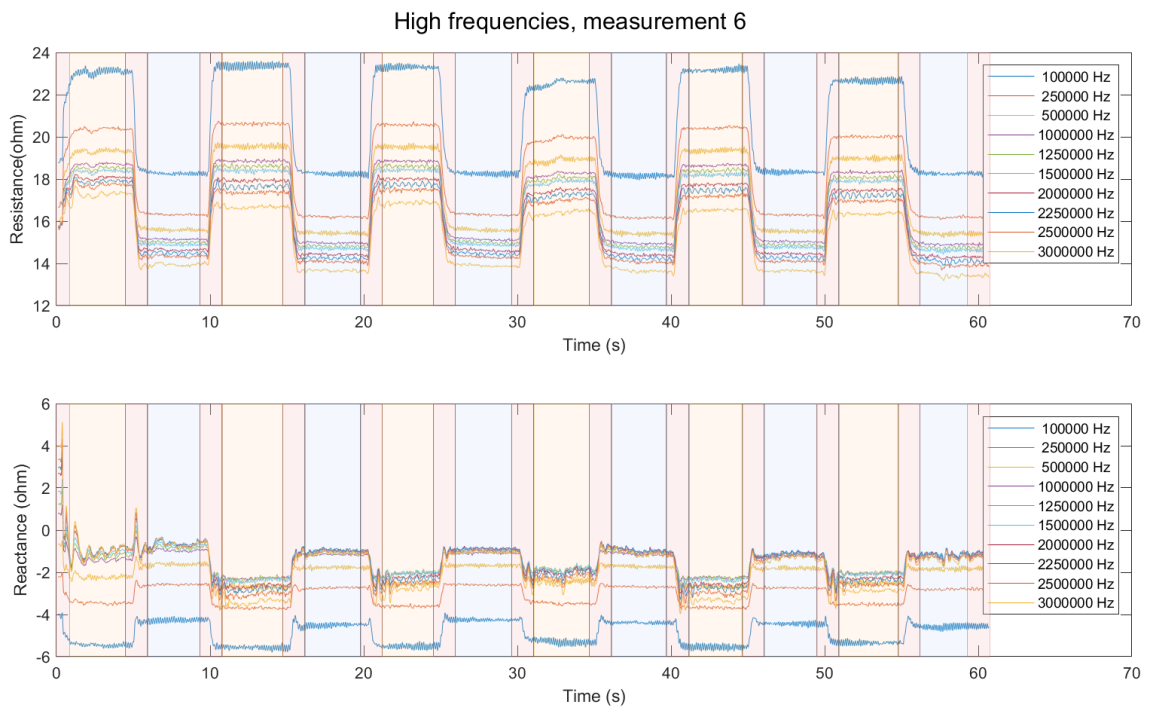


Figure 4.2: The resistance and reactance measured at high frequencies during an isotonic movement, the second pattern as described in section 3.3.3. Red shaded area: this part of the signal is thrown away since it is either start/stop of the signal or around a switching point. Yellow shaded area: the biceps was in a relaxed state. Blue shaded area: the biceps was in a contracted state.

4.3 Cole's model

In Section 2.1 Cole's model is introduced to represent bio-impedance. The model consists of two resistors and a constant phase element and has four parameters, R_0 , R_∞ , n and Q as is given in Figure 4.3. By varying the parameters it is possible to represent the bio-impedance of different materials. Therefore it could be possible to distinguish contracted muscle from relaxed muscle based on these parameters.

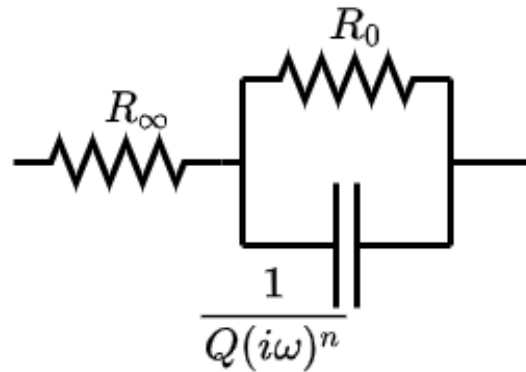


Figure 4.3: The Cole model represented by electrical components. The electrical resistance at high frequencies is given by R_∞ and the resistance at lower frequencies is given by $R_\infty + R_0$.

4.3.1 Cole's impedance representation

When the Cole-Cole model is mentioned its typical way of plotting should be mentioned as well. The impedance of the Cole-Cole model is commonly plotted on an adapted version of a nyquist diagram. It has the resistance on the x-axis and the negative reactance on the y-axis. When the impedance of the Cole model at all real positive frequencies is plotted on these axis it looks like a semicircle.

The typical nyquist plot can be insight full since it shows both the resistance and reactance in one plot. On the other hand is it difficult to see which impedance to expect at which frequency. The frequency information is important when the measurement frequencies shall be chosen. A method which does include the frequency aspect is introduced in Figure 4.4. The x-axis shows the frequency on a logarithmic scale while the y-axis of the first plot shows the resistance and of the second plot shows the reactance. This representation will be used when the frequencies are selected as well as to represent the fitting of the Cole-Cole model to the measured data.

4.3.2 Fitting Cole's model

Fitting the Cole-Cole model to the measured data includes multiple steps. First the data is separated such as is described in Section 4.2. This way a resistance and reactance graph such as Figure 4.4 can be created for all states, e.g. contracted and relaxed. A digital matlab model is made of the Cole model including the estimate, upper bound and lower bound of the parameters. This way it is known "n" is always between 0 and 1 and the resistors and capacitance do not result in a negative value. The impedance and the error of the estimated model is calculated for all measurement frequencies. The parameters are altered based on the fitting algorithm and afterwards the impedance and the error of the model using the new parameters are calculated again. Three different fitting algorithms will be used and compared. These are described in Matlab as, `lsqnonlin`, `fmincon` and `patternsearch`.

- The `lsqnonlin` fitting algorithm solves a nonlinear least squares function by finding the minimum of the sum of squares of a user defined function as is given in Equ-

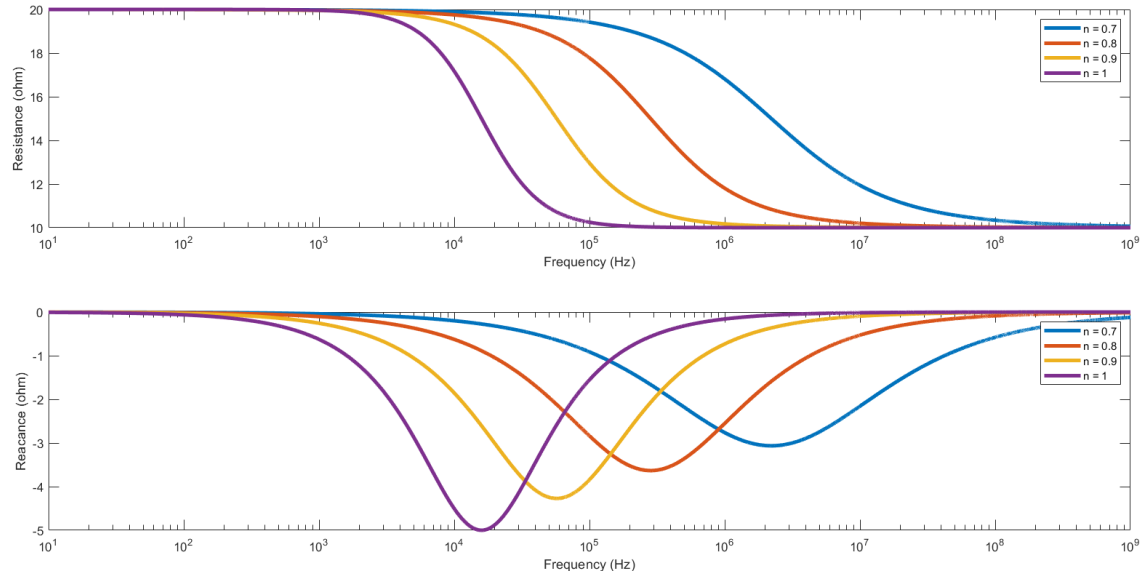


Figure 4.4: The impedance of the Cole model between 0 Hz and 1 GHz for different values of n . $R_\infty = 10 \Omega$, $R_0 = 10 \Omega$ and $Q = 1 \mu\text{F}$.

tion 4.1 [59]. The fitting algorithm is a gradient-based solver which directly means the function to be minimized should be continuous [60]. This function should return the error between the model and the measurement for both the resistance and the reactance for all measurement frequencies. The function $f(Z_{\text{model}}(\omega), Z_{\text{meas}}(\omega))$ in Equation 4.1 takes the impedance of the model $Z_{\text{model}}(\omega)$ and the impedance of the measurement $Z_{\text{meas}}(\omega)$ at all measurement frequencies $\omega_1 \dots \omega_p$ and returns a vector including all values of $f(Z_{\text{model}}(\omega_1), Z_{\text{meas}}(\omega_1))$ up to $f(Z_{\text{model}}(\omega_p), Z_{\text{meas}}(\omega_p))$ where ω_a indicates measurement frequency a and p is the index of the last measurement frequency.

$$\begin{aligned} \min_{Z_{\text{model}}(\omega)} \|f(Z_{\text{model}}(\omega), Z_{\text{meas}}(\omega))\|_2^2 = \\ \min_{Z_{\text{model}}(\omega)} (f(Z_{\text{model}}(\omega_1), Z_{\text{meas}}(\omega_1))^2 + \dots + f(Z_{\text{model}}(\omega_p), Z_{\text{meas}}(\omega_p))^2) \end{aligned} \quad (4.1)$$

- The `fmincon` fitting algorithm has some similarity with the nonlinear least-squares algorithm. The fitting algorithm is again gradient-based [61]. However the error function should in this case return one value instead of a vector. The error is directly used instead of squaring and summing the error of all frequencies. This makes it possible to use a custom error function. The used error function is the sum over all frequencies of the sum of the absolute error of the resistance and the absolute value of the reactance, as denoted by Equation 4.2. Here $X_{\text{meas}}(\omega_a)$ and $X_{\text{model}}(\omega_a)$ denote the resistance of the measurement and the model at measurement frequency ω_a . The reactances are denoted by $Y_{\text{meas}}(\omega_a)$ and $Y_{\text{model}}(\omega_a)$ and the index of the last measurement frequency is again given by p .

$$E_{\text{fmincon}} = \sum_{a=1}^p |X_{\text{meas}}(\omega_a) - X_{\text{model}}(\omega_a)| + |Y_{\text{meas}}(\omega_a) - Y_{\text{model}}(\omega_a)| \quad (4.2)$$

- The `patternsearch` algorithm finds a local minimum of the user defined function using pattern search [62, 63]. The algorithm is not gradient-based like the first two mentioned algorithms. A mesh is made with in the center the estimated parameters. The mesh size is set to 1 for all values. The error of the current and all surrounding mesh parameters is calculated. If a parameter combination is found with a lower error these

parameters are used for the next iteration and the mesh size is doubled. If no parameter combination is found with a lower error than the current one, the same combination is used and the mesh size is halved [63]. This is repeated until one of the end criteria is reached such as, the addition/subtraction value is lower than a given value, the previous error and new error difference becomes lower than a specified value or the maximum number of iterations is reached [62].

All parameters have a completely different order of magnitude. As described in Section 3.2.3 lays R_∞ probably between $100\ \Omega$ and $300\ \Omega$ while Q is expected to be somewhere between $1\ \mu\text{F}$ and $6\ \mu\text{F}$. To make sure the difference in order of magnitude does not influence the fitting algorithms all estimates are set to one and the upper and lower bound are divided by the estimated parameter value. This ensures all parameters are weighted equally in the error function. Otherwise the parameter with the lowest order of magnitude will add little to the error function simple because its magnitude is the lowest. After the fit is performed the result is multiplied by the estimated value again to come to the real fitted parameters.

All fitting algorithms shall be evaluated based on the mean squared error between the measured data and the fitted model on all frequencies. Using the fitting algorithm the Cole parameters for both different states can be compared. It should become clear if and based on which parameters it is possible to distinguish different states from each other.

4.4 Filtering

General muscle movements are expected to be slower than 10 Hz [64]. The measurements are done even slower, the maximum movement state switching frequency used in the measurements is 1 Hz. Therefore is it possible to filter every signal directly at 10 Hz or for these measurements even at 1 Hz. On the other hand there is no need to introduce filters if they are not required. Less filtering would be beneficial for the implementation of EIT, since fewer components, computations and phase shifts are introduced. A filter will only be implemented for the measurements which require it, based on the power of the signal in the frequency range outside the expected movement frequencies. The cut-off frequency will also be determined per case and the reason for a specific cut off frequency will be elaborated on. None of the signal processing is done in real time. This means the processing time is not a problem and the filters can be used such that no extra time delay is introduced.

4.5 Neural network

The used measurement frequencies are chosen such that different states should be distinguishable based on the measured impedance's. If it is indeed possible to distinguish different states based on the measured impedance there should be a function which uses all data of one moment and is able to output the amount of muscle contraction at this moment. Finding a function like this can be cumbersome and time consuming. A neural network should be able to do the job as well.

A neural network (NN) is in general represented as is given in Figure 4.5. Each colored circle in this figure represents a node. A neural network has one or multiple input nodes. These x input nodes represent data points which are used to calculate an output. All nodes of the input layer are connected to all nodes of the first hidden layer. These nodes multiply each input with a specific weight and add the results, a bias is added as well. This calculation is described by:

$$O_{i,j} = \sum_{j=1}^m (N_{i-1,j} W_{i-1,j}) + b_{i-1} \quad (4.3)$$

where $O_{i,j}$ represents the sum of node j in layer i , $N_{i-1,j}$ the result of node j of the previous layer and $W_{i-1,j}$ its corresponding weight. Lastly the bias is represented by b_{i-1} . An activation

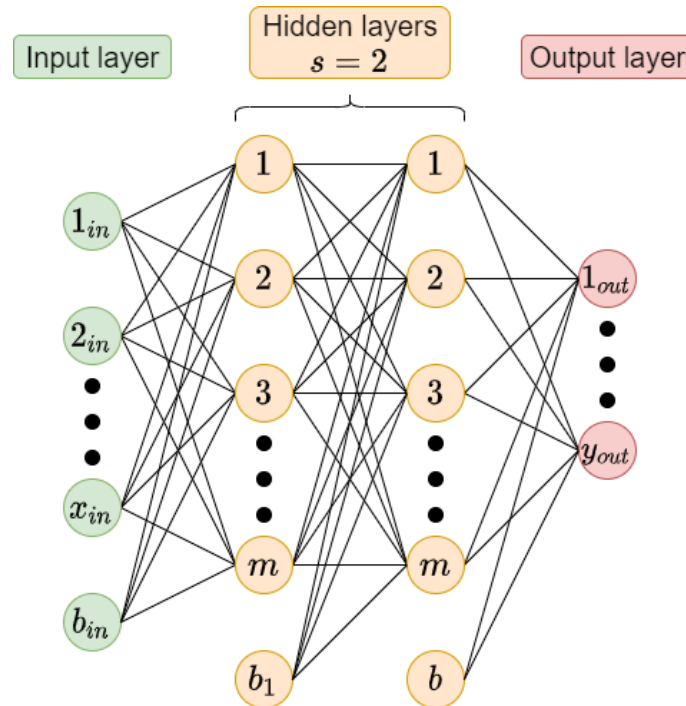


Figure 4.5: A general representation of a neural network. This network has x inputs, m hidden neurons, s hidden layers and y outputs.

function f scales this sum to a certain range, mostly between 0 and 1 or between -1 and 1. In this case Matlab's `tansig` function is used which has a minimum of -1 and a maximum of 1 [65]. It is preferred since in most cases it converges faster than the `sigmoid` function which scales between 0 and 1 [66].

$$N_{i,j,out} = f(O_{i,j}) \quad (4.4)$$

This calculation is graphically represented for one of the nodes in Figure 4.6, where the highlighted nodes and weights are used to calculate the output of the first node $j = 1$ of the second hidden layer $i = 2$. The output of any node of any layer is the input of any node of the next layer. Again these nodes weight and sum the input of all nodes and apply the activation function on the result. The output layer consist of y different outputs. These work the same as all hidden layer nodes, however this time the activation function scales not between 0 and 1 or -1 and 1 but to the “correct” output of the neural network.

The neural network has to adapt all weights and biases in every node in order to come (as close as possible) to the desired output every time. The adaption of these weights and biases is called training. A neural network adapts its weights by calculating the difference between the current output and the desired output of a certain input. This difference is back propagated to every weight of every node such that next time it hopefully functions better. In order to do this the desired output of the training data should be known. This is called labeled data, the desired output is called the target [67].

All labeled data which is present is split in three groups [68], one training data, one validation data and one testing data group. The training data group is used to adapt the weights to come to the best neural network possible for this situation. The validation data is used to test if the network performs well on this data too. If the error of the validation data is higher than last training iteration a counter is increased. If this counter reaches a specified value the training is stopped. The reason for this is that the NN for each new iteration keeps performing worse on the validation data which is data outside of the training data. This indicates that the NN will

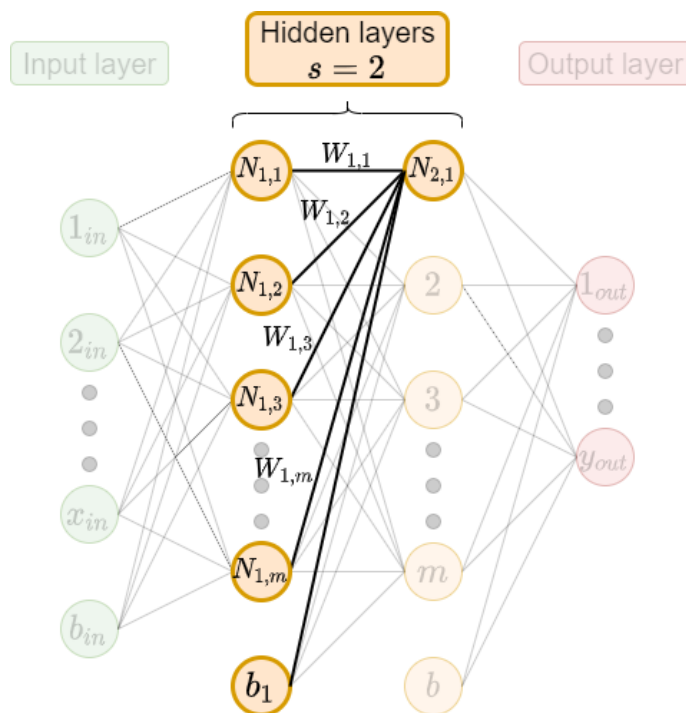


Figure 4.6: A graphical representation of the calculation done for one node. All inputs to the first node of the second layer $N_{2,1}$ are weighted and summed. The activation function is applied to the sum which scales the output to 0 and 1 or -1 and 1.

probably also perform worse in the future if it keeps on training. In order to give an indication of how well the network performs in the future the test data is used. With the test data no training is performed only the error is calculated. The error shows how well the network performs on new data and thus indicates how well the network will perform in the future.

4.5.1 Time delay neural network

A neural network is able to match one input sample to one output sample. In the case of bio-impedance signals there is no certainty that muscle contraction and bio-impedance changes happen at the exact same time. This means it could be the case that the desired output of one sample is muscle contraction while the input sample still matches to muscle relaxation or the other way around. In order to make the neural network resistant against these cases a small range of input data is used. Instead of using only the current data sample to calculate the output the current and the previous $z - 1$ data samples are used. The input which can be represented by a vector with size x becomes a matrix of x rows by z columns. Each row representing either the resistance or reactance on a certain measurement frequency and each column represents one data sample back in time.

The $z - 1$ number of data samples are always data points from the past relative to the time instance of the target. There is only one input sample taken at the same time instance as the target. If the muscle contraction in the target happens before the bio-impedance changes there is no way to predict the muscle is contracted using the previous samples. A work around is to make sure the input of the NN is not only from the past and present but also from the future time instances compared to the target time instance. This is achieved by shifting the target in time. This is made clear using Figure 4.7. The red signal of the top figure shows the target state while the green one shows the input state. At t_1 the target is switched to the contracted state while the input is not. All z samples between t_0 and t_1 are in the relaxed state. Intuitively it seems there is no way the neural network could get to the correct output based on the current

and previous $z - 1$ samples of the input. In the bottom graph of Figure 4.7 a (blue) time shifted target signal is shown. At $t_{1 \text{ shifted}}$ the target is again in a contracted state, now some of the data points of the previous z samples between $t_{0 \text{ shifted}}$ and $t_{1 \text{ shifted}}$ of the input are in the contracted state as well. It is up to the NN to find out which samples to be used and to what extend. Shifting the target is possible since the training of the NN is done offline. Whenever the bio-impedance is processed real time this shift is not possible. This will result in a delay between the moment of contraction and the moment the NN indicates the muscle is contracted. This delay can not be altered since it's origin is from within the body.

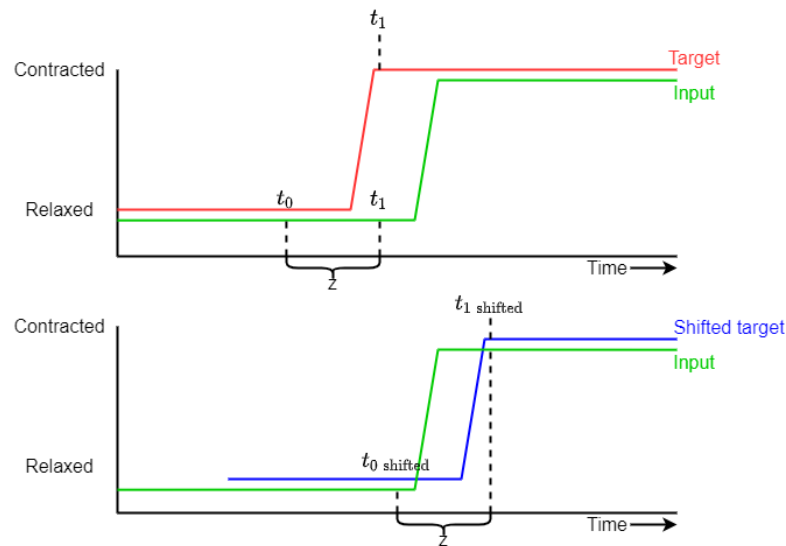


Figure 4.7: If the target switches before the input switches the neural network has not the correct input to match the target. A shifted version of the target should be used.

4.5.2 Implementation

The neural network is implemented using Matlab's Deep Learning Toolbox. Four steps can be distinguished when using a NN in Matlab. The first step is sorting the data, the second is building the network, the third step is training the network and finally testing it and showing the results.

All data should be labeled and each target should match the right input. In which manner the data is presented to the network depends on three parameters these are, the amount of performed measurements l , the amount of samples per measurement k and the amount of measured values per sample x . Two things must be noted, first the amount of measured values per sample equals the amount of inputs to the NN, therefore both indicated by x . In fact the amount of NN inputs is determined by the amount of measured values per sample. If this were not the case there exist a measured value which is not presented to the NN input and is thus not used. In this case if four measurement frequencies are used to measure a resistance and reactance this means that the amount of measured values per sample and thus the amount of inputs for the NN is $x = 4 \cdot 2 = 8$. Secondly the amount of samples per measurement k should be equal for all measurements. The amount of samples per measurement depends on the length of the measurement in seconds T_{meas} and the sampling frequency $f_{s,\text{meas}}$ and is given by $k = T_{\text{meas}} \cdot f_{s,\text{meas}}$. Since the sampling frequency will be constant some measurements have to be cropped such that they take the same amount of time as others.

Matlab requires a specific structure for data which will be used in the NN. A set of input data is build up as in Figure 4.8. The orange box indicates one data set. The data set consist of $k = 20$ samples, each sample is taken at a certain time instance indicated by t_1 for the first and in this

example up to t_{20} for the 20th time instance.

Each of the samples, indicated in blue in Figure 4.8, consist of an l by x 2D array. Here l represents the amount of performed measurements for this data set. Each new measurement is indicated with a different shade of green in Figure 4.8. As explained is x the amount of NN inputs. In Figure 4.8 the inputs are four resistance values indicated by $X_1 \dots X_4$ and four reactance values indicated by $Y_1 \dots Y_4$, measured at four frequencies.

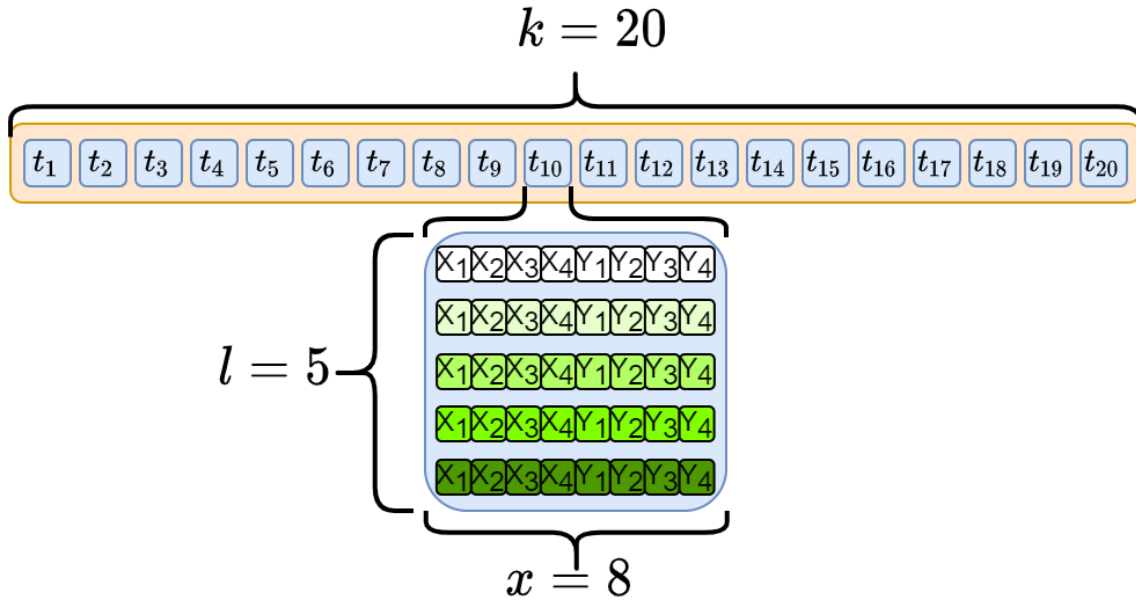


Figure 4.8: The data structure required by Matlab for a NN. The orange box represents one data set. The blue box represents a time instance. All input data belonging to one time instance of one measurement is indicated by $X_1 \dots X_4$ and $Y_1 \dots Y_4$. Each measurement is a different shade of green. This data set consist of $l = 5$ separate measurements consisting of $k = 20$ data samples where $x = 8$ data points are collected.

Since a time delay net is used, the first z out of k samples of each measurement are used to come to target number z . The first $z-1$ targets are thus thrown away. The first z samples separated from the other samples. Every measurement has its own unique z first samples, therefore every time the NN is used these need to be pre-loaded into the NN and thus need to be handled separately. After the first z samples are loaded and used to generate an output an new sample is shifted in and the last one is shifted out to generate a new output. This shifting in and out continuous until the last sample is reached..

Finally the training, validation and test ratio is set. This ratio indicates which percentage of all measurements should be used to train the NN, to validate and to test it. Which measurements are used for training, which are used for validation and which for testing is determined randomly. This to prevent any influence of factors outside of the measurements to influence the training, such as muscle fatigue or sweat. Creating the network can be done with one command, the function `timedelaynet` returns a network type variable. The function needs three inputs which are the number of input delays, z , the number of neurons per layer as array, $[m_1, m_2, \dots, m_n]$, and the trainings function. Many different trainings functions exist and each has its advantages and disadvantages. The most important thing to keep in mind is that train scaled conjugate gradient (`trainscg`) uses less memory. This is an important advantage since during training the computer can run out of free memory making it impossible to train further. Besides that, when less memory is used, less read and write actions are performed which ben-

efits the training speed. By default every network is created with one input and one output. In order to set the number of inputs and outputs the function `configure` can be used. The network, the input data and targets are given and the network is returned where the number of in and outputs matches the data. This is the reason why the first step is to store the data correctly. A visual representation of the network created by Matlab is given in Figure 4.9

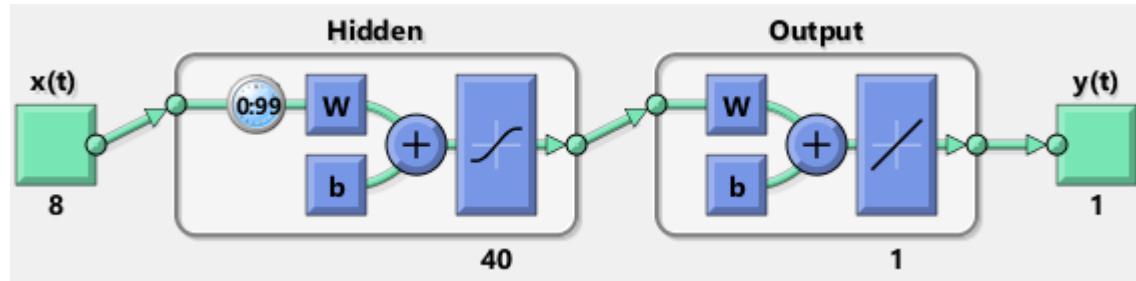


Figure 4.9: A visual representation of a NN created in matlab. This network has $x = 8$ inputs, $y = 1$ output, $z = 100$ time delays, $n = 1$ hidden layer and $m = 40$ neurons in this hidden layer.

Training the network can be done by asserting the `train` function and providing the network, input data and the targets. However before training many parameters can and should be adjusted. The training goal, performance function, minimum gradient and maximum number of epochs are four important settings.

- The **training goal** specifies at which point the error is low enough and the training can stop. This is just one of the many stopping conditions.
- The **performance function** is the function used to calculate the performance and thus the error. Most of the cases a mean squared error function is used.
- The **minimum gradient** again specifies a stop condition. If the learning gradient is lower than the specified value the training stops.
- The **maximum number of epochs** is also a stop condition. This stop condition differs from the others since the others are based on the performance of the NN whereas this one only specifies how many times it has to be trained. If the maximum number of epochs is reached it is likely that the NN is not yet properly trained. However it can function as a hard stop when training takes up to long or might even go on forever without this stop condition.

After the network has been trained it can be tested. By supplying all data and the targets to the net all NN outputs can be calculated. Using the masks made to distinguish the training, validation and test data the data groups can be tested separately. Using the function **perform** the performance of the network on the data group is calculated. The performance can also be studied visually by plotting the target and NN output in one graph.

4.6 Down sampling

To train a neural network every input needs a target, as mentioned in Section 4.5. However the sampling frequency of the EMG signal is 3 kHz while the sampling frequency of the bio-impedance measurements is 350 Hz. To get one target for every bio-impedance measurement the EMG signal is down sampled. When down sampling an anti-aliasing filter is required. Since the down sampled signal should have a sample frequency of 350 Hz the Nyquist frequency is 175 Hz which is thus the maximum cutoff frequency of the low pass filter. Since the processing

of the EMG ends with a low pass filter which is much lower, around 4 Hz, the anti aliasing filter becomes obsolete.

The down-sampling factor is not a round integer, $N = 8.57$. Therefore it is not possible to take all bio-impedance time instances and only use the EMG samples at these time instances. A neat method is to take the weighted average of the EMG samples just before and after the bio-impedance time instance. The weights should depend on how close the EMG sample is to the bio-impedance time instance. However this takes up a lot of computational time. Therefore instead of using the weighted average the EMG time instances which are closest to the bio-impedance time instances are used for the down sampled signal. This does introduce a small error. However when a maximum EMG frequency of 4 Hz is assumed, the error is less than 0.21 %. Since every periodic movement or contraction will be much slower than 4 Hz it is expected that this error will be even much lower.

4.7 Conclusion

It is expected that using these data processing methods the research questions can be answered. The data grouping will be used for the frequency and amplitude selection. The other movement patterns will all be used in combination with a Neural network. It is expected that the contraction and movement information is present in the bio-impedance signal. Therefore should the Neural Network be able to distill this information from the bio-impedance signals. This expectation is based on the fact that the bio-impedance does change when the muscle contracts or moves.

5 Results

5.1 Introduction

All movement patterns given in Chapter 3 are performed and the bio-impedance is measured. The data processing methods as described in Chapter 4 are used on these measurements. The results and the settings of the data processing are given in this section. Section 5.2 shows the results for the amplitude selection. In Section 5.3 the measurements for the frequency selection are given. The Cole-Cole model is fitted onto the measurements, Section 5.4.2 shows the fitted Cole parameters. Section 5.5 describes the performance of a NN with the EMG and movement as targets. Various levels of force are used as target in Section 5.6. The time delay between a EMG measurement and a bio-impedance measurement is discussed in Section 5.7.

5.2 Amplitude selection

The measurements as described in Section 3.3.2 are conducted. Each measurement is done three times. This means for every amplitude 6 measurements are done, 3 using the low frequencies and 3 using the high frequencies as given in Table 3.1. For the lowest amplitude first the three low frequency measurements are conducted, the second amplitude starts with the three high frequency measurements, the third again with low frequencies etcetera. The contracted and relaxed data is separated using the algorithm of Section 4.2. The data of all 3 measurements is used to generate the mean and standard deviation per frequency. A typical graph of the mean and standard deviation of the contracted and relaxed bio-impedance data is given in Figure 5.1. Measurements with different amplitudes have comparable figures, those are given in Appendix A. There is a clear difference between the resistance of the contracted and relaxed state. This is less the case for the reactance. For the low frequencies the values of the reactance in the contracted and relaxed state are almost equal. On the other hand at the higher frequencies, above 100 kHz, the difference is larger however for those frequencies the standard deviation is much larger as well. Therefore only the resistance is used in the following calculations and the reactance is excluded.

The criterion for the amplitude selection is the total amount of difference in the resistance between the contracted and relaxed state as described in Section 3.3.2, calculated using Equation 3.7. The resistance sum is calculated over all frequencies as well of all low and all high frequencies separately. The results of these calculations are given in Figure 5.2.

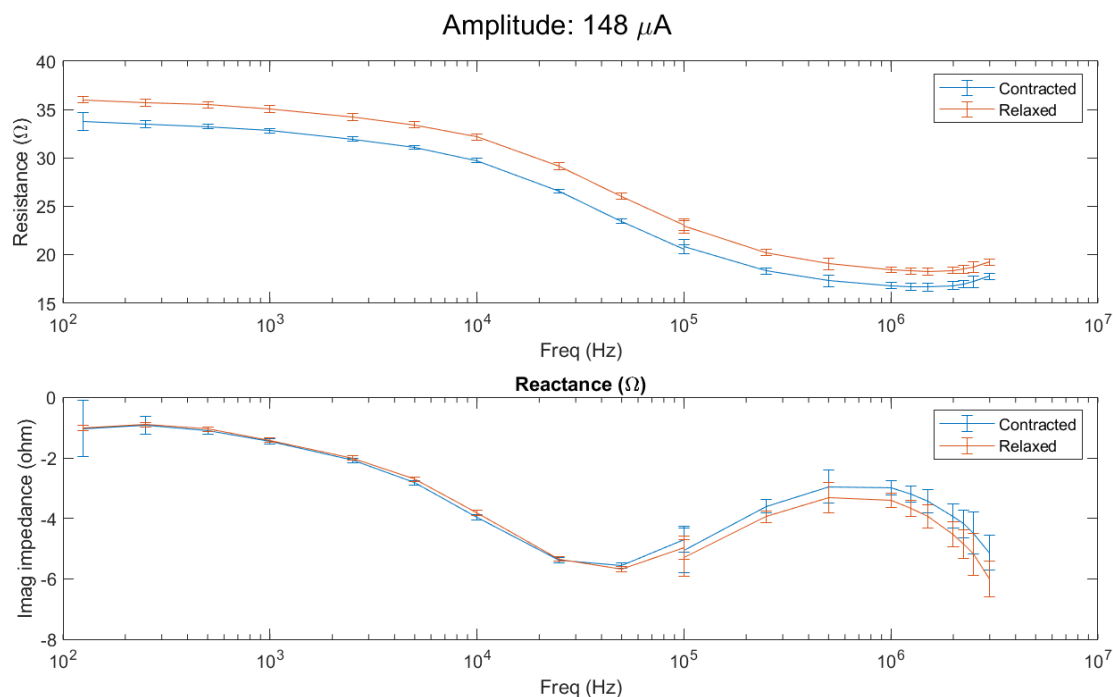


Figure 5.1: The mean and standard deviation of the bio-impedance of the relaxed and contracted state per frequency. The top figure shows the resistance and the bottom the reactance. Three measurements are conducted as described in Section 3.3.2 the data is processed as described in Section 4.2.

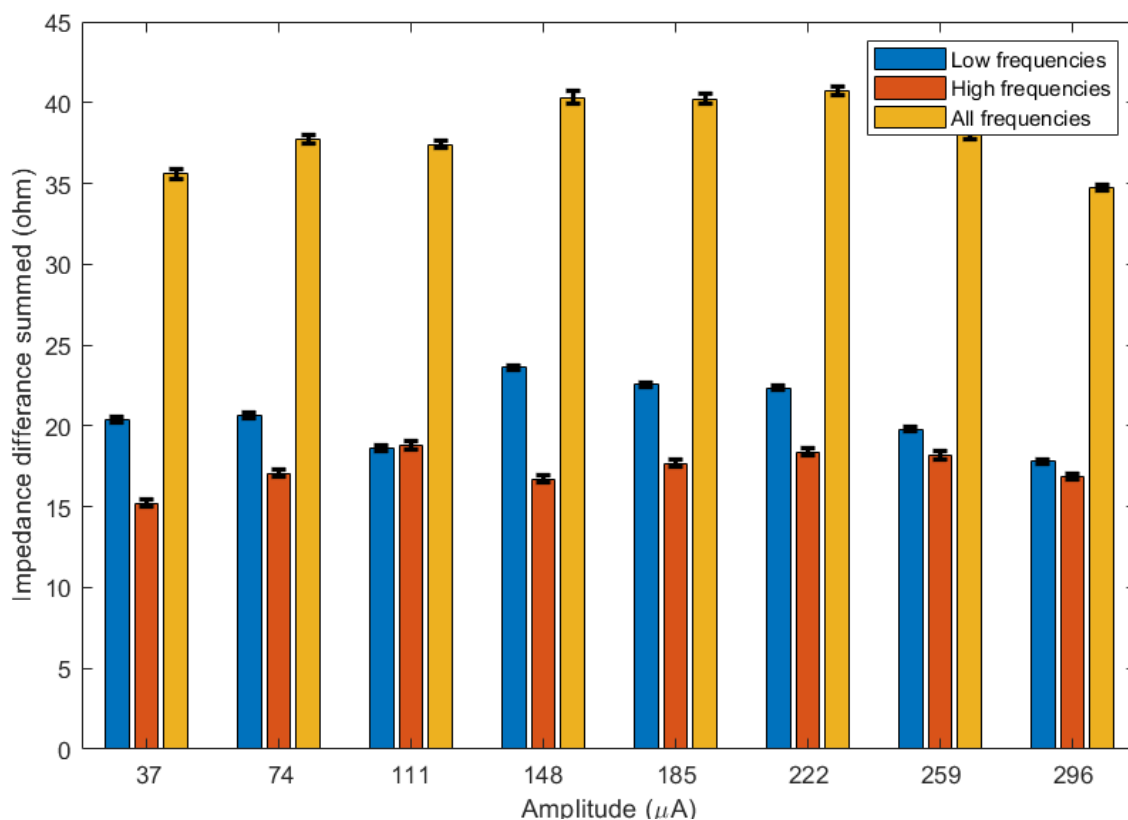


Figure 5.2: The summed difference in mean of the resistance of the contracted and relaxed bio-impedance, Equation 3.7. Movement pattern 1 is used, Figure 3.8, three measurements are done for the low and high frequencies as described in Section 3.3.2.

5.3 Frequency selection

The isometric movement pattern is performed 15 times while the isotonic movement pattern is performed 12 times. The measurements are done for both the high and low frequencies which gives in total $2 \times 15 + 2 \times 12 = 54$ measurements. The electrodes were removed and replaced between the isometric and isotonic movement measurements. All measurements including the switching moments as determined by the data grouping processing are given in Appendix B and Appendix C. The data grouping process of 4.2 groups the data in 4 different groups, isometric relaxing, isometric contraction, isotonic elbow 90° and isotonic elbow 180°. For both movement patterns the mean value and standard deviation of the resistance and reactance of both states are plotted against the frequency.

Figure 5.3 shows the mean and standard deviation of the isometric contraction and relaxation. The resistance is for all frequencies around 2Ω lower when the muscle is contracted compared to relaxed. The reactance can be separated into two parts. One where the relaxed reactance is higher than the contracted, just as with the real impedance is the case, and one where it is the other way around. The switching point seems to be at 50 kHz. At higher frequencies the standard deviations of both the contracted and relaxed state increase for the resistance and the reactance.

Figure 5.4 shows the mean and standard deviation of the isotonic contraction and relaxation states. Just as with the isometric movement pattern there is a difference in the resistance at all frequencies between the two states. For the isotonic movement this difference is about 4Ω . The reactance again has a switching point, however this lays around 25 kHz instead of 50 kHz. Again the standard deviation of the reactance increases for higher measurement frequencies.

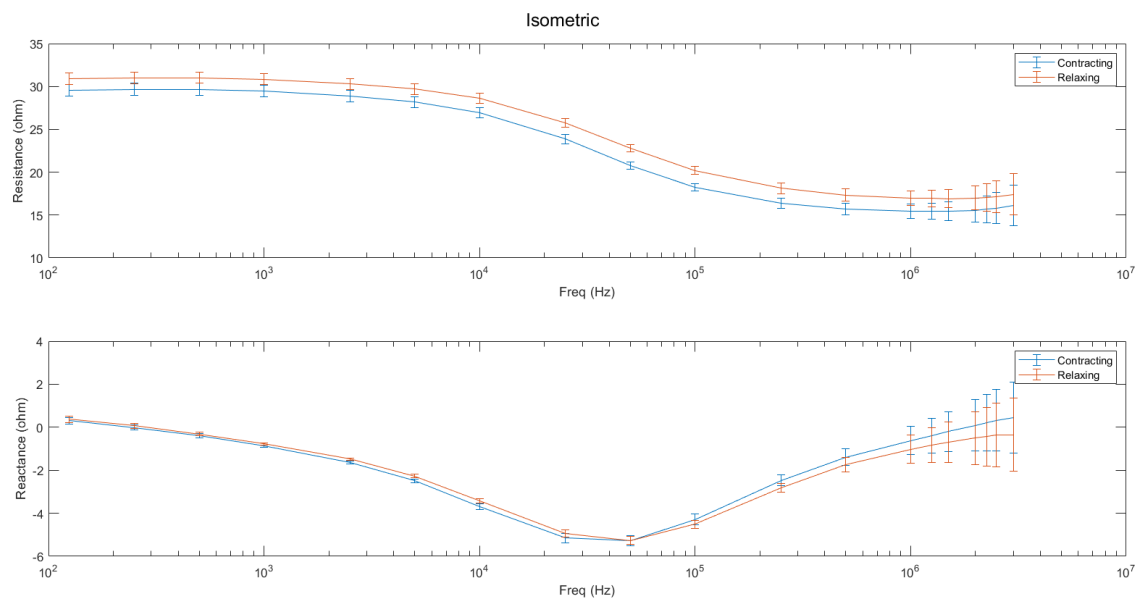


Figure 5.3: The mean and standard deviation of the bio-impedance at different frequencies, using movement pattern 1, shown in Section 3.3.1. Mean and standard deviation are calculated over all data gathered as described in section 3.3.3.

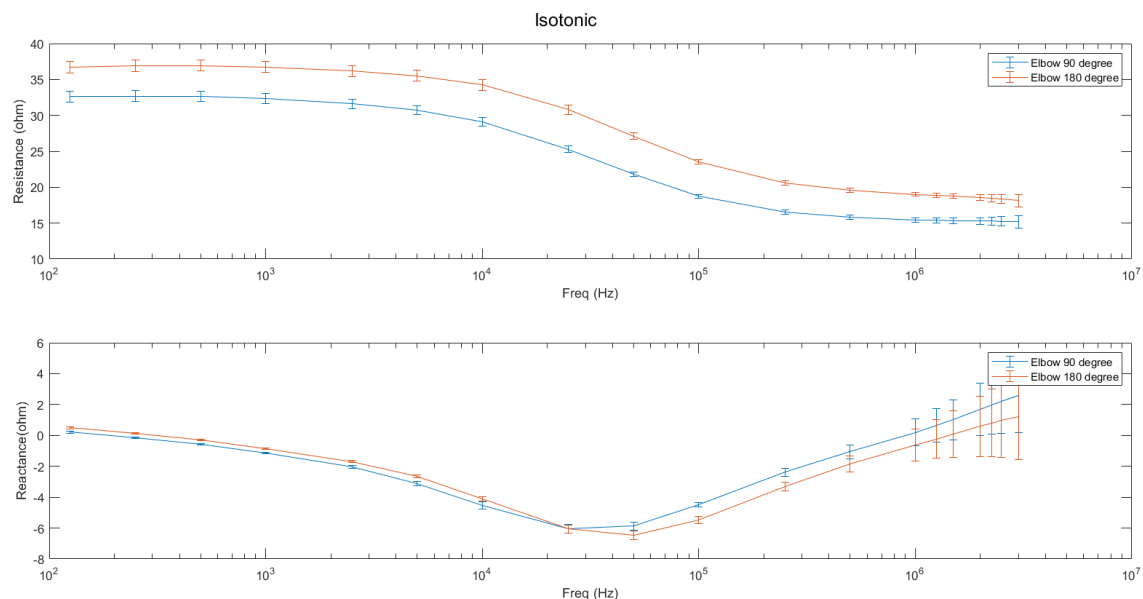


Figure 5.4: The mean and standard deviation of the bio-impedance at different frequencies, using movement pattern 2, shown in Section 3.3.1. Mean and standard deviation are calculated over all data gathered as described in section 3.3.3.

5.4 Cole Model

The Cole model as described in Section 2.1 consist of four unknown parameters. As described in Section 4.3 the parameters can be deduced using a fitting algorithm. The results of the different fitting algorithms are given in Section 5.4.1.

The mean of the bio-impedance for all measured frequencies per state, given in Section 5.3, are used to fit the Cole-Cole model. Each fit starts with an estimated value for each parameter, based on the research done by T. J. Freeborn these are chosen to be $R_\infty = 200 \Omega$, $Q = 3 \mu\text{F}$, $n = 0.65$ and $R_0 = 100 \Omega$ [54]. A typical figure of the measured frequency spectrum and a Cole model fitted to the measurement is given in Figure 5.5. Note that for low frequencies the fit almost exactly equals the measured data, especially for the resistance. However for 10 kHz and higher the error increases. The model does not include the increase in resistance after 1 MHz at all.

5.4.1 Fitting Cole's model

Each fitting algorithm is used for every measurement. The frequency spectrum of one measurement and the Cole model fitted to the measurement is given for all fitting algorithms and all states in Appendix D. The mean and standard deviation of all parameters for all fitting algorithms over all measurements are calculated. The resulting parameters are given in Figure 5.6. There is little difference in the impedance of R_∞ for all different fitting algorithms, the same holds for R_0 . Bigger differences arise when looking at Q and n . This indicates that the parameters of the CPE element vary more depending on the fitting algorithm. The error between the measured and the fitted spectrum for every frequency is calculated. The error is squared and per measurement the mean is calculated. The mean squared error of each measurement is summed. The result of this sum is shown in 5.7. The error of “fmincon” is the lowest of the three. This shows that using “fmincon” the most optimal Cole parameters can be found.

5.4.2 Cole parameters

The Cole parameters of all 15 isometric and all 12 isotonic measurements are calculated using the “fmincon” algorithm. The mean and standard deviation over all measurements are calcu-

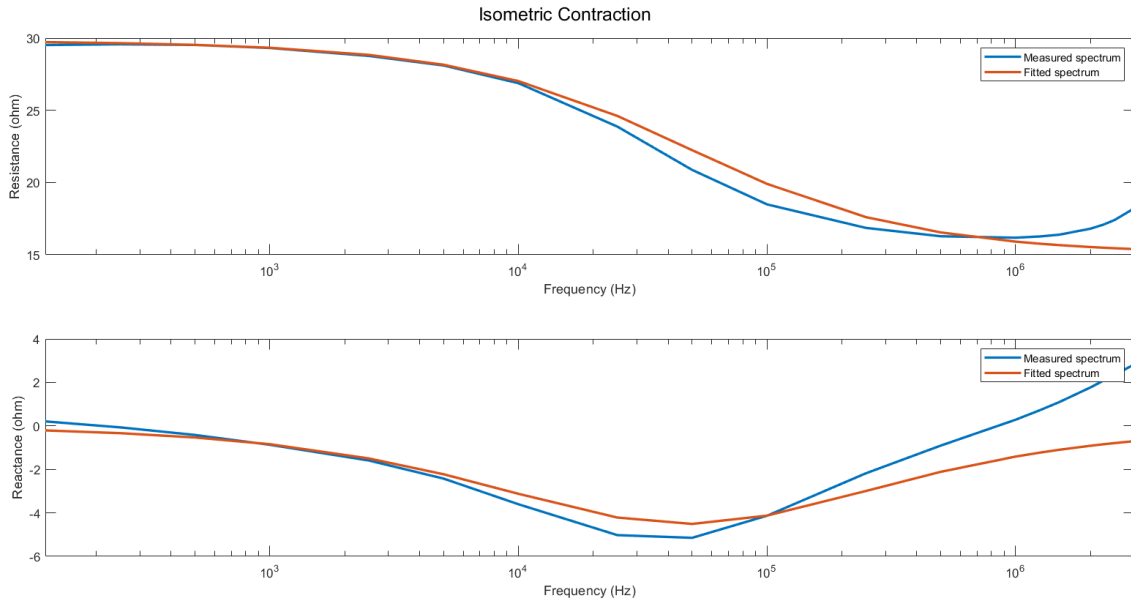


Figure 5.5: The resistance and reactance of the bio-impedance, the measured data and the Cole fit of the measured data is given. The measurement data is that of a contracted state of an isometric movement pattern, pattern 1 of Figure 3.8. The fitting algorithm used is “fmincon” [69].

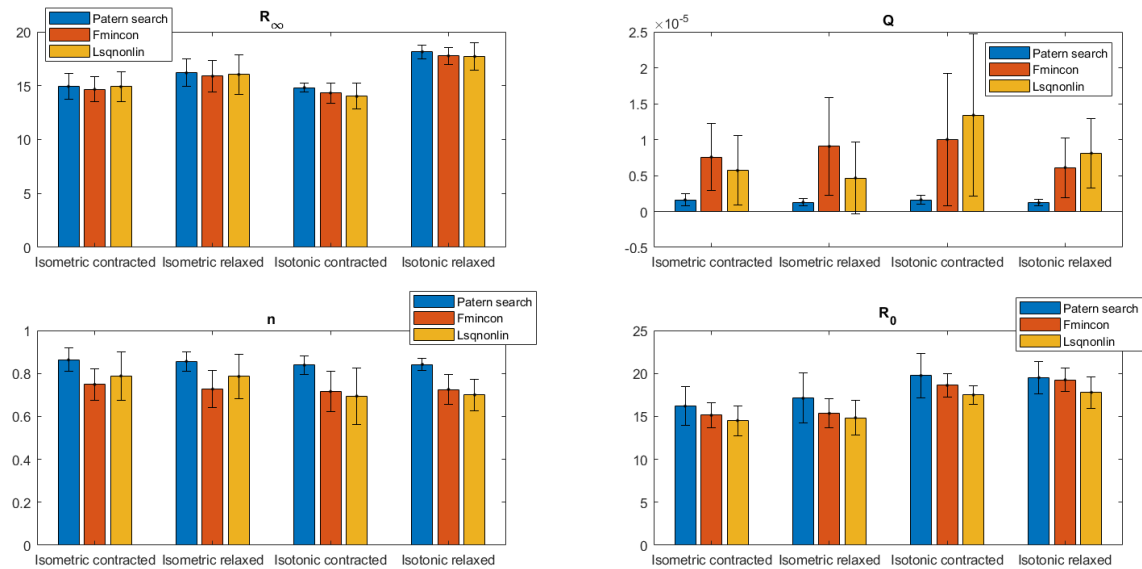


Figure 5.6: The mean and standard deviation of the parameters for each fitting algorithm. The mean and standard deviation are calculated over 15 isometric movement measurements and 12 isotonic movement measurements.

lated of all parameters and shown in Figure 5.8. The standard deviation of Q is high compared to the mean value and the difference in mean between the different states. Therefore it is difficult to distinguish the different states based on Q . The standard deviations of the n parameters are lower compared to the mean value. However in this case the mean values of the n parameter of the different states are almost equal to each other. The different states and arm position can be distinguished based on the both resistances. There is a clear difference in the mean values of R_0 between the isometric and isotonic movement patterns. In the standard deviations there is almost no overlap, therefore these different arm positions can be distinguished based

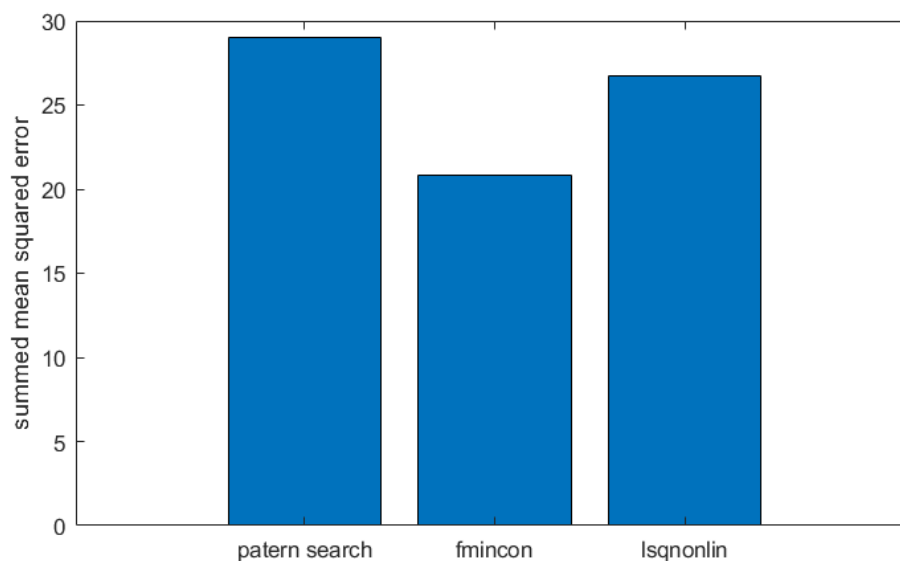


Figure 5.7: The sum of the mean squared error of all measurements for each fitting algorithm.

on R_0 . Distinguishing the contracted from the relaxed state can be done based on the value of R_∞ as can be seen in the top right graph of Figure 5.8. The contracted state has for both the isometric as the isotonic a lower value of R_∞ than the relaxed state. However for the isometric states the difference is lower and the standard deviation higher than for the isotonic states. This would make distinguishing a relaxed from a contracted muscle more difficult in an isometric situation.

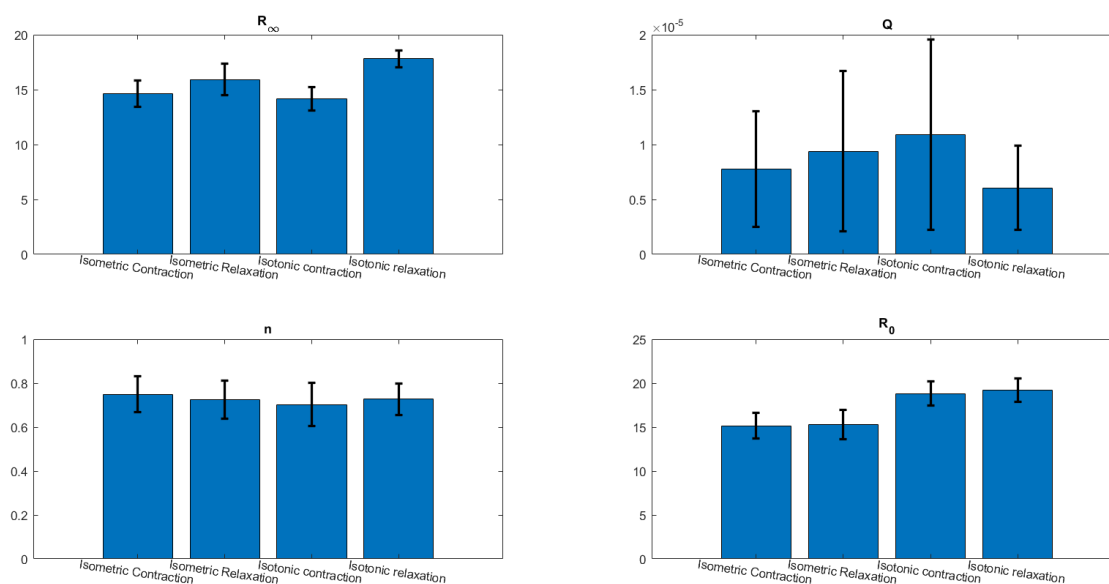


Figure 5.8: The mean and standard deviation of the Cole parameters for the `fmincon` fitting algorithm. The mean and standard deviation are calculated over 15 isometric movement measurements and 12 isotonic movement measurements.

5.5 Movement

The measurements of Section 3.4.1 are performed, which include movement pattern 3 and 4 given in Figure 3.10 and Figure 3.11. The data is structured according to the matlab neural

network implementation requirements as described in Section 4.5.2 and a Neural network is created. In Chapter 6 four measurement frequencies are chosen this means the Neural Network has 8 inputs, 4 of the resistance and 4 of the reactance. The neural network is shown in Figure 5.9 it has a time delay of 100 samples, one hidden layer of 40 nodes and one output layer of one node. The neural network is trained and tested for both movemen patterns.

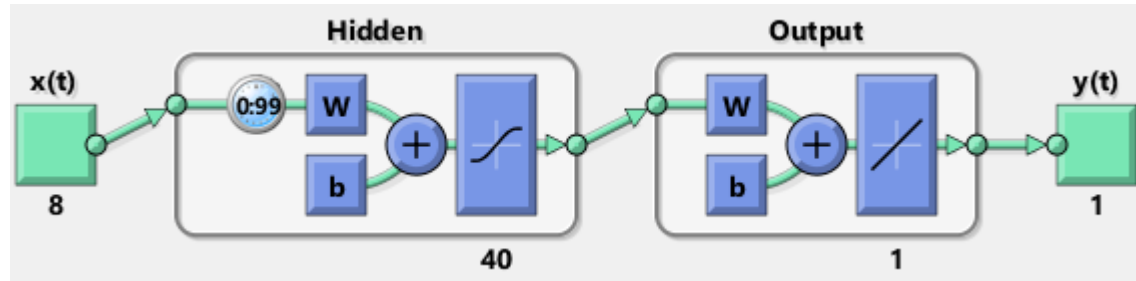


Figure 5.9: A visual representation of the used Neural network created in matlab. This network has $x = 8$ inputs, $y = 1$ output, $z = 100$ time delays, $n = 1$ hidden layer and $m = 40$ neurons in this hidden layer.

5.5.1 Muscle contraction in movement pattern 3

Movement pattern 3 depicted in Figure 3.10 is performed 54 times. The movement pattern has 6 different states and each is performed for ten seconds, the two transitions between the arm positions also take 10 s each, this means one measurements takes 80 s. The movement pattern is performed each time in the same manner, starting at “A” an ending with state “F”. It is important to note that the smaller electrodes where used and a frequency of 1 MHz instead of 75 kHz. One of the measurements is given in Figure 5.10, all measurements are given in Appendix E. A few things can be noticed about the resistance, the reactance and the output of the neural network. The resistance at 50 kHz, 100 kHz and 1 MHz decreases from “A” to “B” as well as from “C” to “D”, in both situations the muscle goes from a relaxed state to a contracted state. However from “E” to “F” the muscle also goes from a relaxed to a contracted state but nevertheless the resistance increases on all frequencies. Besides this increase is more significant than the two decreases.

The reactance at 1 MHz behaves at some moments opposite to the reactance at 50 kHz and 100 kHz. When the switch from “D” to “E” is made the reactance at 1 MHz strongly decreases while the other two strongly increase. The same happens when the muscle is contracted in state “F”.

The output of the neural network follows the target in some way . The same shape can be recognized at multiple points such as just after 20 s, from 40 s to 60 s and after 70 s. However there are also some clear differences. Multiple fluctuations are visible in the target of state “B” and “F” while the output of the NN doesn’t have these fluctuations. In these states the output looks more like a flat line compared to the target.

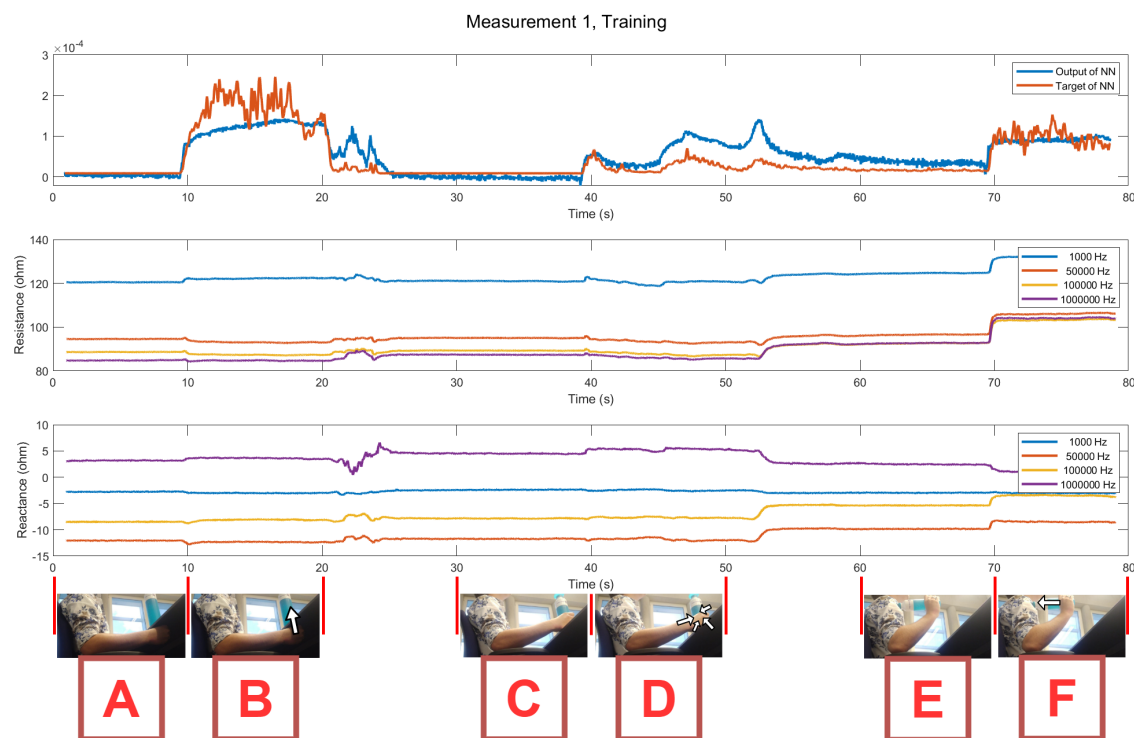


Figure 5.10: Top figure: the target and the output of the time delay Neural network. Middle figure: the 4 measured resistances, which are 4 of the 8 inputs for the NN. Bottom figure: the 4 measured reactances, which form the other 4 of 8 inputs for the NN. The measurement is done while movement pattern 3 (Figure 3.10) is performed from state “A” to “F”.

5.5.2 Muscle contraction in movement pattern 4

Movement pattern 4 depicted in Figure 3.11 is performed 20 times, 10 times from state “A” to “D” and ten times the other way around. Each state is performed for 10 seconds. The movement pattern has 4 states, relaxing on arm rest, pushing against table top, resting against shoulder and pushing bottle towards shoulder. One measurement takes therefore 40 seconds. The NN as given in Figure 5.9 is trained using the resistance and reactance signals.

All measurements are given in Appendix F. Figure 5.11 shows one measurement. The top figure of Figure 5.11 shows the target of the neural network and the output of the neural network. The target of the neural network is a down-sampled version of the EMG signal as described in Section 4.6. The figure in the middle is the resistance of the measured bio-impedance and the bottom figure is the reactance of the measured bio-impedance. Note that in this figure (Figure 5.11) the movement pattern is performed in reverse, meaning it is starting at state “D” and finishing with state “A”.

State “D” and “B” of Figure 5.11 both include a muscle contraction. When the muscle changes from contraction to relaxation from “D” to “C” the resistance decreases for all frequencies. However in the other case where the muscle goes from contraction to relaxation from “B” to “A” the resistance increases. The reactance shows different behaviour for all measurement frequencies. From “D” to “A” the amplitude of the reactance of the measurement at 1 kHz decreases every step, while at 50 kHz and 75 kHz the amplitude increases every step. At 10 kHz the reactance amplitude decreases when the muscle goes from contracted to a relaxed state and increases when it goes from the state “C” where the hand is near the shoulder to state “B” where the hand is near the table. This can be seen when comparing the reactance in Figure 5.11 of state “D” with “B” and “C” with “A” at 10 kHz. A similar observation can be made about the reactance at 50 kHz and 75 kHz, as mentioned increases the reactance amplitude

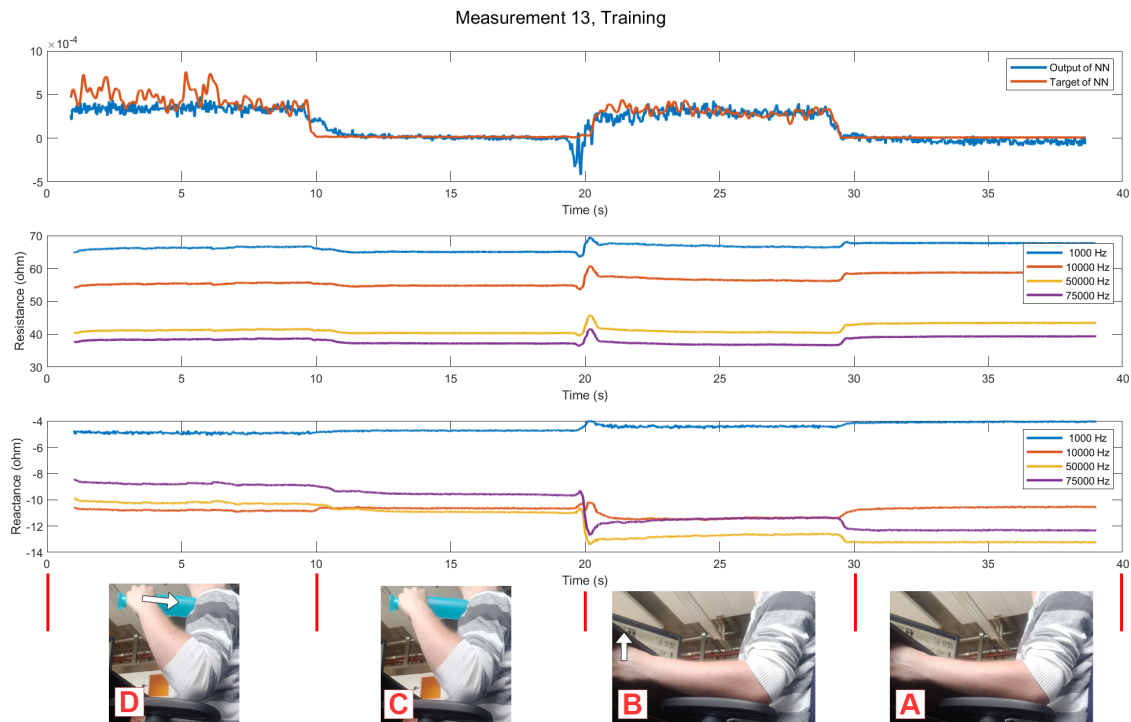


Figure 5.11: Top figure: the target and the output of the time delay Neural network. Middle figure: the 4 measured resistances, which are 4 of the 8 inputs for the NN. Bottom figure: the 4 measured reactances, which form the other 4 of 8 inputs for the NN. The measurement is done while movement pattern 4 (Figure 3.11) is performed from state “D” to “A”.

when the muscle is relaxed, logically it can be expected that it thus decreases again when the muscle contracts. However even though the muscle goes from a relaxed to a contracted state from “C” to “B” the reactance amplitude still increases, at 50 kHz and 75 kHz. The amplitude change is even bigger than the changes when the muscle is contracted. This means the reactance at 50 kHz and 75 kHz is greatly influenced by the arm position. The measured reactance increases and decreases differently at different measurement frequencies. This is the result of the frequency selection of Chapter 6 and is expected to be beneficial for the results of the neural network.

Figure 5.11 shows, besides the resistance and the reactance, also the neural network target and output. In general it can be seen that the output of the NN somewhat looks like the target. When the muscle is contracted in state “D” and “B” the output is relatively higher than when the muscle is relaxed, state “C” and “A”. This means the neural network is in some sense able to detect muscle contraction based on the measured bio-impedance signals. Even though the bio-impedances differ for both relaxed and both contracted states, the output of the NN is about the same in both states. During the first 6 seconds the NN doesn’t follow the target properly. Again is the output of the NN smoother than the EMG signal, especially when comparing the target and the output in the first 6 seconds. Besides it seems the output of the NN is strongly influenced by the movement which happens around 20 s.

5.5.3 Muscle contraction and arm movement

In the previous two sections, Section 5.5.1 and Section 5.5.2, it is shown that the bio-impedance does change when the muscle contracts as well when the arm is moved. This change in bio-impedance can be used to detect arm movement. The same measurements as in Section 5.5.2 are used. This means movement pattern 4, Figure 3.11, is used. There is only one movement in

this movement pattern. Since the measurements are done in both directions, the arm is moved ten times from the arm rest towards the shoulder and ten times from the shoulder to the arm rest. The position where the arm is on the arm rest is given the value “0” and the position where the hand is near the shoulder equals “1”. The transition between these states is made using a scaled sinusoidal function. The switching point is determined by the change in reactance at 75 kHz around 20 s. This because the reactance at 75 kHz shows the highest difference in value between both arm positions, as can be seen in Figure 5.11 and Appendix F. The EMG signal is filtered at 4 Hz and down-sampled to match the bio-impedance sampling frequency of 350 Hz. The EMG signal is scaled between 0 and 1 such that both the EMG and movement signal lay in the same range.

A neural network is created with 50 time delays, one hidden layer of 40 neurons, 8 inputs and 2 outputs. The eight inputs are the resistance and reactance at the four measurement frequencies. The two outputs are the EMG signal and the movement signal. The neural network is depicted in Figure 5.12. As can be expected from Section 5.5.2 is the neural network able to

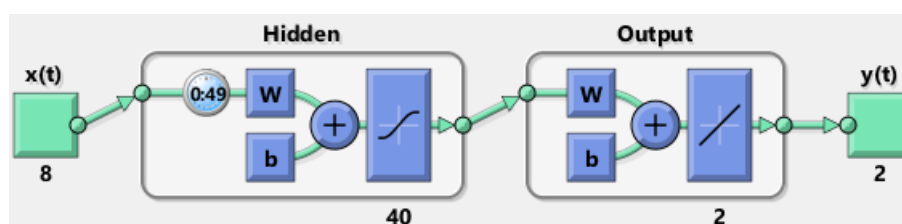


Figure 5.12: The neural network used for the EMG and movement signals. The NN has 50 delays, 40 neurons, 8 inputs and 2 outputs.

come close to the EMG target signal as can be seen in Figure 5.13. More in dept analysis of the NN with the EMG signal as target is given in Section 5.5.2. The output of the NN with the movement signal as target seems even better than with the EMG as target, as can be deduced from the top and bottom figure of Figure 5.13. The targets and outputs of the NN for all measurements are given in Appendix G. The NN is able to find a combination of inputs which seem to reflect the difference in the two arm positions rather well. Since the movement signal is artificially created no statements can be made about the real performance of a NN with as target e.g. the elbow angle or distance between hand and shoulder.

5.6 Force

The force measurement described in Section 3.4.2 is performed 20 times. The weighting scale is placed between the hand and the bottom of the table leaf. In ten of the measurements the arm starts in a relaxed state and each ten seconds the user tries to increase the weight indicated on the weighting scale by 1 kg. The measurement is ended after the subject has reached and held he weighting scale around 5 kg for 10 s. In the other ten measurements the pattern is performed in reverse, the subject starts pushing at 5 kg and each 10 s the desired weight is reduced by 1 kg. The last state where the subject doesn't push against the scale is again held for ten seconds before the measurement is ended.

The measured bio-impedance and the EMG signals are used as input for two neural networks with as target the weighting scale value. This is done to compare the results of the bio-impedance with those of the EMG. The sampling frequency of the weighting scale is around 5.8 Hz. The bio-impedance and EMG signals are both sampled at a much higher frequency, 350 Hz and 3 kHz respectively. Therefore both the bio-impedance and the EMG signals have to be down-sampled. Before down-sampling a fourth order Butter-worth anti-aliasing filter is applied at 2 kHz to both signals after which both signals are down sampled. The EMG processing would normally end with an envelope detection filter at 4 Hz however since the anti-aliasing

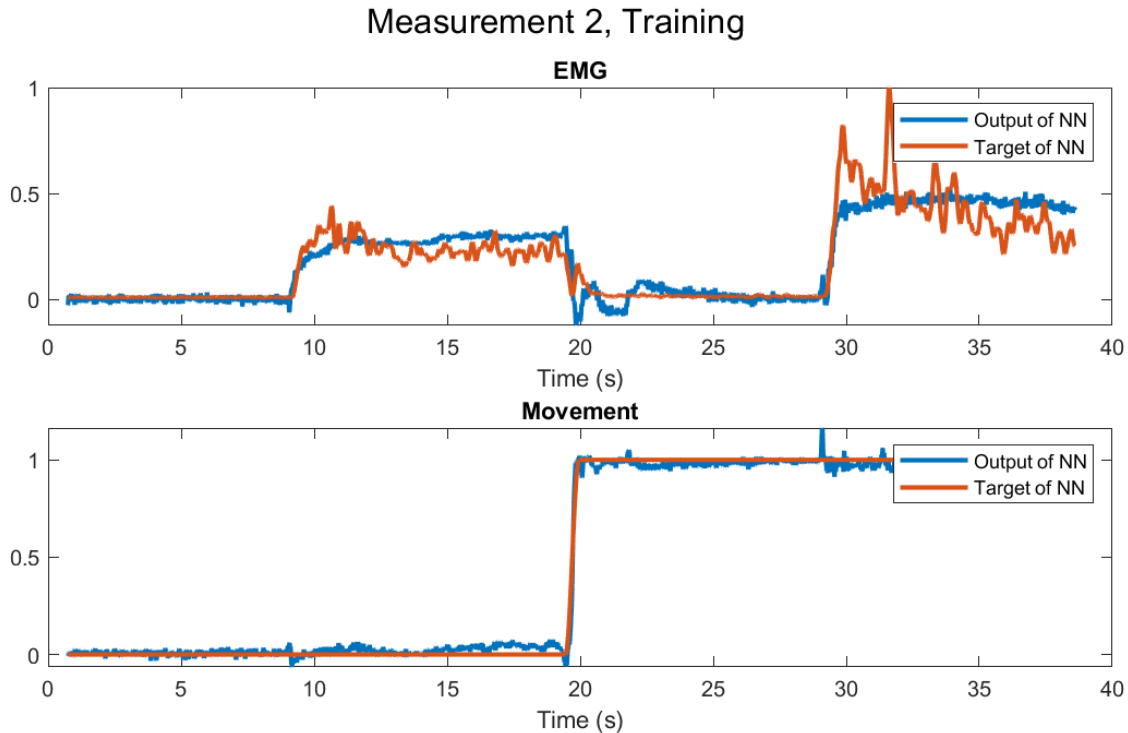


Figure 5.13: Top figure: the first target and output of the NN. The target is the measured EMG which is down sampled and normalized between 0 and 1. Bottom figure: the second target and output of the NN. The target represents the arm position which is either 0 or 1. The switching point is based on the switching point in the reactance at 75 kHz around 20 s.

filter comes right after it with an even lower cut-off the envelope detection filter becomes obsolete and is therefore removed. The reactance measured at 50 kHz showed a strong increase in power present around 13.3 Hz. Therefore another fourth order butter-worth stop-band filter was applied to the bio-impedance between 12 Hz and 14 Hz.

The data is structured as required described in Section 4.5.2 and two neural networks are created one for the EMG and one for the bio-impedance. The bio-impedance NN is given in Figure 5.14, the NN for the EMG is identical except for the input which is of size 1 instead of 8. The neural network used has no time delays and fewer neurons compared to the previously used neural networks. When the muscle exerts force the EMG signal as well as the change in bio-impedance have already happened. The actual exertion of force is the last step of the three. At every moment when the weighting scale takes a sample the muscle and EMG signals are likely to be in the same state as indicated by the weighting scale. This means that the neural network doesn't need any time delay and no signal has to be shifted as well. In these measurements the only performed contraction is isometric. This means there is only one arm position. The different arm positions resulted in different bio-impedance changes between relaxed and contracted muscle as described in Section 5.5. With only one arm position this problem disappears which would make the learning a lot easier for the neural network. This is the reason why the network has only 10 instead of 40 nodes.

The target, the bio-impedance NN output and EMG NN output of one of the measurements is given in Figure 5.15. The weighting scale signal is the most smooth of all three whilst the output of the EMG NN has the most fluctuations. The fact that the weighting scale is the smoothest seems logical since the subject tries to keep the weight indicated by the scale as stable as pos-

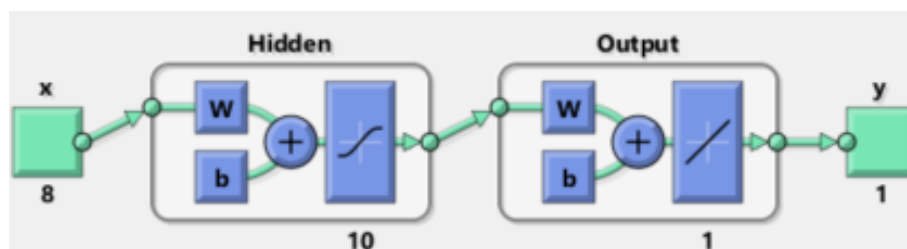


Figure 5.14: The used neural network for the bio-impedance input signals. The EMG NN is exactly the same except that it has only one input instead of 8. No time delay is used because all signals are in the same state at the time of measurement. Only ten neurons are used because there is no movement within the contraction.

sible. The fluctuations within the EMG signal do introduce a lot of error and another low-pass filter should be implemented to filter it out. However when done real time this again introduces an undesired delay.



Figure 5.15: The target, output of the bio-impedance NN and the output of the EMG NN of measurement number 14 of the force measurement as described in Section 3.4.2. The desired force is increased with 1 kg every 10 s.

The output of the neural networks and the target for all measurements are given in Appendix H. The calculated output of both networks for all inputs of both the EMG and the bio-impedance is plotted against the target in Figure 5.16. Multiple clusters can be indicated which are present around all desired weight values. This comes from the fact that the subject was asked to hold the weight at a certain level for 10 s. If the NN worked perfectly the clusters would transform in a straight line, since for a perfect NN the output always matches the target. Every deviation from this line is an error. It seems that the EMG NN has a bigger error for 0 kg than the bio-impedance NN. The output of the EMG lays around 1 kg while the target is 0 kg. The EMG has again a higher error for the targets around 4 kg most of the EMG NN outputs are around 3 kg instead of 4 kg. However, besides these observations, it is hard to conclude which method is better, based on

this graph. Therefore to get an indication of the expected error per measurement the mean of the absolute error of all measurements is calculated by:

$$E = \frac{1}{N} \sum_{n=1}^N |T_{NN}(n) - Y_{NN}(n)| \quad (5.1)$$

Here E is the calculated error, N the number of sample points, $T_{NN}(n)$ the target of the NN for sample n and $Y_{NN}(n)$ the output of the NN for sample n . This calculation is performed for both the EMG NN and the bio-impedance NN. The expected error for an EMG sample equals 475.05 g for this trained network. The expected error for the bio-impedance is equal to 385.70 g.

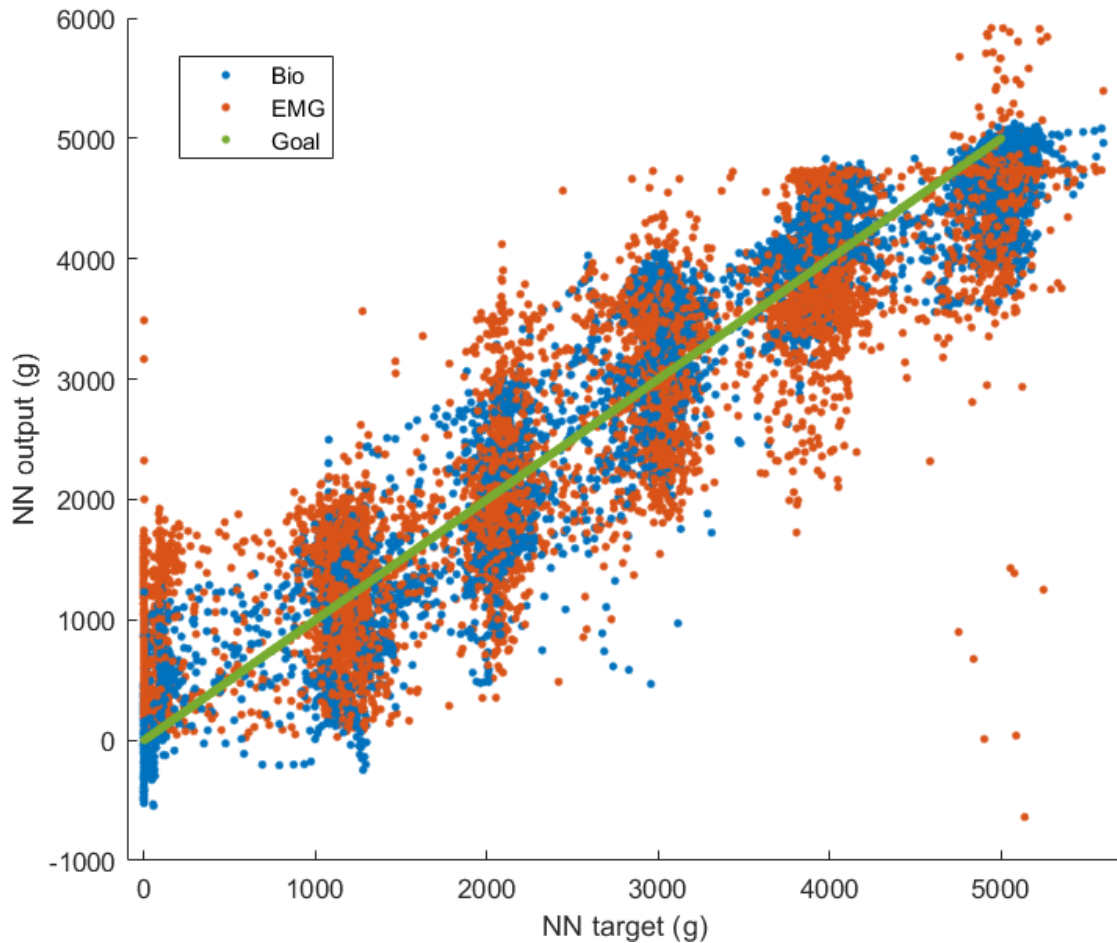


Figure 5.16: The output of the bio-impedance and the EMG NN plotted against the NN target. The goal is indicated by green, which represents the exact correct NN output for every NN target.

5.7 Time delay

Movement pattern 1 of Section 3.3.1 depicted by Figure 3.8 is performed 7 times. The subject is sitting in a chair with its hand beneath a table resting on an arm rest. When contracting the subject tries to push the table top up. When relaxing the arm is resting on the arm rest. Each second a switch is made between the relaxing and contracting state, the subject is assisted by a metronome set at 60 beats per minute as described in Section 3.4.3.

The EMG signal low pass filter is set at 5 Hz. All signals are normalized between 0 and 1. In Section 5.3 it is shown in Figure 5.3 that the resistance at all and reactance at some frequencies decreases when the muscle is contracted using movement pattern 1. However the EMG signal

always increases when the muscle contracts. Therefore all of the resistance and some of the reactance signals are inverted around the middle which is at 0.5 since all signals are normalized between 0 and 1. It is expected that no time delay is bigger than 0.5 s. Every cross correlation for which the maximum value has a time delay of 0.5 s or bigger is discarded. Next the signal is inverted and the cross-correlation is done again. This takes more computational time however it automates the process of selecting the signals which need to be inverted. To decrease the computational time the cross-correlation is performed for a range of -1.5 s to 1.5 s. The time delay corresponding to the maximum value of every cross-correlation is assumed to be the delay of that signal with respect to the EMG signal.

Seven measurements are performed with each 4 resistance and 4 reactance signals this gives in total $7 \cdot 8 = 56$ time delay calculations. One of the measurements is given in Figure 5.17, the signals are already inverted if needed. The same shape can be recognized in the EMG as in the bio-impedance signals which gives confidence that the cross-correlation indeed finds the delay between these two signals. This is also the case for all other measurements given in Appendix I. The mean and standard deviation of the calculated time delays are -0.2009 s and 0.0882 s respectively. On average the bio-impedance signal is 0.2009 s slower than the EMG signal. The mean of the time delay of the measurement system and signal processing is equal to 0.0569 s with a standard deviation of 9.818×10^{-4} s, determined over 20 measurements as explained in Appendix J. This leaves a time delay of about 0.144 s.

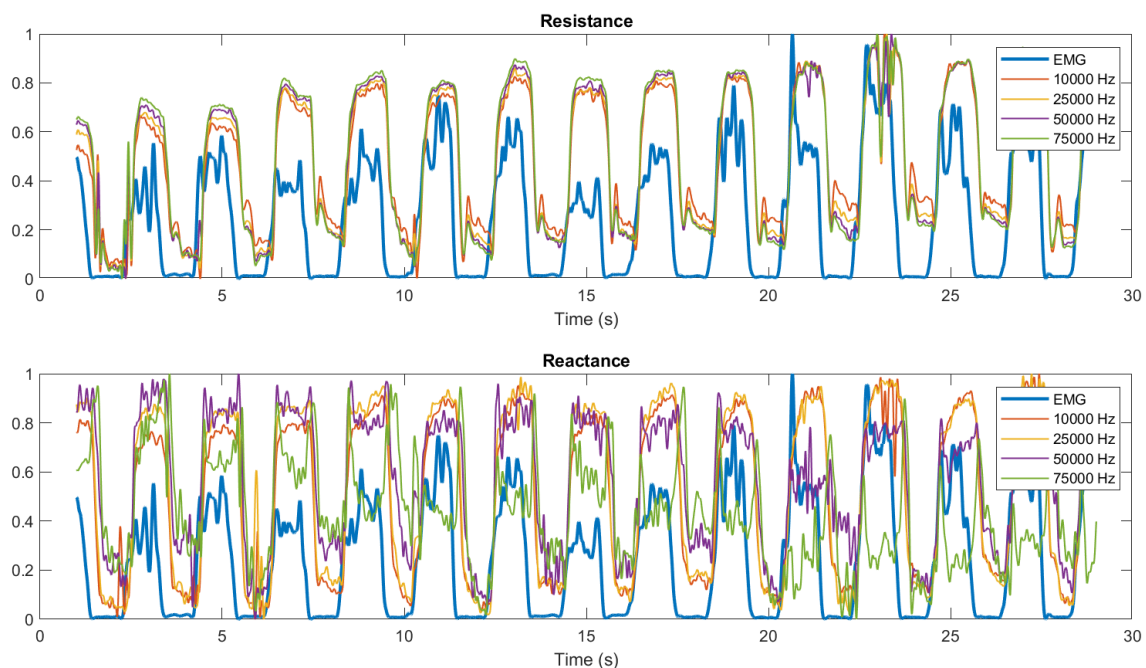


Figure 5.17: The measured bio-impedance and EMG signal while movement pattern 1 (Figure 3.8) is performed. Each second the subject switches between relaxing and contracting for 30 seconds assisted by a metronome beating at 60 beats per minute. All signals are normalized between 0 and 1. All of the resistance and some of the reactance signals are inverted around $y = 0.5$ such that the shape of these signals is the same as the EMG signal.

5.8 Conclusion

Multiple neural networks have been trained with each its own purpose. The first two used the 4 resistance and 4 reactance inputs to get to the EMG signal. It was shown that the NN was in some sense able to recreate the EMG signal from the bio-impedance signal. Next a NN was not only used to recreate the EMG signal but also an artificial movement signal.

The movement signal represented the arm position which was held in two different states during the measurements. The neural network was able to recreate the signal and distinguish in which position the arm was at the time of the measurements.

The last two NNs were trained using the EMG and bio-impedance as input and the weight of the weighing scale as output. Some relation was found between the EMG and the weight and the bio-impedance and the weight however the expected error is 475.05 g and 385.70 g.

The time delay of the bio-impedance changes with respect to the EMG signal was found to be 0.144 s .

6 Conclusion and Discussion

The goal of this project was to study the possibility of predicting muscle activity using mfEIT and hfEIT as an alternative to EMG for the control of a prosthetic arm. A choice had to be made for the right measurement parameters, regarding the measurements frequencies and current amplitude. Four main research questions arose within the goal of the project. Below the choice for the measurement parameters is elaborated. All research questions are repeated after which the corresponding results and conclusions are given.

The first movement pattern is used for the amplitude selection, as described in Section 3.3.2. The difference in the resistance of a contracted muscle and relaxed muscle is summed over all frequencies as described in Section 5.2. The resistance difference is the lowest for a current amplitude of $37\ \mu\text{A}$ and $296\ \mu\text{A}$, which are the largest and the smallest used current amplitudes. The total resistance difference is the highest for an AC amplitude of $222\ \mu\text{A}$. There is a low standard deviation for all amplitudes. Therefore has the standard deviation no influence on the amplitude choice. It could be argued that there is an amplitude which is not used in these measurement for which the difference in resistance is even higher. However it is expected that this sum of resistance is about equal to the sum of resistance measured using an amplitude of $222\ \mu\text{A}$. This expectation is based on the small differences between the three highest measured sum of resistances. These are $40.32\ \Omega$ for an amplitude of $148\ \mu\text{A}$, $40.24\ \Omega$ for an amplitude of $185\ \mu\text{A}$ and $40.71\ \Omega$ for an amplitude of $222\ \mu\text{A}$. Therefore it is likely that any amplitude in between of these measured amplitudes will have an sum of resistance which is almost equal to the total resistance of $222\ \mu\Omega$ and will therefore not significantly benefit the measurements. Therefore for all measurements the amplitude will be set to $222\ \mu\text{A}$.

The isometric and isotonic movement pattern, movement pattern 1 and 2, are used for the frequency selection as described in Section 3.3.3. The choice for which frequencies will be used is based on the criteria mentioned in Section 3.3.3 and are repeated below.

- The standard deviation over multiple measurements is low.
- The difference in impedance between the two states of Figure 3.8, contracted and relaxed muscle, is high.
- The difference in impedance between the two states of Figure 3.9, elbow 90° and 180° , is high.
- A distinction can be made between the (difference in impedance) of the isometric and the isotonic movement pattern.

As given in Section 5.3 the standard deviation starts to increase after $100\ \text{kHz}$. Therefore to meet the first criterion the used frequencies should not be higher than $100\ \text{kHz}$. For the second and third criterion it is easy to find a solution. The resistance is in both cases a good measure to distinguish the two states. The last criterion can be met using the difference in the switching points of the reactance. The reactance of the relaxed state and the elbow in 90° state where lower than the contracted state and the elbow in 180° state for the low frequencies. However for the higher frequencies this was the other way around. The switching points where around $25\ \text{kHz}$ and $50\ \text{kHz}$ respectively. Using one measurement frequency between the two switching points is not an option since the standard deviations for both the isometric and isotonic movement are too high to make a clear distinction between the different states. A more robust solution is using multiple measurement frequencies, a few at a lower and a few at a

higher frequency than both switching points. The mean of the contracted and the relaxed state differ more from each other outside this switching region, especially for the isotonic movement. Therefore four measurement frequencies are chosen. Two in the low region 10 kHz and 25 kHz, both have low standard deviation compared to the impedance difference and are at frequencies below the switching region. For the other two in the higher region 75 kHz and 100 kHz are used, both also still have a low standard deviation and are on the high side of the switching region. With the impedance measurements of those four frequencies it is possible to distinguish contraction from relaxation and isometric movement from isotonic movement.

- To what extent is it possible to predict muscle activation in various arm positions using mf-EIT and/or hf-EIT?

In order to predict muscle activation it is required that there is a measurable difference between the reactance and/or resistance of a muscle in a relaxed state and a muscle in a contracted state. Detecting muscle activation can be done if this difference is significant and repeatable. Besides should it be distinguishable from other factors which influence the bio-impedance such as movement. A resistance difference of 2Ω over all measurement frequencies was shown in Section 5.2. However this difference was for one arm position only, the arm resting on the arm rest and contracting against the down side of the table top. The resistance and reactance changes between a relaxed and a contracted muscle are different in various arm positions as shown in Section 5.5.1.

A neural network (NN) was trained to handle this increase in complexity. The neural networks input consisted of multiple measurements with in each measurements at least two muscle contractions and relaxations in different arm positions. The target of the neural network was the simultaneously recorded EMG signal. Section 5.5.1 and Section 5.5.2 showed one measurement including the NN training result of this approach. It was shown that the NN is able to recreate the EMG in some sense however many fluctuations present in the EMG where missing in the NN output. The NN is able to predict the EMG signal with a mean R^2 of 0.75 for the third movement pattern and a mean R^2 of 0.57 for the fourth movement pattern. Therefore can it be concluded that based on the bio-impedance signal the NN is able to predict the muscle activation in different arm positions with an currently maximum mean R^2 of 0.75. It must it be noted that for the fourth movement pattern only 20 measurements where available while for the third movement pattern 54 measurements where performed. Since a NN in general performs better when more training data is available it can be expected that the NN for the fourth movement pattern can be improved when more measurements are performed.

- How precise and accurate can different levels of muscle contraction be distinguished?

For the second research question different levels of contraction were created using a weighting scale. The bio-impedance was measured while the isometric contraction was performed pushing onto the scale. The weight indicates the amount of force delivered by the hand which is mostly a result of the contraction of the bicep. Again a NN was used with as target the weight as indicated by the weighting scale. The mean of the error between the target and the output of the NN is 385.7 g when the bio-impedance is used as input and 475.1 g when the EMG is used as input. This is also called the accuracy. The standard deviation of the error for the bio-impedance and EMG signals are 282.3 g and 397.7 g respectively, also called the precision. Besides is it shown that the bio-impedance resulted in a smoother output signal compared to the EMG output. The mean and standard deviation of the error are smaller when the bio-impedance is used as input to the NN. However the mean error is still almost 40 % of the used resolution of 1 kg. Besides is the standard deviation almost 30 % of the used resolution. In order to use the bio-impedance as measure for the level of contraction the accuracy and the preci-

sion should both increase especially when a higher resolution than 1 kg is required. A solution for this can be by increasing the sampling frequency of the weighting scale and measuring the time delay between the bio-impedance change and the extruded force. In Section 5.6 it is assumed that the bio-impedance is in the same state as the extruded force. However when the extruded force lags the bio-impedance signal part of the error can be explained by this time delay.

- What is the time delay between muscle activation and bio-impedance changes?

The delay between the EMG signal and the bio-impedance was found based on the cross correlation of these signals. The delay was calculated to be 0.20 s with a standard deviation of 0.0882 s. The delay between the EMG signal and the bio-impedance introduced by the system and the signal processing was found using two resistors and a capacitor. This delay turned out to have a mean of 0.0569 s and a standard deviation of 9.818×10^{-4} s. The remaining delay is expected to be the delay between the EMG signal and the change in bio-impedance due to the same contraction and equals 0.14 s with a standard deviation of 0.0882 s. The time delay has a standard deviation of 63 % of the mean value. This is mainly caused by the reactance measured at 75 kHz. Removing these measurements gives a time delay mean and standard deviation of 0.1322 and 0.0173 between the bio-impedance and EMG signal. In order to conclude if this is only the case for the currently performed measurements or that the reactance at higher frequencies always has a more variable time delay more research has to be done.

- To what extent is it possible to distinguish muscle contraction and arm movement?

The last research question is based on the observation that the bio-impedance changes when the arm is moved to a new position as shown in Section 5.5.1. The actual movement is not captured by a separate measurement. Therefore it is implemented based on the knowledge that there are only two arm positions in movement pattern 4, and the fact that there is a rapid change in reactance around 20 s which is the switching moment between the two arm positions. The NN is given two targets, both the EMG and the created movement signal. The NN is able to distinguish the arm movement from the contraction and the other way around. It seems that the contraction has little to no influence on the movement signal and the other way around. It must be noted that the movement signal is 0, 1 or is switching from one to another. When measuring the real arm position small deviations from the current state can be expected due to the imperfect nature of the measurement and the ability to hold the arm steady in one position. To what extent the neural network is able to recognize these small changes in the arm position remains a question for further research.

Bibliography

- [1] W. Williams, "Bionic hand price list." <https://bionicsforeveryone.com/bionic-hand-price-list/>.
- [2] N. Ahamed, K. Sundaraj, M. Alqahtani, O. Altwijri, M. A. Ali, and M. A. Islam, "Emg-force relationship during static contraction: Effects on sensor placement locations on biceps brachii muscle," *Technology and health care : official journal of the European Society for Engineering and Medicine*, vol. 22, pp. 505–513, 07 2014.
- [3] A. Hof, "The relationship between electromyogram and muscle force," *Sportverletzung Sportschaden : Organ der Gesellschaft für Orthopädisch-Traumatologische Sportmedizin*, vol. 11, pp. 79–86, 10 1997.
- [4] M. Sartori, M. Reggiani, D. Farina, and D. G. Lloyd, "Emg-driven forward-dynamic estimation of muscle force and joint moment about multiple degrees of freedom in the human lower extremity," *PLOS ONE*, vol. 7, pp. 1–11, 12 2012.
- [5] A. Ubeda, A. D. Vecchio, M. Sartori, S. T. Puente, F. Torres, J. M. Azorin, and D. Farina, "Electromechanical delay in the tibialis anterior muscle during time-varying ankle dorsiflexion," in *2017 International Conference on Rehabilitation Robotics (ICORR)*, IEEE, July 2017.
- [6] Ş. U. Yavuz, A. Şendemir-Ürkmez, and K. S. Türker, "Effect of gender, age, fatigue and contraction level on electromechanical delay," *Clinical Neurophysiology*, vol. 121, pp. 1700–1706, Oct. 2010.
- [7] L. Shaw and S. Bhaga, "Online emg signal analysis for diagnosis of neuromuscular diseases by using pca and pnn.," *International Journal Of Engineering Science and Technology* 0975-5462, vol. 4, pp. 4453–4459, 10 2012.
- [8] B. Freriks and H. J. Hermens, *SENIAM: European recommendations for surface electromyography: results of the SENIAM project*. Roessingh Research and Development, 2000.
- [9] Infinity Mesh Teams, "The cocktail party problem." <https://www.infinitymesh.com/blog/the-cocktail-party-problem/>.
- [10] R. E. P. Sica, A. J. McComas, A. R. M. Upton, and D. Longmire, "Motor unit estimations in small muscles of the hand," *Journal of Neurology, Neurosurgery & Psychiatry*, vol. 37, no. 1, pp. 55–67, 1974.
- [11] M. Grossi and B. Riccò, "Electrical impedance spectroscopy (eis) for biological analysis and food characterization: a review," *Journal of Sensors and Sensor Systems*, vol. 6, no. 2, pp. 303–325, 2017.
- [12] M. Dubuisson, "Impedance changes in muscle during contraction, and their possible relation to chemical processes," *The Journal of Physiology*, vol. 89, no. 2, pp. 132–152, 1937.
- [13] C. A. Shiffman, R. Aaron, and S. B. Rutkove, "Electrical impedance of muscle during isometric contraction," *Physiological Measurement*, vol. 24, pp. 213–234, feb 2003.
- [14] T. Orth, "Impedance changes in biceps brachii due to isometric contractions and muscle fatigue using electrical impedance myography (eim)," 2013).

- [15] L. T. L. Fiuza, "Feasibility of eit measurements of functional muscular activity as control signals for prosthetics," Master's thesis, University College London, k.aristovich@ucl.ac.uk, 8 2018. Department of Medical Physics and Biomedical Engineering.
- [16] A. Liston, R. Bayford, and D. Holder, "A cable theory based biophysical model of resistance change in crab peripheral nerve and human cerebral cortex during neuronal depolarisation: implications for electrical impedance tomography of fast neural activity in the brain," *Medical and Biological Engineering and Computing*, vol. 50, pp. 425–37, 05 2012. Copyright - International Federation for Medical and Biological Engineering 2012.
- [17] K. Patton and G. Thibodeau, *Structure & Function of the Body*. 15 ed., 2015. page. 163.
- [18] K. S. Cole, "PERMEABILITY AND IMPERMEABILITY OF CELL MEMBRANES FOR IONS," *Cold Spring Harbor Symposia on Quantitative Biology*, vol. 8, pp. 110–122, Jan. 1940.
- [19] K. S. Cole and R. H. Cole, "Dispersion and absorption in dielectrics i. alternating current characteristics," *The Journal of Chemical Physics*, vol. 9, pp. 341–351, Apr. 1941.
- [20] M. E. Orazem, I. Frateur, B. Tribollet, V. Vivier, S. Marcelin, N. Pébère, A. L. Bunge, E. A. White, D. P. Riemer, and M. Musiani, "Dielectric properties of materials showing constant-phase-element (CPE) impedance response," *Journal of The Electrochemical Society*, vol. 160, no. 6, pp. C215–C225, 2013.
- [21] D. Ayllon, F. Seoane, and R. Gil-Pita, "Cole equation and parameter estimation from electrical bioimpedance spectroscopy measurements - a comparative study," vol. 2009, pp. 3779–82, 07 2009.
- [22] B. Fu and T. J. Freeborn, "Cole-impedance parameters representing biceps tissue bioimpedance in healthy adults and their alterations following eccentric exercise," *Journal of Advanced Research*, vol. 25, pp. 285–293, 2020. Recent Advances in the Fractional-Order Circuits and Systems: Theory, Design and Applications.
- [23] E. Teschner, M. Imhoff, and S. Leonhardt, *Electrical Impedance Tomography: The realisation of regional ventilation Monitoring, 2nd edition*. 01 2015.
- [24] C. Xu, X. Dong, F. Fu, W. Shuai, X. Liu, and C. Zhang, *A Novel Image Monitoring Software System of Electrical Impedance Tomography for Internal Hemorrhage*, vol. 14, pp. 3882–3885. 01 2007.
- [25] Y. Zhang and C. Harrison, "Tomo: Wearable, low-cost electrical impedance tomography for hand gesture recognition," pp. 167–173, 11 2015.
- [26] O. L. Silva, "Muscle contraction detection using electrical impedance tomography," Master's thesis, Escola Politécnica da Universidade de São Paulo, 12 2012.
- [27] T.-J. LIAO and H. NISHIKAWA, "The variation of action potential and impedance in human skeletal muscle during voluntary contraction," *The Tohoku Journal of Experimental Medicine*, vol. 173, no. 3, pp. 303–309, 1994.
- [28] R. Kusche and M. Ryschka, "Combining bioimpedance and emg measurements for reliable muscle contraction detection," *IEEE Sensors Journal*, vol. 19, no. 23, pp. 11687–11696, 2019.
- [29] A. Coutinho, B. Jotta, A. Pino, and M. Souza, "Behaviour of the electrical impedance myography in isometric contraction of biceps brachii at different elbow joint angles," *Journal of Physics Conference Series*, vol. 407, pp. 2017–, 12 2012.

- [30] T. Zagar and D. Krizaj, "Multivariate analysis of electrical impedance spectra for relaxed and contracted skeletal muscle," *Physiological Measurement*, vol. 29, pp. S365–S372, jun 2008.
- [31] A. Hof, "The relationship between electromyogram and muscle force," *Sportverletzung Sportschaden : Organ der Gesellschaft für Orthopädisch-Traumatologische Sportmedizin*, vol. 11, pp. 79–86, 10 1997.
- [32] G. C. Ray and S. K. Guha, "Relationship between the surface e.m.g. and muscular force," *Medical and Biological Engineering and Computing*, vol. 21, pp. 579–586, Sep 1983.
- [33] S. Grimnes and Ørjan G Martinsen, "Chapter 6 - geometrical analysis," in *Bioimpedance and Bioelectricity Basics (Third Edition)* (S. Grimnes and Ørjan G Martinsen, eds.), pp. 141–178, Oxford: Academic Press, third edition ed., 2015.
- [34] C. A. Shiffman, H. Kashuri, and R. Aaron, "Electrical impedance myography at frequencies up to 2 MHz," *Physiological Measurement*, vol. 29, pp. S345–S363, June 2008.
- [35] N. Goren, J. Avery, T. Dowrick, E. Mackle, A. Witkowska-Wrobel, D. Werring, and D. Holder, "Multi-frequency electrical impedance tomography and neuroimaging data in stroke patients," *Scientific Data*, vol. 5, July 2018.
- [36] A. Romsauerova, A. Ewan, L. Horesh, T. Oh, E. J. Woo, and D. Holder, *A comparison of Multi-Frequency EIT systems intended for acute stroke imaging*, vol. 14, pp. 3918–3920. 01 2007.
- [37] S. X. Zhang, *Electrical Impedance Based Spectroscopy and Tomography Techniques for Obesity and Heart Diseases*. PhD thesis, 2017.
- [38] M. C. Staff, "Arteriosclerosis / atherosclerosis." <https://www.mayoclinic.org/diseases-conditions/arteriosclerosis-atherosclerosis/symptoms-causes/syc-20350569>.
- [39] T. A. Hope and S. E. Iles *Breast Cancer Research*, vol. 6, no. 2, p. 69, 2003.
- [40] M. Schouten and C. Baars, "Tiepielcr design document." "Unpublished".
- [41] NVIDIA Developer, "Nvidia cuda." <https://developer.nvidia.com/cuda-downloads>.
- [42] CADENCE PCB SOLUTIONS, "What are the maximum power output and data transfer rates for the usb standards?." <https://resources.pcb.cadence.com/blog/2020-what-are-the-maximum-power-output-and-data-transfer-rates-for-the-usb-standards>.
- [43] TiePie engineering, "Tiepie handyscope hs5 usb oscilloscope specifications." <https://www.tiepie.com/nl/usb-oscilloscope/handyscope-hs5#specifications>.
- [44] Covidien, "Kendall™ ecg electrodes product data sheet h124sg." <https://cdn.sparkfun.com/datasheets/Sensors/Biometric/H124SG.pdf>.
- [45] S. Lee and J. Kruse, "Biopotential electrode sensors in ecg/eeg/emg systems."
- [46] TMSI, "Unipolar micro electrode (microcoax)." <https://tmsi.wiljekoffie.dev/product/unipolar-micro-electrode-microcoax>.

- [47] TMSI, “Electrode gel sonogel.” <https://tmsi.wiljekoffie.dev/product/electrode-gel-sonogel-100gr>.
- [48] M. H. Jung, K. Namkoong, Y. Lee, Y. Koh, K. Eom, H. Jang, W. Jung, J. Bae, and J. Park, “Wrist-wearable bioelectrical impedance analyzer with miniature electrodes for daily obesity management,” *Scientific Reports*, vol. 11, 01 2021.
- [49] S. Day, “Important factors in surface emg measurement,” 2002.
- [50] J. Liu, X. Qiao, M. Wang, W. Zhang, G. Li, and L. Lin, “The differential howland current source with high signal to noise ratio for bioimpedance measurement system,” *Review of Scientific Instruments*, vol. 85, p. 055111, May 2014.
- [51] H. Yazdanian, M. Mosayebi Samani, and A. Mahnam, “Characteristics of the howland current source for bioelectric impedance measurements systems,” pp. 189–193, 12 2013.
- [52] TiePie engineering, “Tiepie handyscope hs5 usb oscilloscope drivers.” <https://www.tiepie.com/nl/usb-oscilloscope/handyscope-hs5#downloads>.
- [53] Eric W. Weisstein, “Convolution theorem.” <https://mathworld.wolfram.com/ConvolutionTheorem.html>, May 2021.
- [54] T. J. Freeborn and S. Critcher, “Cole-impedance model representations of right-side segmental arm, leg, and full-body bioimpedances of healthy adults: Comparison of fractional-order,” *Fractal and Fractional*, vol. 5, no. 1, 2021.
- [55] Ohaus Corporation, “Scout® pro portable electronic balances.” <https://us.ohaus.com/en-US/Products/Balances-Scales/Portable-Balances/Scout-Pro/Electronic-Balance-SP6001-AM>.
- [56] Google. Inc, “Google metronome.” https://www.google.com/search?q=Metronoom&oq=metronoom&aqs=chrome.0.69i59j0i512l9.1743j0j7&sourceid=chrome&ie=UTF-8&stick=H4sIAAAAAAAAAA0OwfcQoxS3w8sc9YSnBSWtOXmPk5uL0TS0pys_Lz03lAQAKTh3AHwAAAA.
- [57] The MathWorks Inc, “Matlab r2020a.” https://nl.mathworks.com/products/new_products/release2020a.html.
- [58] The MathWorks Inc, “Matlab function findchangepts.” <https://nl.mathworks.com/help/signal/ref/findchangepts.html>.
- [59] The MathWorks Inc., “Matlab function lsqnonlin.” <https://nl.mathworks.com/help/optim/ug/lsqnonlin.html#buuhch7-fun>.
- [60] Northwestern University, “Optimization toolbox lsqnonlin.” <http://www.ece.northwestern.edu/local-apps/matlabhelp/toolbox/optim/lsqnonlin.html>.
- [61] Northwestern University, “Optimization toolbox fmincon.” <http://www.ece.northwestern.edu/local-apps/matlabhelp/toolbox/optim/fmincon.html>.
- [62] The MathWorks Inc., “Matlab function patternsearch.” <https://nl.mathworks.com/help/gads/how-pattern-search-polling-works.html>.
- [63] The MathWorks Inc, “Matlab function patternsearch polling.” <https://nl.mathworks.com/help/gads/how-pattern-search-polling-works.html>.

-
- [64] R. Khusainov, D. Azzi, I. Achumba, and S. Bersch, “Real-time human ambulation, activity, and physiological monitoring: Taxonomy of issues, techniques, applications, challenges and limitations,” *Sensors*, vol. 13, pp. 12852–12902, Sept. 2013.
- [65] The MathWorks Inc, “Activation functions : Why “tanh” outperforms “logistic sigmoid”?.” <https://nl.mathworks.com/help/deeplearning/ref/tansig.html>.
- [66] Chamanth MVS, “Matlab function tansig.” <https://medium.com/analytics-vidhya/activation-functions-why-tanh-outperforms-logistic-sigmoid-3f26469ac0d11>.
- [67] The MathWorks Inc, “Matlab function feedforwardnet.” <https://nl.mathworks.com/help/deeplearning/ref/feedforwardnet.html>.
- [68] The MathWorks Inc., “Divide data for optimal neural network training.” <https://nl.mathworks.com/help/deeplearning/ug/divide-data-for-optimal-neural-network-training.html>.
- [69] The MathWorks Inc., “Matlab function fmincon.” https://nl.mathworks.com/help/optim/ug/fmincon.html#busog7r_sep_shared-A.

A Amplitude selection data

The mean and standard deviation of all measurements per amplitude are given in the following figures.

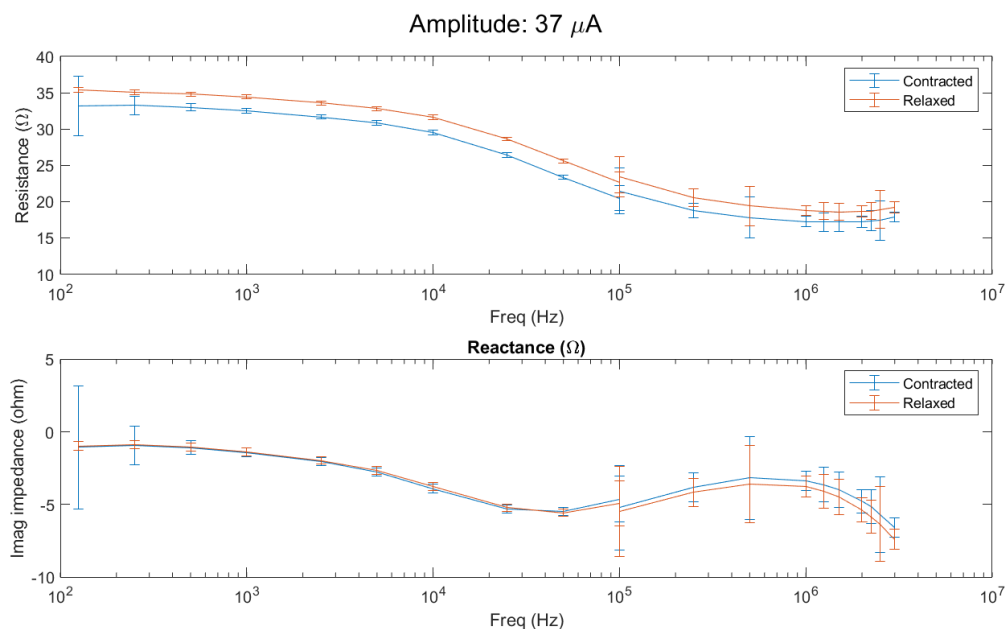


Figure A.1: The mean and standard deviation of the bio-impedance of the relaxed and contracted state per frequency. The top figure shows the resistance and the bottom the reactance. Three measurements are conducted as described in Section 3.3.2 the data is processed as described in Section 4.2.

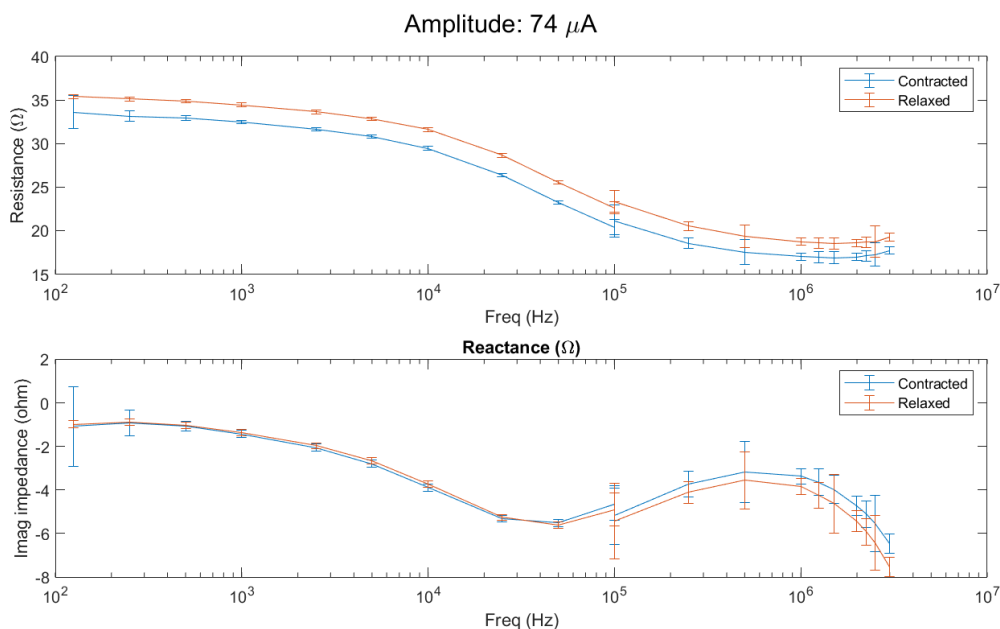


Figure A.2: The mean and standard deviation of the bio-impedance of the relaxed and contracted state per frequency. The top figure shows the resistance and the bottom the reactance. Three measurements are conducted as described in Section 3.3.2 the data is processed as described in Section 4.2.

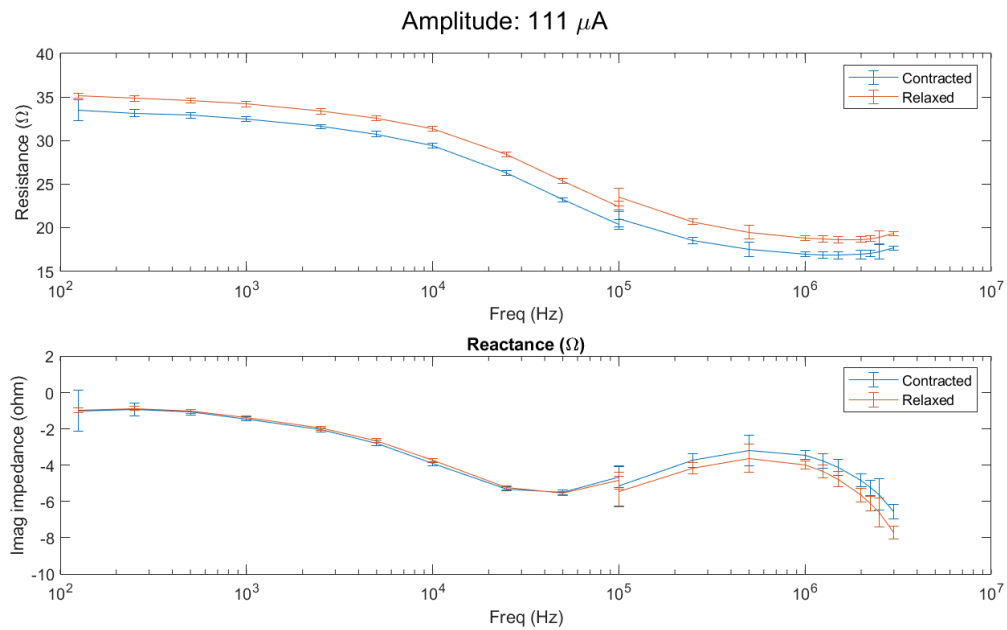


Figure A.3: The mean and standard deviation of the bio-impedance of the relaxed and contracted state per frequency. The top figure shows the resistance and the bottom the reactance. Three measurements are conducted as described in Section 3.3.2 the data is processed as described in Section 4.2.

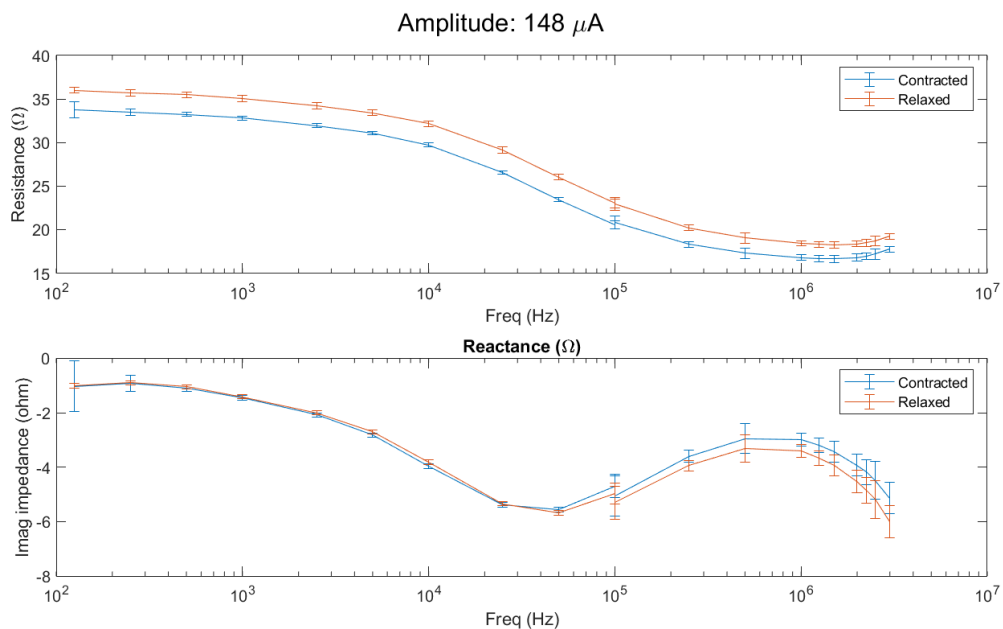


Figure A.4: The mean and standard deviation of the bio-impedance of the relaxed and contracted state per frequency. The top figure shows the resistance and the bottom the reactance. Three measurements are conducted as described in Section 3.3.2 the data is processed as described in Section 4.2.

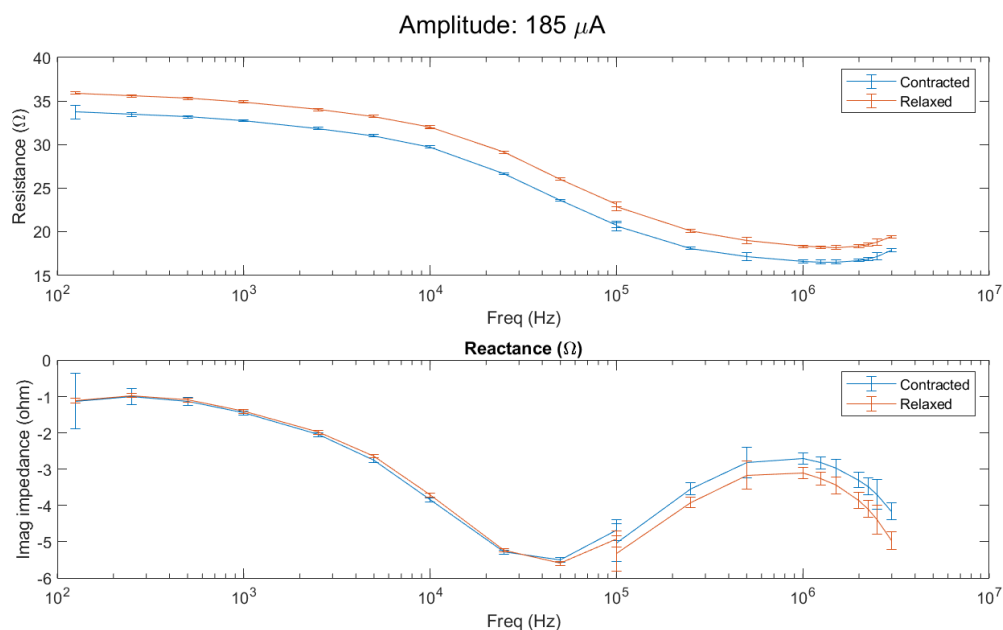


Figure A.5: The mean and standard deviation of the bio-impedance of the relaxed and contracted state per frequency. The top figure shows the resistance and the bottom the reactance. Three measurements are conducted as described in Section 3.3.2 the data is processed as described in Section 4.2.

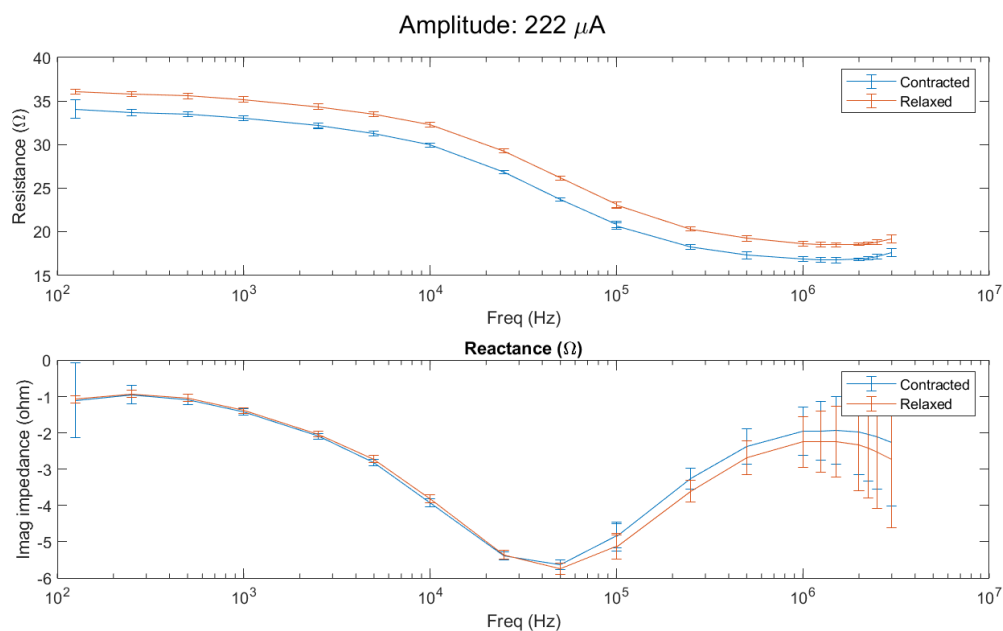


Figure A.6: The mean and standard deviation of the bio-impedance of the relaxed and contracted state per frequency. The top figure shows the resistance and the bottom the reactance. Three measurements are conducted as described in Section 3.3.2 the data is processed as described in Section 4.2.

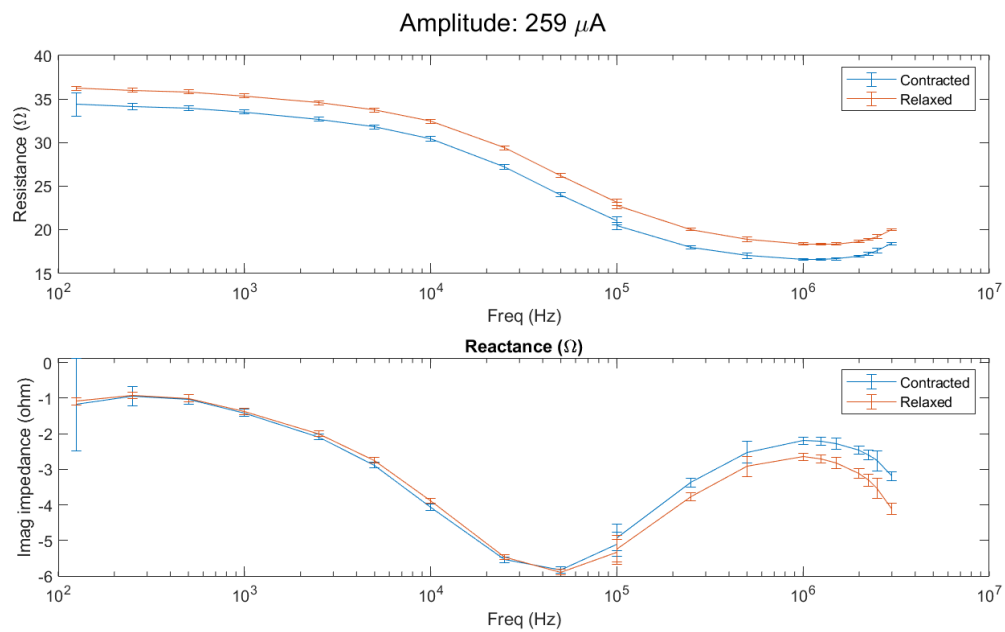


Figure A.7: The mean and standard deviation of the bio-impedance of the relaxed and contracted state per frequency. The top figure shows the resistance and the bottom the reactance. Three measurements are conducted as described in Section 3.3.2 the data is processed as described in Section 4.2.

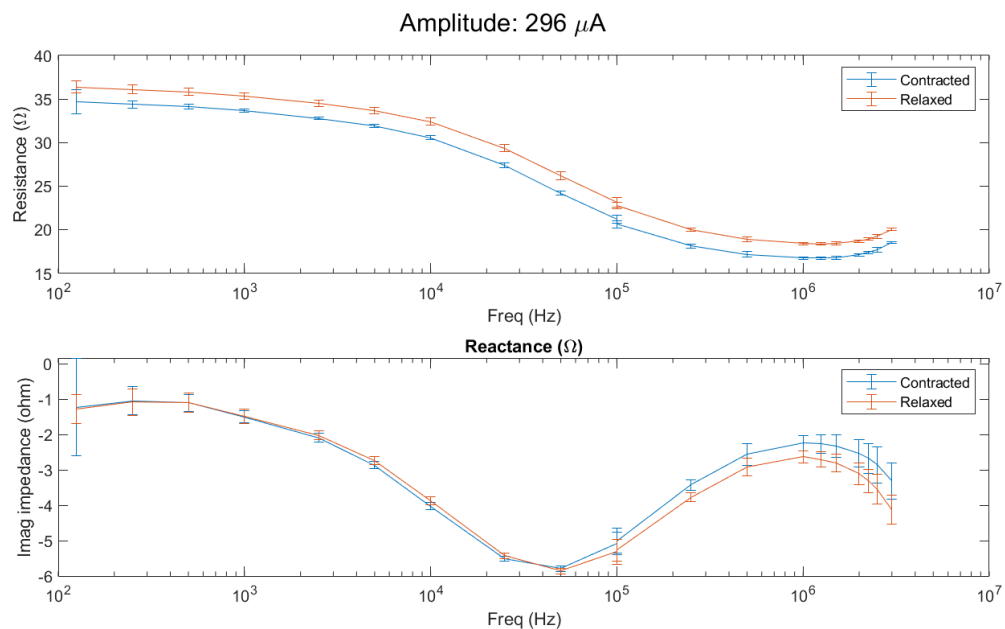


Figure A.8: The mean and standard deviation of the bio-impedance of the relaxed and contracted state per frequency. The top figure shows the resistance and the bottom the reactance. Three measurements are conducted as described in Section 3.3.2 the data is processed as described in Section 4.2.

B Isometric data

This chapter shows all figures of the data collected using movement pattern 1 of Section 3.3.1, Figure 3.8. The low and high frequencies are shown.

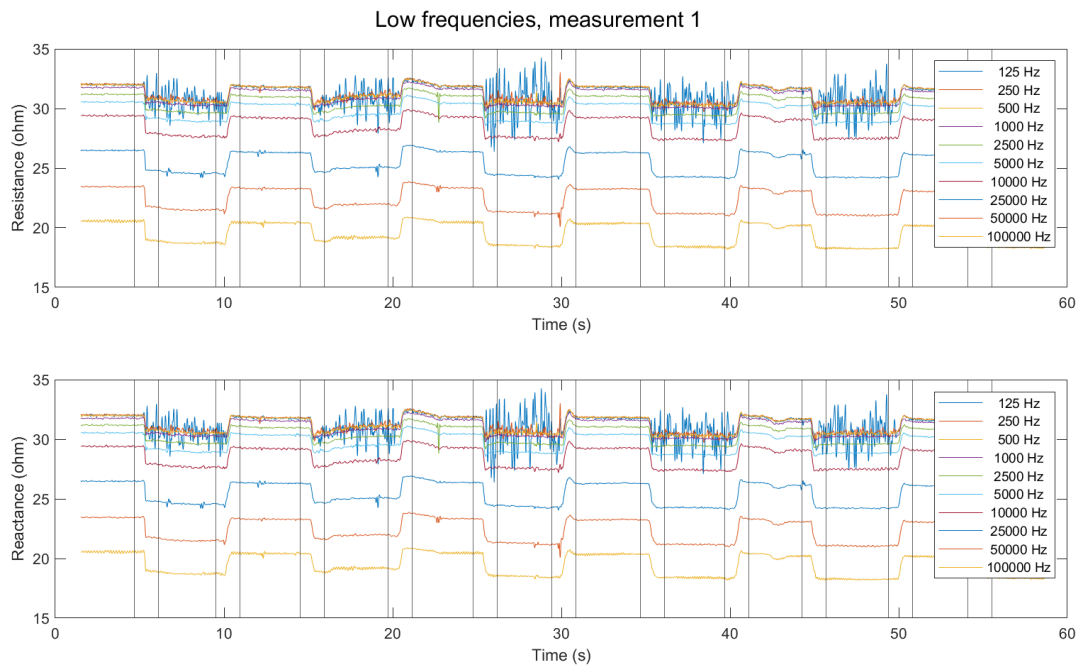


Figure B.1: Measurement number 1 of the resistance and the reactance measured during an isometric movement at low frequencies. The first pattern as described in Section 3.3.1 is used.

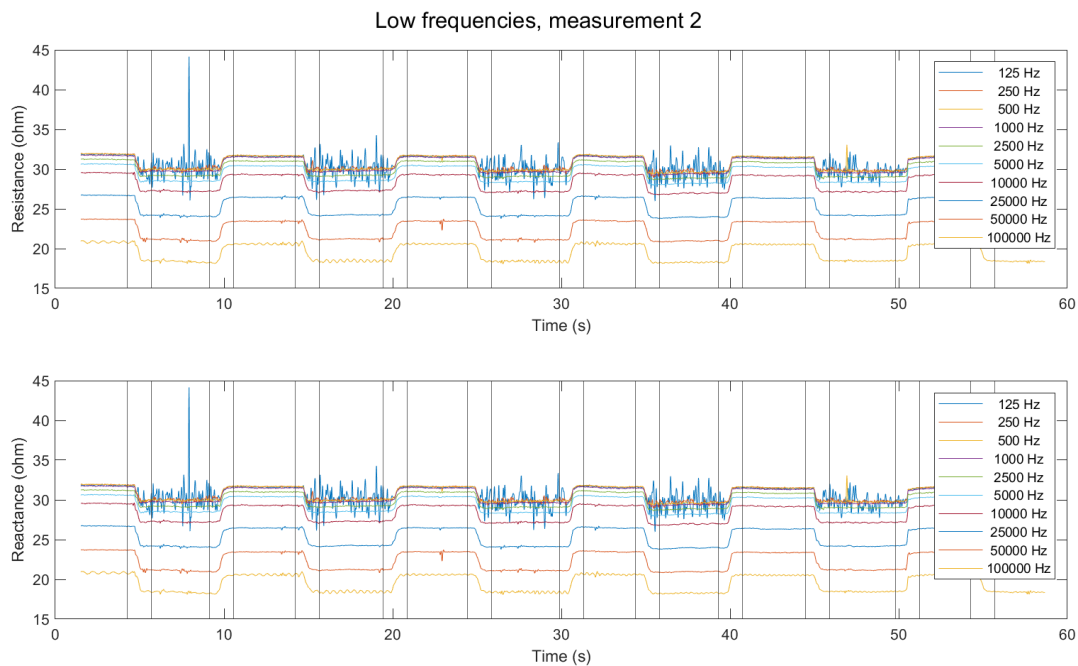


Figure B.2: Measurement number 2 of the resistance and the reactance measured during an isometric movement at low frequencies. The first pattern as described in Section 3.3.1 is used.

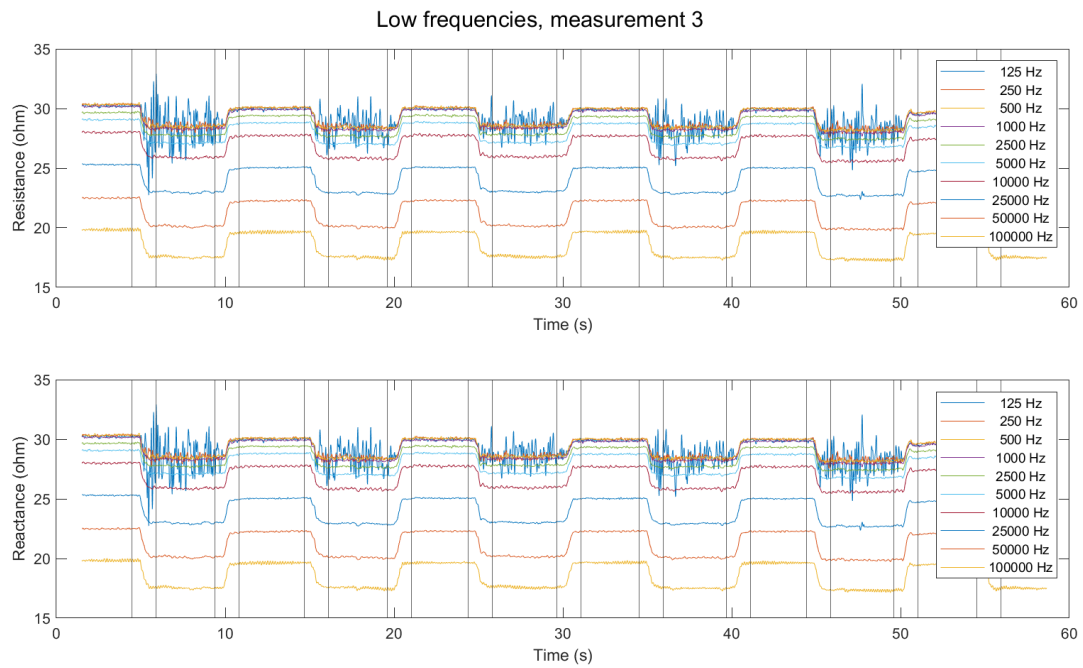


Figure B.3: Measurement number 3 of the resistance and the reactance measured during an isometric movement at low frequencies. The first pattern as described in Section 3.3.1 is used.

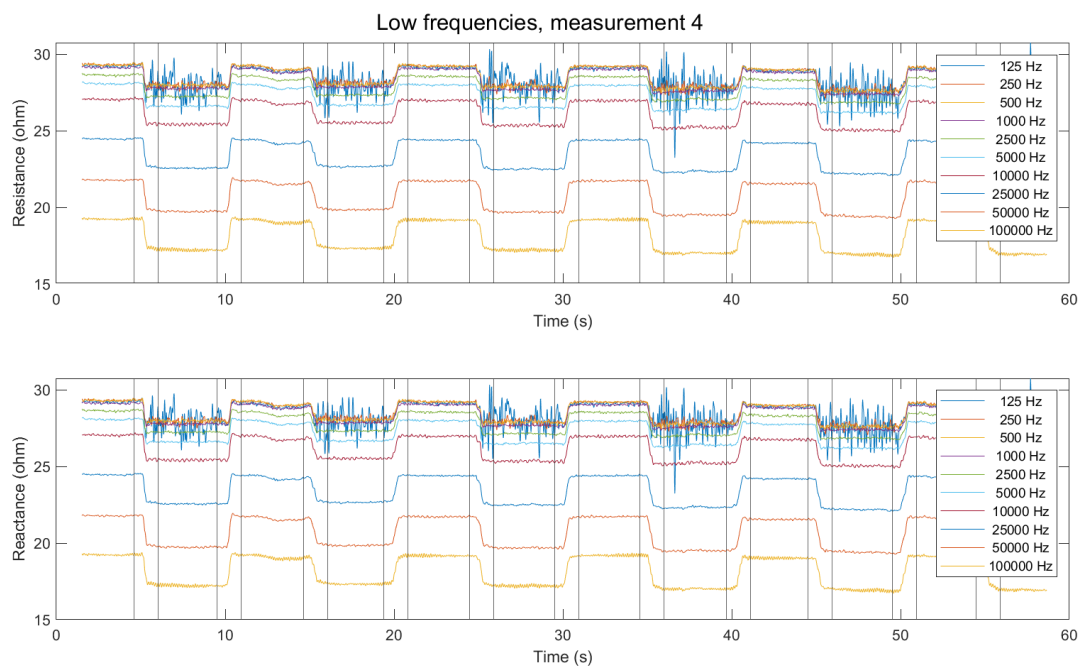


Figure B.4: Measurement number 4 of the resistance and the reactance measured during an isometric movement at low frequencies. The first pattern as described in Section 3.3.1 is used.

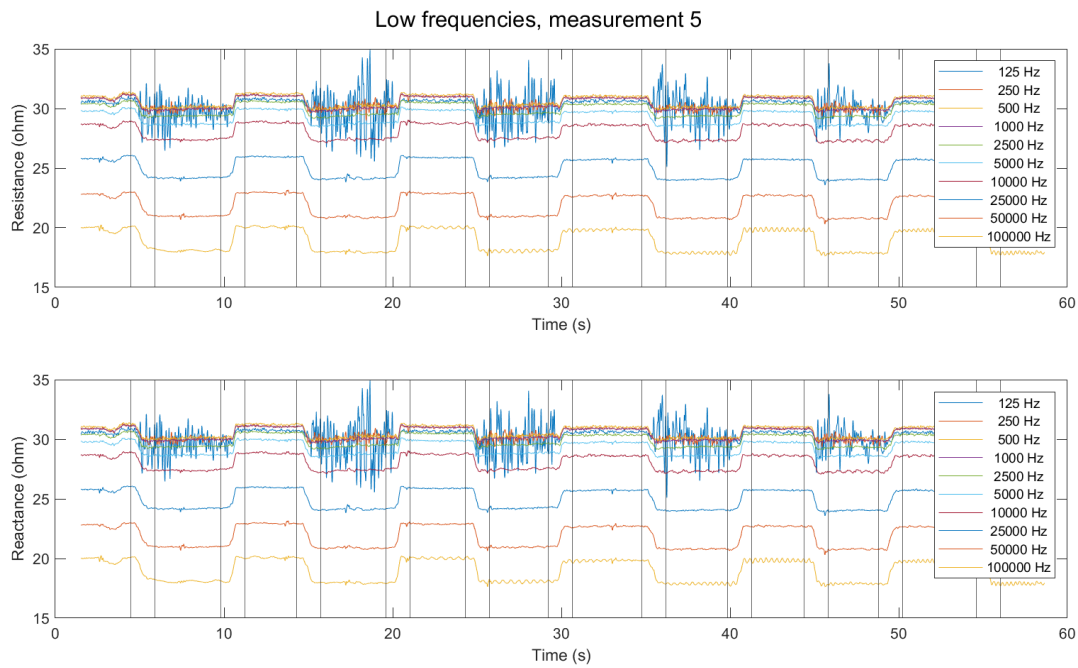


Figure B.5: Measurement number 5 of the resistance and the reactance measured during an isometric movement at low frequencies. The first pattern as described in Section 3.3.1 is used.

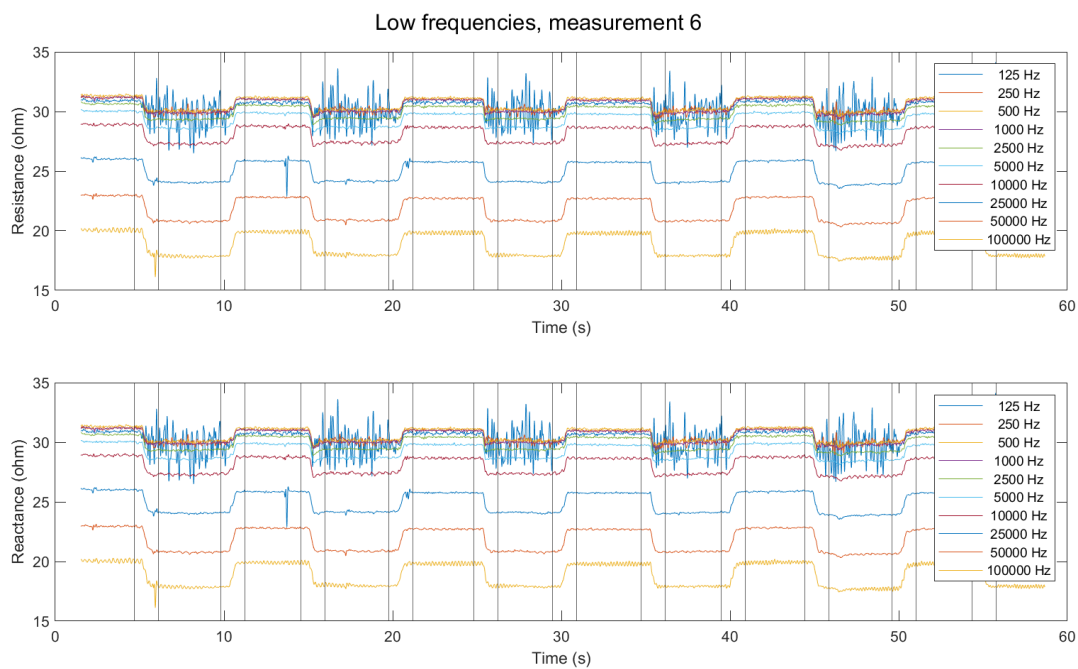


Figure B.6: Measurement number 6 of the resistance and the reactance measured during an isometric movement at low frequencies. The first pattern as described in Section 3.3.1 is used.

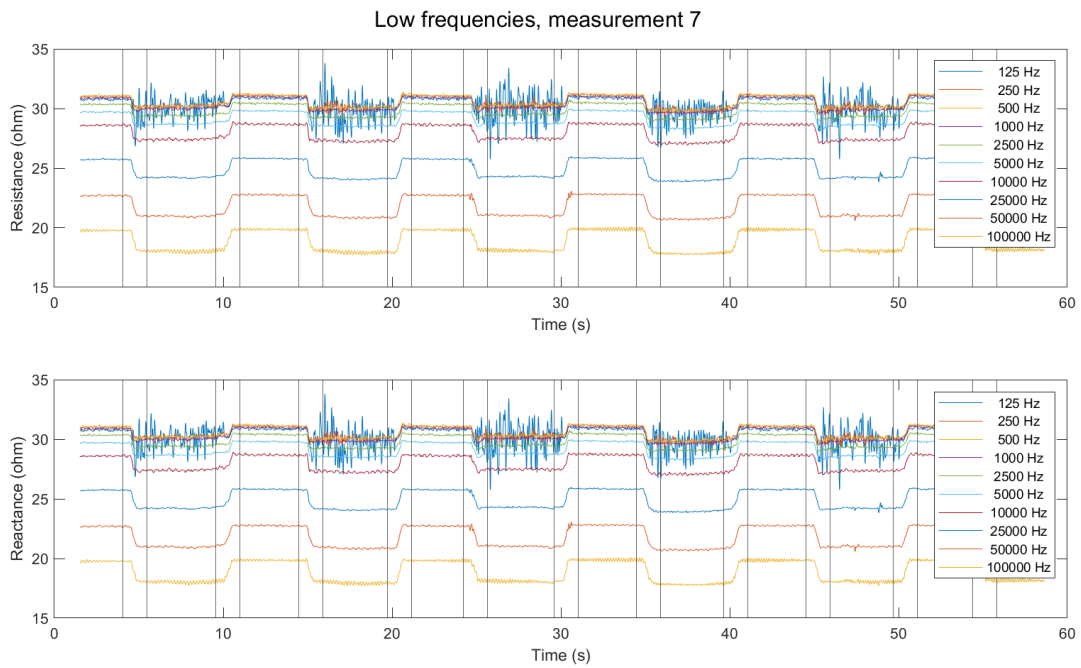


Figure B.7: Measurement number 7 of the resistance and the reactance measured during an isometric movement at low frequencies. The first pattern as described in Section 3.3.1 is used.

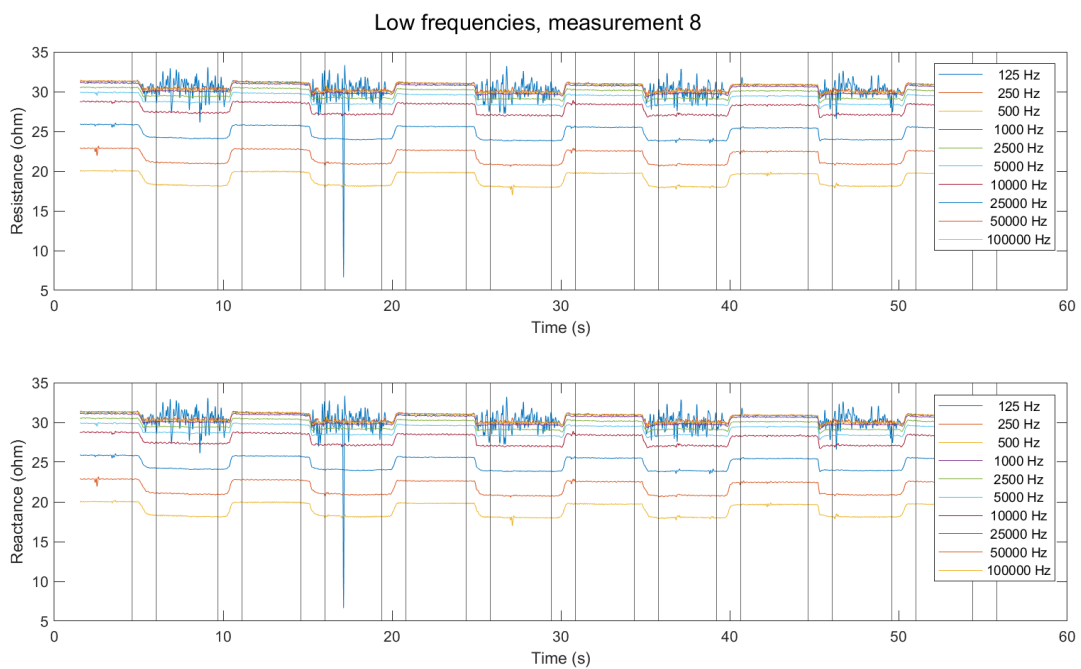


Figure B.8: Measurement number 8 of the resistance and the reactance measured during an isometric movement at low frequencies. The first pattern as described in Section 3.3.1 is used.

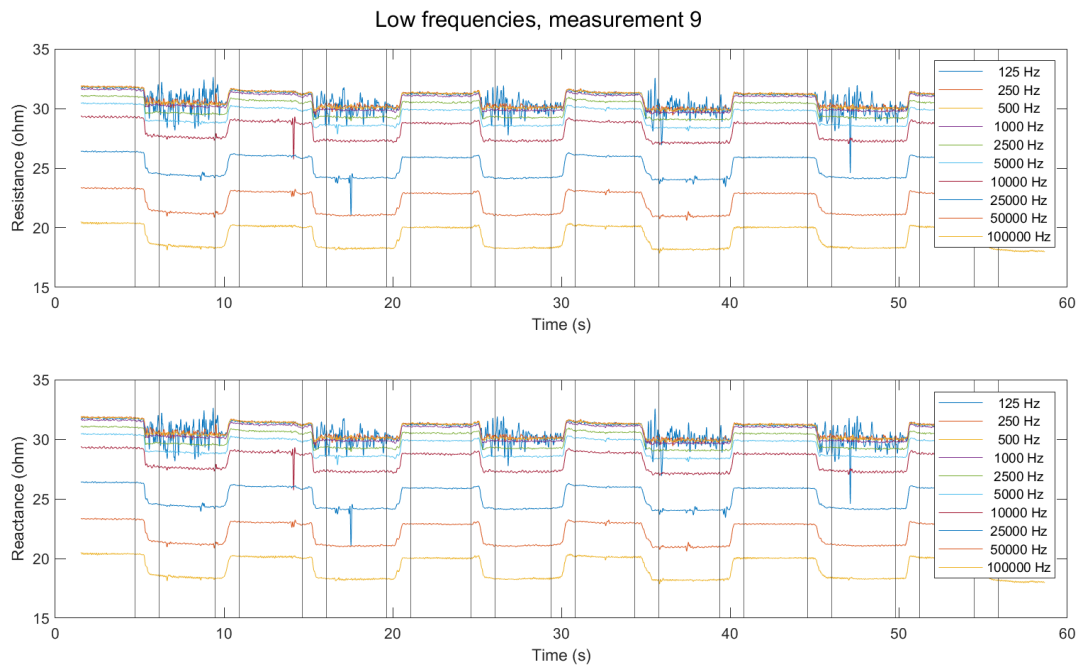


Figure B.9: Measurement number 9 of the resistance and the reactance measured during an isometric movement at low frequencies. The first pattern as described in Section 3.3.1 is used.

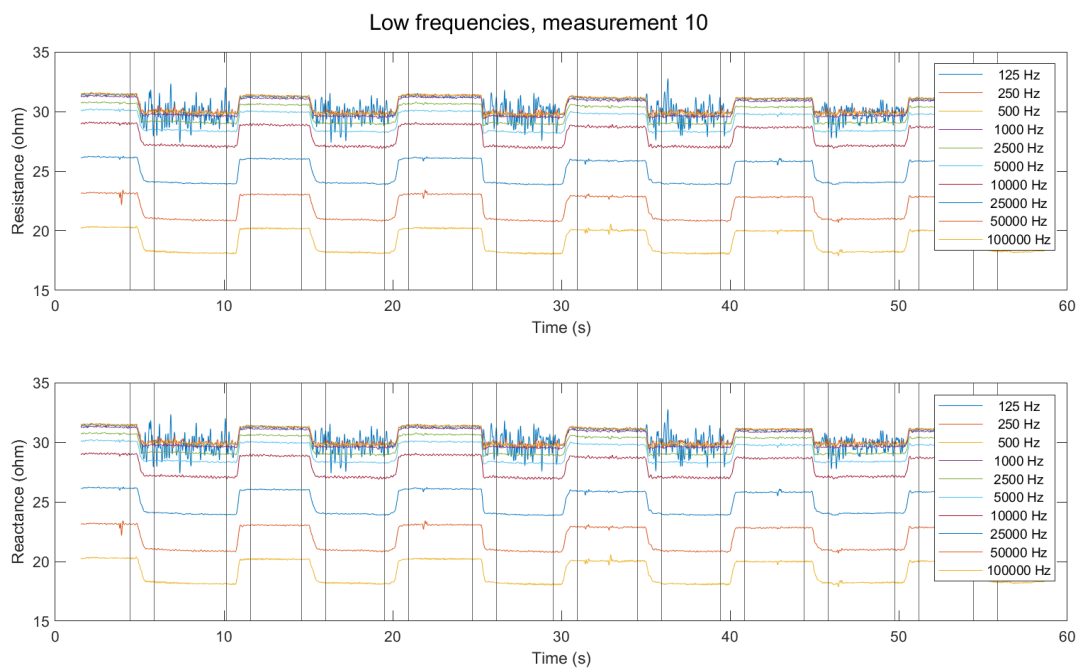


Figure B.10: Measurement number 10 of the resistance and the reactance measured during an isometric movement at low frequencies. The first pattern as described in Section 3.3.1 is used.

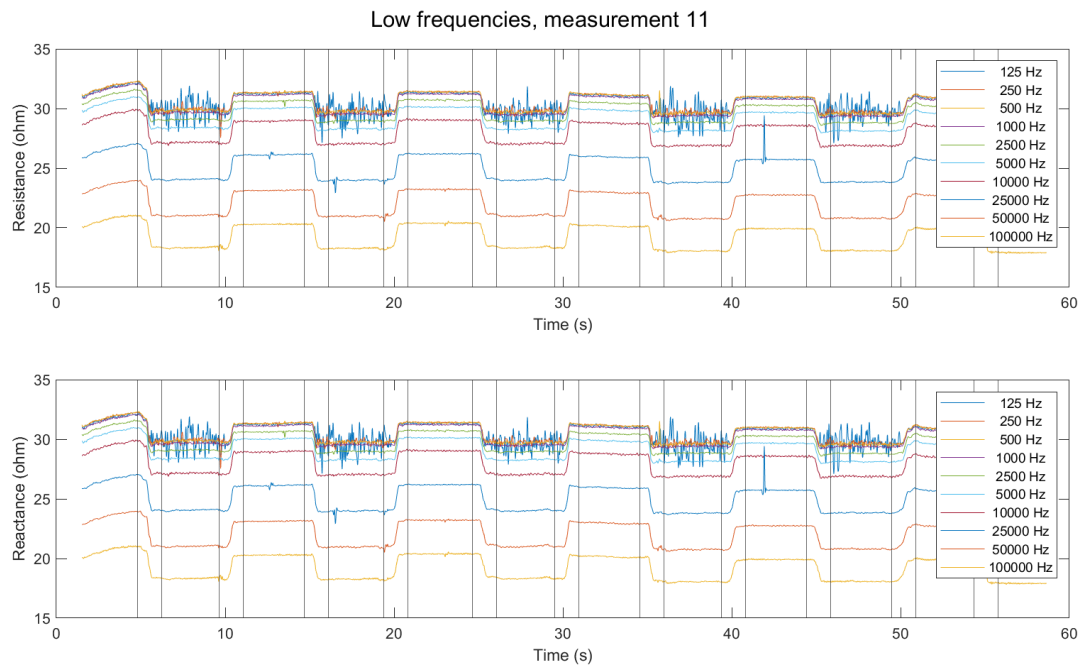


Figure B.11: Measurement number 11 of the resistance and the reactance measured during an isometric movement at low frequencies. The first pattern as described in Section 3.3.1 is used.

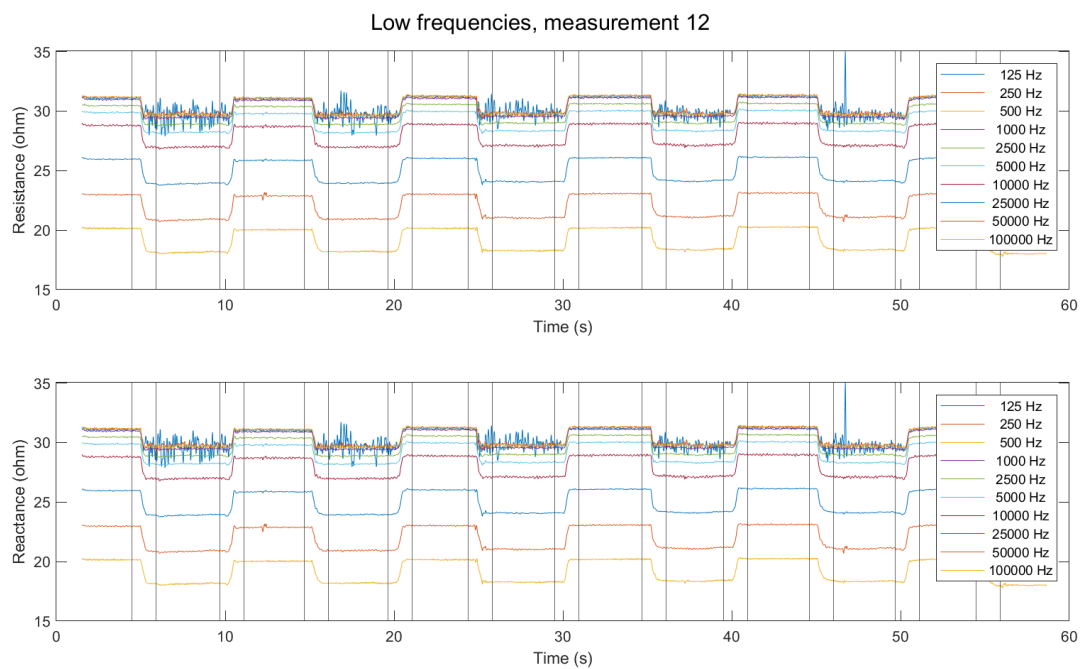


Figure B.12: Measurement number 12 of the resistance and the reactance measured during an isometric movement at low frequencies. The first pattern as described in Section 3.3.1 is used.

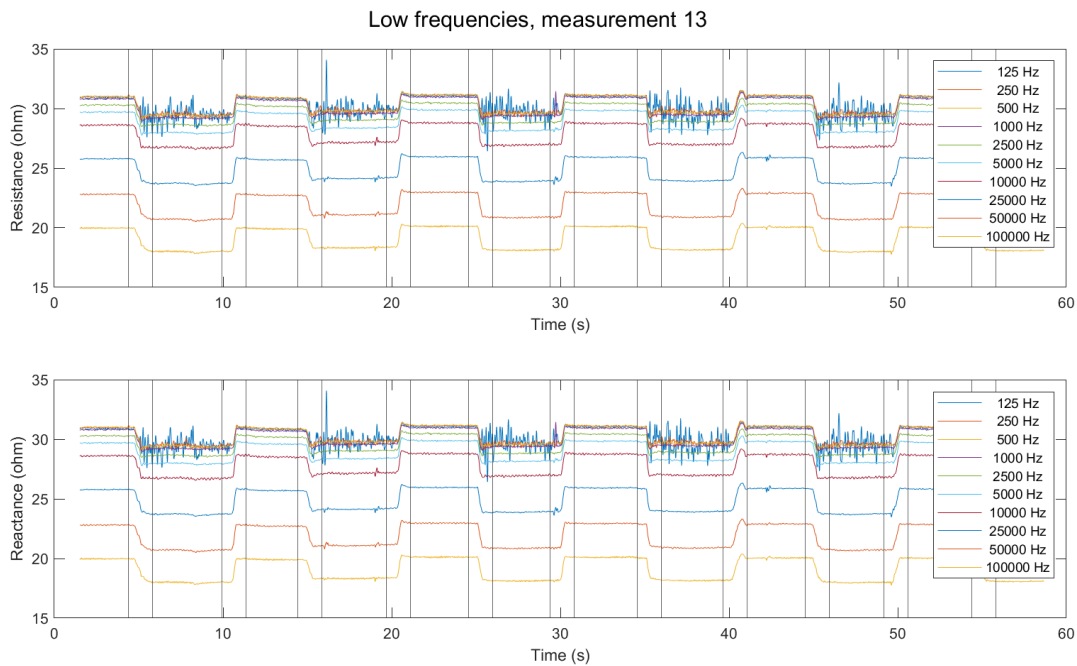


Figure B.13: Measurement number 13 of the resistance and the reactance measured during an isometric movement at low frequencies. The first pattern as described in Section 3.3.1 is used.

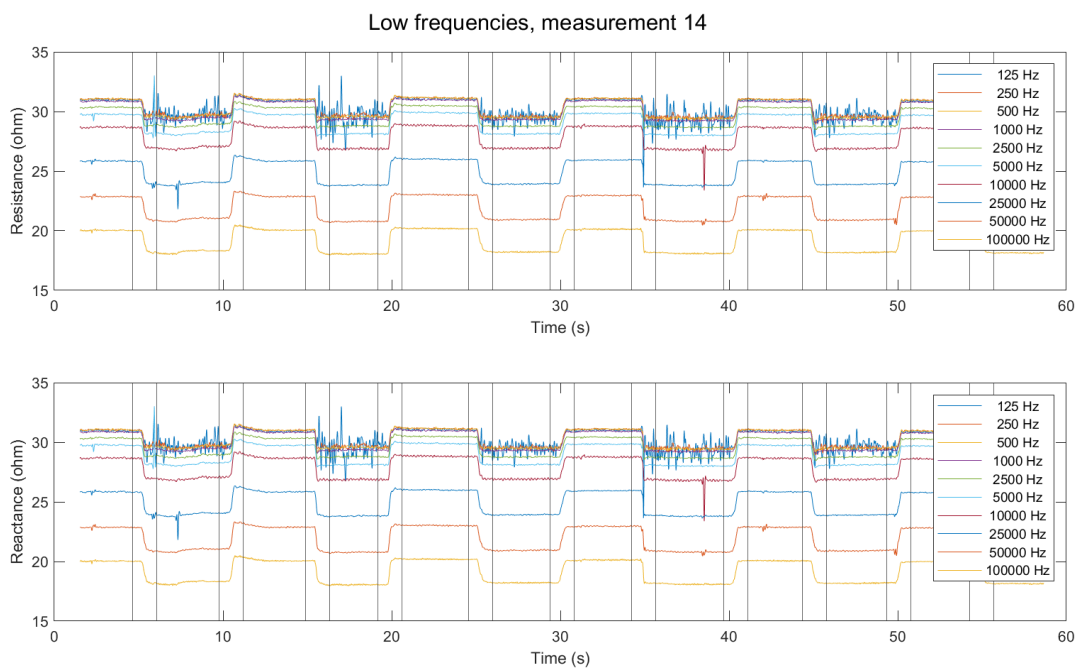


Figure B.14: Measurement number 14 of the resistance and the reactance measured during an isometric movement at low frequencies. The first pattern as described in Section 3.3.1 is used.

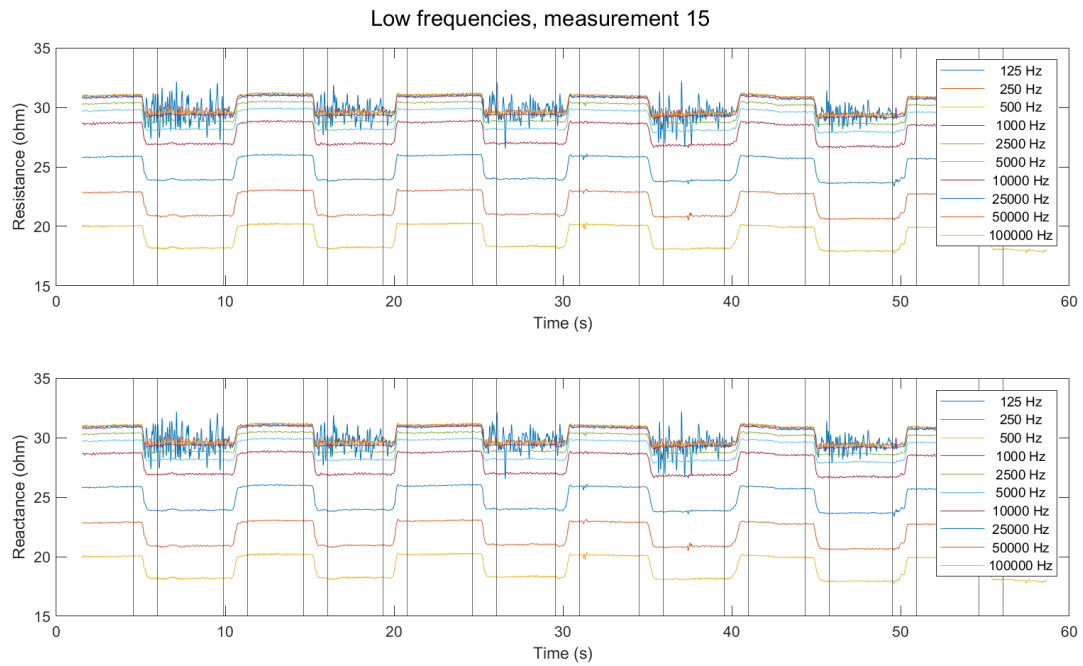


Figure B.15: Measurement number 15 of the resistance and the reactance measured during an isometric movement at low frequencies. The first pattern as described in Section 3.3.1 is used.

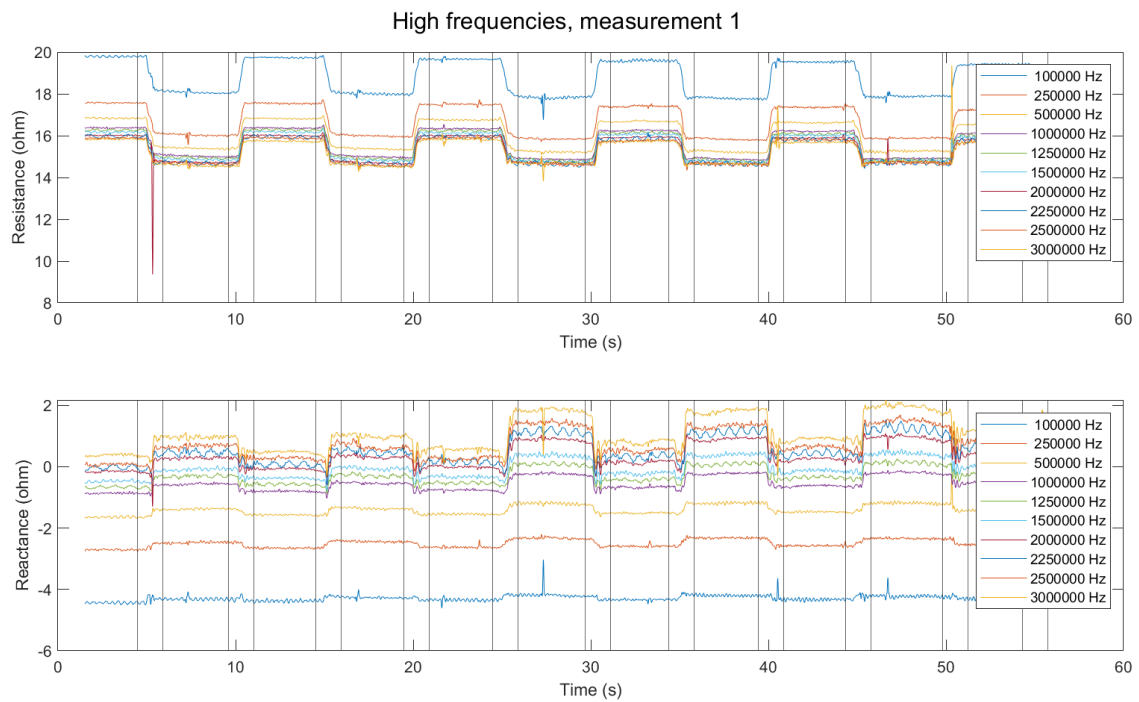


Figure B.16: Measurement number 1 of the resistance and the reactance measured during an isometric movement at high frequencies. The first pattern as described in Section 3.3.1 is used.

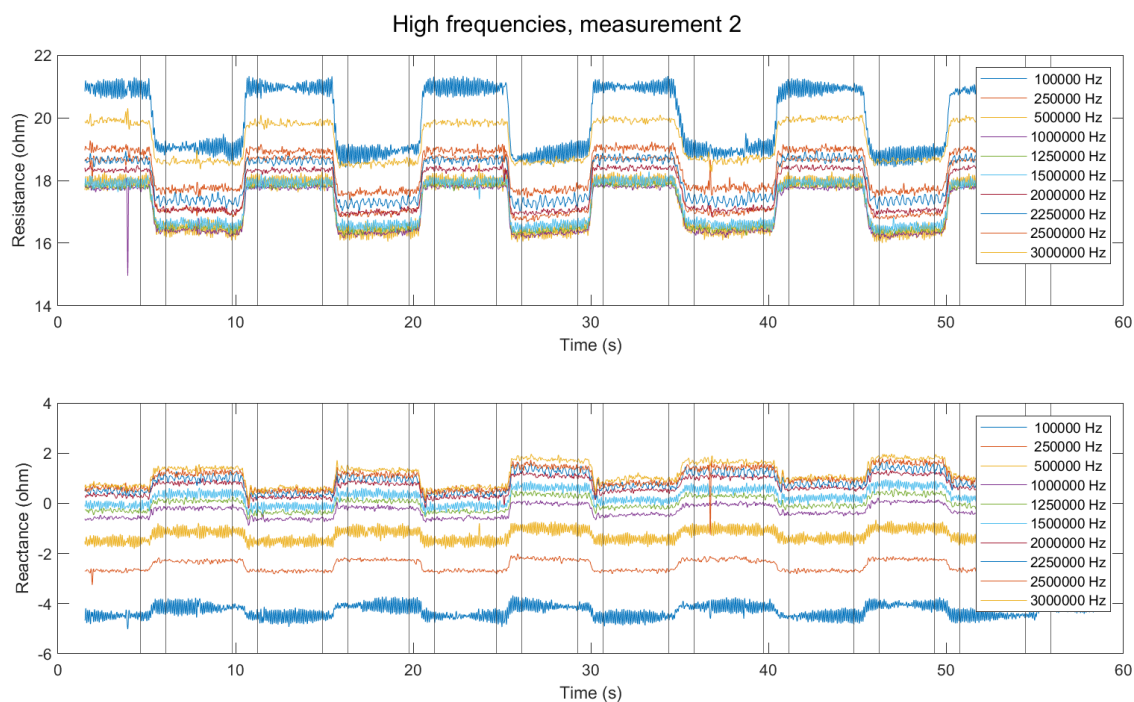


Figure B.17: Measurement number 2 of the resistance and the reactance measured during an isometric movement at high frequencies. The first pattern as described in Section 3.3.1 is used.

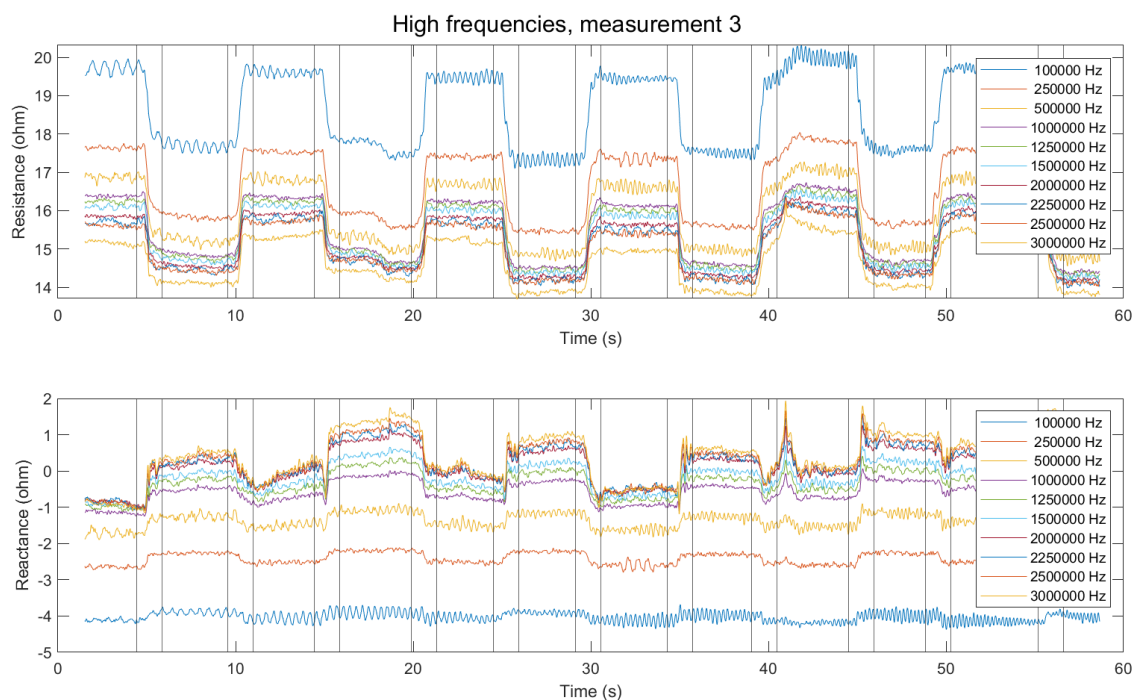


Figure B.18: Measurement number 3 of the resistance and the reactance measured during an isometric movement at high frequencies. The first pattern as described in Section 3.3.1 is used.

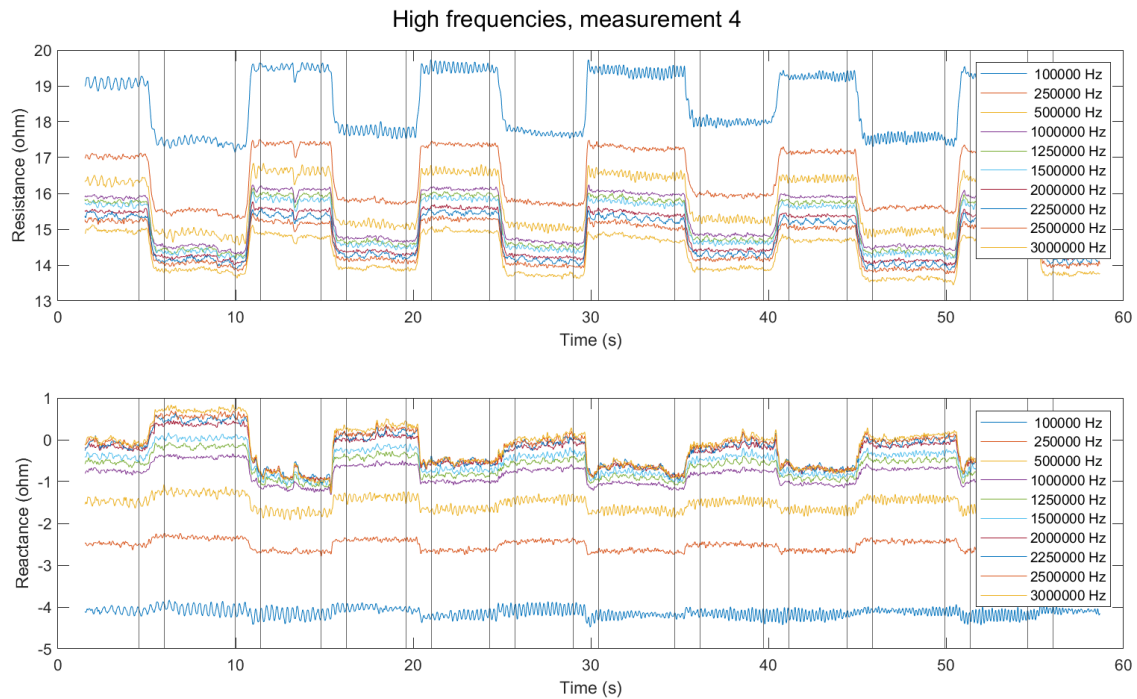


Figure B.19: Measurement number 4 of the resistance and the reactance measured during an isometric movement at high frequencies. The first pattern as described in Section 3.3.1 is used.

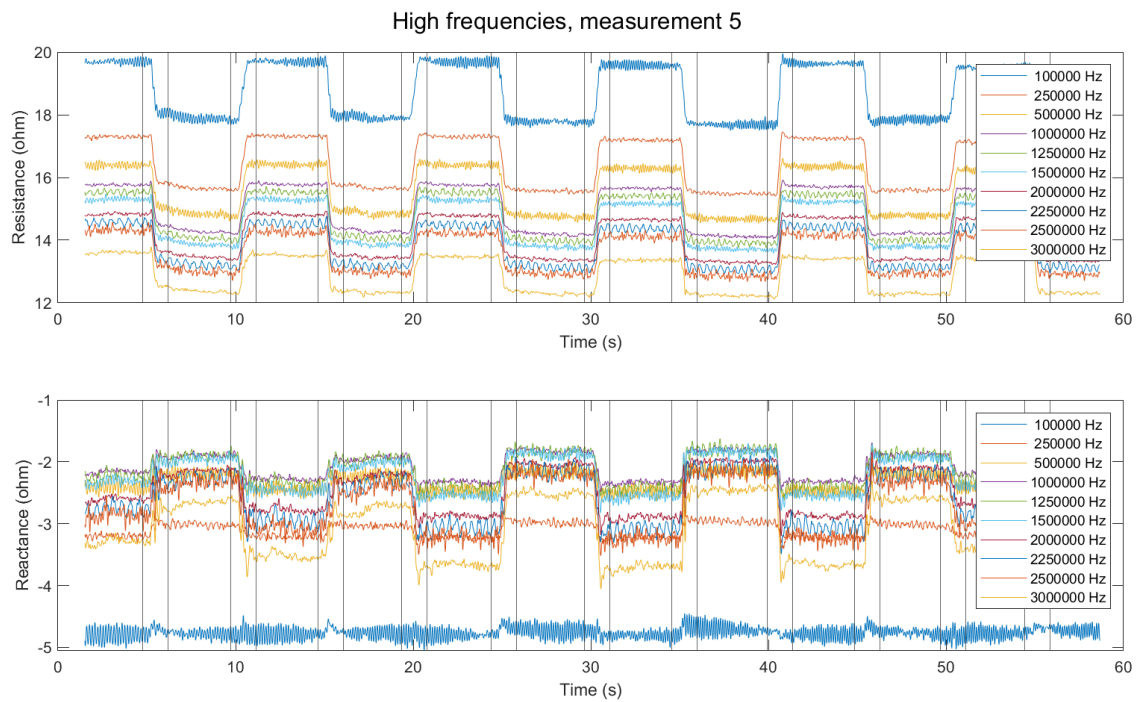


Figure B.20: Measurement number 5 of the resistance and the reactance measured during an isometric movement at high frequencies. The first pattern as described in Section 3.3.1 is used.

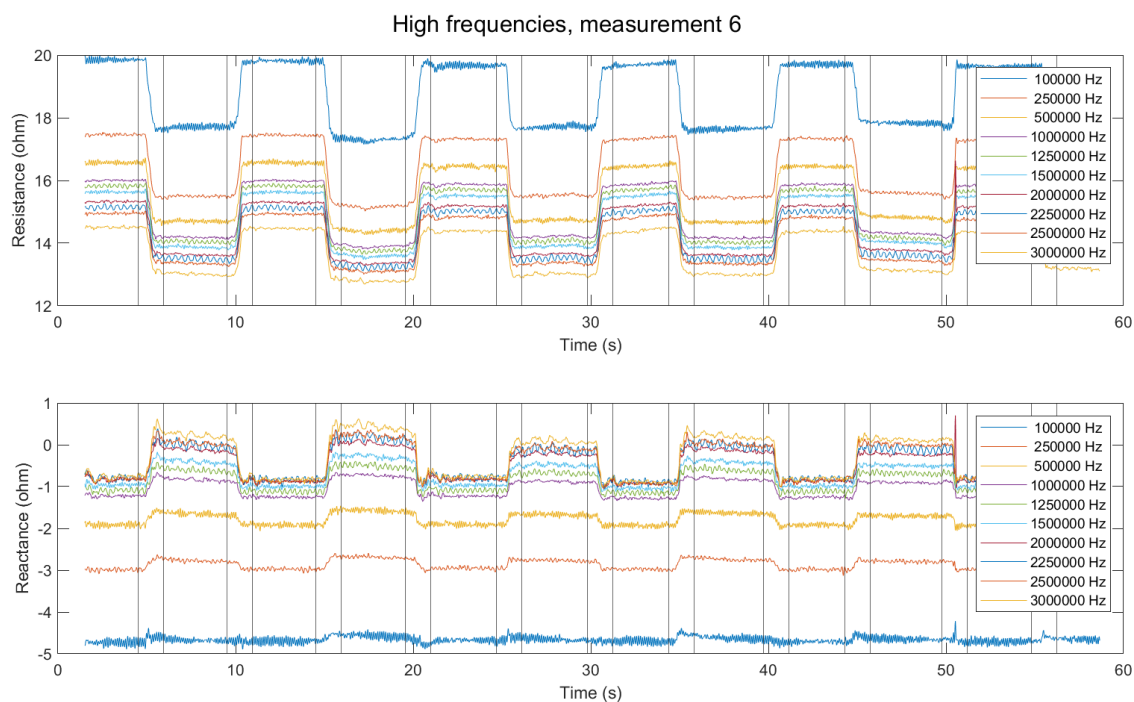


Figure B.21: Measurement number 6 of the resistance and the reactance measured during an isometric movement at high frequencies. The first pattern as described in Section 3.3.1 is used.

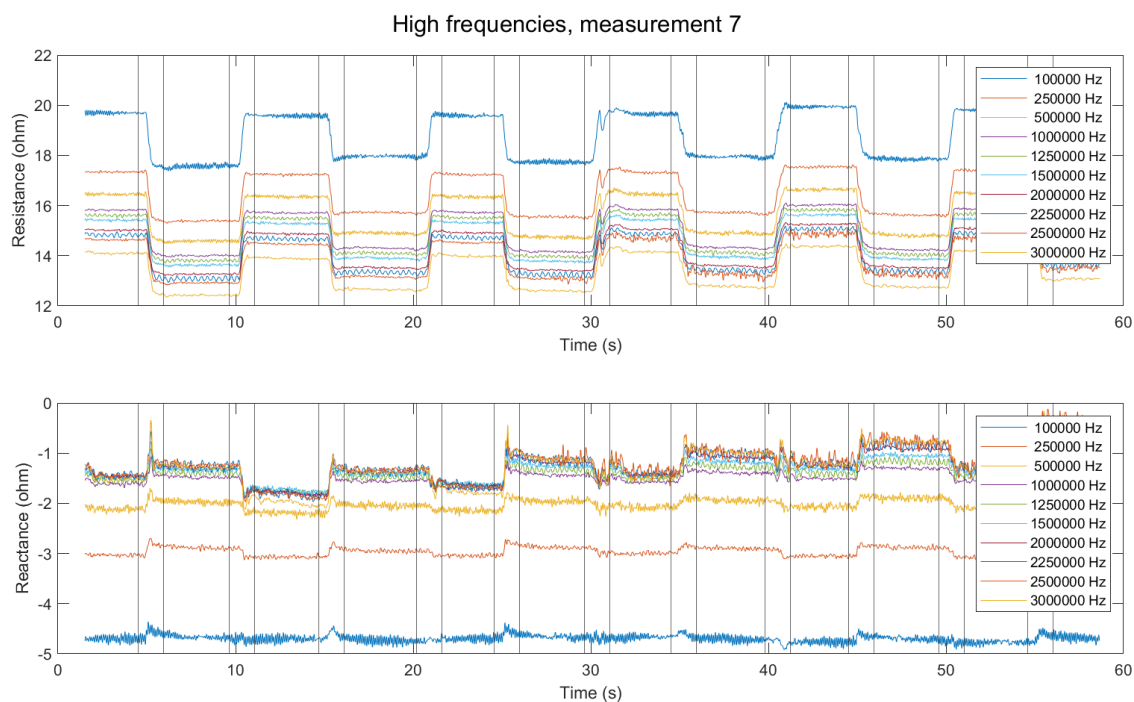


Figure B.22: Measurement number 7 of the resistance and the reactance measured during an isometric movement at high frequencies. The first pattern as described in Section 3.3.1 is used.

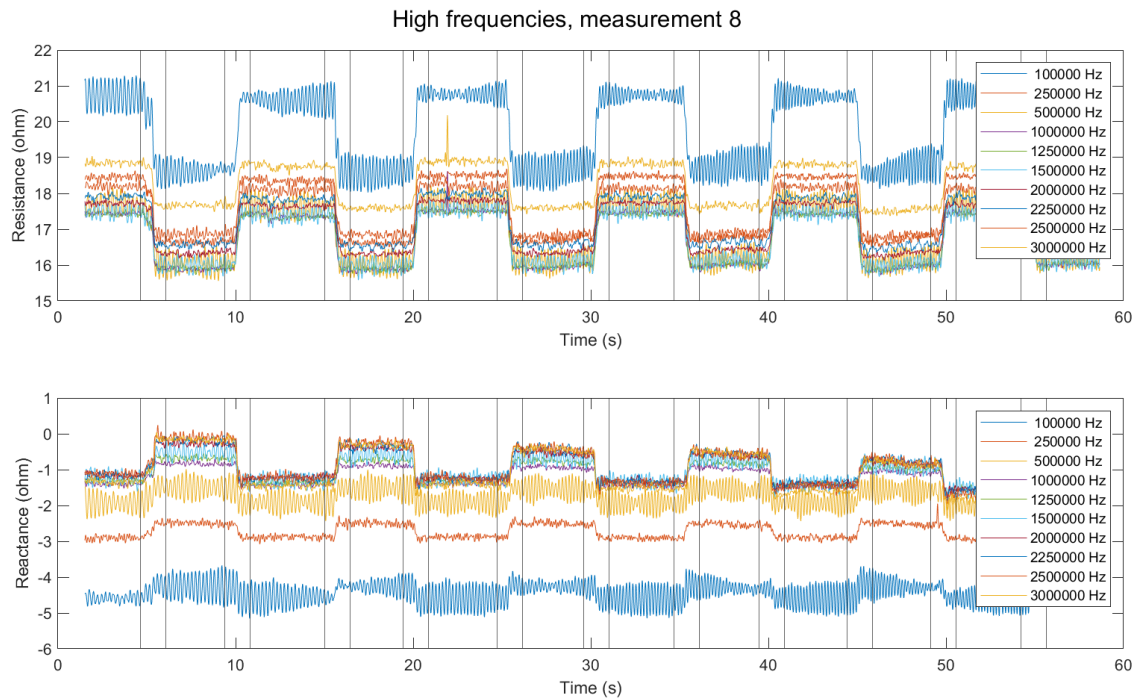


Figure B.23: Measurement number 8 of the resistance and the reactance measured during an isometric movement at high frequencies. The first pattern as described in Section 3.3.1 is used.

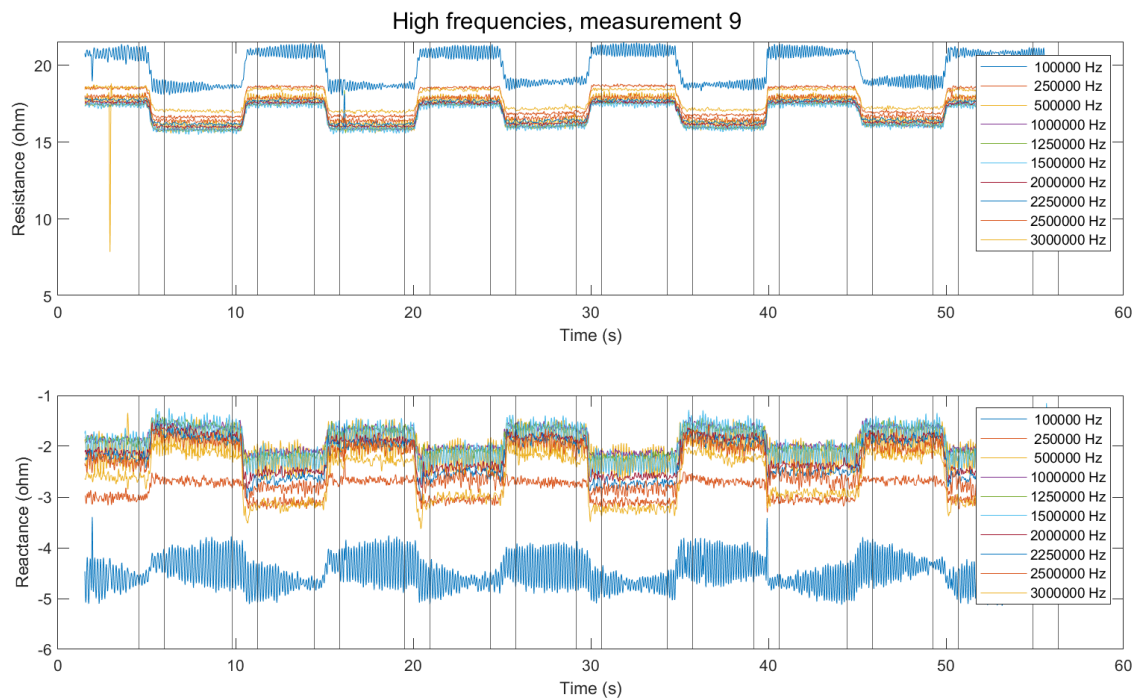


Figure B.24: Measurement number 9 of the resistance and the reactance measured during an isometric movement at high frequencies. The first pattern as described in Section 3.3.1 is used.

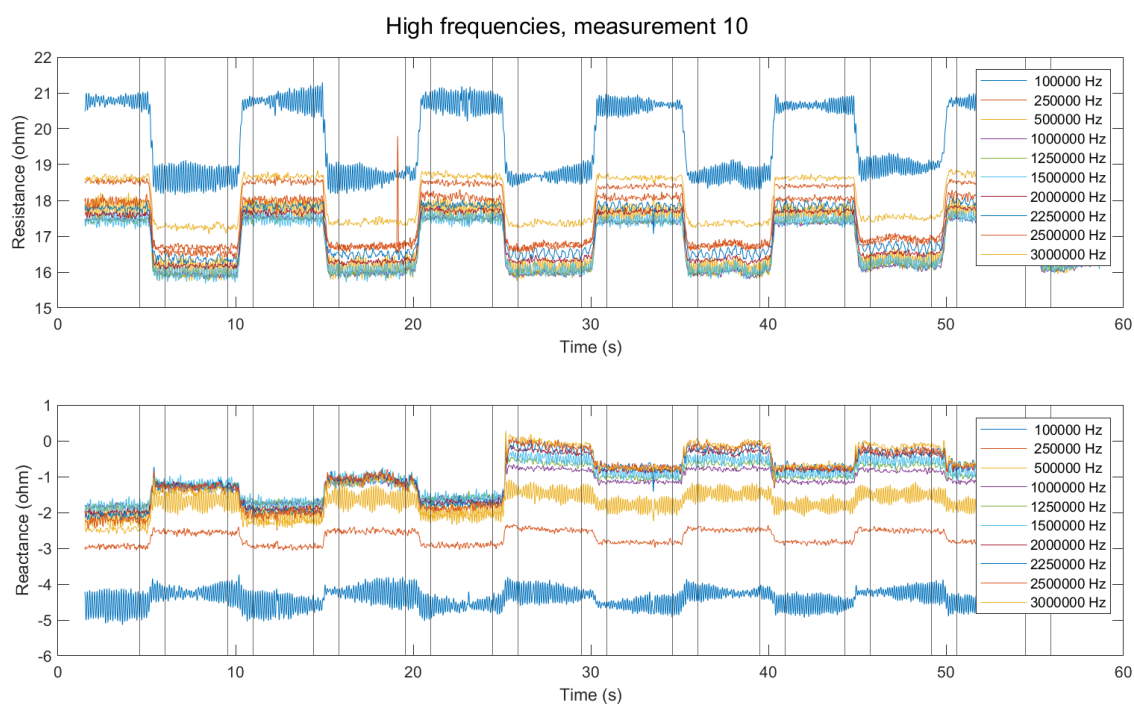


Figure B.25: Measurement number 10 of the resistance and the reactance measured during an isometric movement at high frequencies. The first pattern as described in Section 3.3.1 is used.

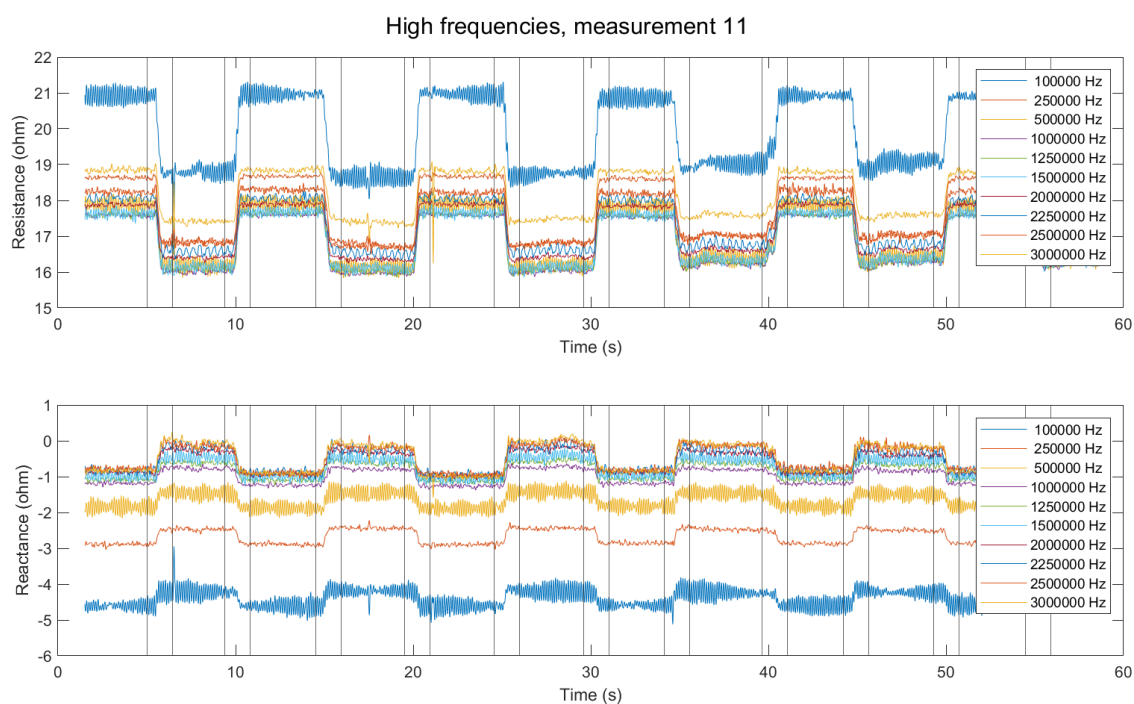


Figure B.26: Measurement number 11 of the resistance and the reactance measured during an isometric movement at high frequencies. The first pattern as described in Section 3.3.1 is used.

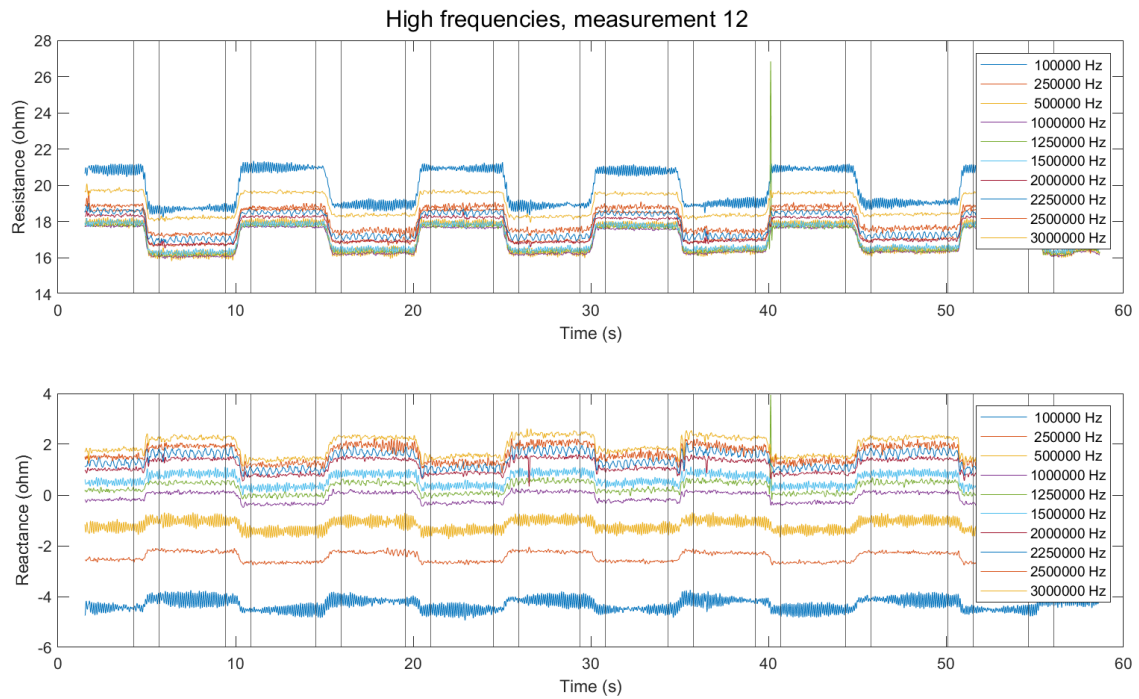


Figure B.27: Measurement number 12 of the resistance and the reactance measured during an isometric movement at high frequencies. The first pattern as described in Section 3.3.1 is used.

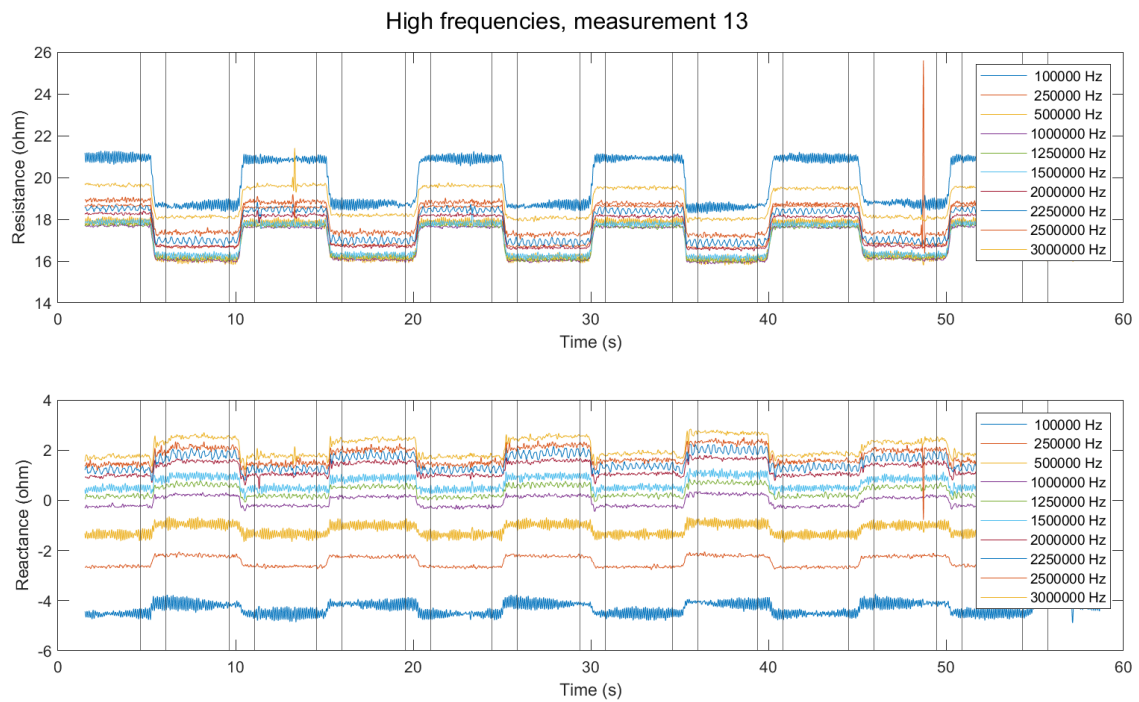


Figure B.28: Measurement number 13 of the resistance and the reactance measured during an isometric movement at high frequencies. The first pattern as described in Section 3.3.1 is used.

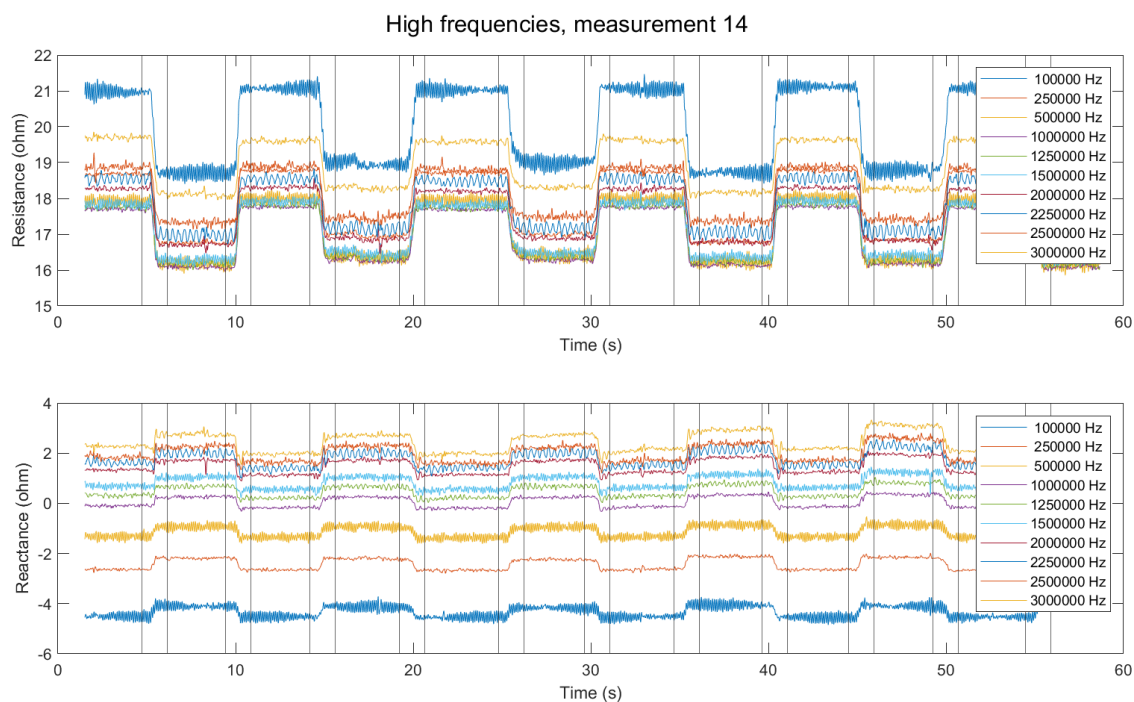


Figure B.29: Measurement number 14 of the resistance and the reactance measured during an isometric movement at high frequencies. The first pattern as described in Section 3.3.1 is used.

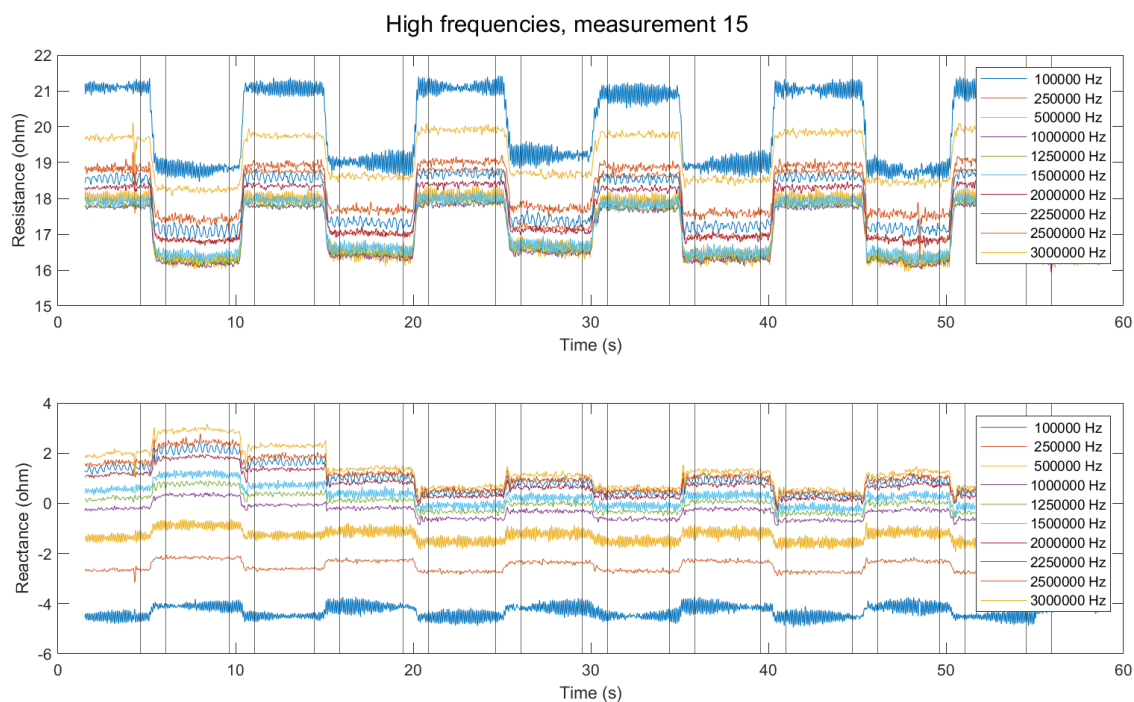


Figure B.30: Measurement number 15 of the resistance and the reactance measured during an isometric movement at high frequencies. The first pattern as described in Section 3.3.1 is used.

C Isotonic data

This chapter shows all figures of the data collected using movement pattern 2 of Section 3.3.1, Figure 3.9. The low and high frequencies are shown.

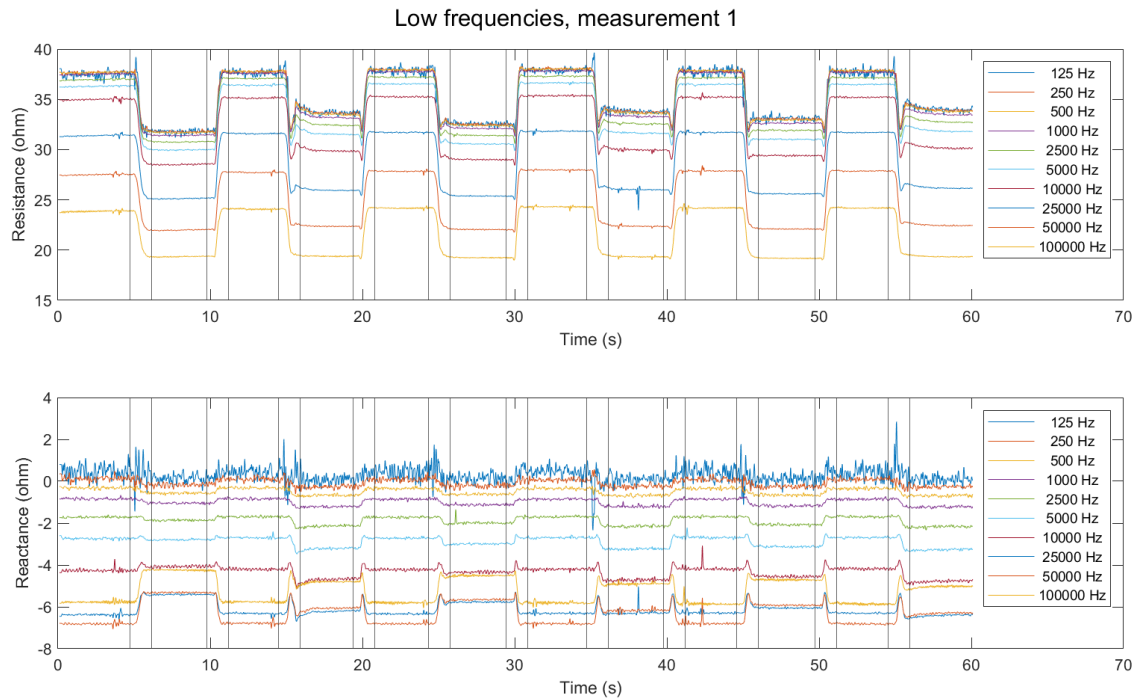


Figure C.1: The resistance and reactance of the bio-impedance measured during an isotonic movement at low frequencies. The second pattern as described in Section 3.3.1 is used.

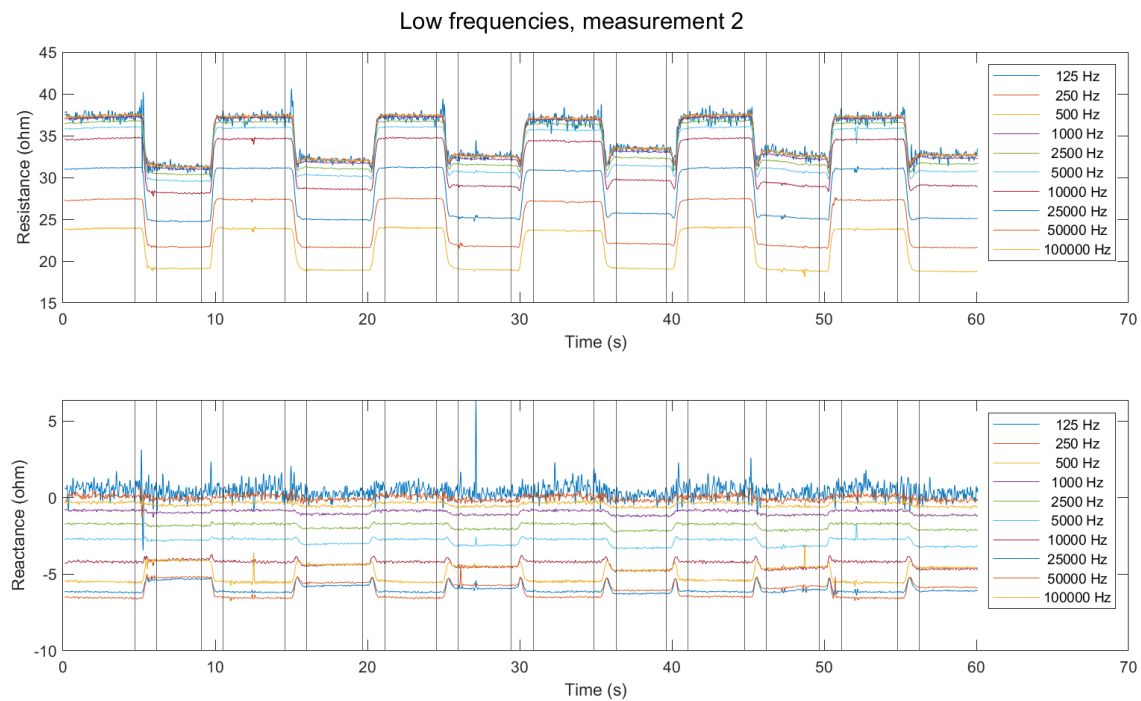


Figure C.2: The resistance and reactance of the bio-impedance measured during an isotonic movement at low frequencies. The second pattern as described in Section 3.3.1 is used.

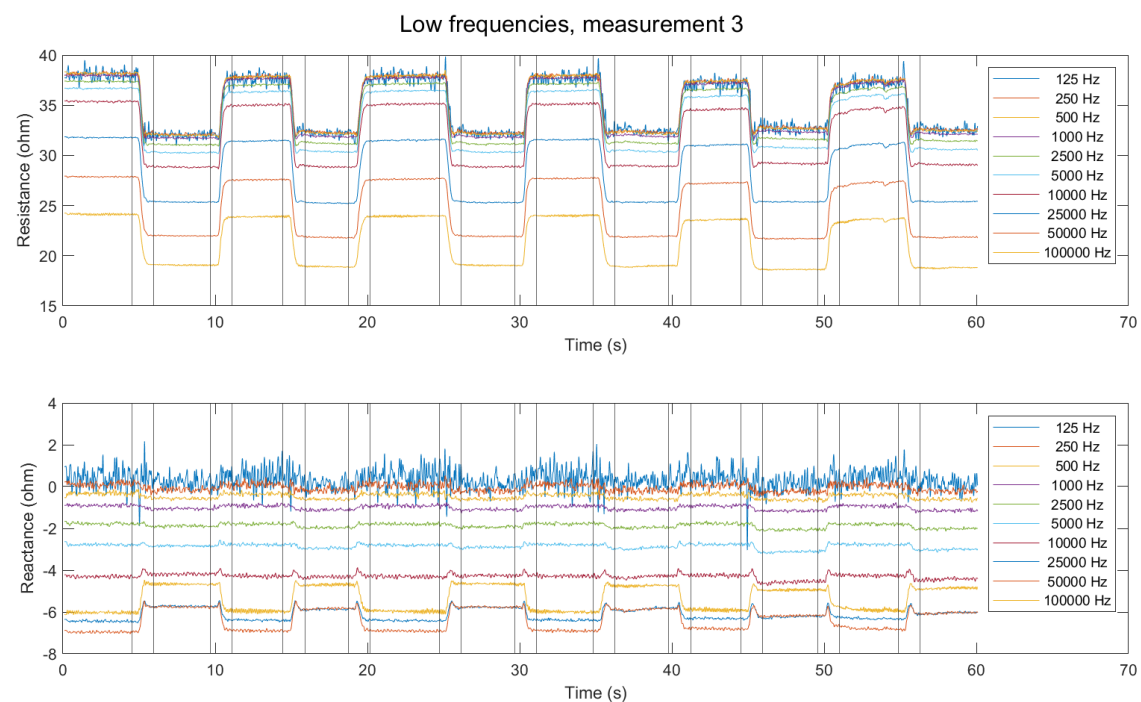


Figure C.3: The resistance and reactance of the bio-impedance measured during an isotonic movement at low frequencies. The second pattern as described in Section 3.3.1 is used.

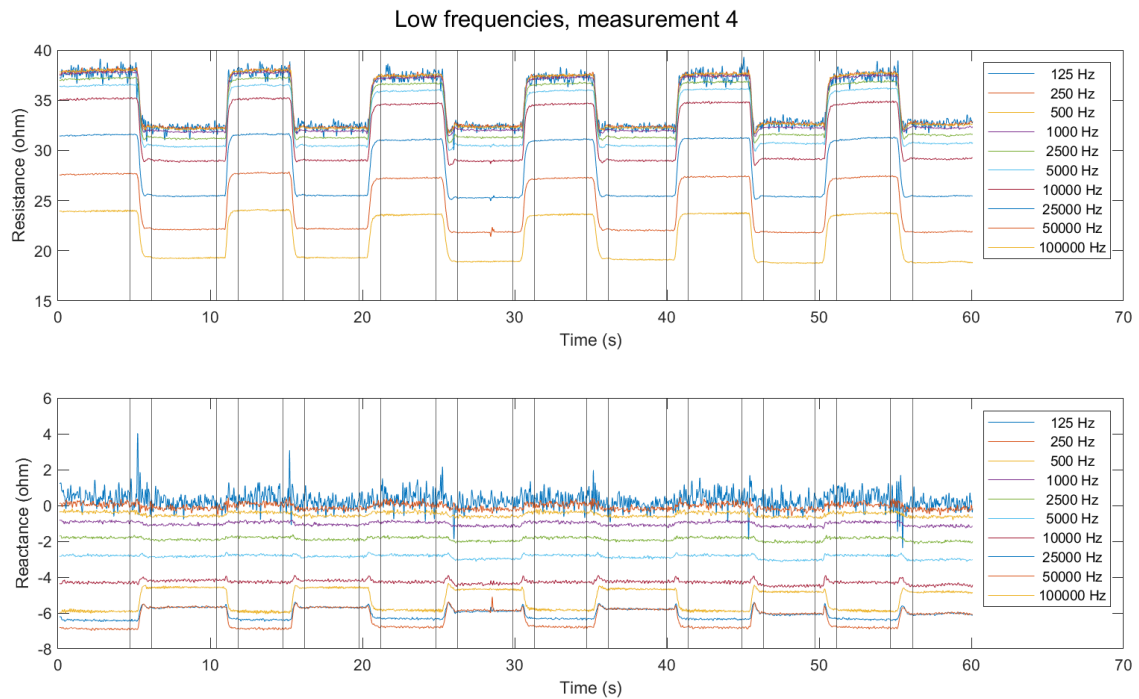


Figure C.4: The resistance and reactance of the bio-impedance measured during an isotonic movement at low frequencies. The second pattern as described in Section 3.3.1 is used.

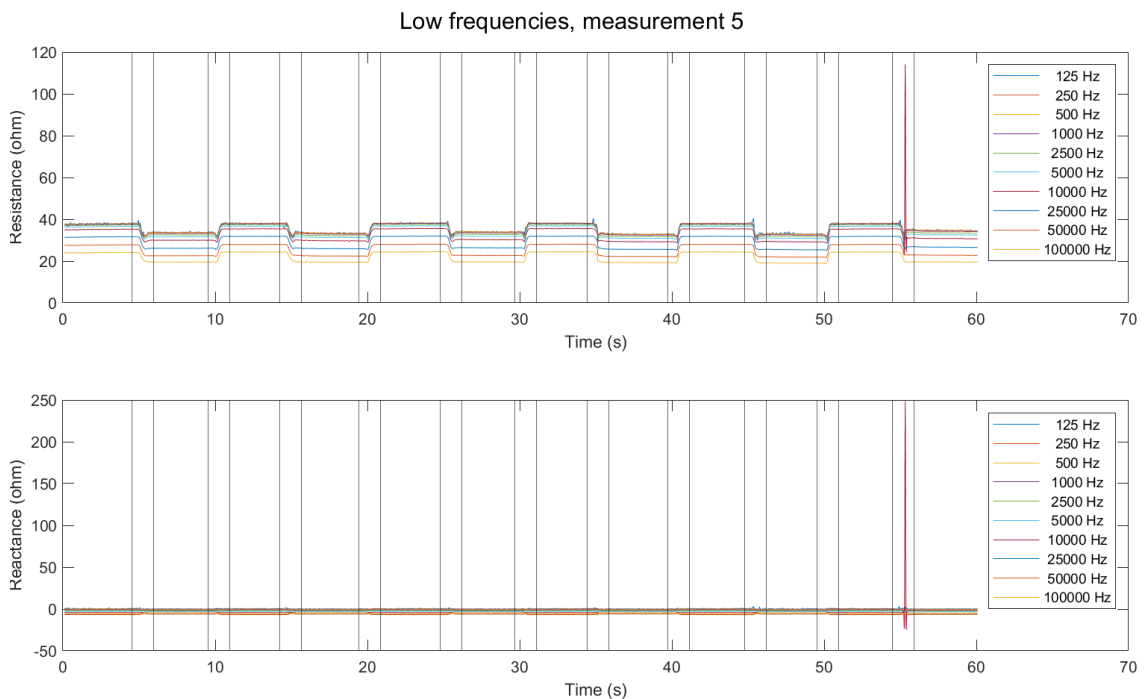


Figure C.5: The resistance and reactance of the bio-impedance measured during an isotonic movement at low frequencies. The second pattern as described in Section 3.3.1 is used.

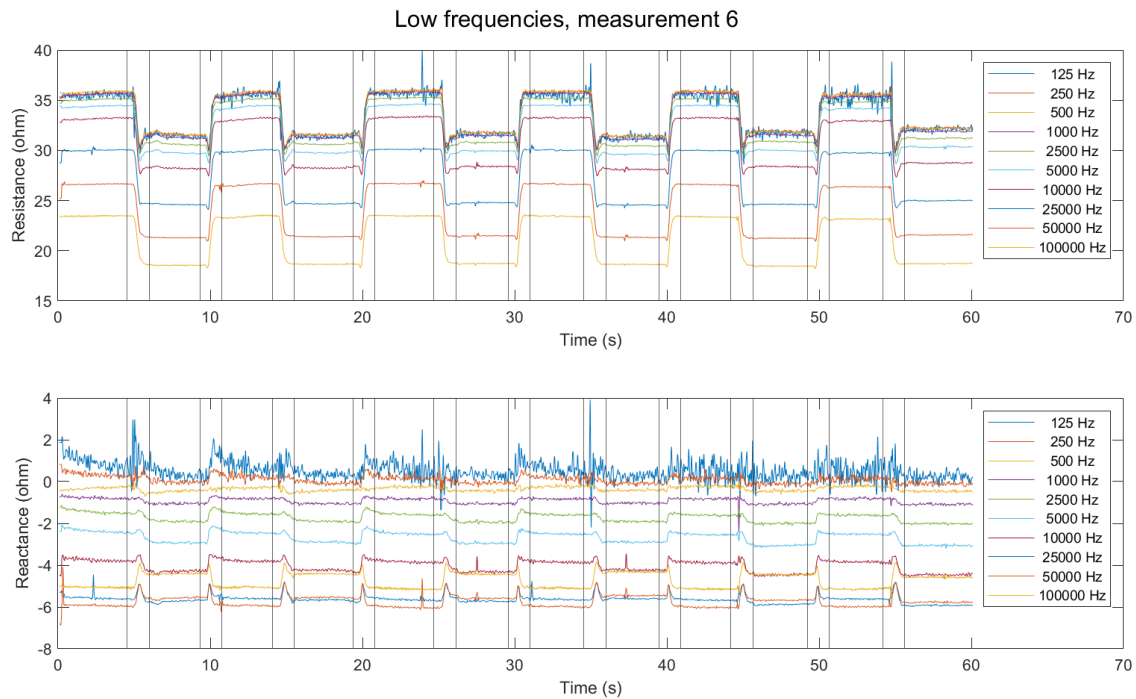


Figure C.6: The resistance and reactance of the bio-impedance measured during an isotonic movement at low frequencies. The second pattern as described in Section 3.3.1 is used.

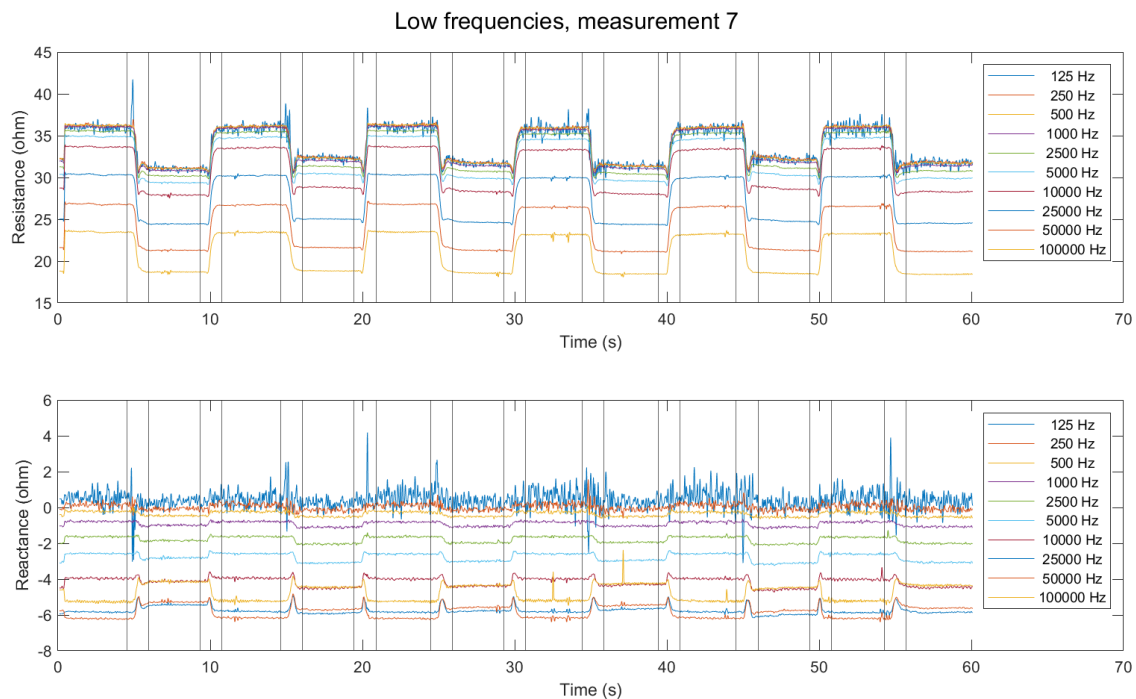


Figure C.7: The resistance and reactance of the bio-impedance measured during an isotonic movement at low frequencies. The second pattern as described in Section 3.3.1 is used.

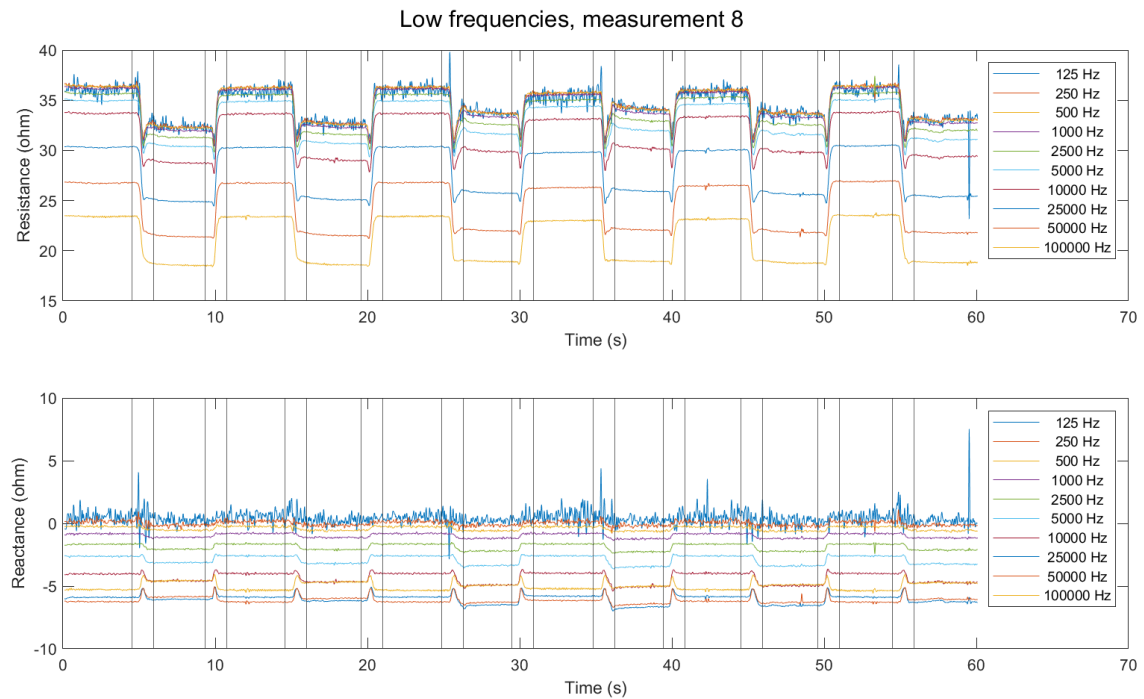


Figure C.8: The resistance and reactance of the bio-impedance measured during an isotonic movement at low frequencies. The second pattern as described in Section 3.3.1 is used.

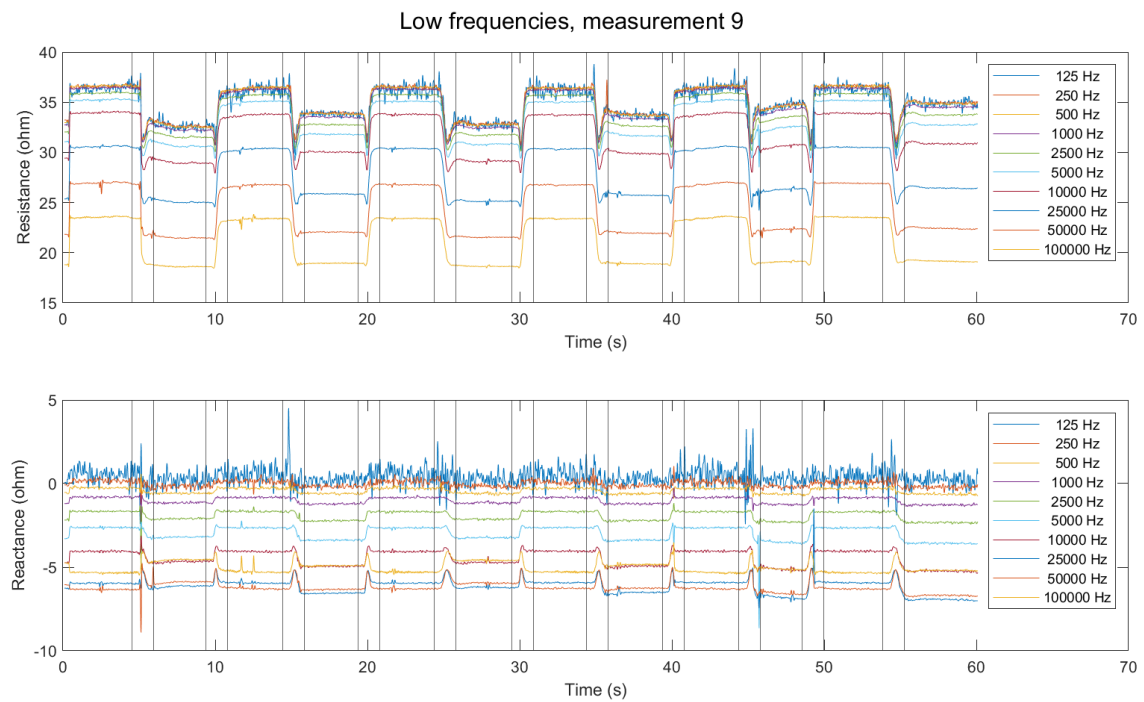


Figure C.9: The resistance and reactance of the bio-impedance measured during an isotonic movement at low frequencies. The second pattern as described in Section 3.3.1 is used.

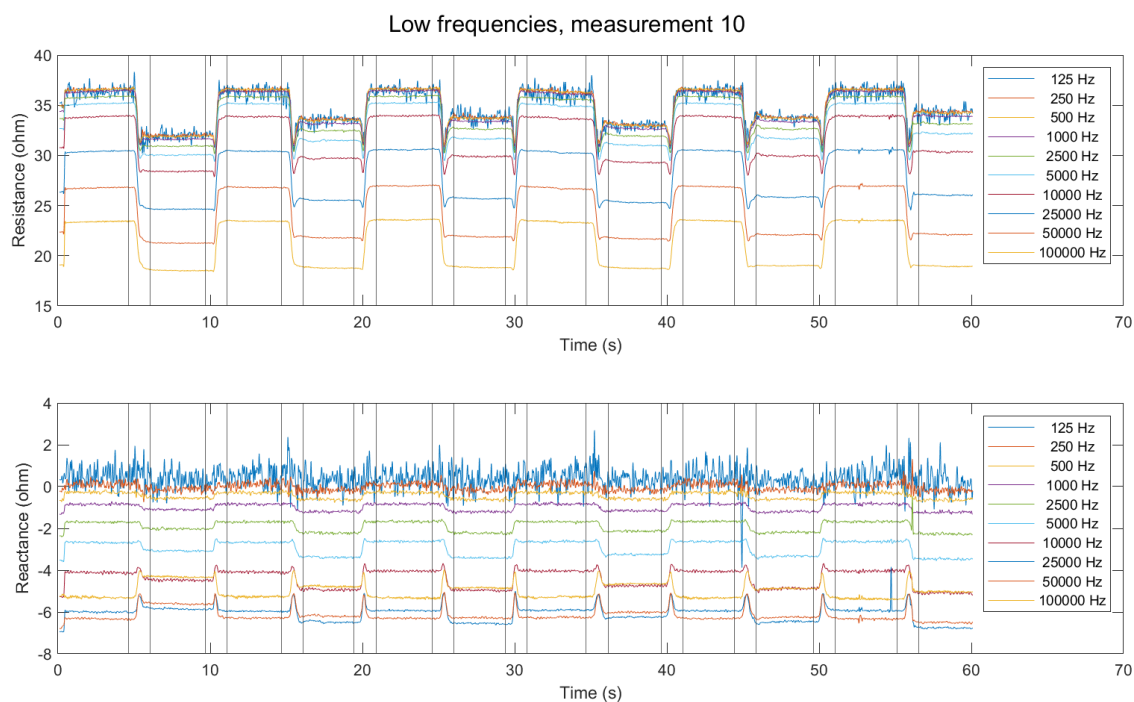


Figure C.10: The resistance and reactance of the bio-impedance measured during an isotonic movement at low frequencies. The second pattern as described in Section 3.3.1 is used.

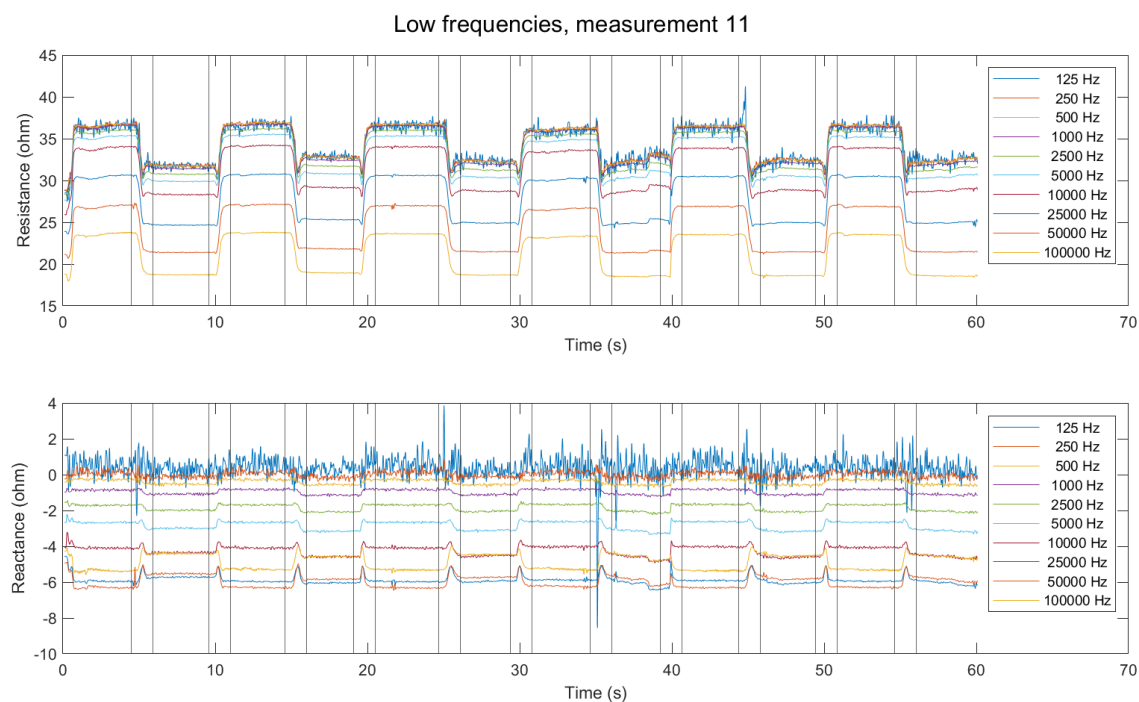


Figure C.11: The resistance and reactance of the bio-impedance measured during an isotonic movement at low frequencies. The second pattern as described in Section 3.3.1 is used.

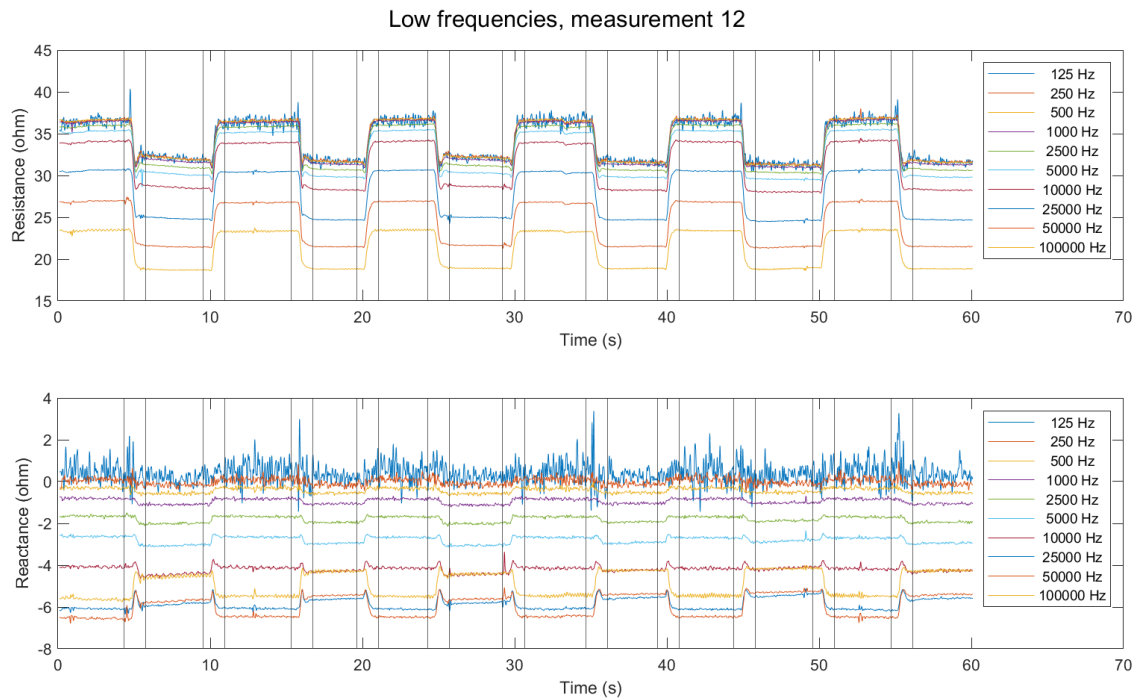


Figure C.12: The resistance and reactance of the bio-impedance measured during an isotonic movement at low frequencies. The second pattern as described in Section 3.3.1 is used.

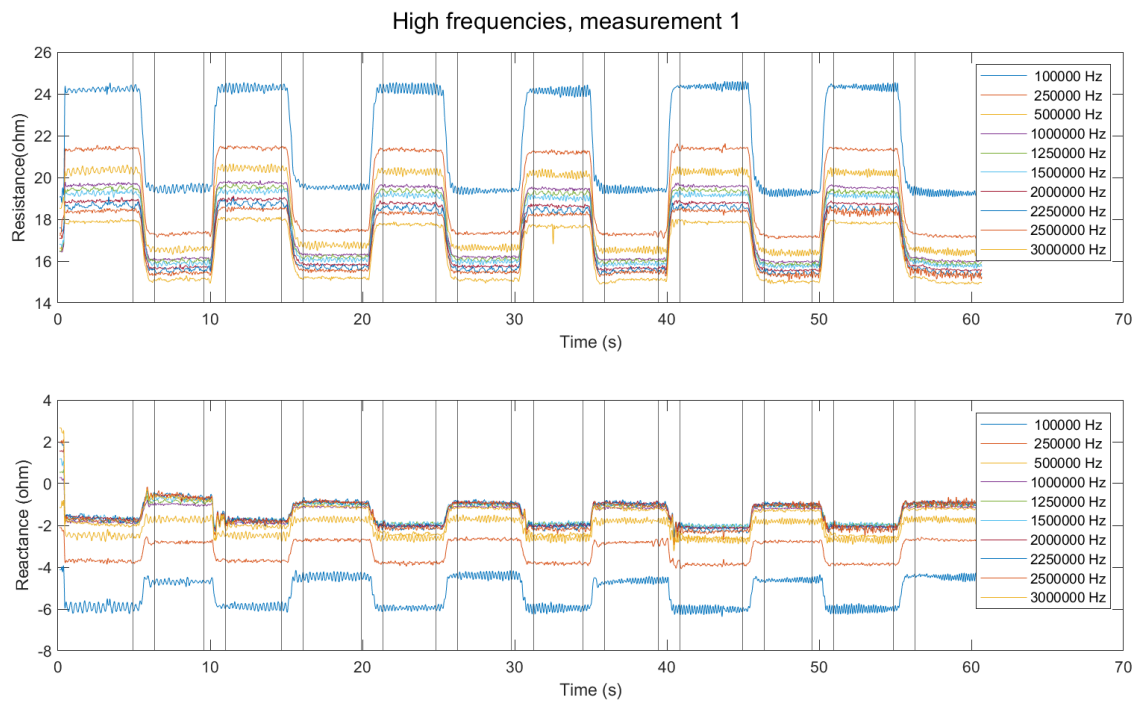


Figure C.13: The resistance and reactance of the bio-impedance measured during an isotonic movement at high frequencies. The second pattern as described in Section 3.3.1 is used.

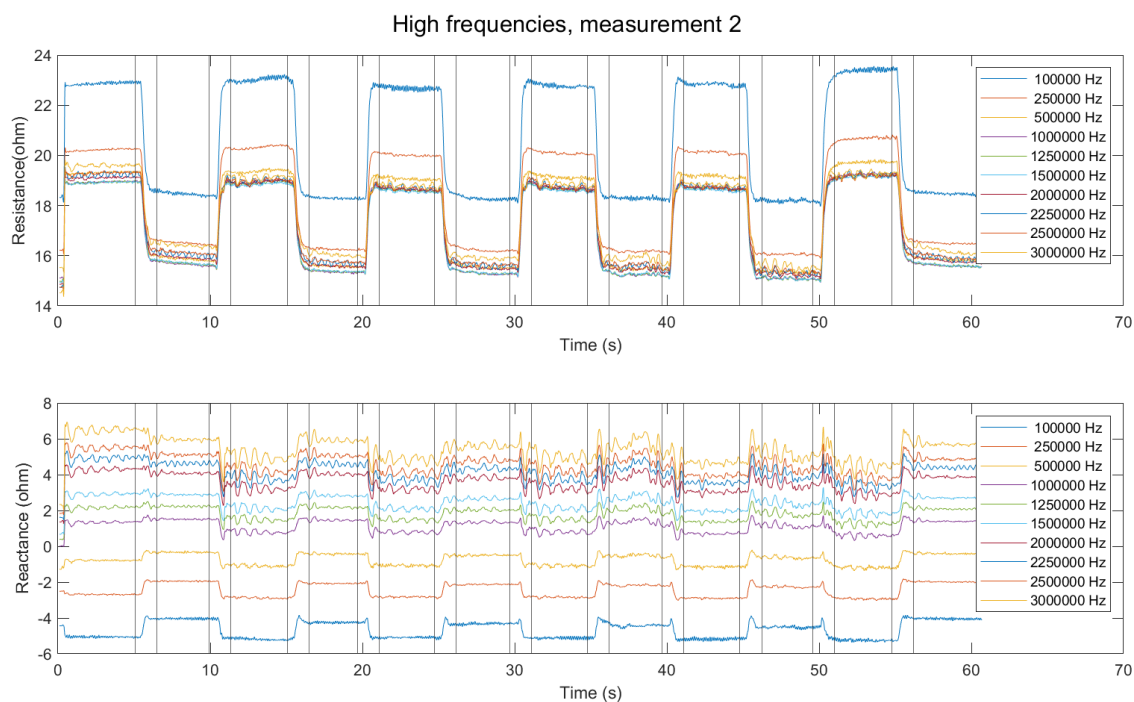


Figure C.14: The resistance and reactance of the bio-impedance measured during an isotonic movement at high frequencies. The second pattern as described in Section 3.3.1 is used.

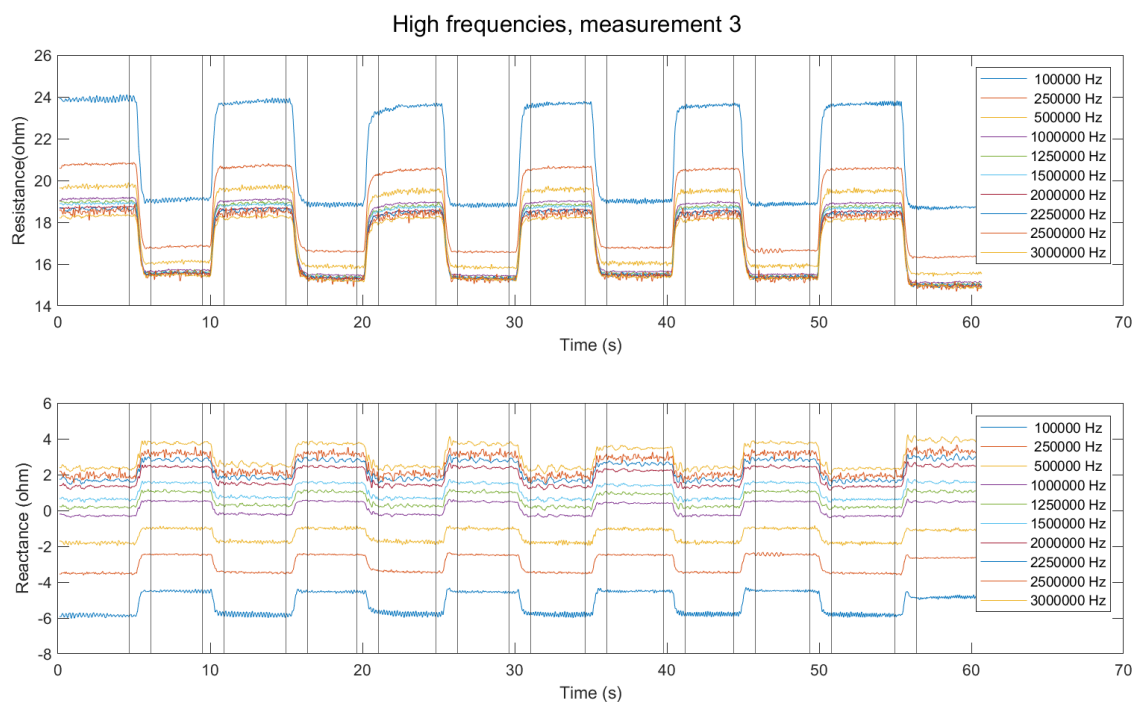


Figure C.15: The resistance and reactance of the bio-impedance measured during an isotonic movement at high frequencies. The second pattern as described in Section 3.3.1 is used.

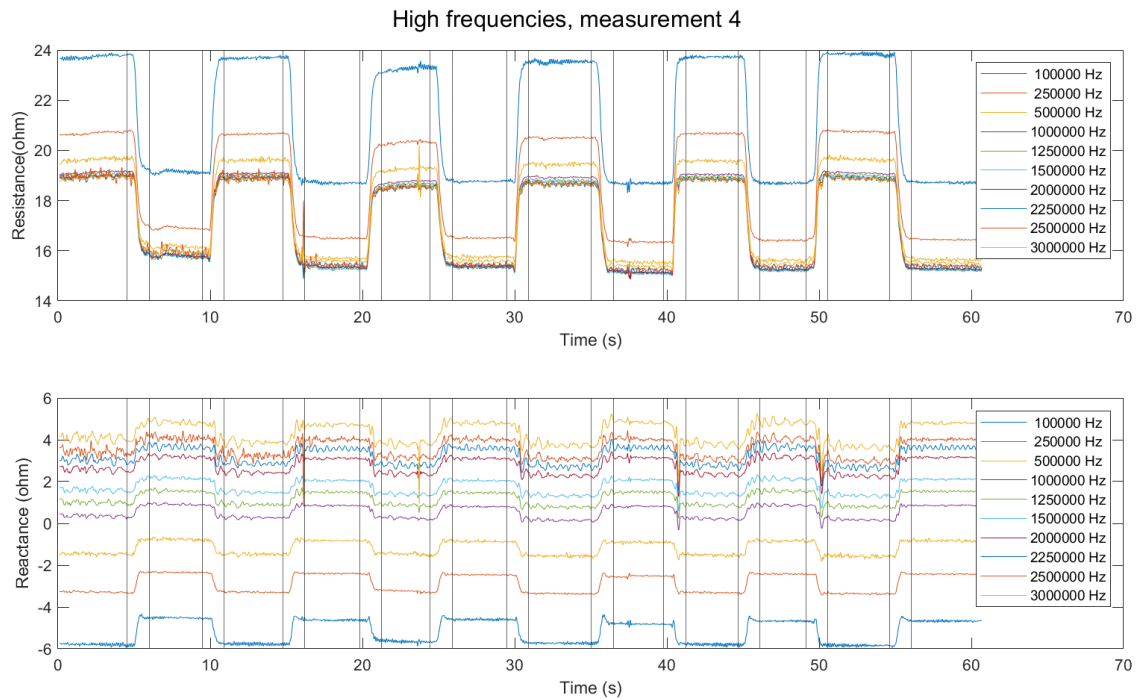


Figure C.16: The resistance and reactance of the bio-impedance measured during an isotonic movement at high frequencies. The second pattern as described in Section 3.3.1 is used.

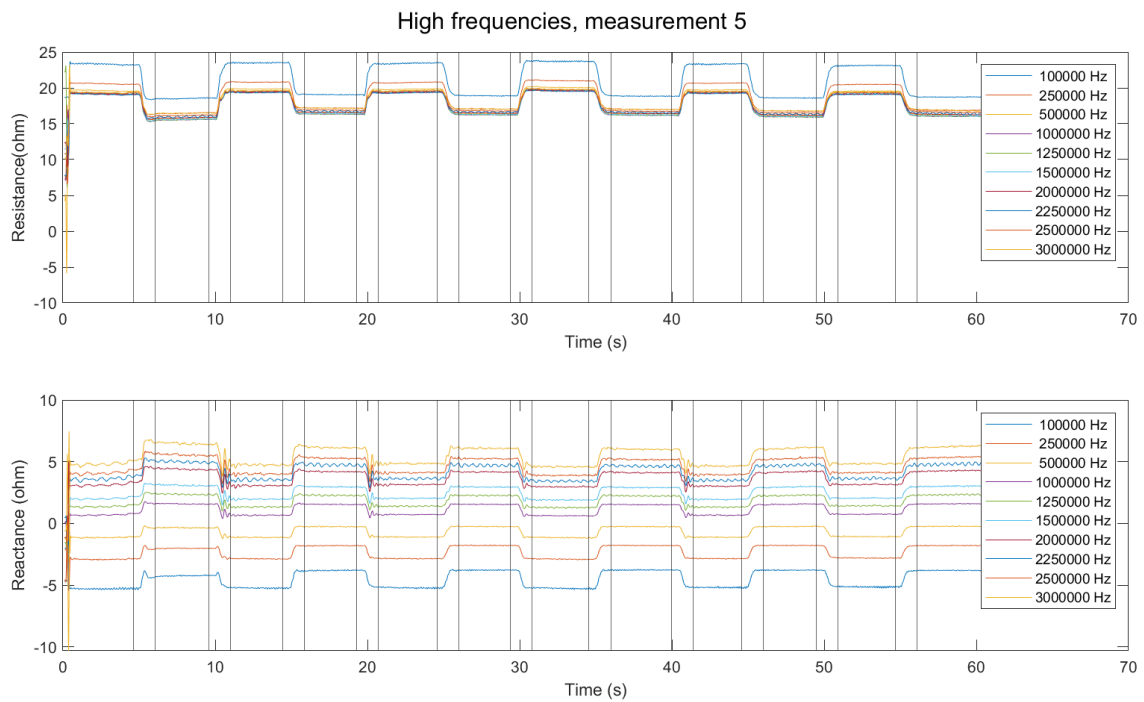


Figure C.17: The resistance and reactance of the bio-impedance measured during an isotonic movement at high frequencies. The second pattern as described in Section 3.3.1 is used.

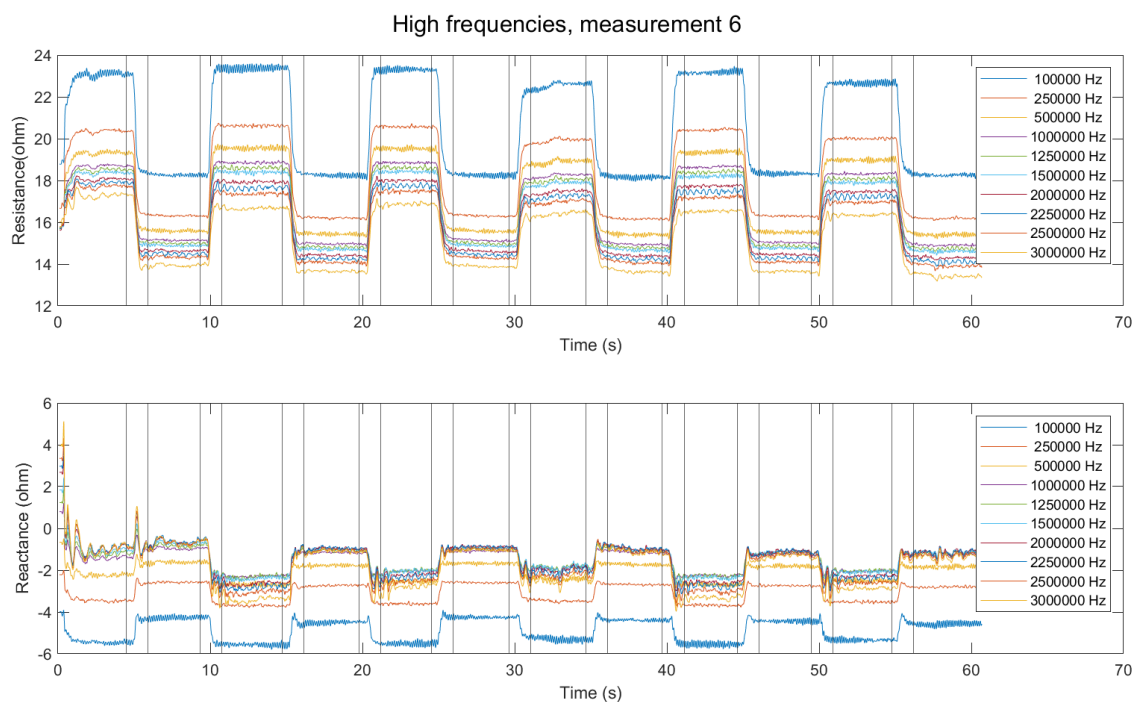


Figure C.18: The resistance and reactance of the bio-impedance measured during an isotonic movement at high frequencies. The second pattern as described in Section 3.3.1 is used.

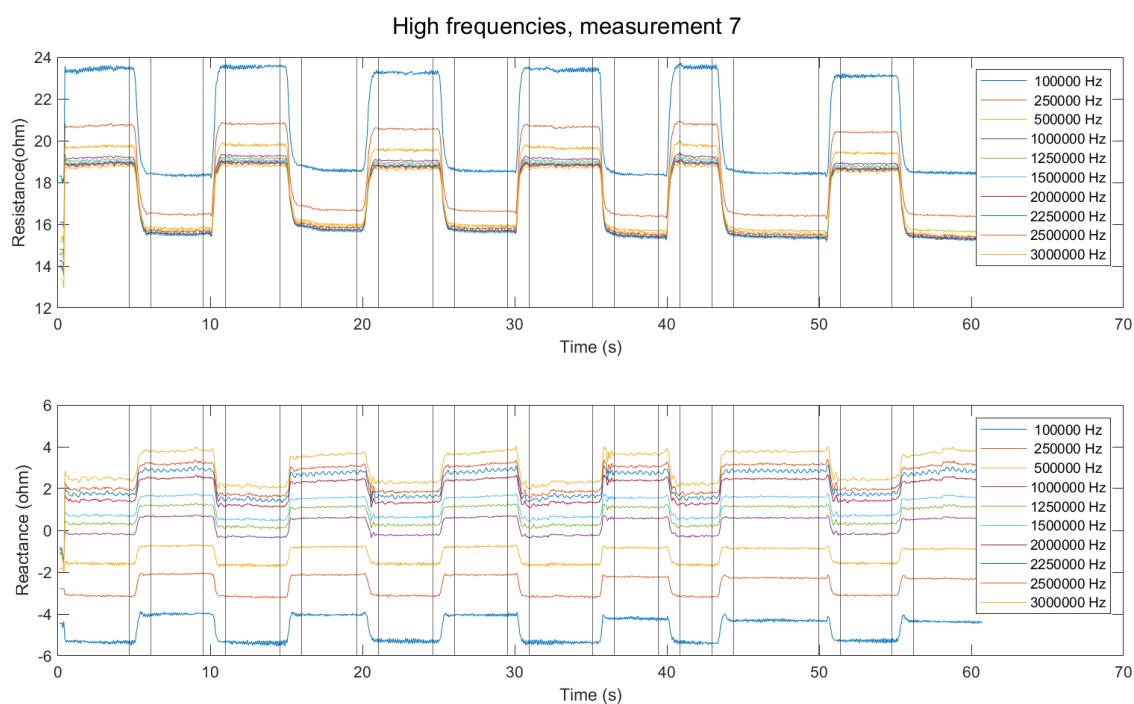


Figure C.19: The resistance and reactance of the bio-impedance measured during an isotonic movement at high frequencies. The second pattern as described in Section 3.3.1 is used.

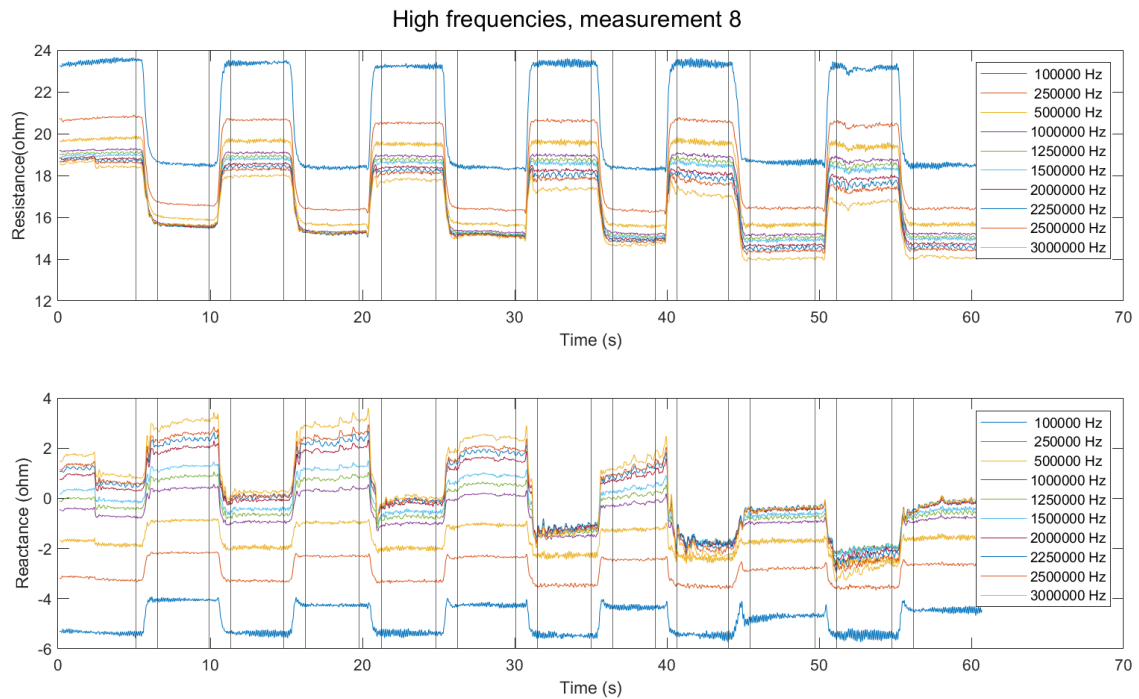


Figure C.20: The resistance and reactance of the bio-impedance measured during an isotonic movement at high frequencies. The second pattern as described in Section 3.3.1 is used.

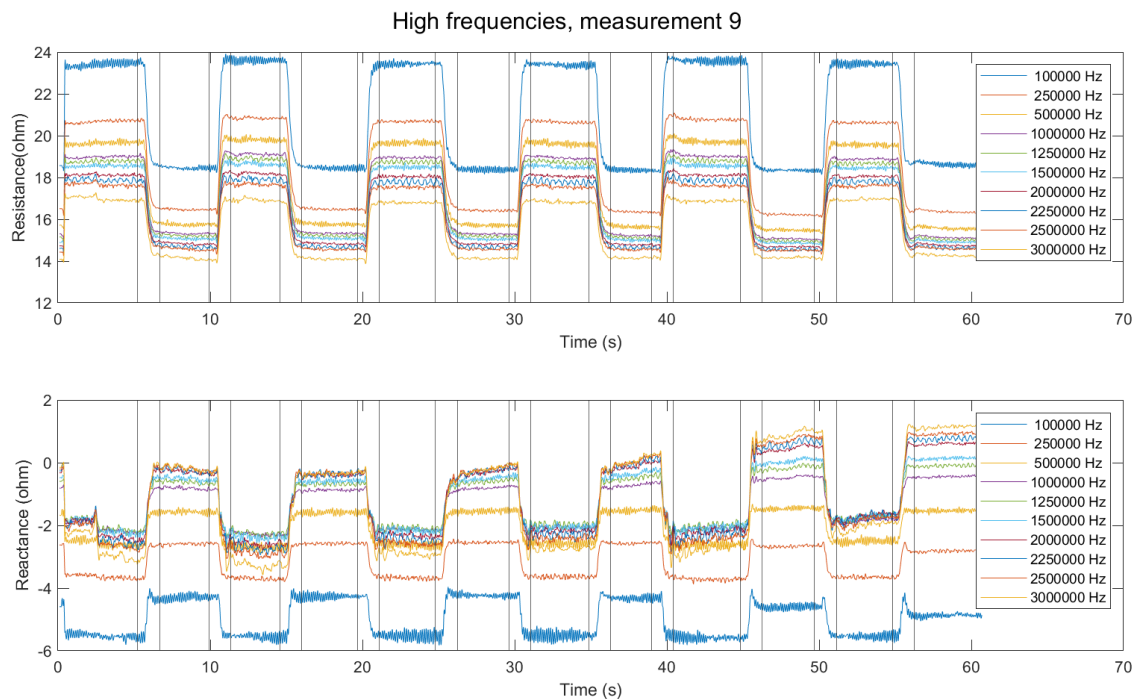


Figure C.21: The resistance and reactance of the bio-impedance measured during an isotonic movement at high frequencies. The second pattern as described in Section 3.3.1 is used.

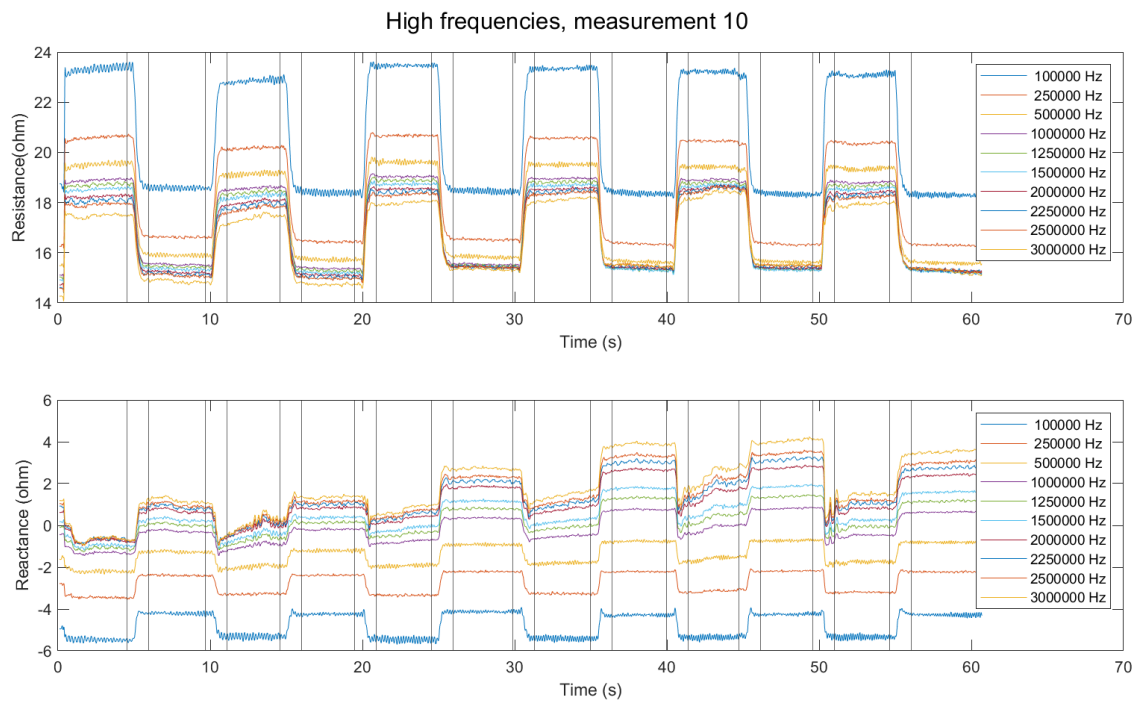


Figure C.22: The resistance and reactance of the bio-impedance measured during an isotonic movement at high frequencies. The second pattern as described in Section 3.3.1 is used.

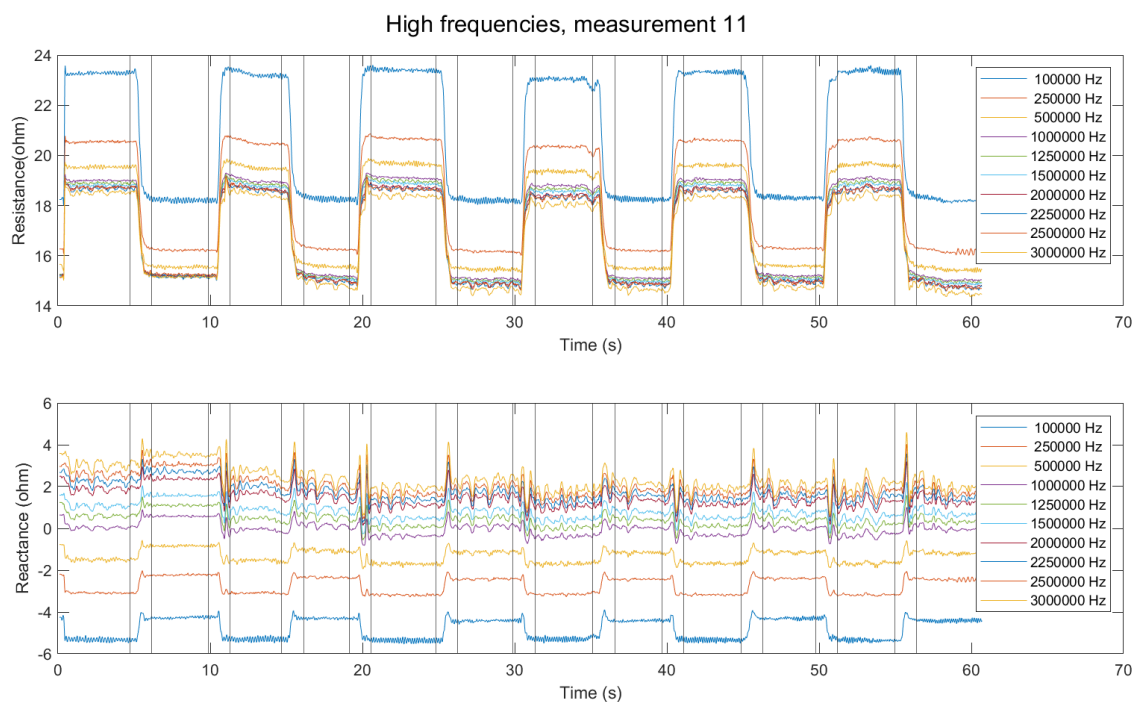


Figure C.23: The resistance and reactance of the bio-impedance measured during an isotonic movement at high frequencies. The second pattern as described in Section 3.3.1 is used.

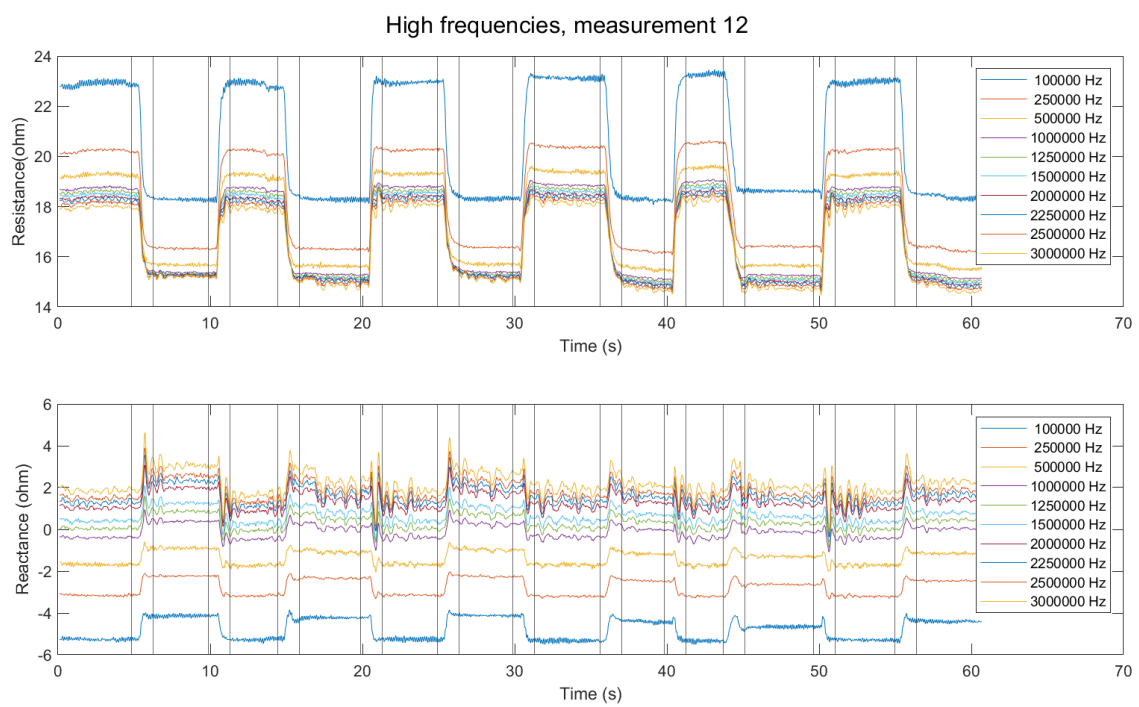


Figure C.24: The resistance and reactance of the bio-impedance measured during an isotonic movement at high frequencies. The second pattern as described in Section 3.3.1 is used.

D Cole fit parameters

Three different fitting algorithms are used, `fmincon`, `pattern search` and `lsqnonlin`. For each fitting algorithm one of the measured spectrum's is given with the corresponding fit.

D.1 `fmincon`

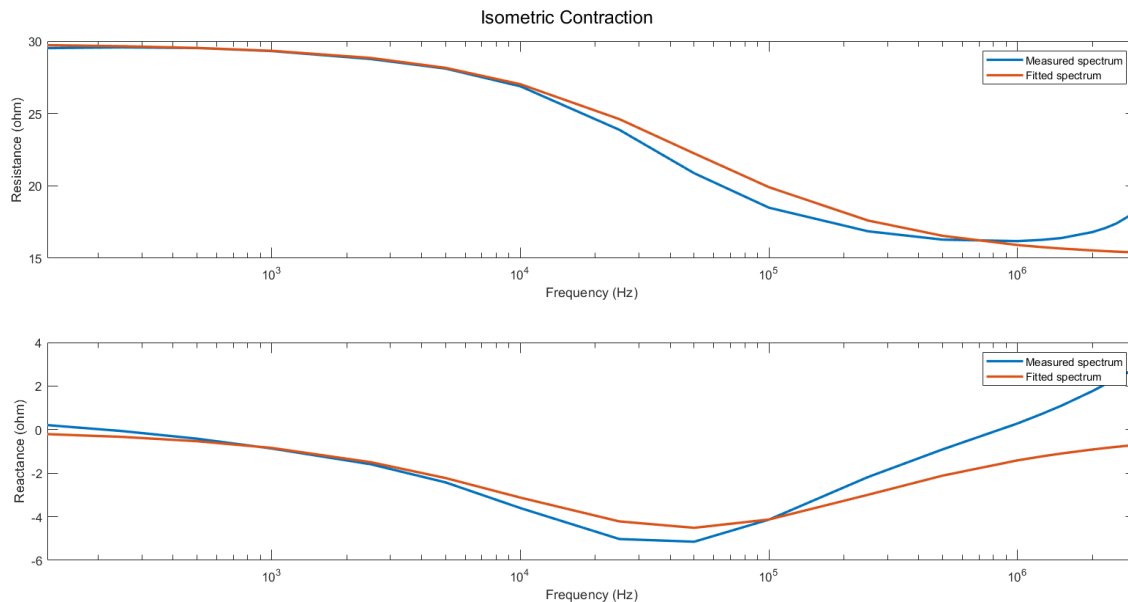


Figure D.1: The resistance and reactance of the bio-impedance. The measured data and the Cole fit of the measured data is given. The fitting algorithm used is `fmincon` [69].

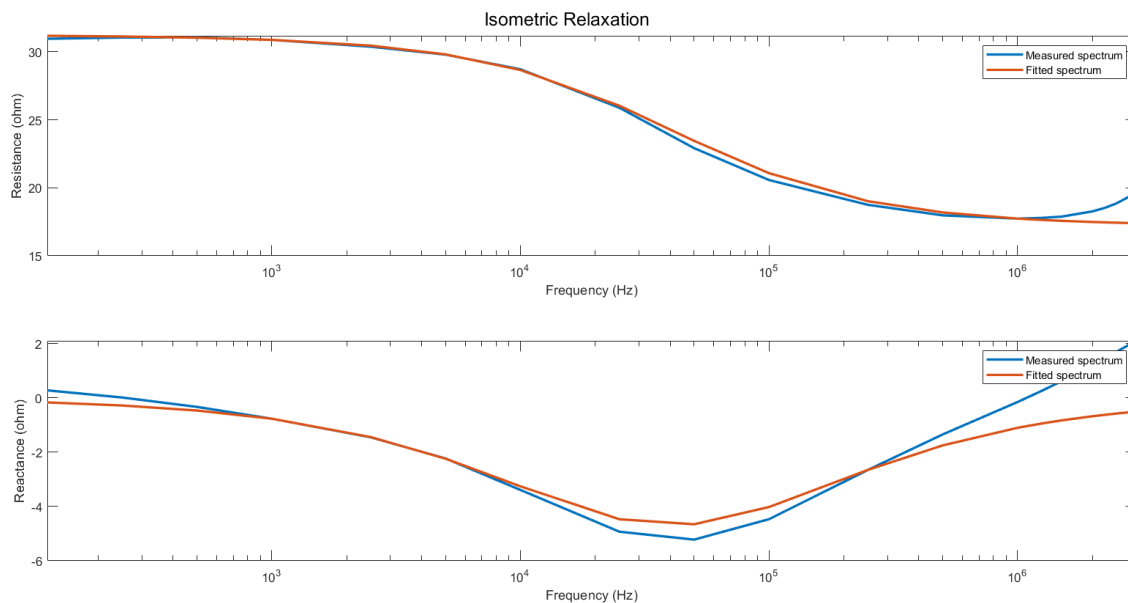


Figure D.2: The resistance and reactance of the bio-impedance. The measured data and the Cole fit of the measured data is given. The fitting algorithm used is `fmincon` [69].

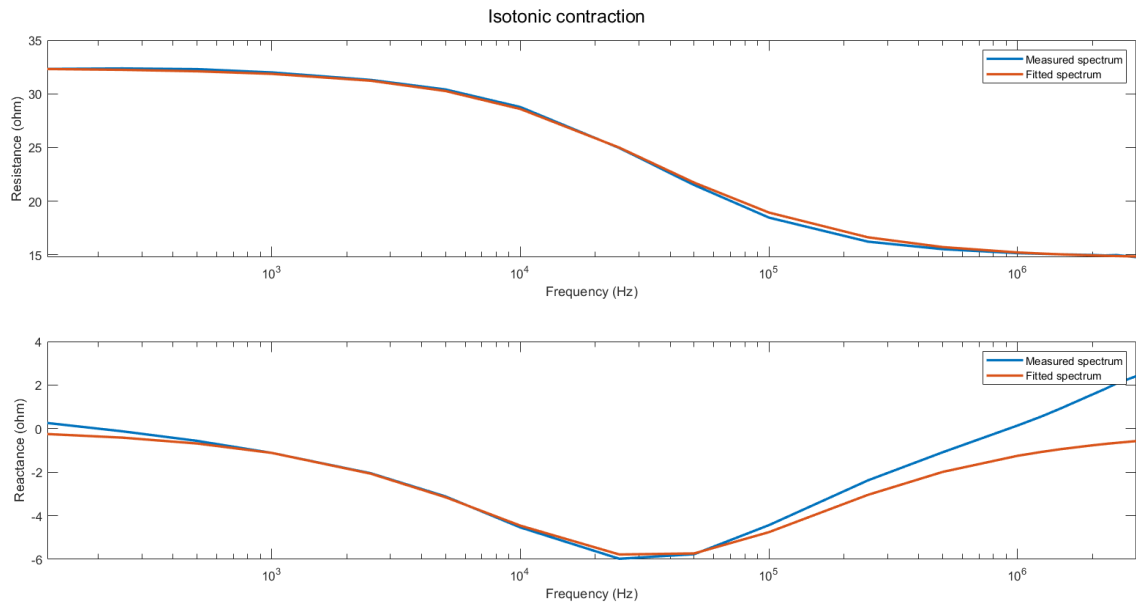


Figure D.3: The resistance and reactance of the bio-impedance. The measured data and the Cole fit of the measured data is given. The fitting algorithm used is `fmincon` [69].

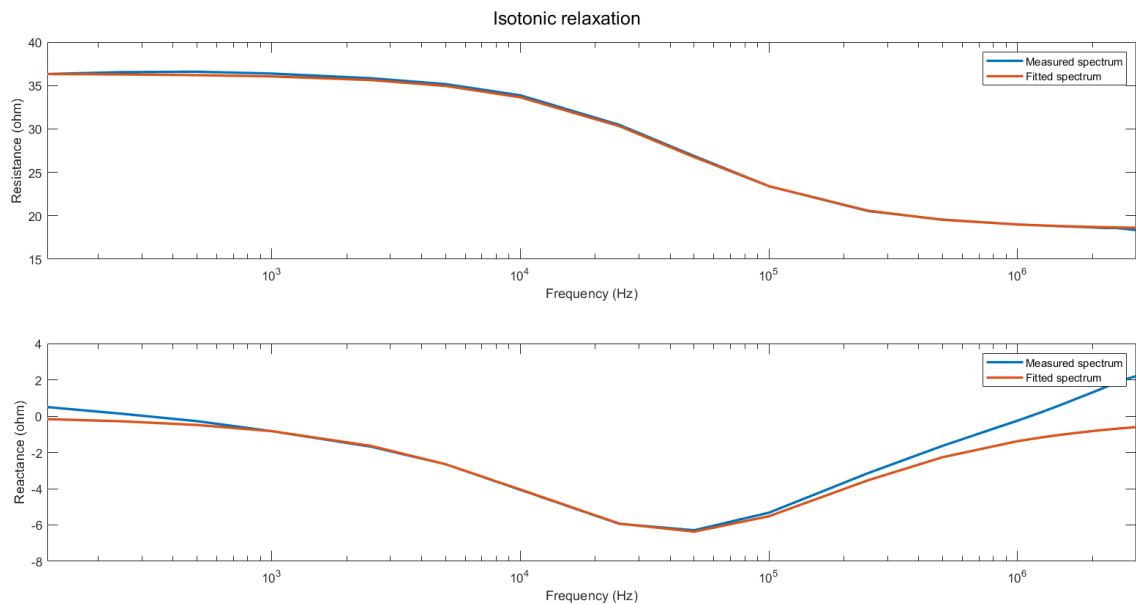


Figure D.4: The resistance and reactance of the bio-impedance. The measured data and the Cole fit of the measured data is given. The fitting algorithm used is `fmincon` [69].

D.2 Lsqnonlin

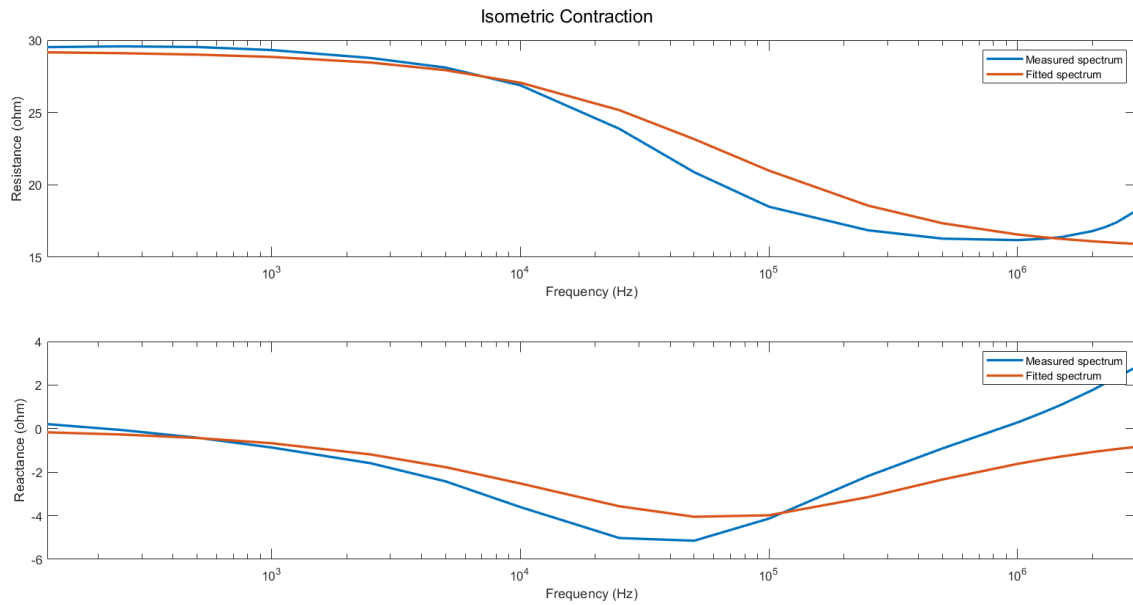


Figure D.5: The resistance and reactance of the bio-impedance. The measured data and the Cole fit of the measured data is given. The fitting algorithm used is `lsqnonlin` [59].

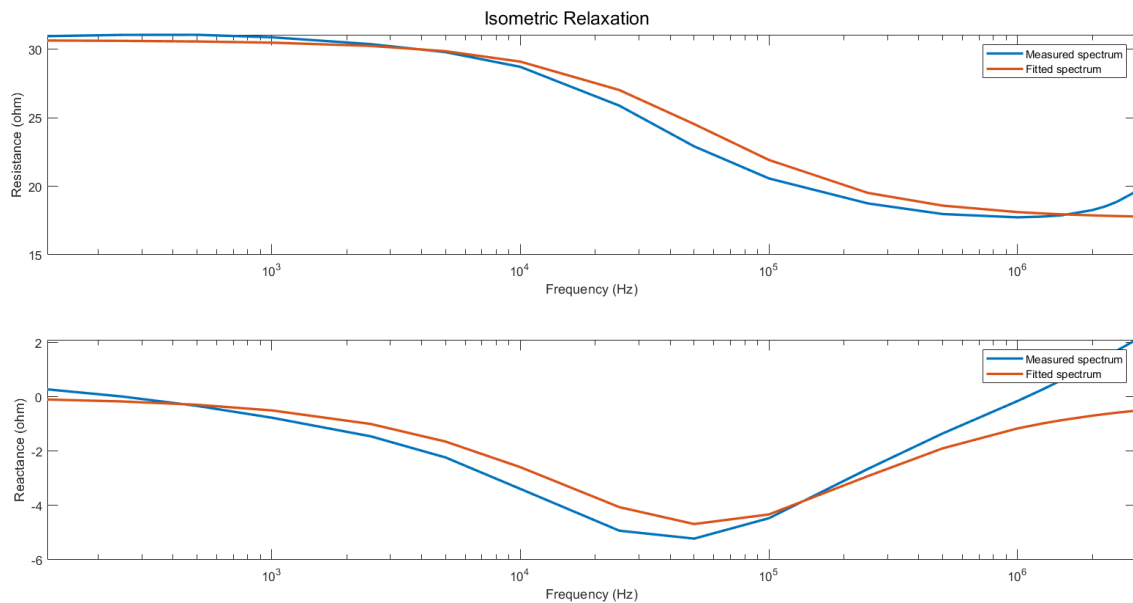


Figure D.6: The resistance and reactance of the bio-impedance. The measured data and the Cole fit of the measured data is given. The fitting algorithm used is `lsqnonlin` [59].

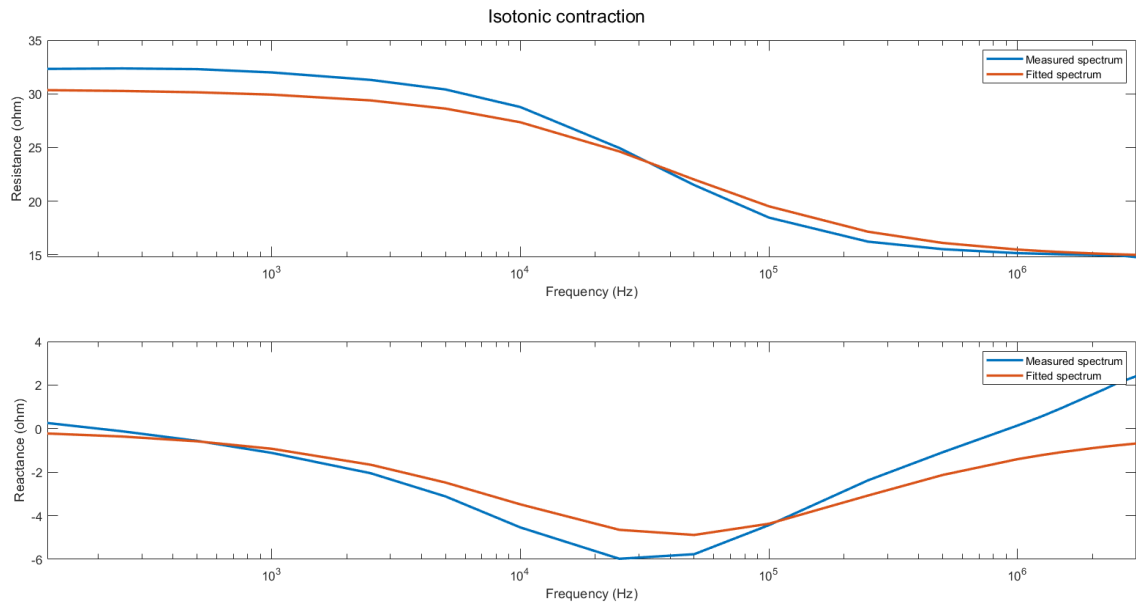


Figure D.7: The resistance and reactance of the bio-impedance. The measured data and the Cole fit of the measured data is given. The fitting algorithm used is `lsqnonlin` [59].

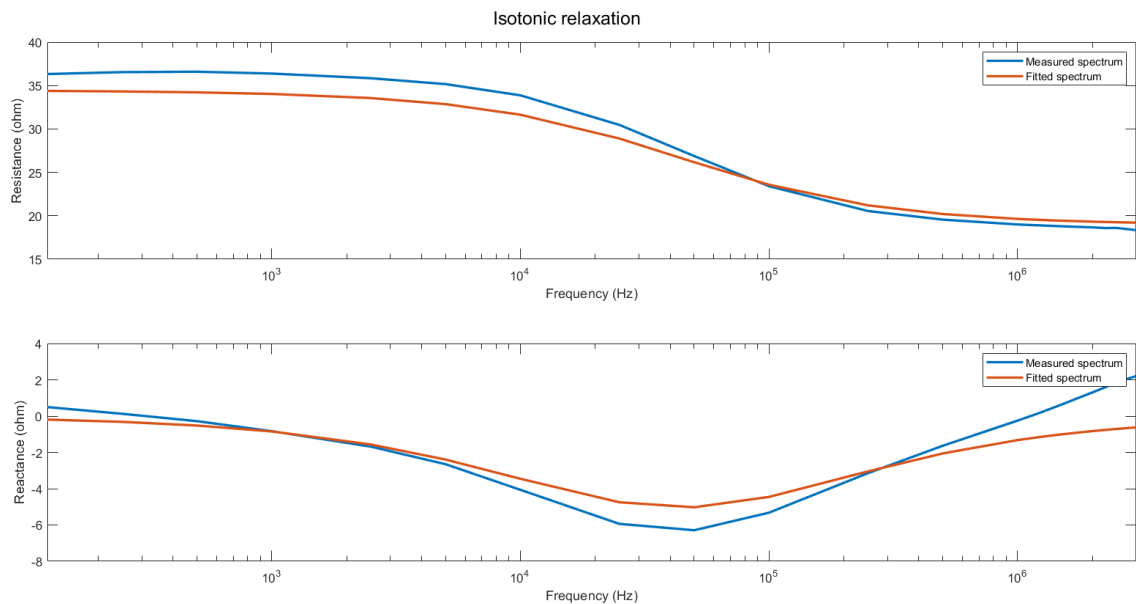


Figure D.8: The resistance and reactance of the bio-impedance. The measured data and the Cole fit of the measured data is given. The fitting algorithm used is `lsqnonlin` [59].

D.3 Pattern search

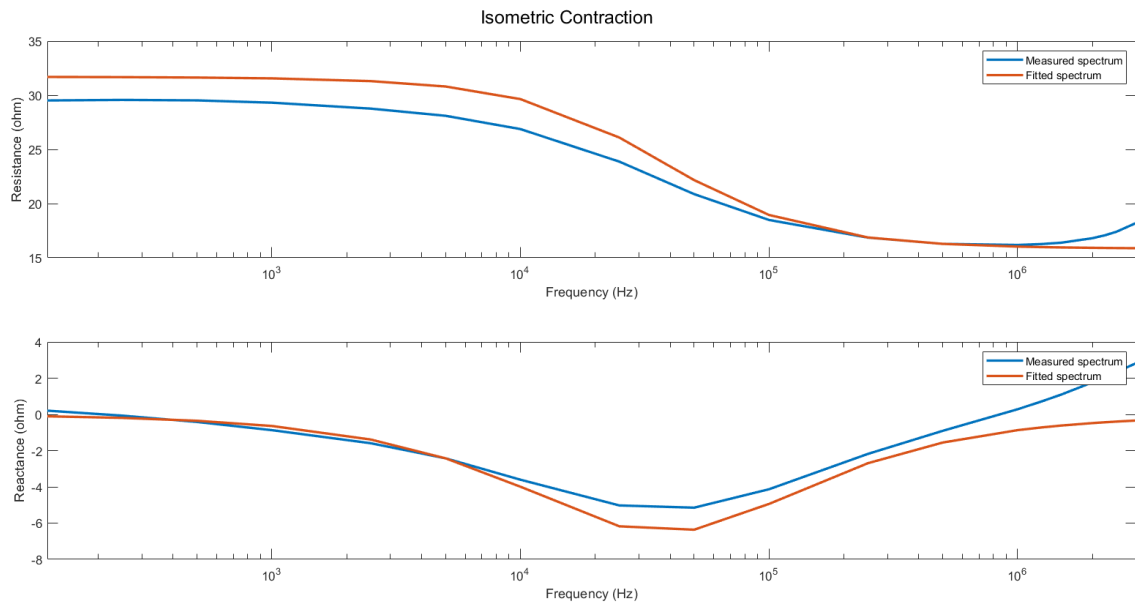


Figure D.9: The resistance and reactance of the bio-impedance. The measured data and the Cole fit of the measured data is given. The fitting algorithm used is `pattern search` [62].

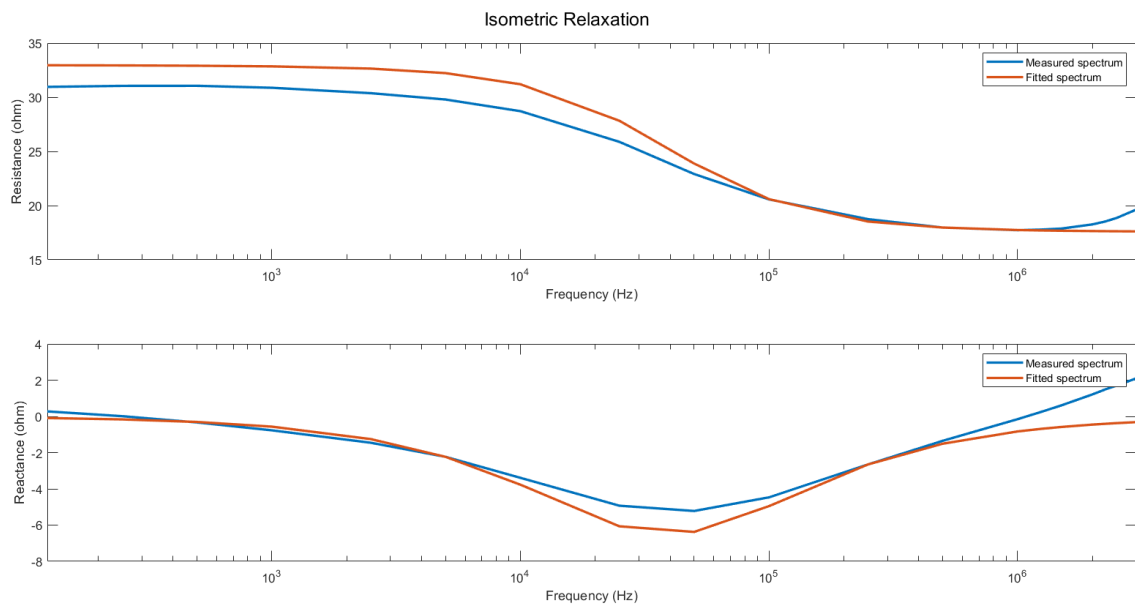


Figure D.10: The resistance and reactance of the bio-impedance. The measured data and the Cole fit of the measured data is given. The fitting algorithm used is `pattern search` [62].

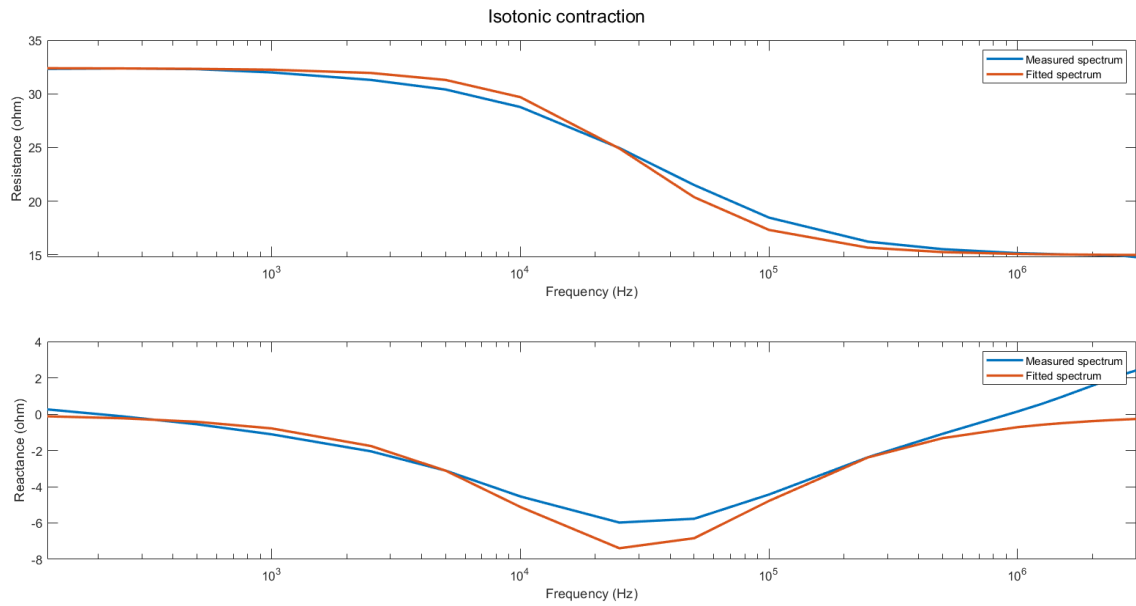


Figure D.11: The resistance and reactance of the bio-impedance. The measured data and the Cole fit of the measured data is given. The fitting algorithm used is `pattern search` [62].

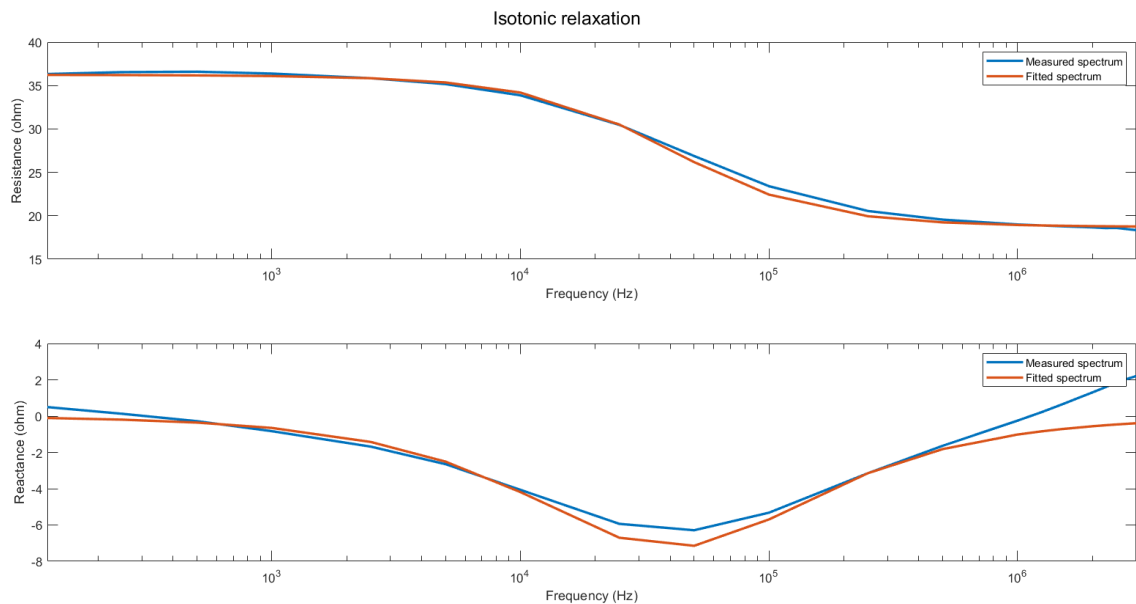


Figure D.12: The resistance and reactance of the bio-impedance. The measured data and the Cole fit of the measured data is given. The fitting algorithm used is `pattern search` [62].

E Movement pattern 3 data

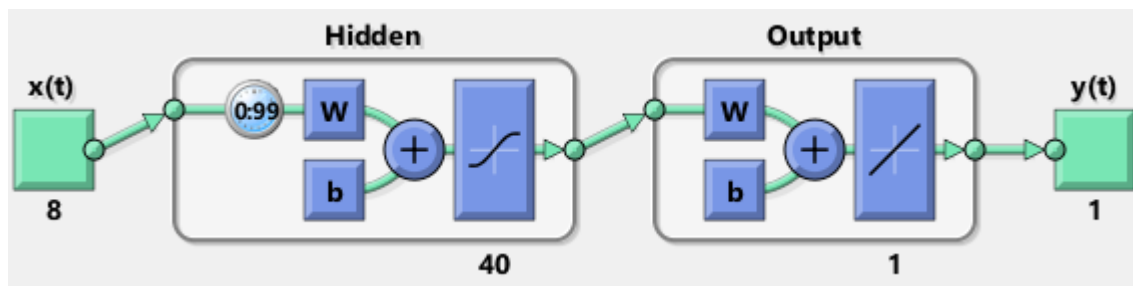


Figure E.1: A visual representation of the used NN created in Matlab. This network has $x = 8$ inputs, $y = 1$ output, $z = 100$ time delays, $n = 1$ hidden layer and $m = 40$ neurons in this hidden layer.



Figure E.2: Top figure: the target and the output of the time delay Neural network. Middle figure: the 4 measured resistances, which are 4 of the 8 inputs for the NN. Bottom figure: the 4 measured reactances, which form the other 4 of 8 inputs for the NN. The measurement is done while movement pattern 3 (Figure 3.10) is performed from state “A” to “F”.

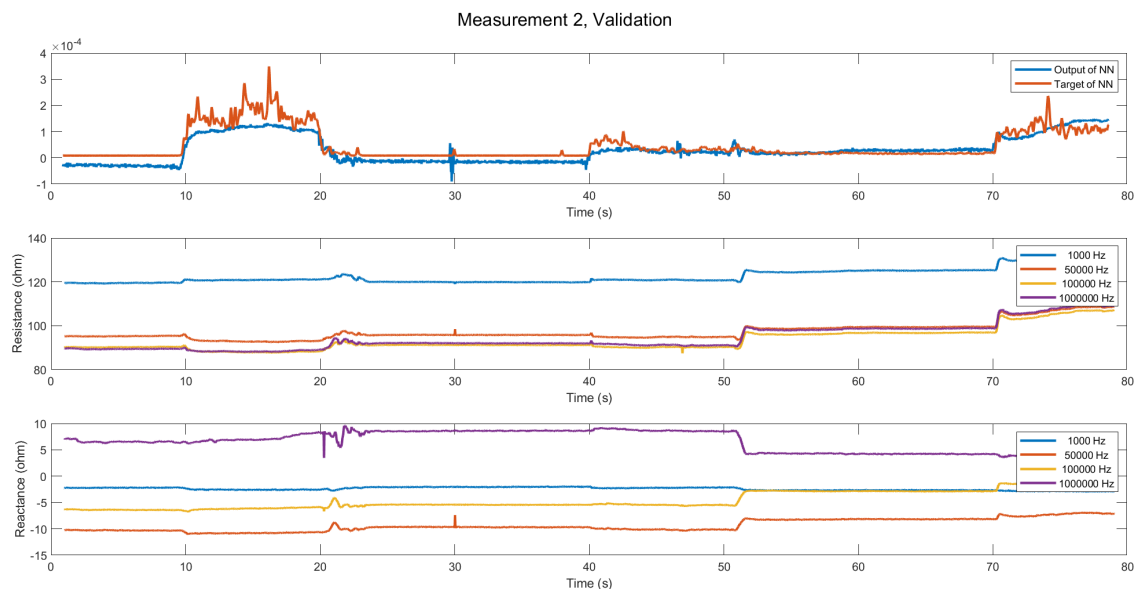


Figure E.3: Top figure: the target and the output of the time delay Neural network. Middle figure: the 4 measured resistances, which are 4 of the 8 inputs for the NN. Bottom figure: the 4 measured reactances, which form the other 4 of 8 inputs for the NN. The measurement is done while movement pattern 3 (Figure 3.10) is performed from state “A” to “F”.

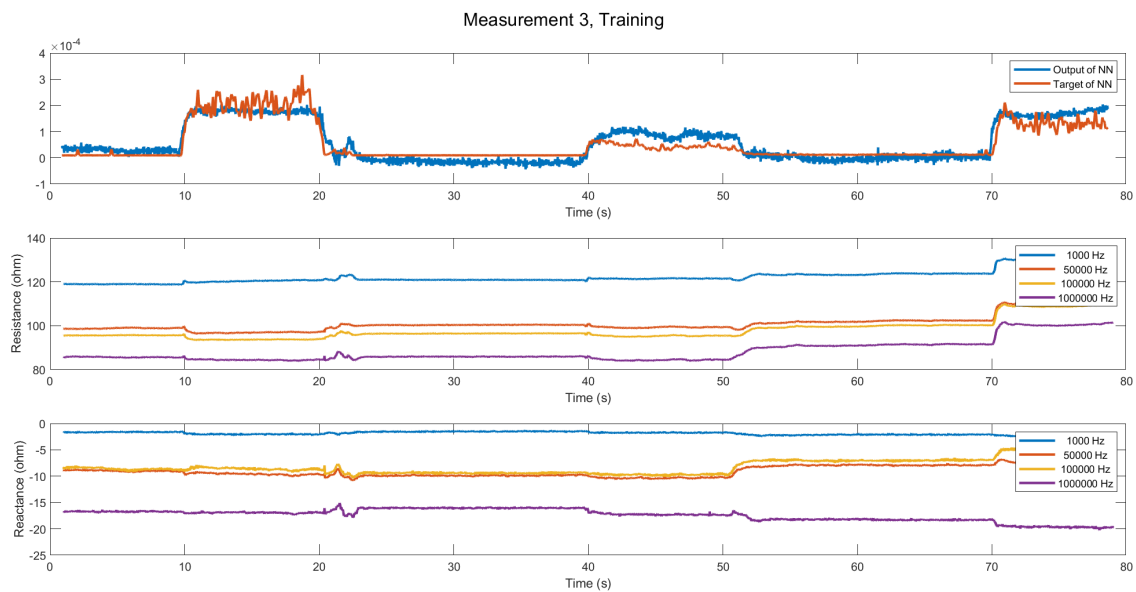


Figure E.4: Top figure: the target and the output of the time delay Neural network. Middle figure: the 4 measured resistances, which are 4 of the 8 inputs for the NN. Bottom figure: the 4 measured reactances, which form the other 4 of 8 inputs for the NN. The measurement is done while movement pattern 3 (Figure 3.10) is performed from state “A” to “F”.

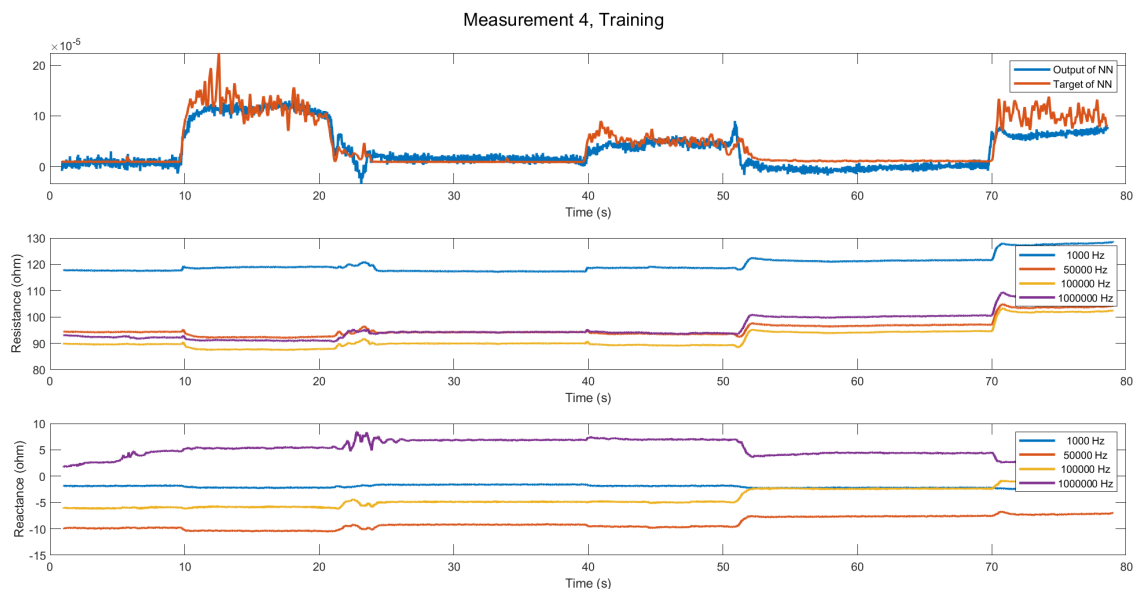


Figure E.5: Top figure: the target and the output of the time delay Neural network. Middle figure: the 4 measured resistances, which are 4 of the 8 inputs for the NN. Bottom figure: the 4 measured reactances, which form the other 4 of 8 inputs for the NN. The measurement is done while movement pattern 3 (Figure 3.10) is performed from state “A” to “F”.

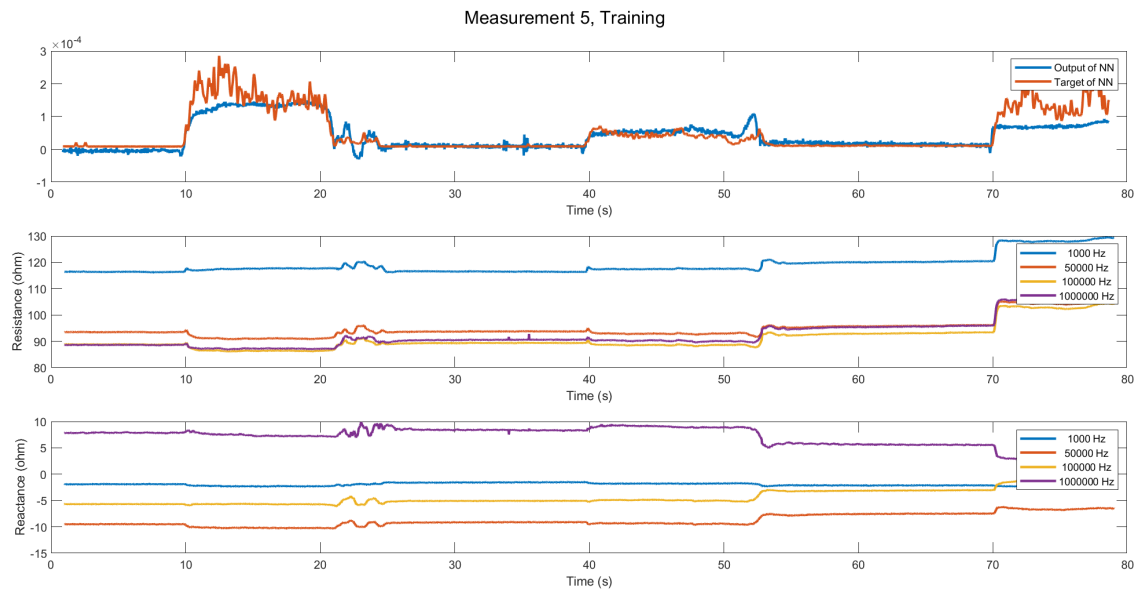


Figure E.6: Top figure: the target and the output of the time delay Neural network. Middle figure: the 4 measured resistances, which are 4 of the 8 inputs for the NN. Bottom figure: the 4 measured reactances, which form the other 4 of 8 inputs for the NN. The measurement is done while movement pattern 3 (Figure 3.10) is performed from state “A” to “F”.

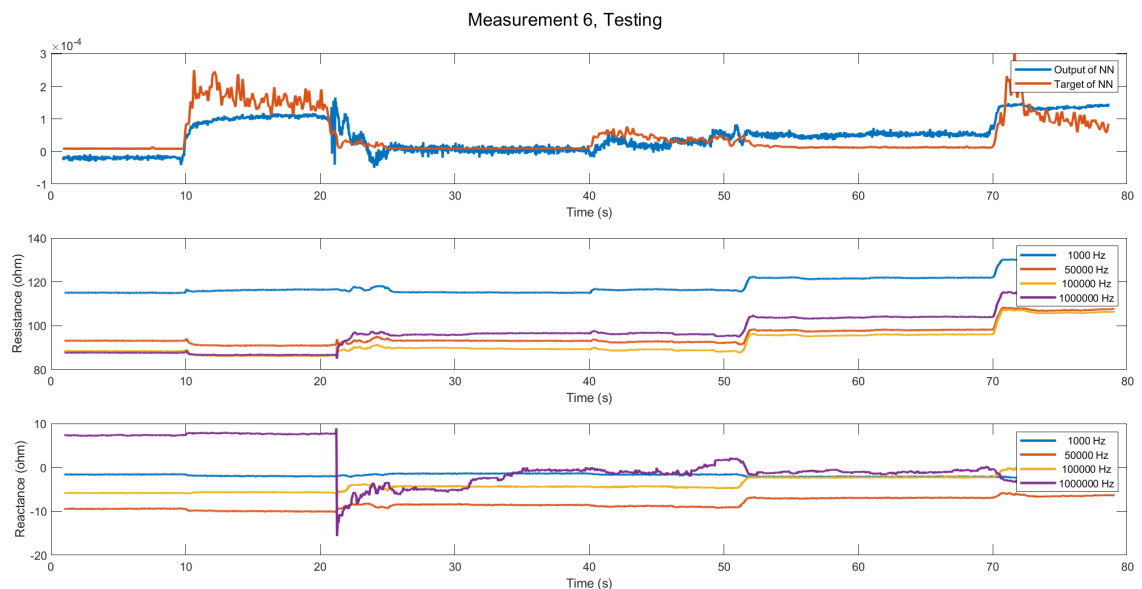


Figure E.7: Top figure: the target and the output of the time delay Neural network. Middle figure: the 4 measured resistances, which are 4 of the 8 inputs for the NN. Bottom figure: the 4 measured reactances, which form the other 4 of 8 inputs for the NN. The measurement is done while movement pattern 3 (Figure 3.10) is performed from state “A” to “F”.

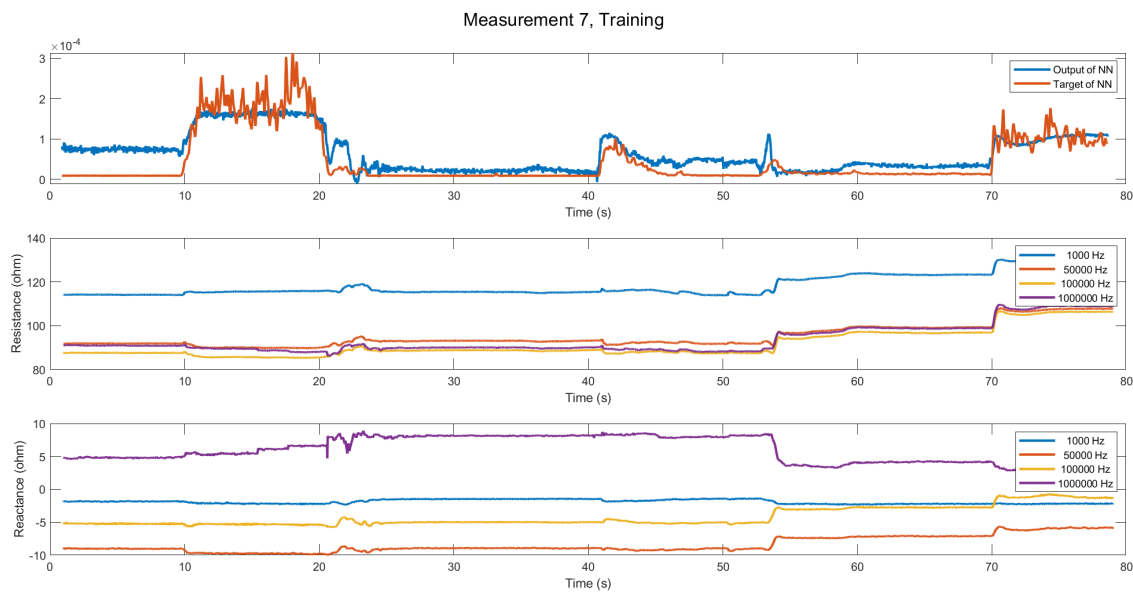


Figure E.8: Top figure: the target and the output of the time delay Neural network. Middle figure: the 4 measured resistances, which are 4 of the 8 inputs for the NN. Bottom figure: the 4 measured reactances, which form the other 4 of 8 inputs for the NN. The measurement is done while movement pattern 3 (Figure 3.10) is performed from state “A” to “F”.

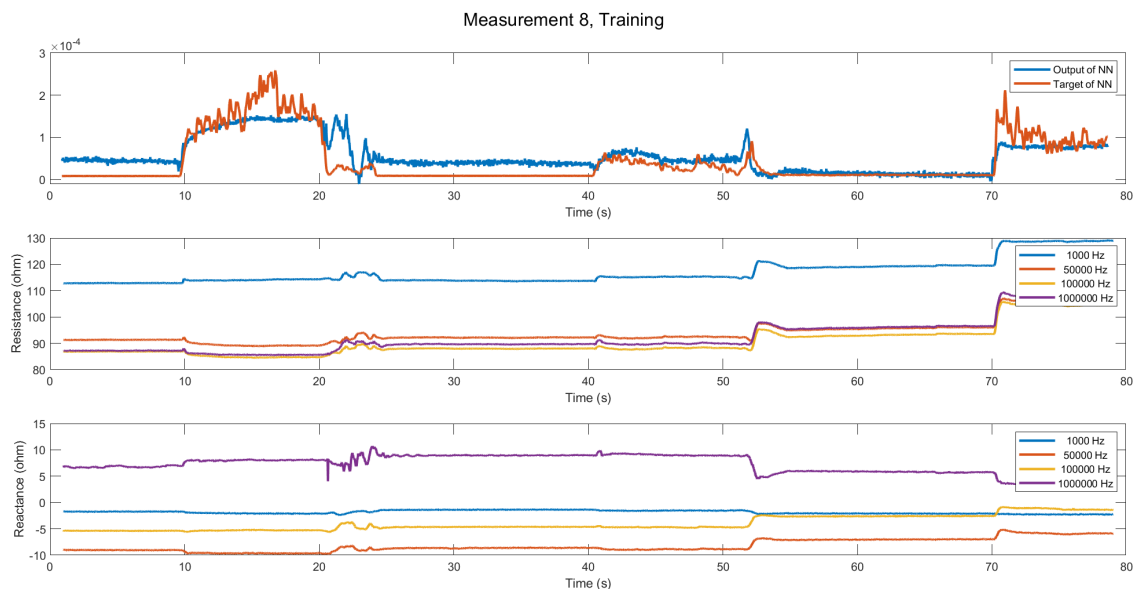


Figure E.9: Top figure: the target and the output of the time delay Neural network. Middle figure: the 4 measured resistances, which are 4 of the 8 inputs for the NN. Bottom figure: the 4 measured reactances, which form the other 4 of 8 inputs for the NN. The measurement is done while movement pattern 3 (Figure 3.10) is performed from state “A” to “F”.

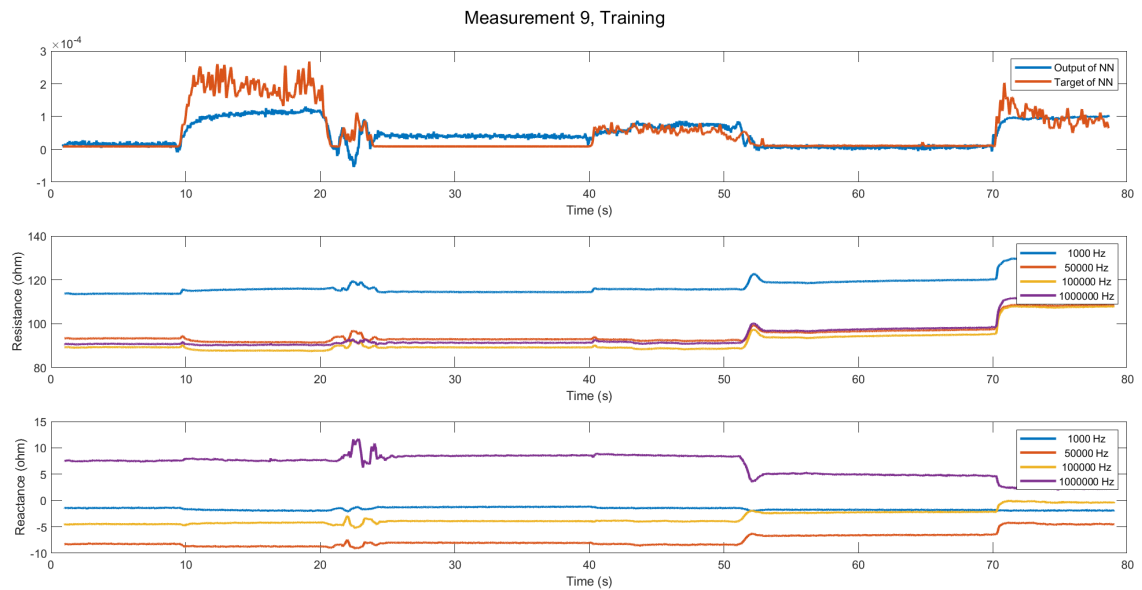


Figure E.10: Top figure: the target and the output of the time delay Neural network. Middle figure: the 4 measured resistances, which are 4 of the 8 inputs for the NN. Bottom figure: the 4 measured reactances, which form the other 4 of 8 inputs for the NN. The measurement is done while movement pattern 3 (Figure 3.10) is performed from state “A” to “F”.

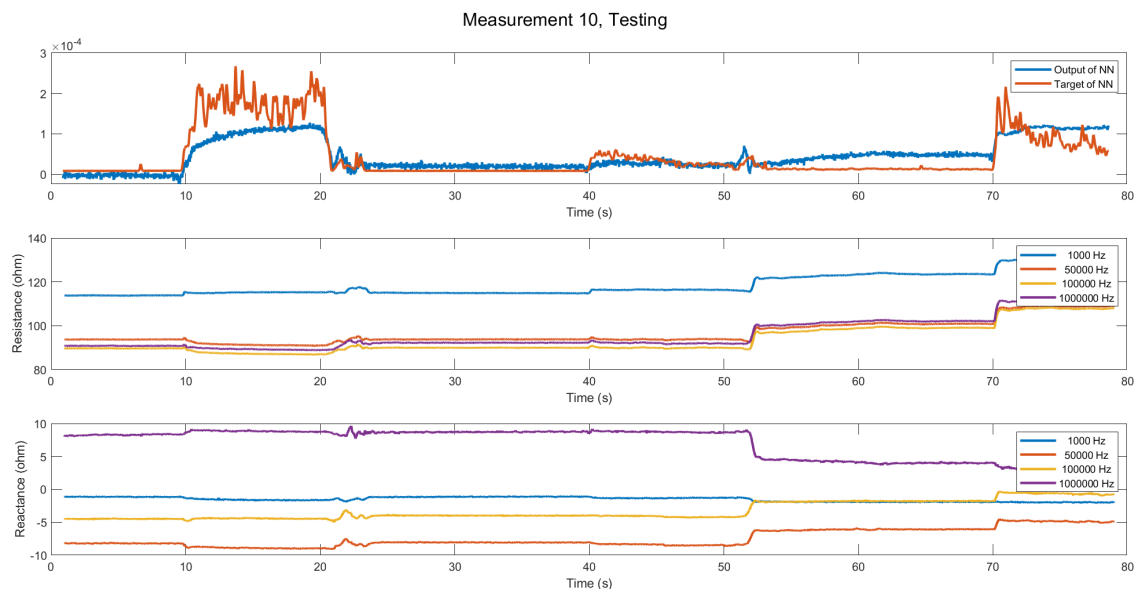


Figure E.11: Top figure: the target and the output of the time delay Neural network. Middle figure: the 4 measured resistances, which are 4 of the 8 inputs for the NN. Bottom figure: the 4 measured reactances, which form the other 4 of 8 inputs for the NN. The measurement is done while movement pattern 3 (Figure 3.10) is performed from state “A” to “F”.



Figure E.12: Top figure: the target and the output of the time delay Neural network. Middle figure: the 4 measured resistances, which are 4 of the 8 inputs for the NN. Bottom figure: the 4 measured reactances, which form the other 4 of 8 inputs for the NN. The measurement is done while movement pattern 3 (Figure 3.10) is performed from state “A” to “F”.

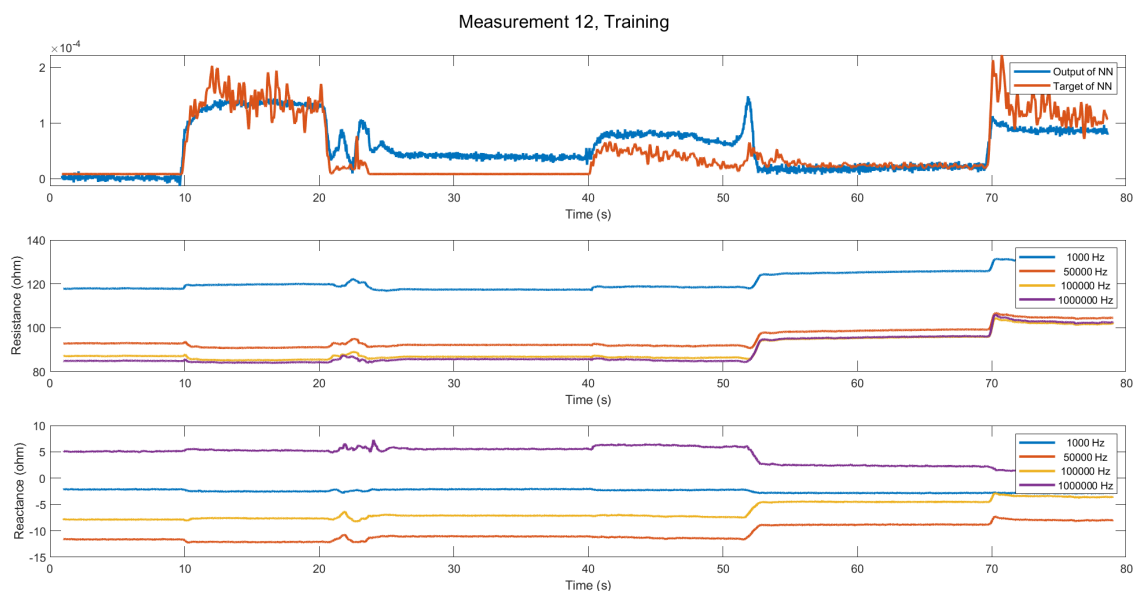


Figure E.13: Top figure: the target and the output of the time delay Neural network. Middle figure: the 4 measured resistances, which are 4 of the 8 inputs for the NN. Bottom figure: the 4 measured reactances, which form the other 4 of 8 inputs for the NN. The measurement is done while movement pattern 3 (Figure 3.10) is performed from state “A” to “F”.

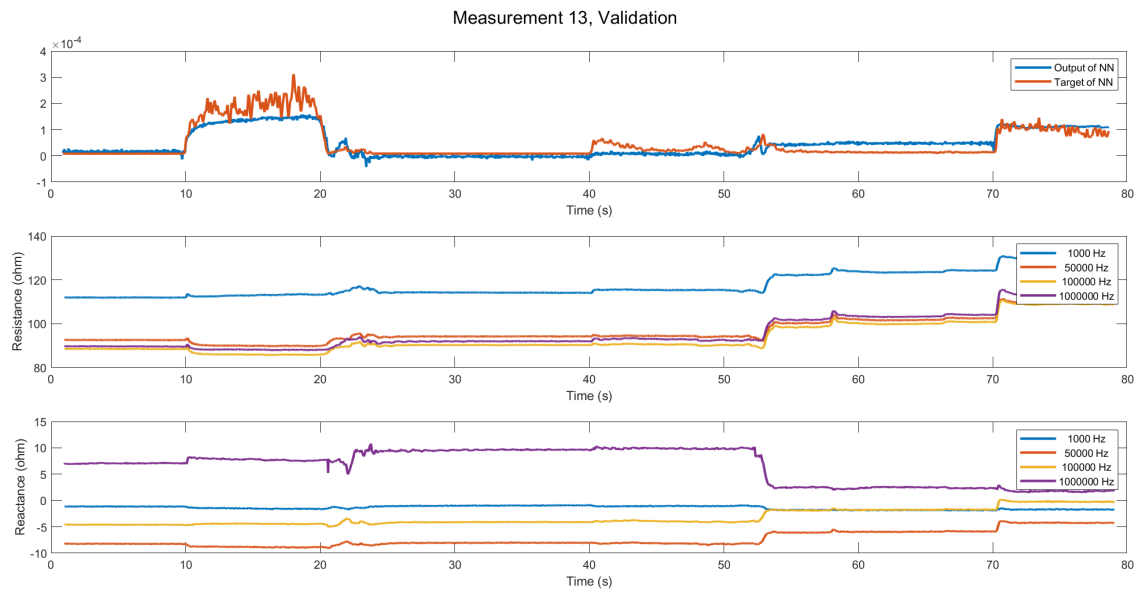


Figure E.14: Top figure: the target and the output of the time delay Neural network. Middle figure: the 4 measured resistances, which are 4 of the 8 inputs for the NN. Bottom figure: the 4 measured reactances, which form the other 4 of 8 inputs for the NN. The measurement is done while movement pattern 3 (Figure 3.10) is performed from state “A” to “F”.

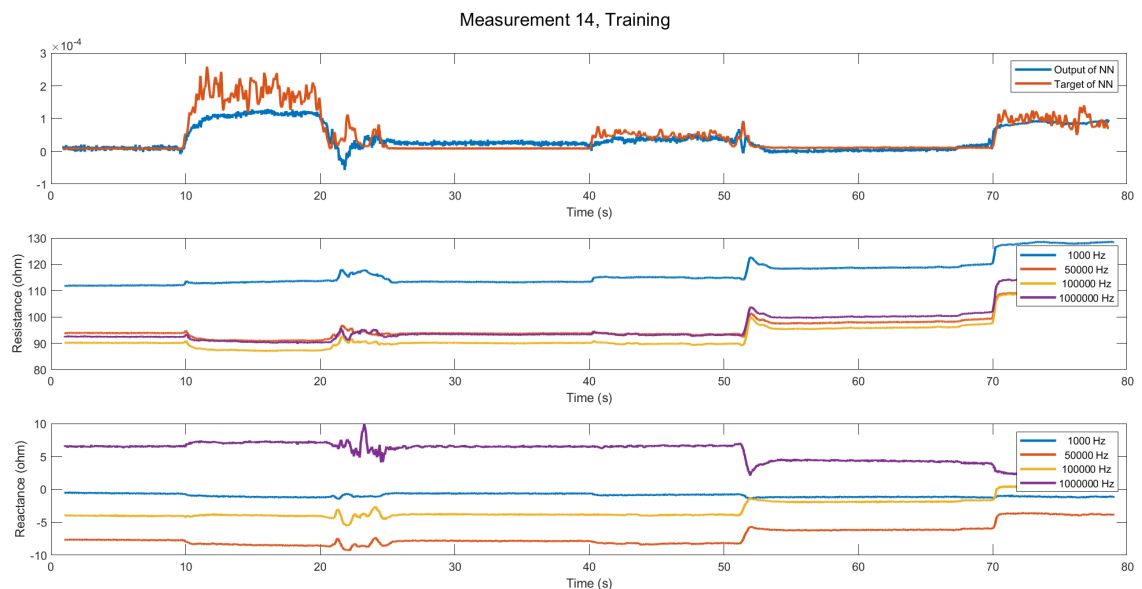


Figure E.15: Top figure: the target and the output of the time delay Neural network. Middle figure: the 4 measured resistances, which are 4 of the 8 inputs for the NN. Bottom figure: the 4 measured reactances, which form the other 4 of 8 inputs for the NN. The measurement is done while movement pattern 3 (Figure 3.10) is performed from state “A” to “F”.

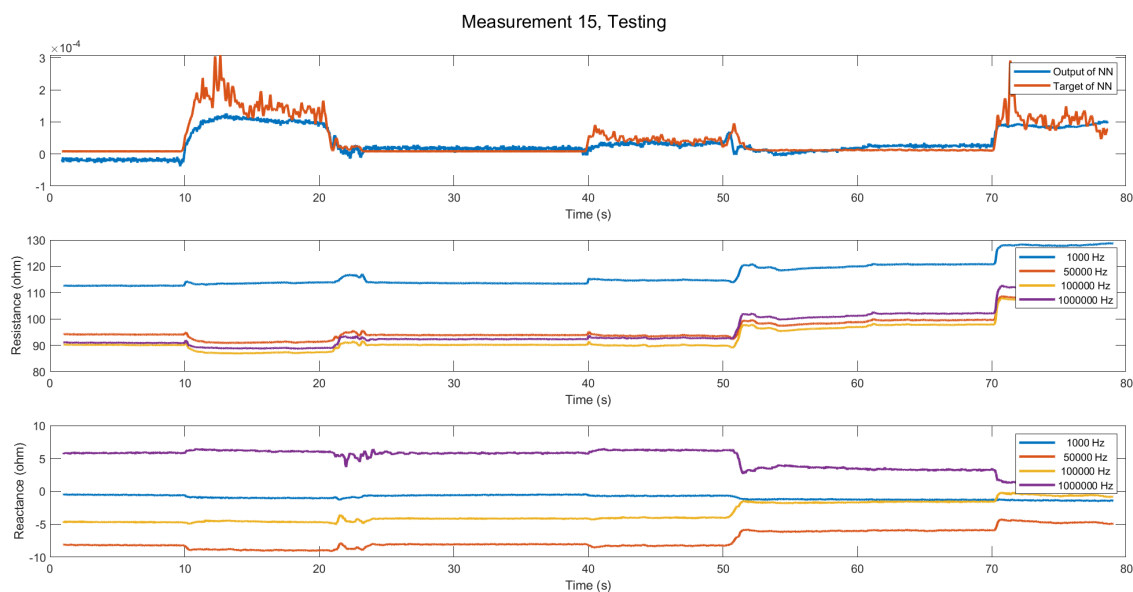


Figure E.16: Top figure: the target and the output of the time delay Neural network. Middle figure: the 4 measured resistances, which are 4 of the 8 inputs for the NN. Bottom figure: the 4 measured reactances, which form the other 4 of 8 inputs for the NN. The measurement is done while movement pattern 3 (Figure 3.10) is performed from state “A” to “F”.

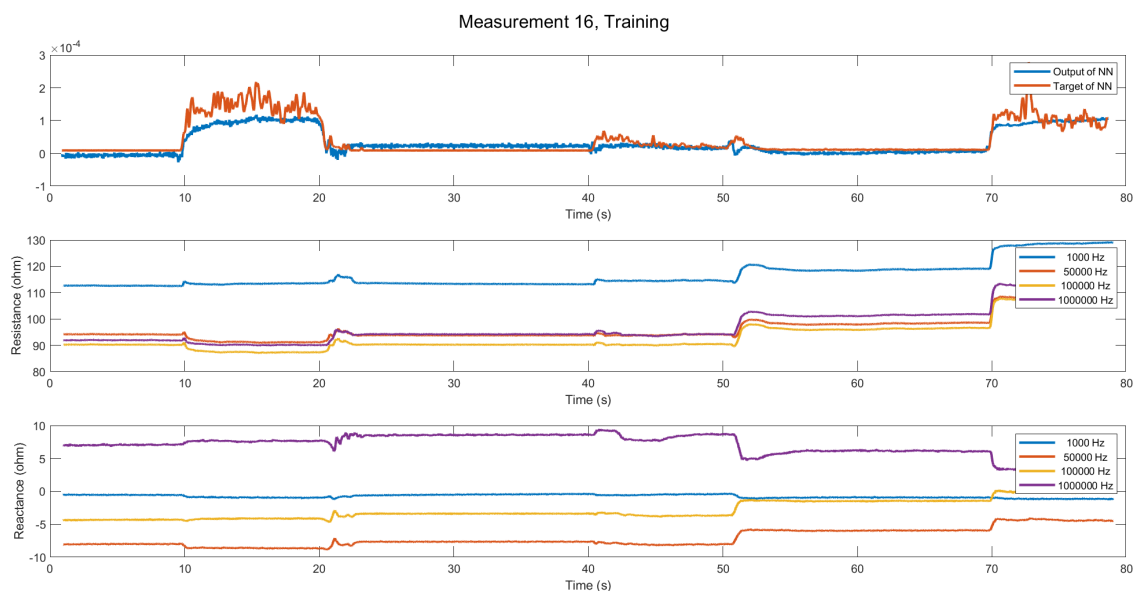


Figure E.17: Top figure: the target and the output of the time delay Neural network. Middle figure: the 4 measured resistances, which are 4 of the 8 inputs for the NN. Bottom figure: the 4 measured reactances, which form the other 4 of 8 inputs for the NN. The measurement is done while movement pattern 3 (Figure 3.10) is performed from state “A” to “F”.



Figure E.18: Top figure: the target and the output of the time delay Neural network. Middle figure: the 4 measured resistances, which are 4 of the 8 inputs for the NN. Bottom figure: the 4 measured reactances, which form the other 4 of 8 inputs for the NN. The measurement is done while movement pattern 3 (Figure 3.10) is performed from state “A” to “F”.

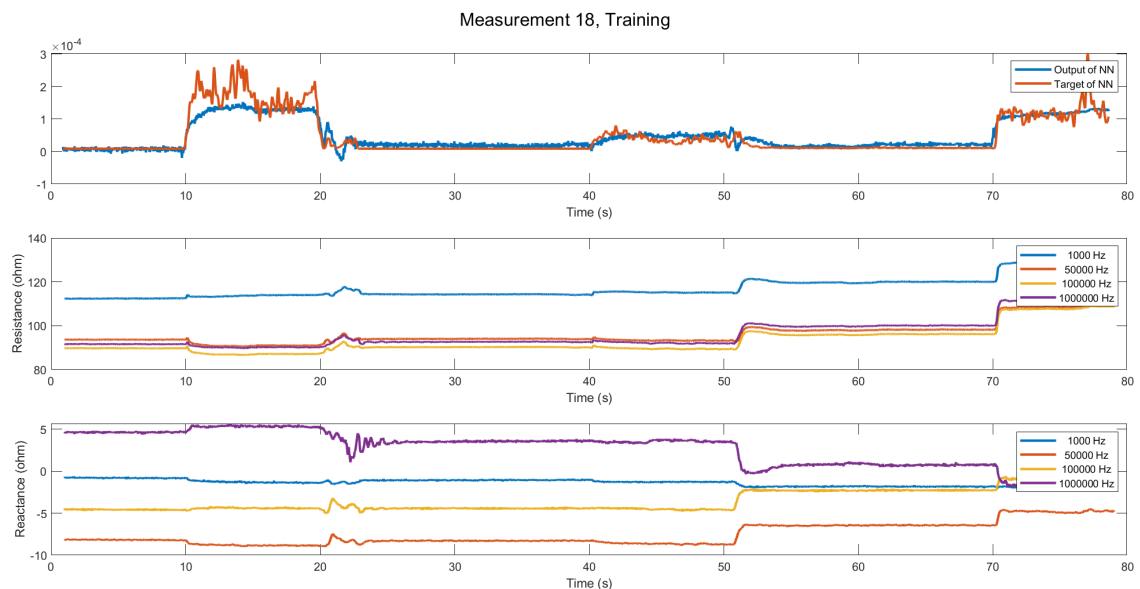


Figure E.19: Top figure: the target and the output of the time delay Neural network. Middle figure: the 4 measured resistances, which are 4 of the 8 inputs for the NN. Bottom figure: the 4 measured reactances, which form the other 4 of 8 inputs for the NN. The measurement is done while movement pattern 3 (Figure 3.10) is performed from state “A” to “F”.

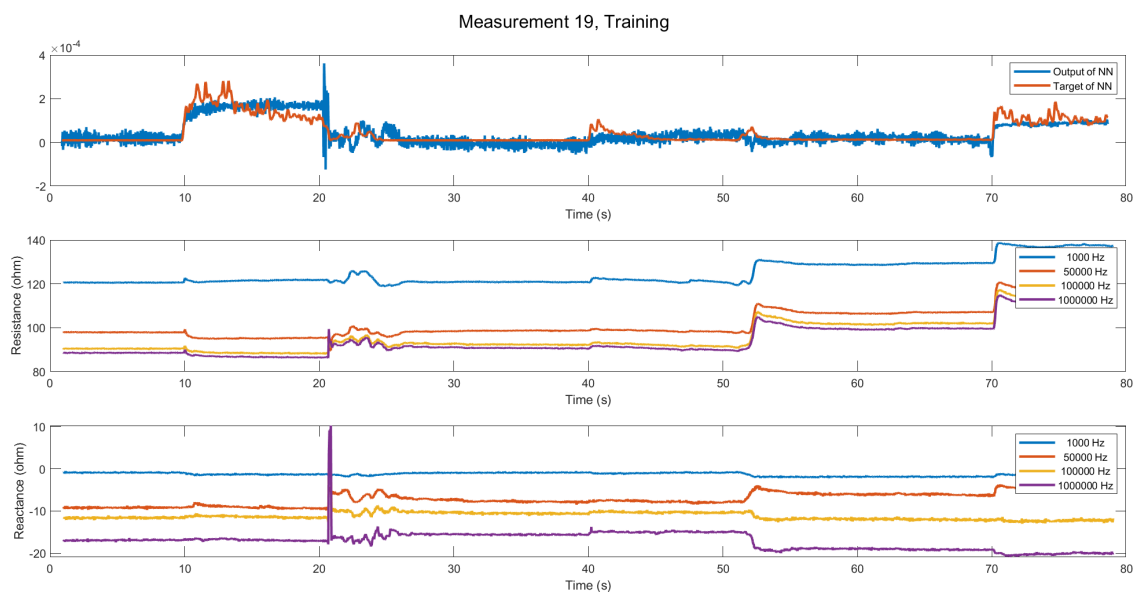


Figure E.20: Top figure: the target and the output of the time delay Neural network. Middle figure: the 4 measured resistances, which are 4 of the 8 inputs for the NN. Bottom figure: the 4 measured reactances, which form the other 4 of 8 inputs for the NN. The measurement is done while movement pattern 3 (Figure 3.10) is performed from state “A” to “F”.



Figure E.21: Top figure: the target and the output of the time delay Neural network. Middle figure: the 4 measured resistances, which are 4 of the 8 inputs for the NN. Bottom figure: the 4 measured reactances, which form the other 4 of 8 inputs for the NN. The measurement is done while movement pattern 3 (Figure 3.10) is performed from state “A” to “F”.



Figure E.22: Top figure: the target and the output of the time delay Neural network. Middle figure: the 4 measured resistances, which are 4 of the 8 inputs for the NN. Bottom figure: the 4 measured reactances, which form the other 4 of 8 inputs for the NN. The measurement is done while movement pattern 3 (Figure 3.10) is performed from state "A" to "F".

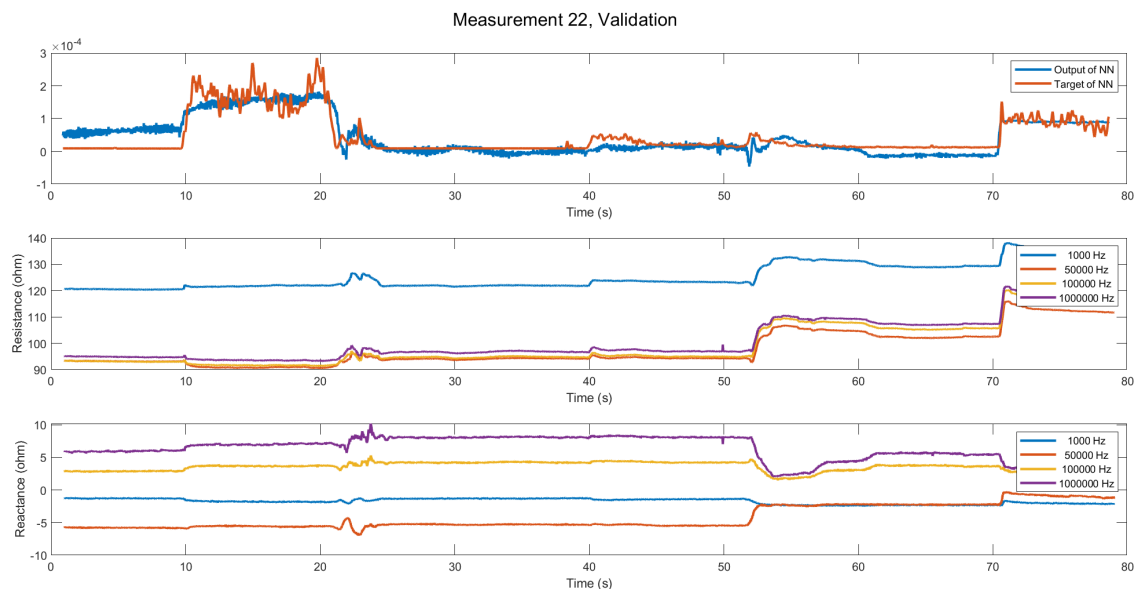


Figure E.23: Top figure: the target and the output of the time delay Neural network. Middle figure: the 4 measured resistances, which are 4 of the 8 inputs for the NN. Bottom figure: the 4 measured reactances, which form the other 4 of 8 inputs for the NN. The measurement is done while movement pattern 3 (Figure 3.10) is performed from state "A" to "F".



Figure E.24: Top figure: the target and the output of the time delay Neural network. Middle figure: the 4 measured resistances, which are 4 of the 8 inputs for the NN. Bottom figure: the 4 measured reactances, which form the other 4 of 8 inputs for the NN. The measurement is done while movement pattern 3 (Figure 3.10) is performed from state “A” to “F”.

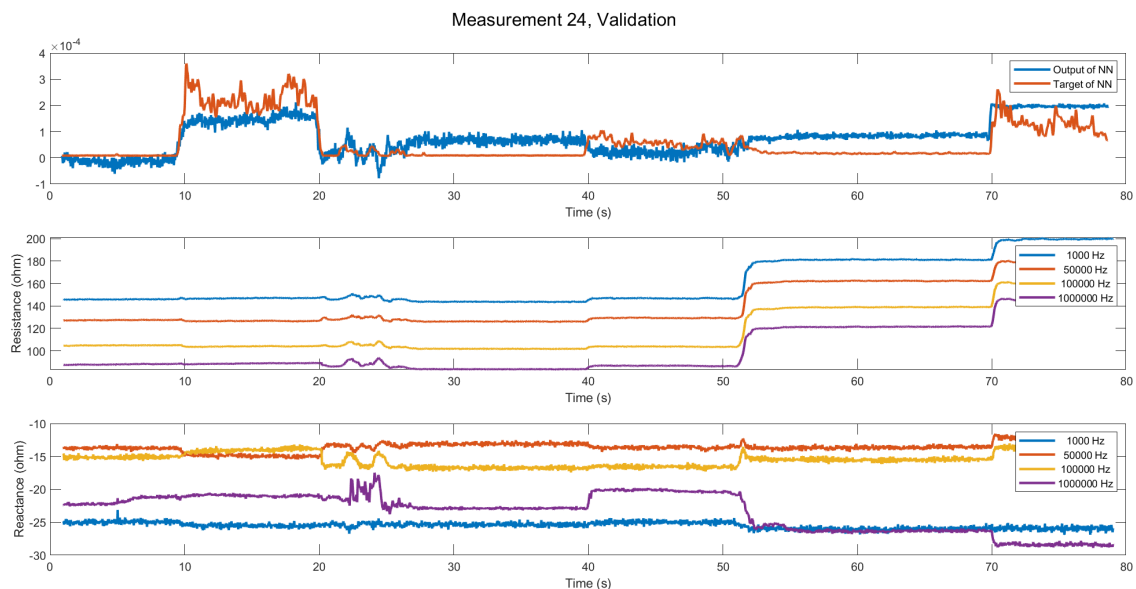


Figure E.25: Top figure: the target and the output of the time delay Neural network. Middle figure: the 4 measured resistances, which are 4 of the 8 inputs for the NN. Bottom figure: the 4 measured reactances, which form the other 4 of 8 inputs for the NN. The measurement is done while movement pattern 3 (Figure 3.10) is performed from state “A” to “F”.

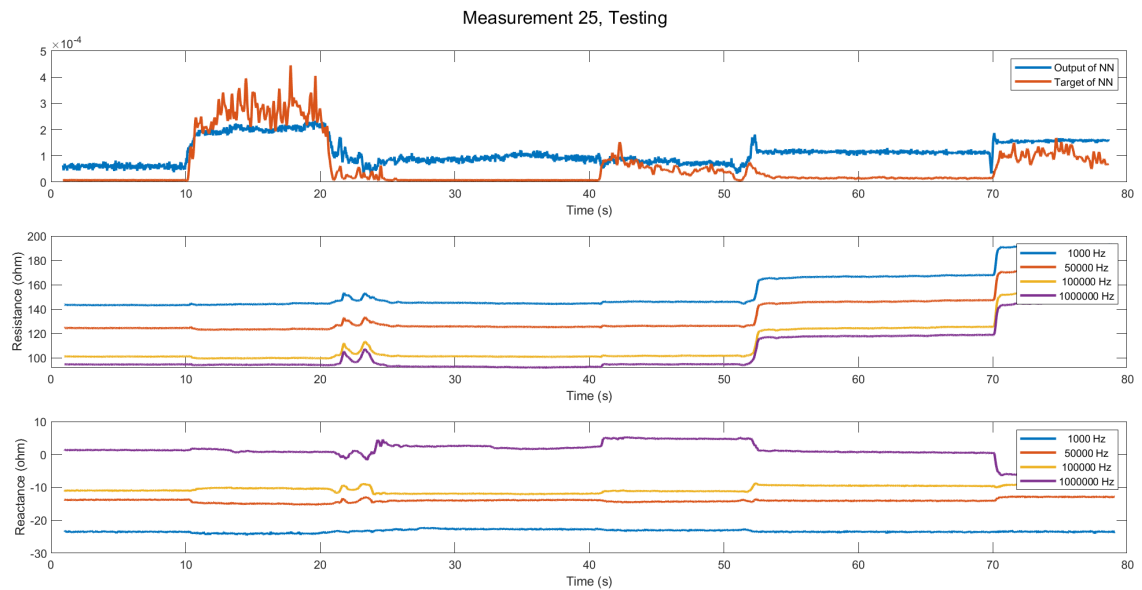


Figure E.26: Top figure: the target and the output of the time delay Neural network. Middle figure: the 4 measured resistances, which are 4 of the 8 inputs for the NN. Bottom figure: the 4 measured reactances, which form the other 4 of 8 inputs for the NN. The measurement is done while movement pattern 3 (Figure 3.10) is performed from state “A” to “F”.

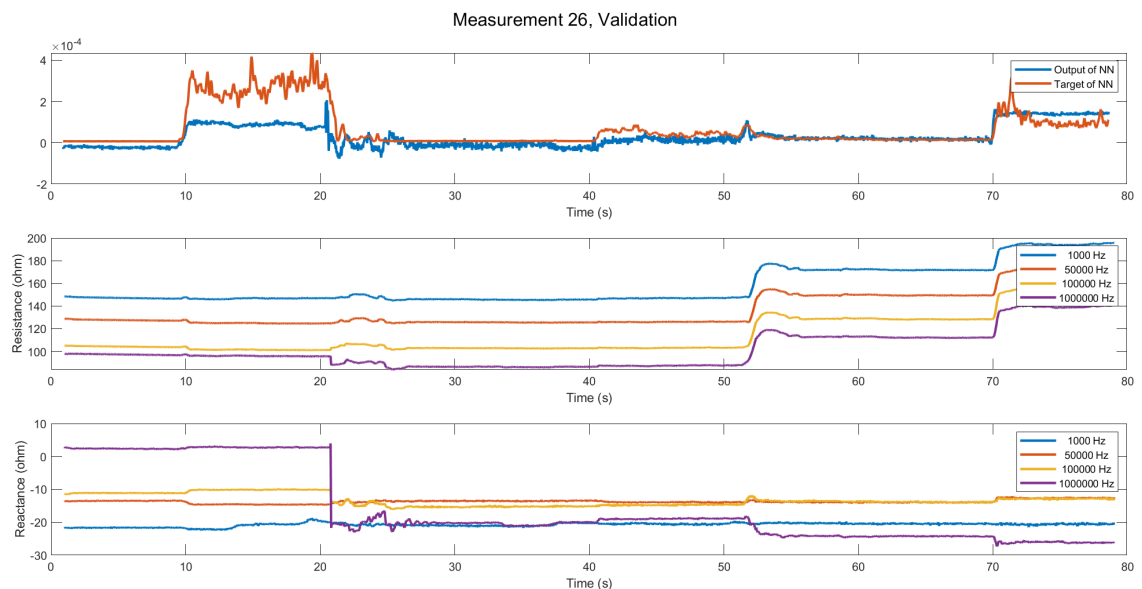


Figure E.27: Top figure: the target and the output of the time delay Neural network. Middle figure: the 4 measured resistances, which are 4 of the 8 inputs for the NN. Bottom figure: the 4 measured reactances, which form the other 4 of 8 inputs for the NN. The measurement is done while movement pattern 3 (Figure 3.10) is performed from state “A” to “F”.

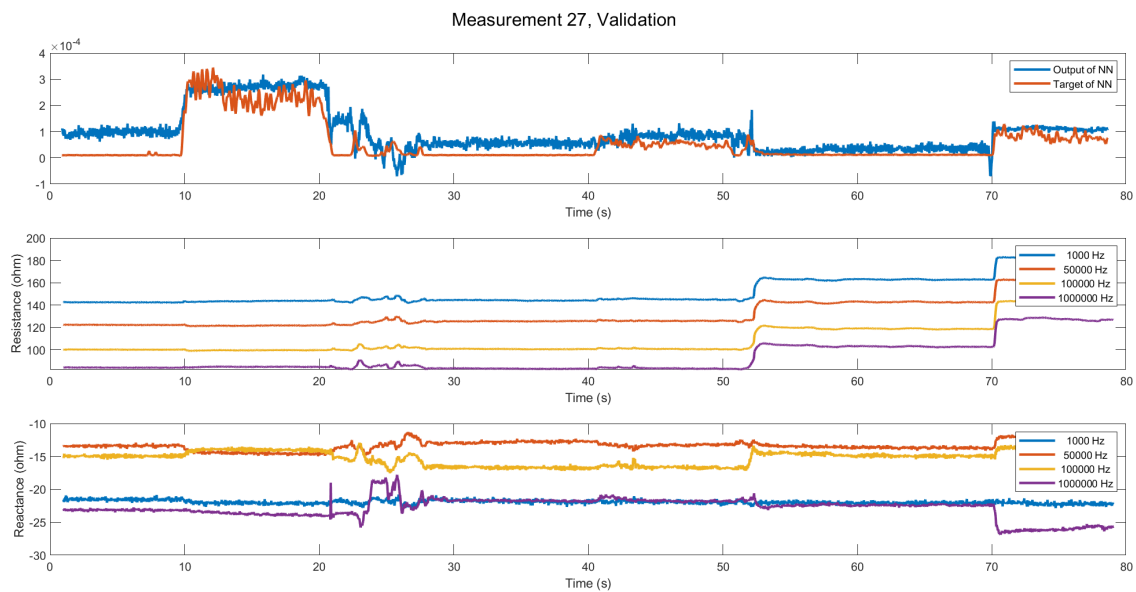


Figure E.28: Top figure: the target and the output of the time delay Neural network. Middle figure: the 4 measured resistances, which are 4 of the 8 inputs for the NN. Bottom figure: the 4 measured reactances, which form the other 4 of 8 inputs for the NN. The measurement is done while movement pattern 3 (Figure 3.10) is performed from state “A” to “F”.



Figure E.29: Top figure: the target and the output of the time delay Neural network. Middle figure: the 4 measured resistances, which are 4 of the 8 inputs for the NN. Bottom figure: the 4 measured reactances, which form the other 4 of 8 inputs for the NN. The measurement is done while movement pattern 3 (Figure 3.10) is performed from state “A” to “F”.

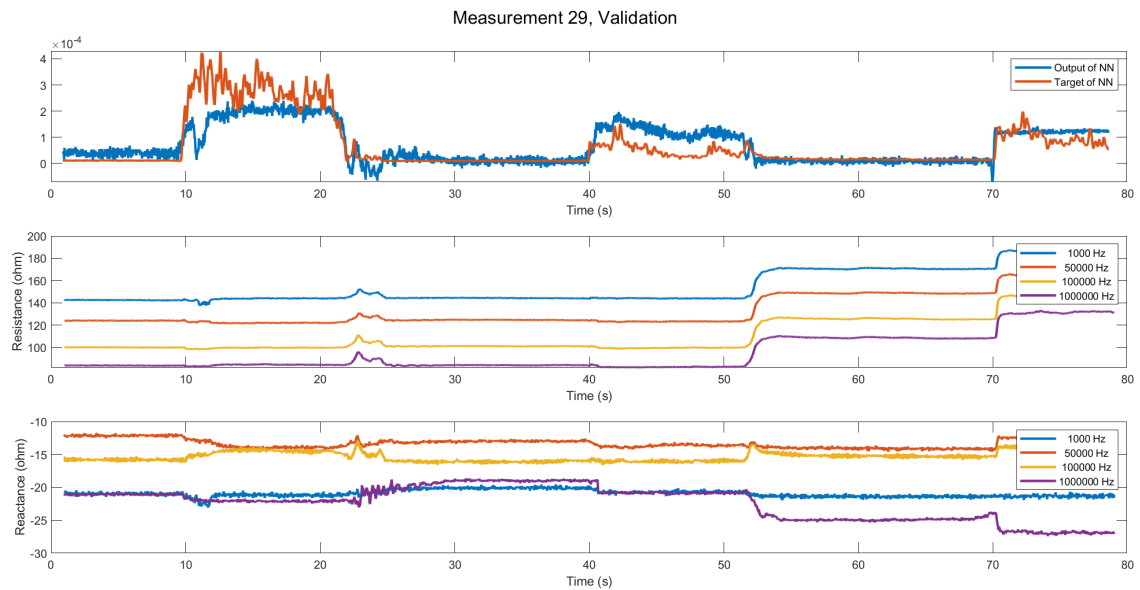


Figure E.30: Top figure: the target and the output of the time delay Neural network. Middle figure: the 4 measured resistances, which are 4 of the 8 inputs for the NN. Bottom figure: the 4 measured reactances, which form the other 4 of 8 inputs for the NN. The measurement is done while movement pattern 3 (Figure 3.10) is performed from state “A” to “F”.

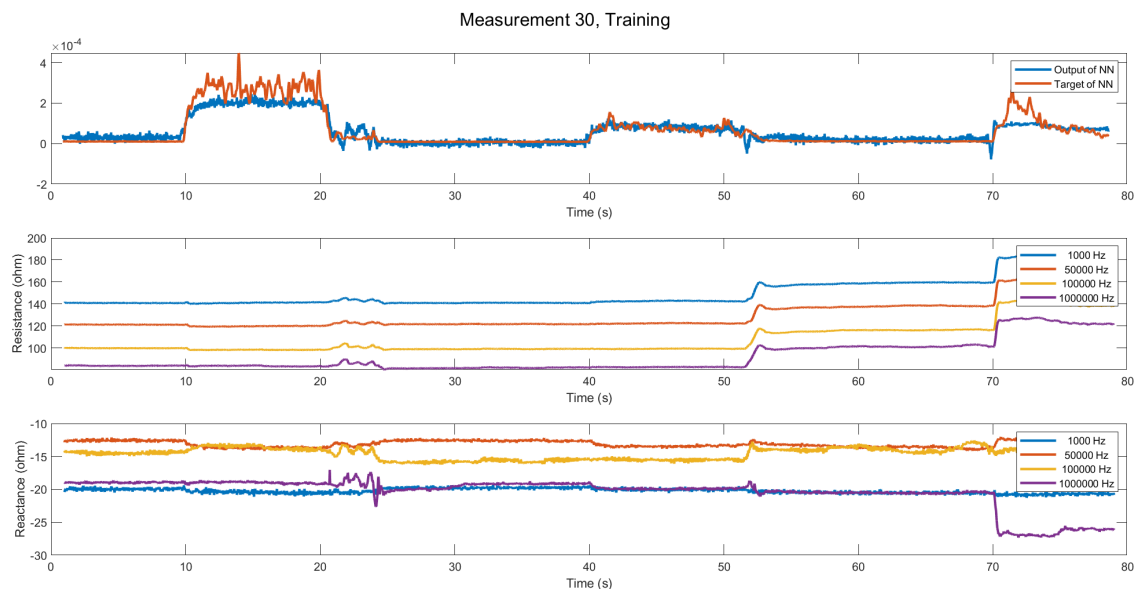


Figure E.31: Top figure: the target and the output of the time delay Neural network. Middle figure: the 4 measured resistances, which are 4 of the 8 inputs for the NN. Bottom figure: the 4 measured reactances, which form the other 4 of 8 inputs for the NN. The measurement is done while movement pattern 3 (Figure 3.10) is performed from state “A” to “F”.

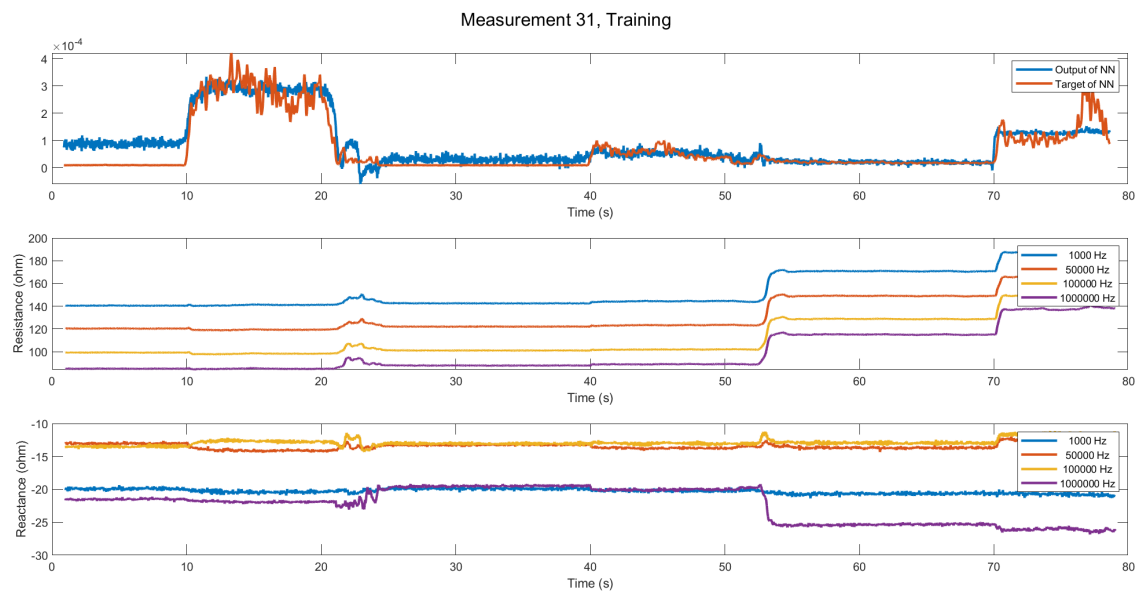


Figure E.32: Top figure: the target and the output of the time delay Neural network. Middle figure: the 4 measured resistances, which are 4 of the 8 inputs for the NN. Bottom figure: the 4 measured reactances, which form the other 4 of 8 inputs for the NN. The measurement is done while movement pattern 3 (Figure 3.10) is performed from state “A” to “F”.



Figure E.33: Top figure: the target and the output of the time delay Neural network. Middle figure: the 4 measured resistances, which are 4 of the 8 inputs for the NN. Bottom figure: the 4 measured reactances, which form the other 4 of 8 inputs for the NN. The measurement is done while movement pattern 3 (Figure 3.10) is performed from state “A” to “F”.



Figure E.34: Top figure: the target and the output of the time delay Neural network. Middle figure: the 4 measured resistances, which are 4 of the 8 inputs for the NN. Bottom figure: the 4 measured reactances, which form the other 4 of 8 inputs for the NN. The measurement is done while movement pattern 3 (Figure 3.10) is performed from state “A” to “F”.



Figure E.35: Top figure: the target and the output of the time delay Neural network. Middle figure: the 4 measured resistances, which are 4 of the 8 inputs for the NN. Bottom figure: the 4 measured reactances, which form the other 4 of 8 inputs for the NN. The measurement is done while movement pattern 3 (Figure 3.10) is performed from state “A” to “F”.

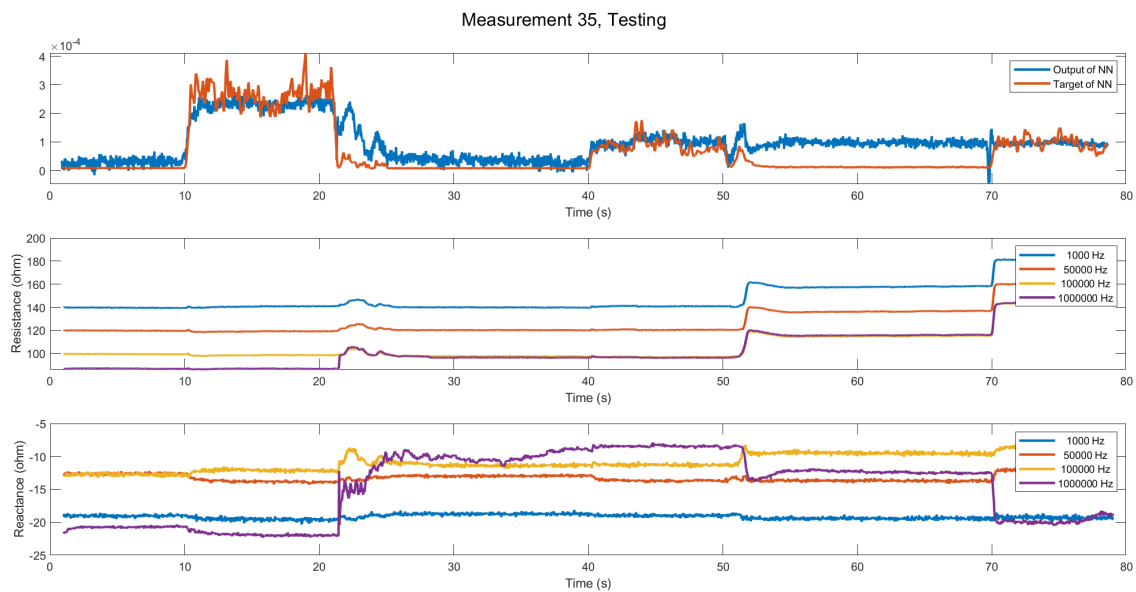


Figure E.36: Top figure: the target and the output of the time delay Neural network. Middle figure: the 4 measured resistances, which are 4 of the 8 inputs for the NN. Bottom figure: the 4 measured reactances, which form the other 4 of 8 inputs for the NN. The measurement is done while movement pattern 3 (Figure 3.10) is performed from state “A” to “F”.

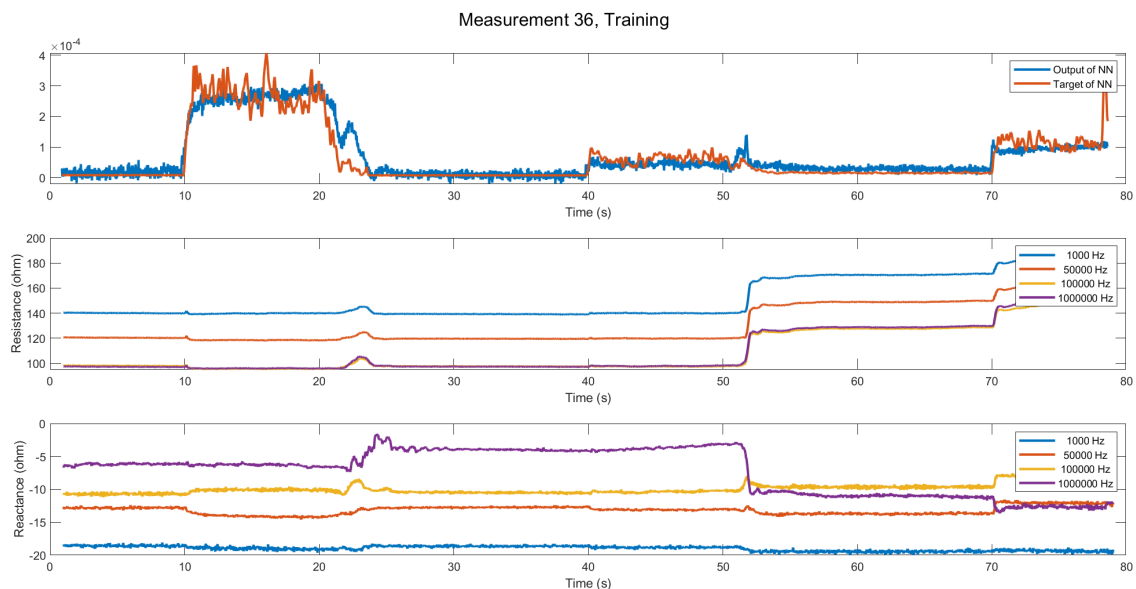


Figure E.37: Top figure: the target and the output of the time delay Neural network. Middle figure: the 4 measured resistances, which are 4 of the 8 inputs for the NN. Bottom figure: the 4 measured reactances, which form the other 4 of 8 inputs for the NN. The measurement is done while movement pattern 3 (Figure 3.10) is performed from state “A” to “F”.



Figure E.38: Top figure: the target and the output of the time delay Neural network. Middle figure: the 4 measured resistances, which are 4 of the 8 inputs for the NN. Bottom figure: the 4 measured reactances, which form the other 4 of 8 inputs for the NN. The measurement is done while movement pattern 3 (Figure 3.10) is performed from state “A” to “F”.

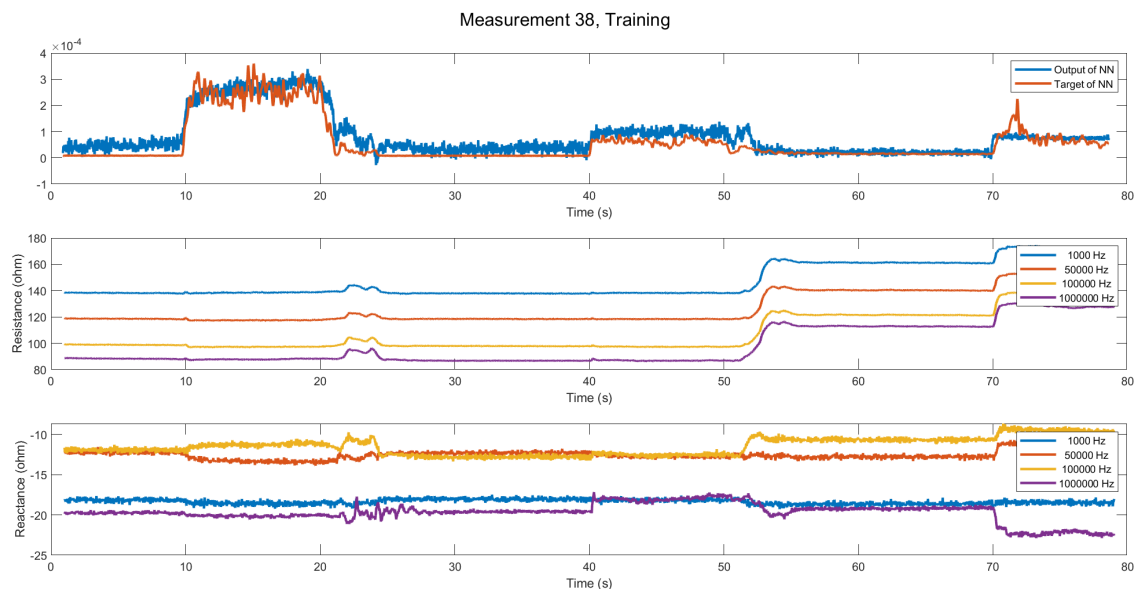


Figure E.39: Top figure: the target and the output of the time delay Neural network. Middle figure: the 4 measured resistances, which are 4 of the 8 inputs for the NN. Bottom figure: the 4 measured reactances, which form the other 4 of 8 inputs for the NN. The measurement is done while movement pattern 3 (Figure 3.10) is performed from state “A” to “F”.

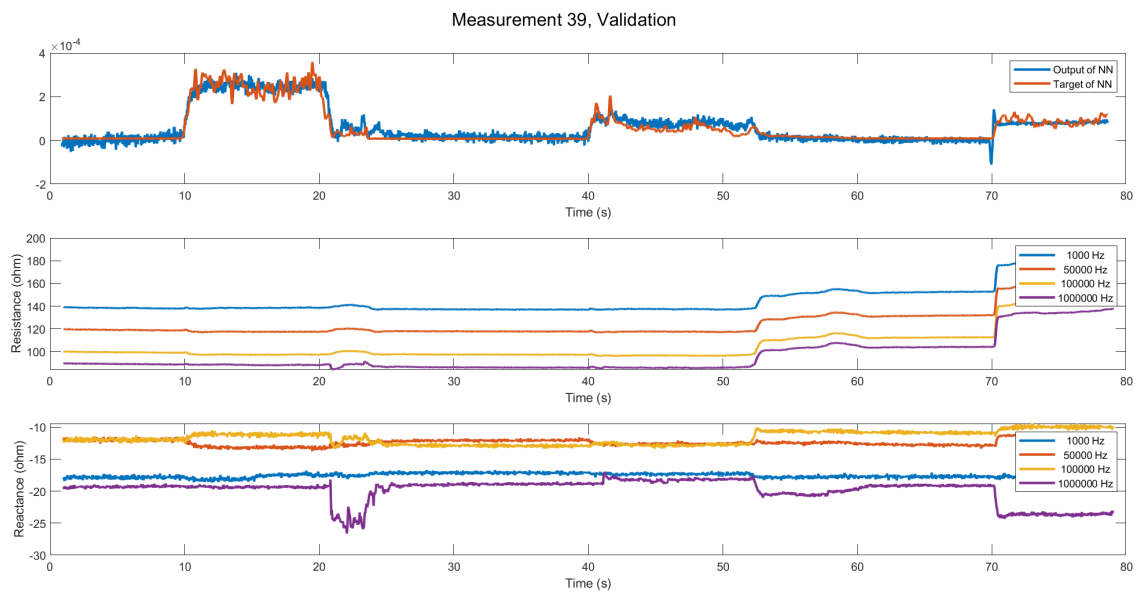


Figure E.40: Top figure: the target and the output of the time delay Neural network. Middle figure: the 4 measured resistances, which are 4 of the 8 inputs for the NN. Bottom figure: the 4 measured reactances, which form the other 4 of 8 inputs for the NN. The measurement is done while movement pattern 3 (Figure 3.10) is performed from state “A” to “F”.

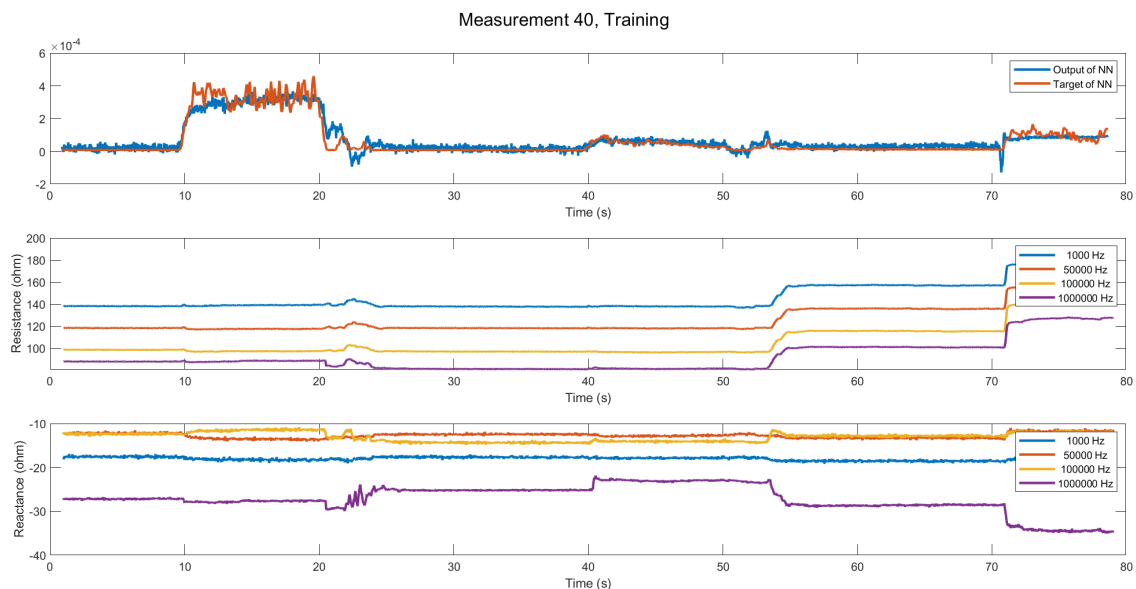


Figure E.41: Top figure: the target and the output of the time delay Neural network. Middle figure: the 4 measured resistances, which are 4 of the 8 inputs for the NN. Bottom figure: the 4 measured reactances, which form the other 4 of 8 inputs for the NN. The measurement is done while movement pattern 3 (Figure 3.10) is performed from state “A” to “F”.

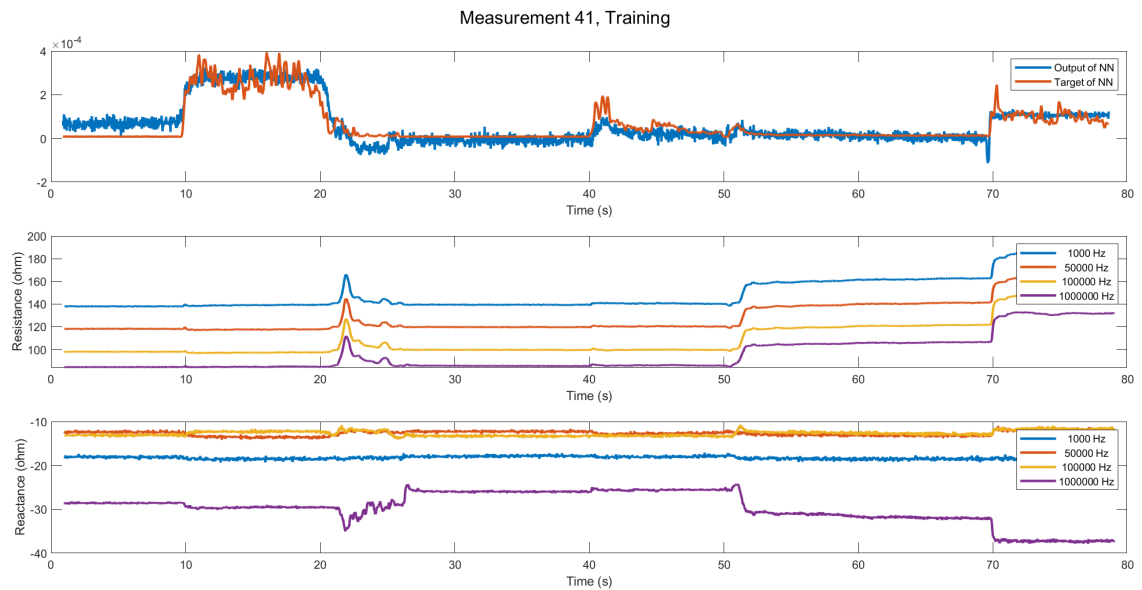


Figure E.42: Top figure: the target and the output of the time delay Neural network. Middle figure: the 4 measured resistances, which are 4 of the 8 inputs for the NN. Bottom figure: the 4 measured reactances, which form the other 4 of 8 inputs for the NN. The measurement is done while movement pattern 3 (Figure 3.10) is performed from state “A” to “F”.

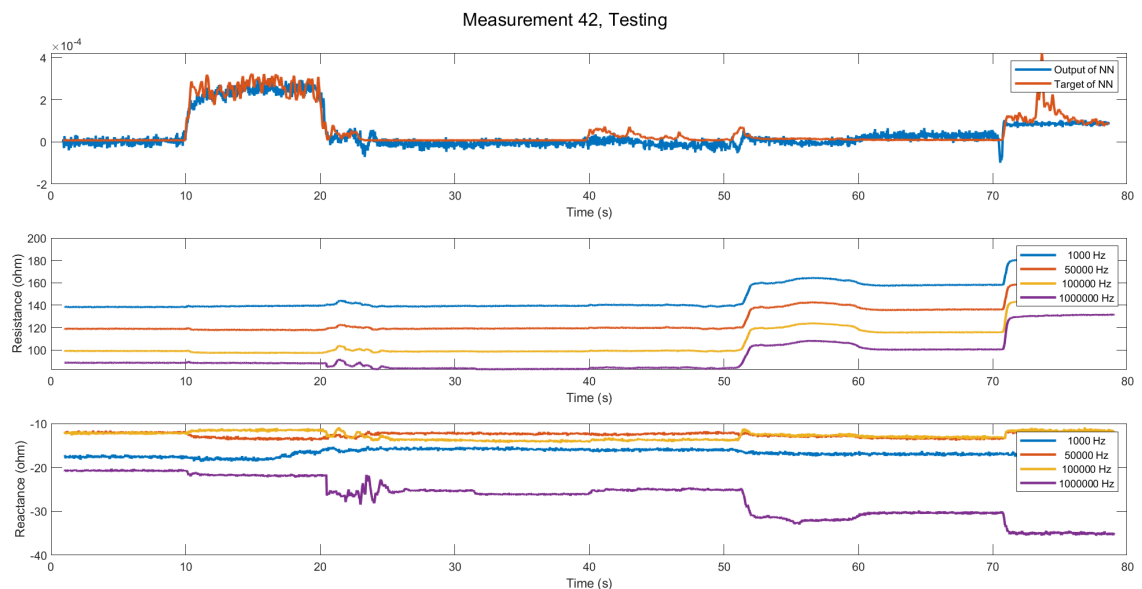


Figure E.43: Top figure: the target and the output of the time delay Neural network. Middle figure: the 4 measured resistances, which are 4 of the 8 inputs for the NN. Bottom figure: the 4 measured reactances, which form the other 4 of 8 inputs for the NN. The measurement is done while movement pattern 3 (Figure 3.10) is performed from state “A” to “F”.

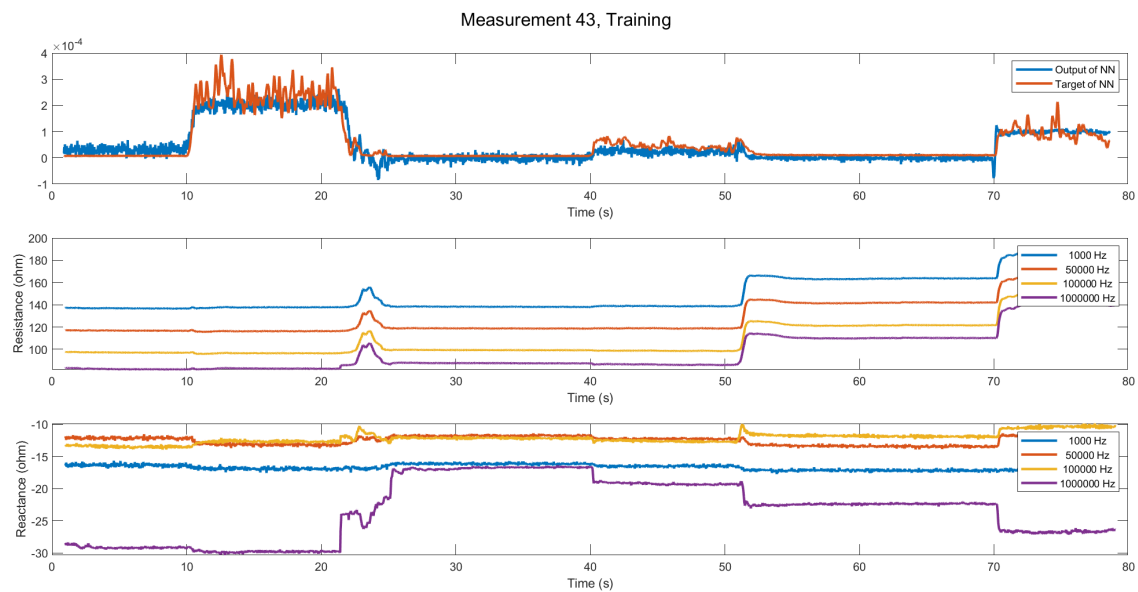


Figure E.44: Top figure: the target and the output of the time delay Neural network. Middle figure: the 4 measured resistances, which are 4 of the 8 inputs for the NN. Bottom figure: the 4 measured reactances, which form the other 4 of 8 inputs for the NN. The measurement is done while movement pattern 3 (Figure 3.10) is performed from state “A” to “F”.

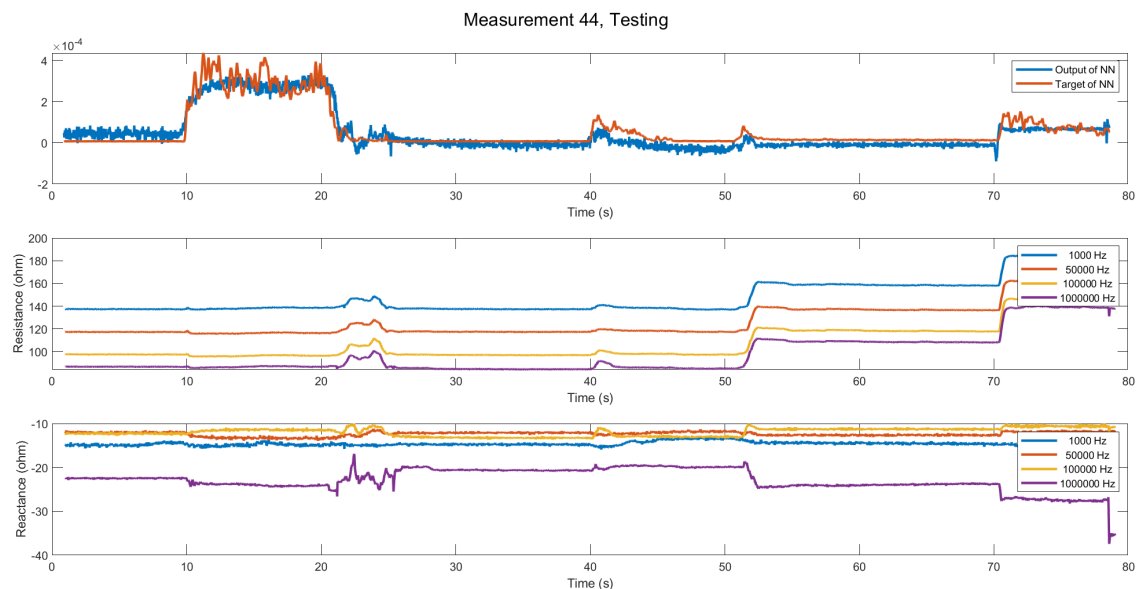


Figure E.45: Top figure: the target and the output of the time delay Neural network. Middle figure: the 4 measured resistances, which are 4 of the 8 inputs for the NN. Bottom figure: the 4 measured reactances, which form the other 4 of 8 inputs for the NN. The measurement is done while movement pattern 3 (Figure 3.10) is performed from state “A” to “F”.



Figure E.46: Top figure: the target and the output of the time delay Neural network. Middle figure: the 4 measured resistances, which are 4 of the 8 inputs for the NN. Bottom figure: the 4 measured reactances, which form the other 4 of 8 inputs for the NN. The measurement is done while movement pattern 3 (Figure 3.10) is performed from state “A” to “F”.

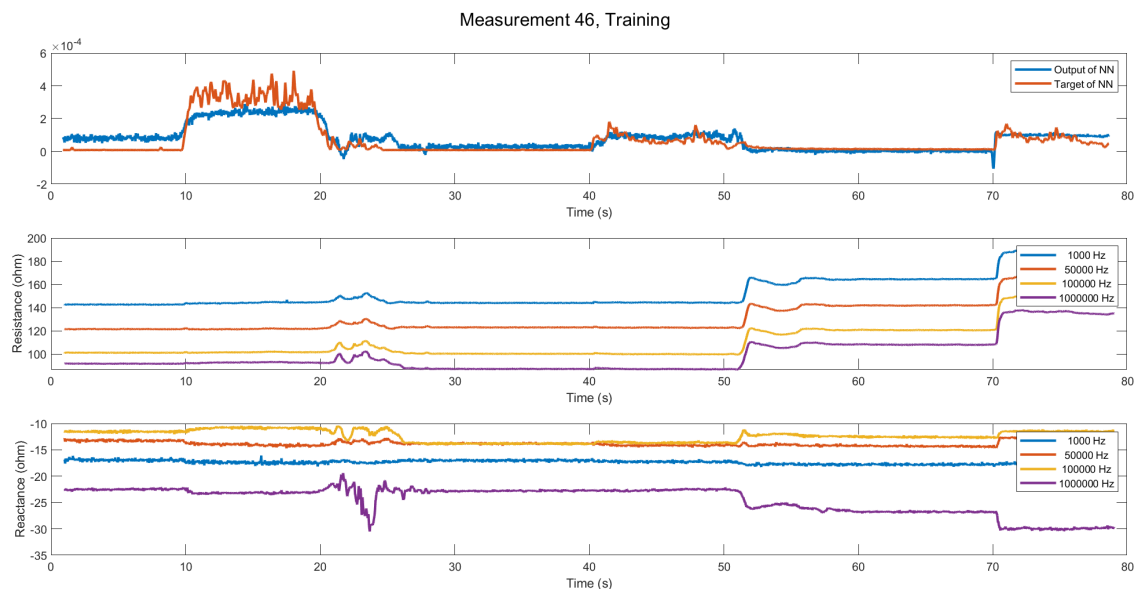


Figure E.47: Top figure: the target and the output of the time delay Neural network. Middle figure: the 4 measured resistances, which are 4 of the 8 inputs for the NN. Bottom figure: the 4 measured reactances, which form the other 4 of 8 inputs for the NN. The measurement is done while movement pattern 3 (Figure 3.10) is performed from state “A” to “F”.

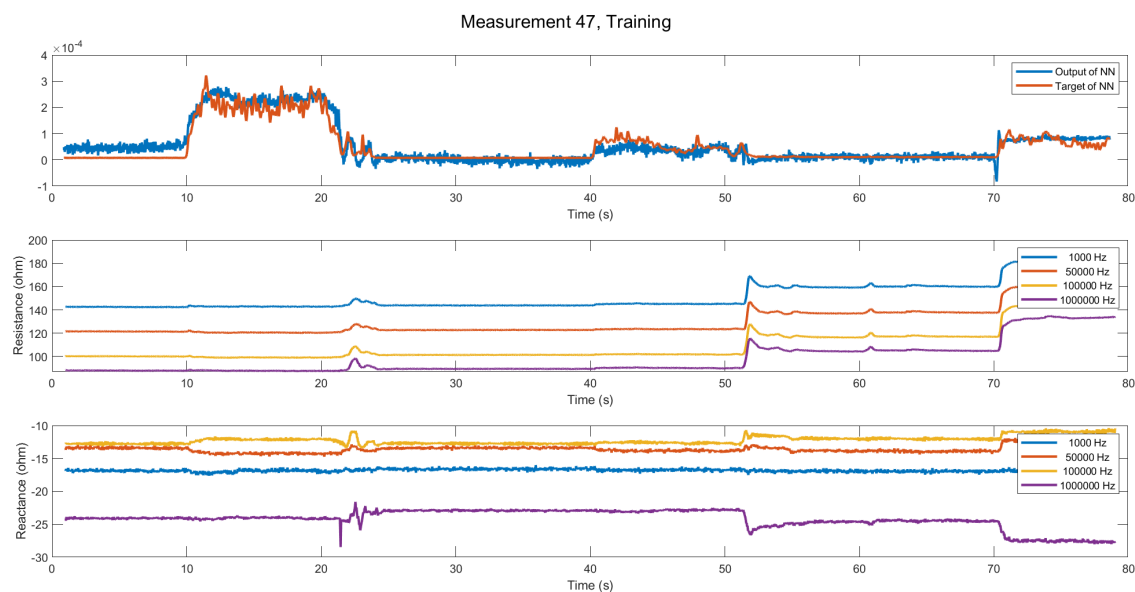


Figure E.48: Top figure: the target and the output of the time delay Neural network. Middle figure: the 4 measured resistances, which are 4 of the 8 inputs for the NN. Bottom figure: the 4 measured reactances, which form the other 4 of 8 inputs for the NN. The measurement is done while movement pattern 3 (Figure 3.10) is performed from state “A” to “F”.

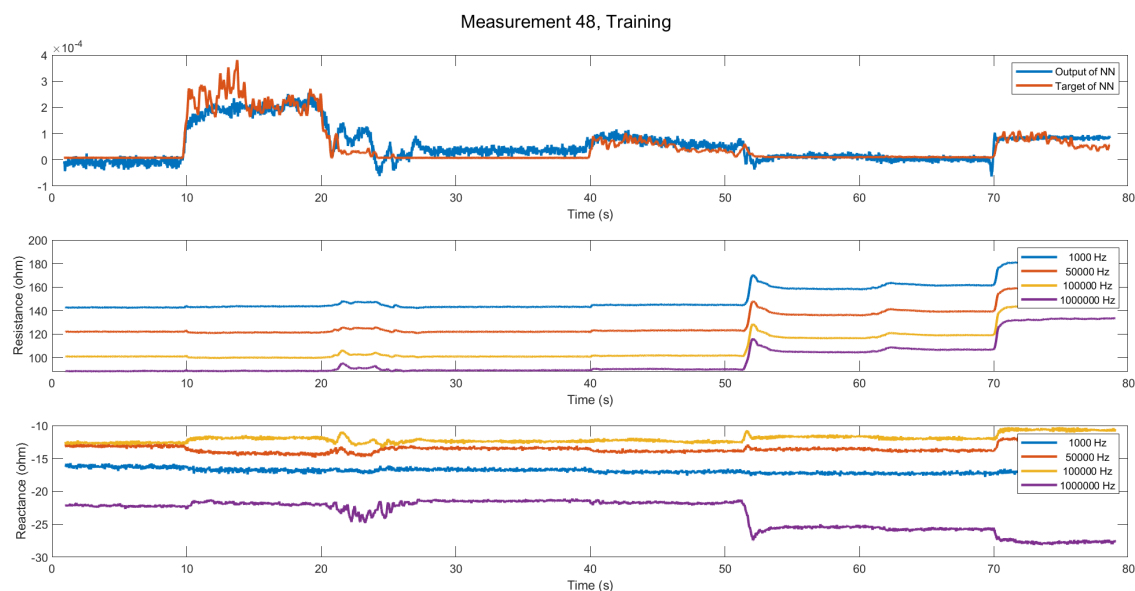


Figure E.49: Top figure: the target and the output of the time delay Neural network. Middle figure: the 4 measured resistances, which are 4 of the 8 inputs for the NN. Bottom figure: the 4 measured reactances, which form the other 4 of 8 inputs for the NN. The measurement is done while movement pattern 3 (Figure 3.10) is performed from state “A” to “F”.

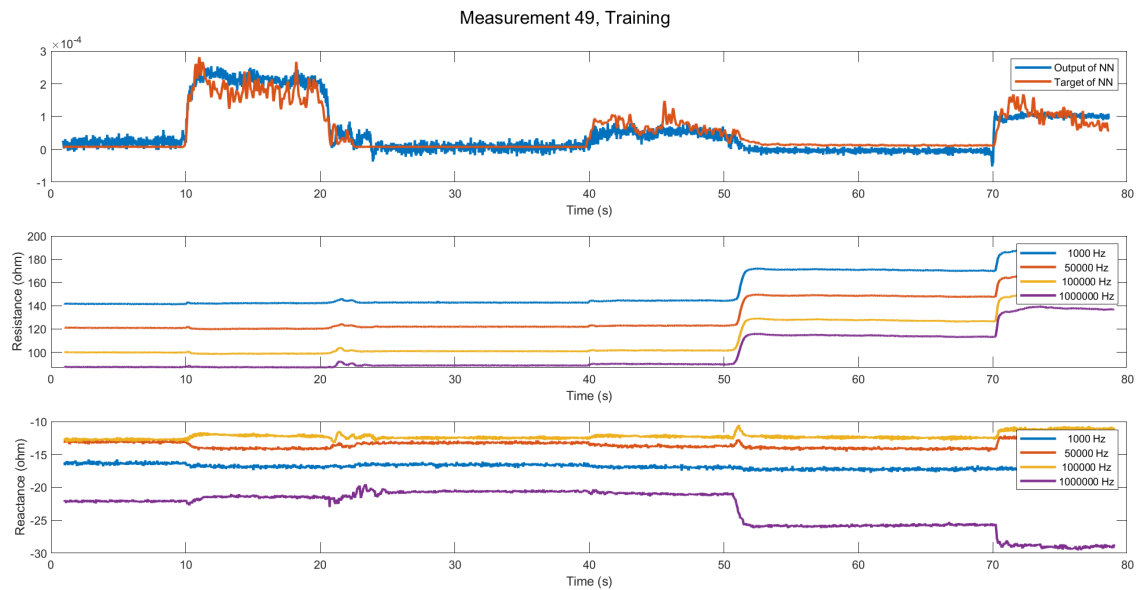


Figure E.50: Top figure: the target and the output of the time delay Neural network. Middle figure: the 4 measured resistances, which are 4 of the 8 inputs for the NN. Bottom figure: the 4 measured reactances, which form the other 4 of 8 inputs for the NN. The measurement is done while movement pattern 3 (Figure 3.10) is performed from state “A” to “F”.



Figure E.51: Top figure: the target and the output of the time delay Neural network. Middle figure: the 4 measured resistances, which are 4 of the 8 inputs for the NN. Bottom figure: the 4 measured reactances, which form the other 4 of 8 inputs for the NN. The measurement is done while movement pattern 3 (Figure 3.10) is performed from state “A” to “F”.



Figure E.52: Top figure: the target and the output of the time delay Neural network. Middle figure: the 4 measured resistances, which are 4 of the 8 inputs for the NN. Bottom figure: the 4 measured reactances, which form the other 4 of 8 inputs for the NN. The measurement is done while movement pattern 3 (Figure 3.10) is performed from state "A" to "F".



Figure E.53: Top figure: the target and the output of the time delay Neural network. Middle figure: the 4 measured resistances, which are 4 of the 8 inputs for the NN. Bottom figure: the 4 measured reactances, which form the other 4 of 8 inputs for the NN. The measurement is done while movement pattern 3 (Figure 3.10) is performed from state "A" to "F".

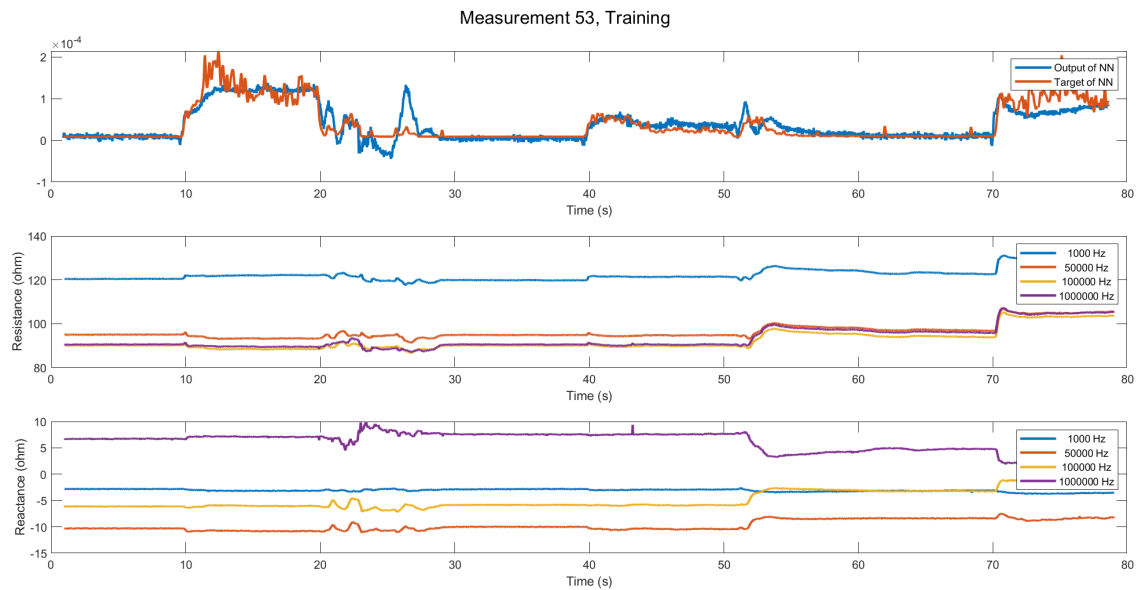


Figure E.54: Top figure: the target and the output of the time delay Neural network. Middle figure: the 4 measured resistances, which are 4 of the 8 inputs for the NN. Bottom figure: the 4 measured reactances, which form the other 4 of 8 inputs for the NN. The measurement is done while movement pattern 3 (Figure 3.10) is performed from state “A” to “F”.



Figure E.55: Top figure: the target and the output of the time delay Neural network. Middle figure: the 4 measured resistances, which are 4 of the 8 inputs for the NN. Bottom figure: the 4 measured reactances, which form the other 4 of 8 inputs for the NN. The measurement is done while movement pattern 3 (Figure 3.10) is performed from state “A” to “F”.

F Movement pattern 4 data

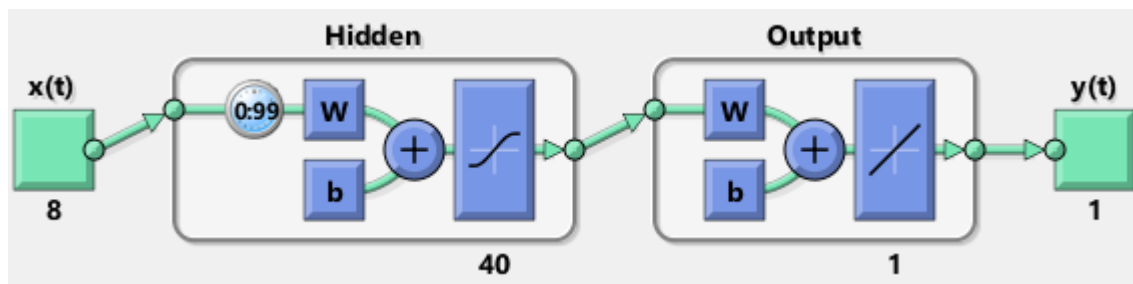


Figure F.1: A visual representation of the used NN created in Matlab. This network has $x = 8$ inputs, $y = 1$ output, $z = 100$ time delays, $n = 1$ hidden layer, $m = 40$ neurons per hidden layer.

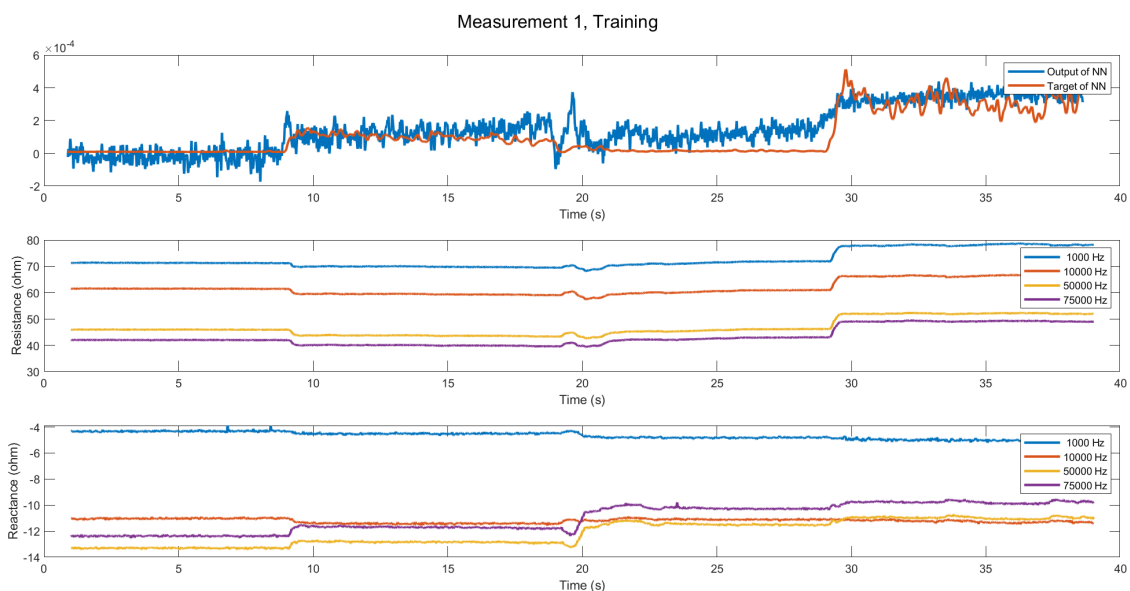


Figure F.2: Top figure: the target and the output of the time delay Neural network. The used Neural Network is given in Figure F.1. Middle figure: the 4 measured resistances, which are 4 of the 8 inputs for the NN. Bottom figure: the 4 measured reactances, which form the other 4 of 8 inputs for the NN.

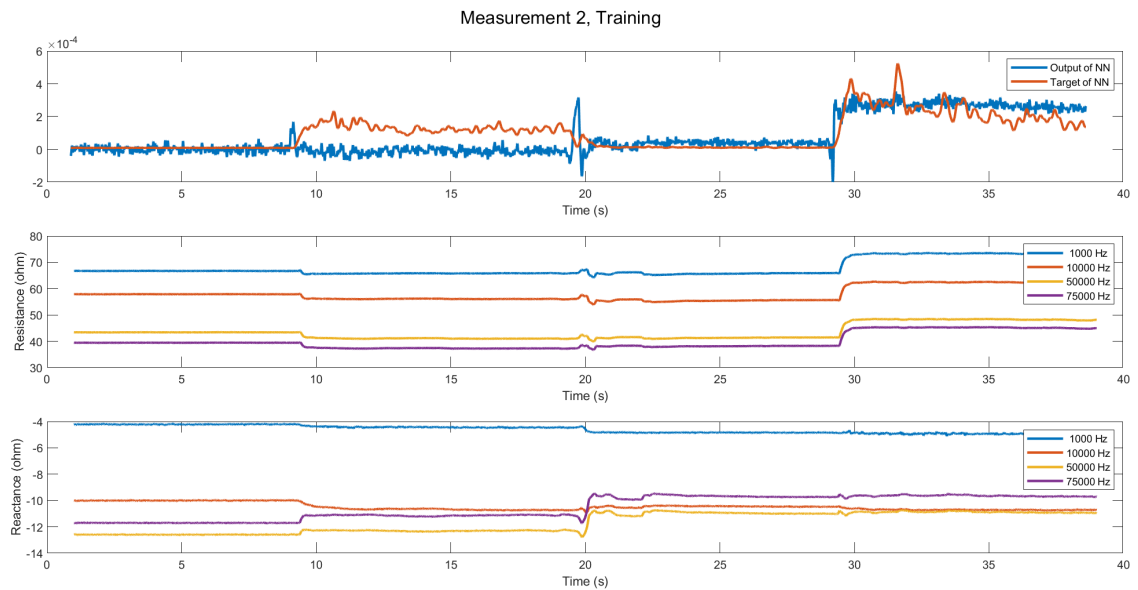


Figure F3: Top figure: the target and the output of the time delay Neural network. The used Neural Network is given in Figure E.1. Middle figure: the 4 measured resistances, which are 4 of the 8 inputs for the NN. Bottom figure: the 4 measured reactances, which form the other 4 of 8 inputs for the NN.

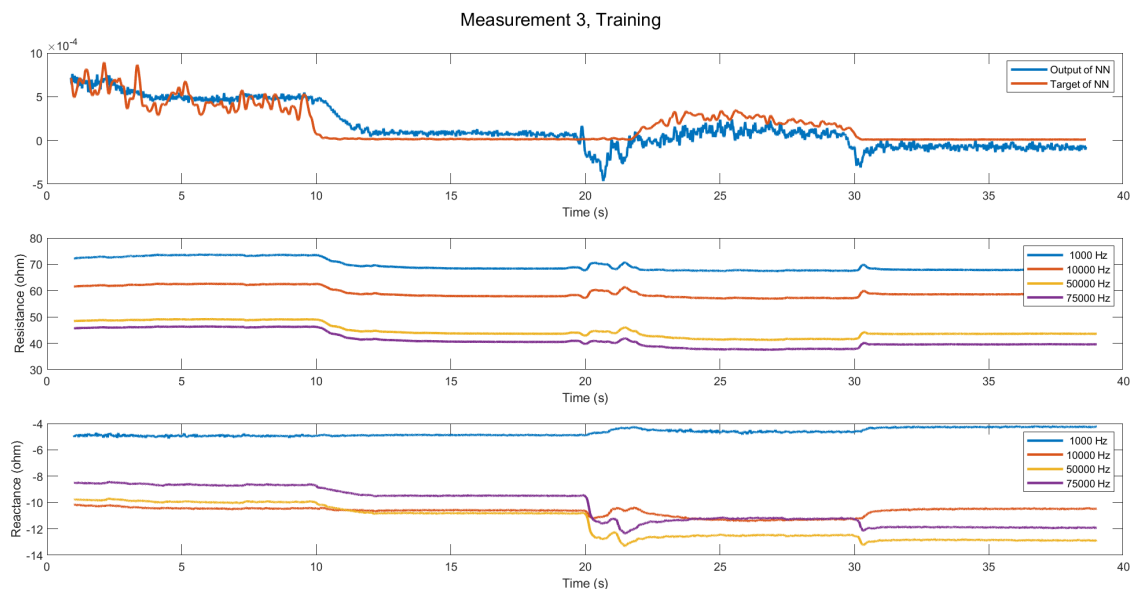


Figure F4: Top figure: the target and the output of the time delay Neural network. The used Neural Network is given in Figure E.1. Middle figure: the 4 measured resistances, which are 4 of the 8 inputs for the NN. Bottom figure: the 4 measured reactances, which form the other 4 of 8 inputs for the NN.

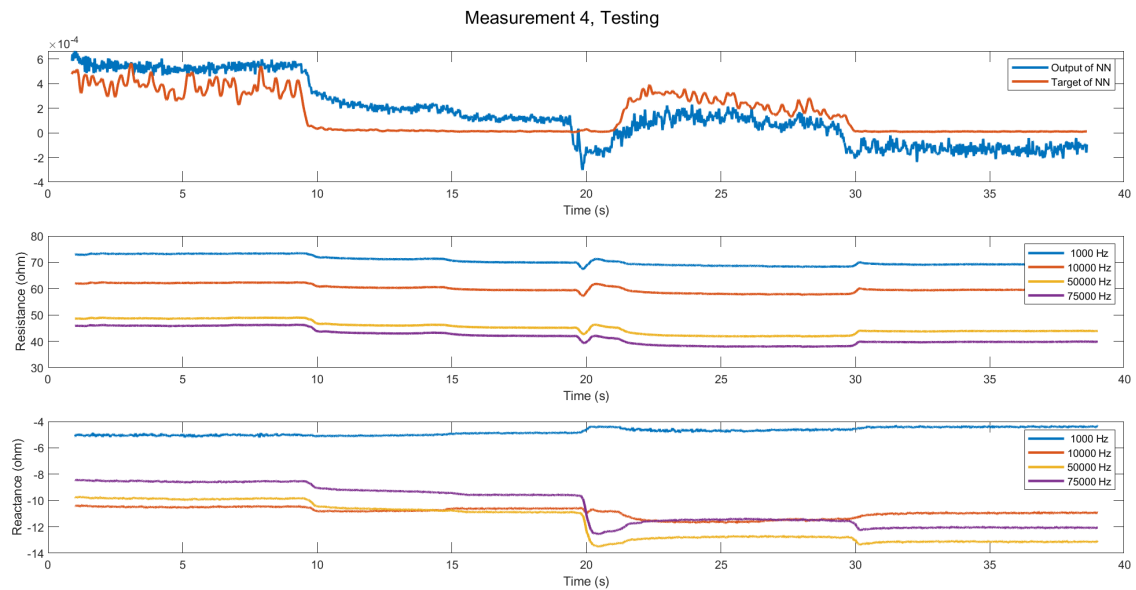


Figure F5: Top figure: the target and the output of the time delay Neural network. The used Neural Network is given in Figure E.1. Middle figure: the 4 measured resistances, which are 4 of the 8 inputs for the NN. Bottom figure: the 4 measured reactances, which form the other 4 of 8 inputs for the NN.

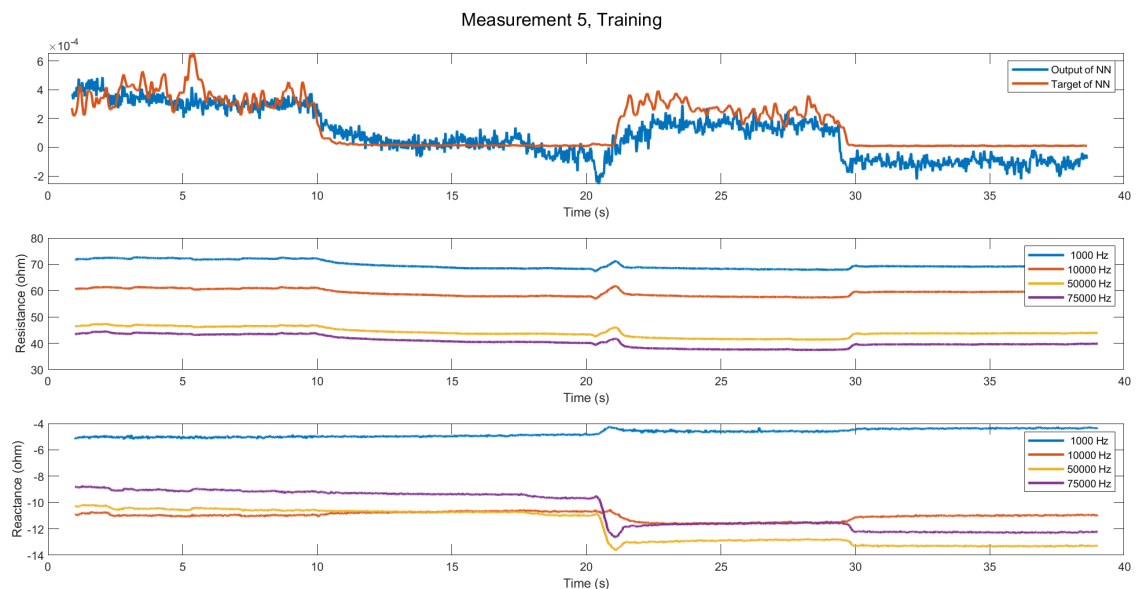


Figure F6: Top figure: the target and the output of the time delay Neural network. The used Neural Network is given in Figure E.1. Middle figure: the 4 measured resistances, which are 4 of the 8 inputs for the NN. Bottom figure: the 4 measured reactances, which form the other 4 of 8 inputs for the NN.

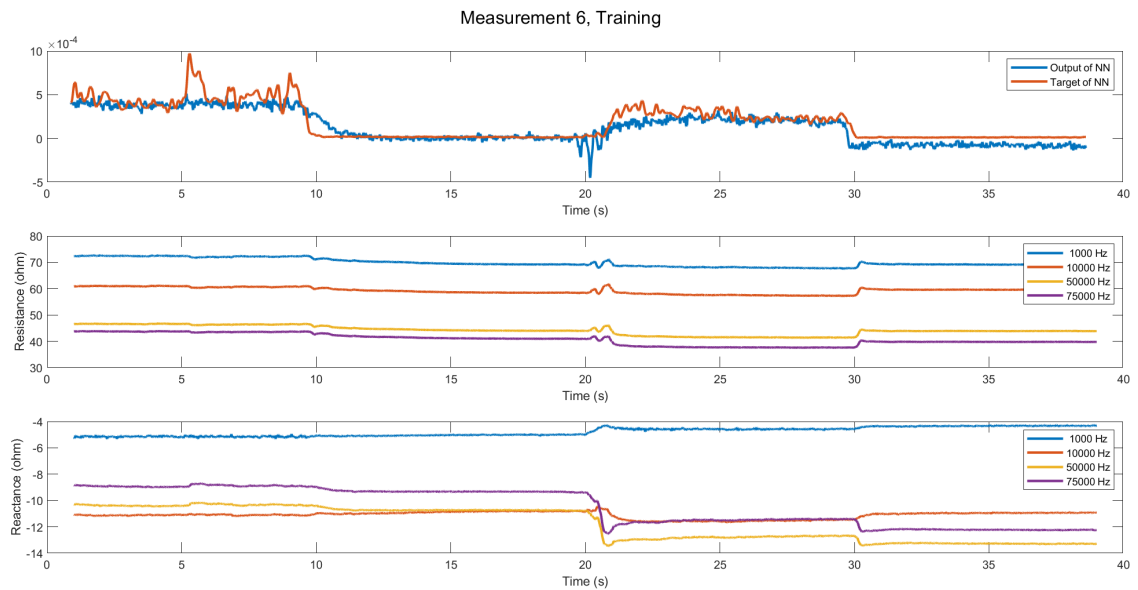


Figure F7: Top figure: the target and the output of the time delay Neural network. The used Neural Network is given in Figure E.1. Middle figure: the 4 measured resistances, which are 4 of the 8 inputs for the NN. Bottom figure: the 4 measured reactances, which form the other 4 of 8 inputs for the NN.

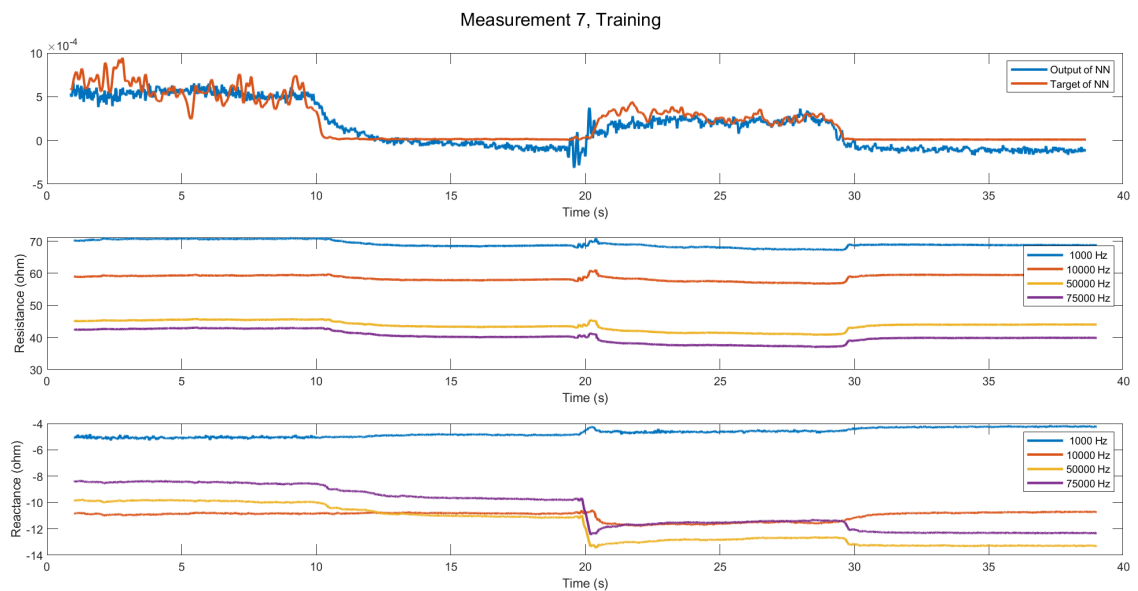


Figure F8: Top figure: the target and the output of the time delay Neural network. The used Neural Network is given in Figure E.1. Middle figure: the 4 measured resistances, which are 4 of the 8 inputs for the NN. Bottom figure: the 4 measured reactances, which form the other 4 of 8 inputs for the NN.

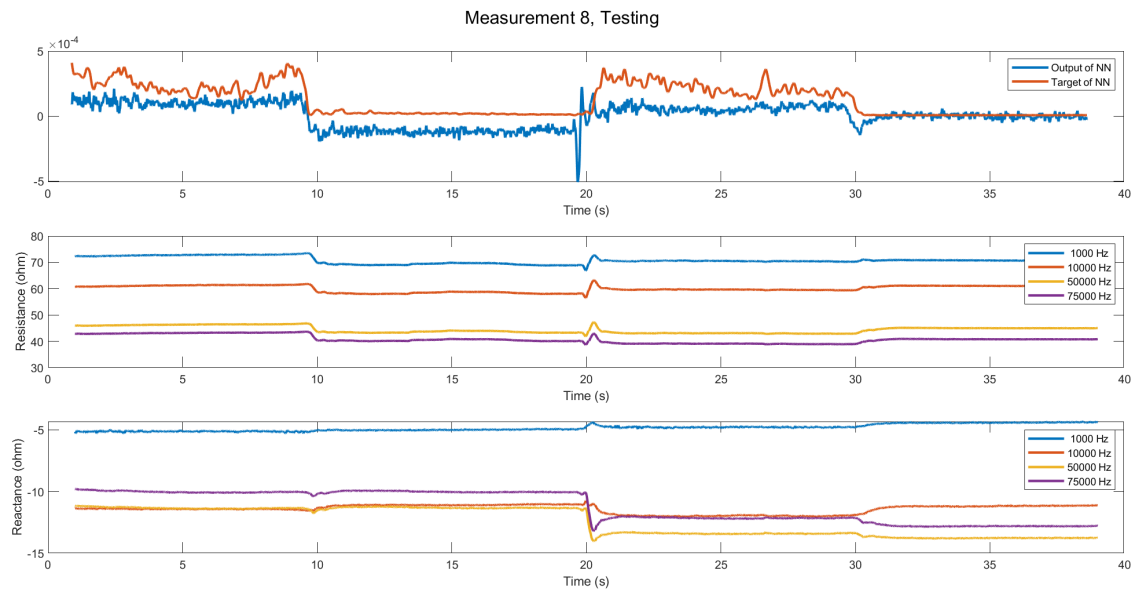


Figure F.9: Top figure: the target and the output of the time delay Neural network. The used Neural Network is given in Figure E.1. Middle figure: the 4 measured resistances, which are 4 of the 8 inputs for the NN. Bottom figure: the 4 measured reactances, which form the other 4 of 8 inputs for the NN.

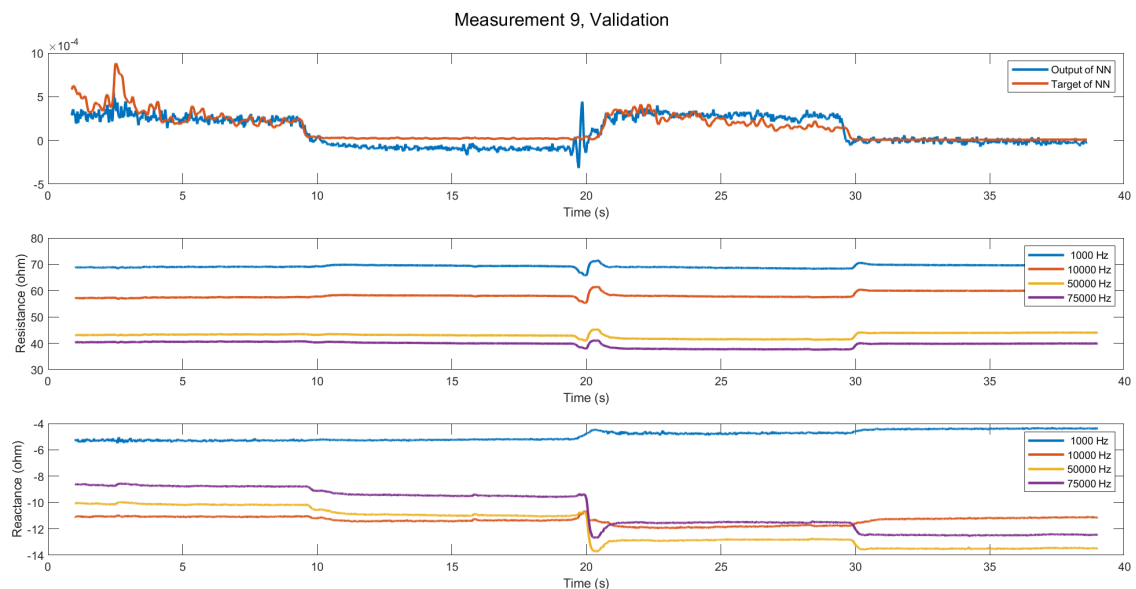


Figure F.10: Top figure: the target and the output of the time delay Neural network. The used Neural Network is given in Figure E.1. Middle figure: the 4 measured resistances, which are 4 of the 8 inputs for the NN. Bottom figure: the 4 measured reactances, which form the other 4 of 8 inputs for the NN.

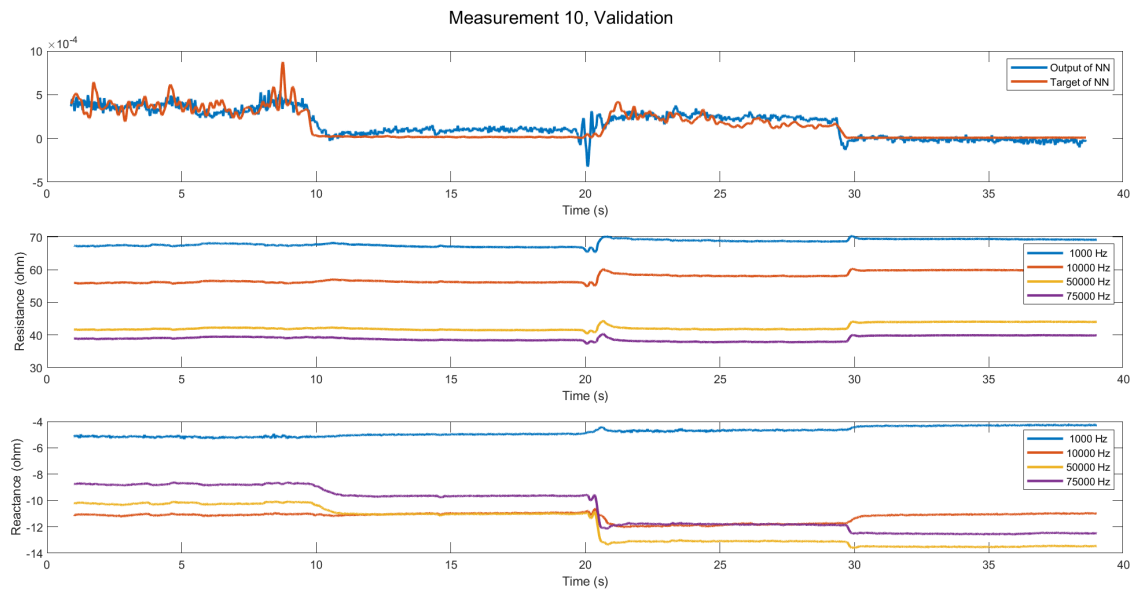


Figure F.11: Top figure: the target and the output of the time delay Neural network. The used Neural Network is given in Figure F.1. Middle figure: the 4 measured resistances, which are 4 of the 8 inputs for the NN. Bottom figure: the 4 measured reactances, which form the other 4 of 8 inputs for the NN.

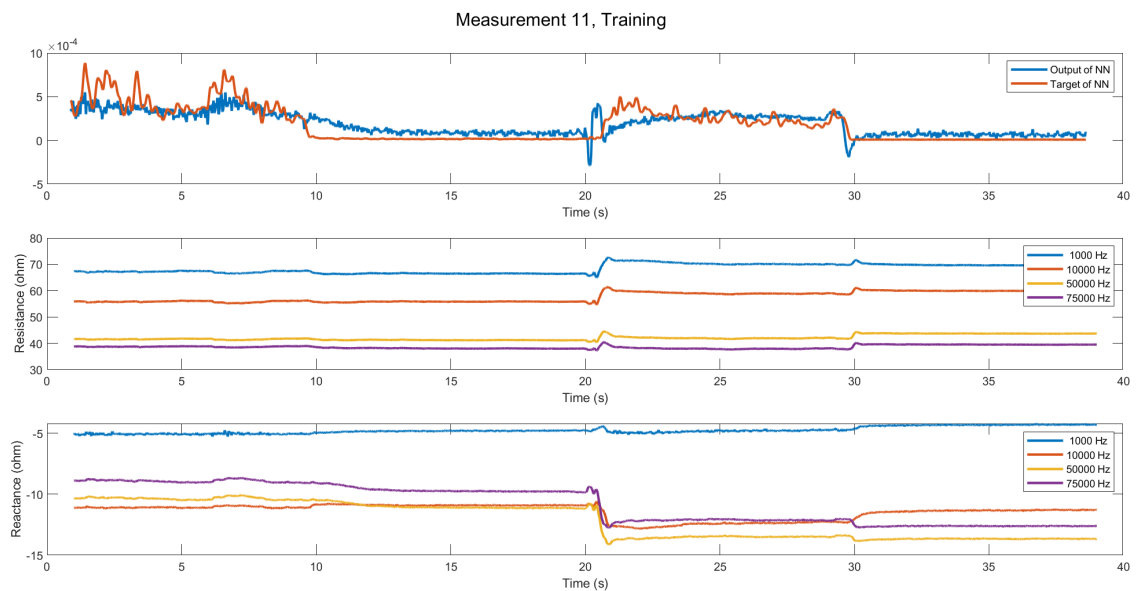


Figure F.12: Top figure: the target and the output of the time delay Neural network. The used Neural Network is given in Figure F.1. Middle figure: the 4 measured resistances, which are 4 of the 8 inputs for the NN. Bottom figure: the 4 measured reactances, which form the other 4 of 8 inputs for the NN.

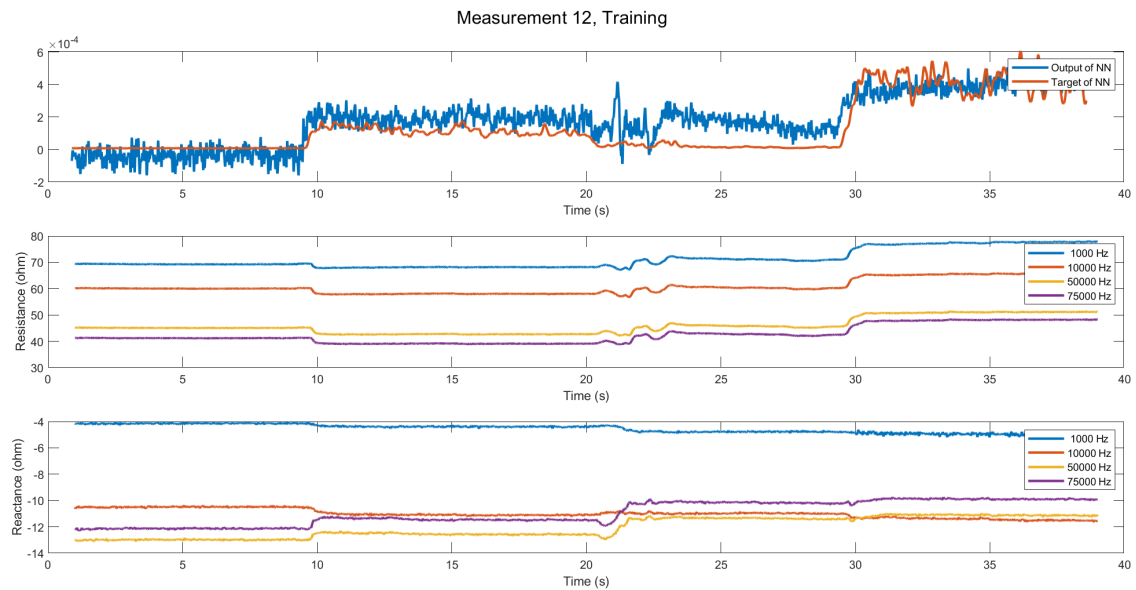


Figure F.13: Top figure: the target and the output of the time delay Neural network. The used Neural Network is given in Figure E.1. Middle figure: the 4 measured resistances, which are 4 of the 8 inputs for the NN. Bottom figure: the 4 measured reactances, which form the other 4 of 8 inputs for the NN.

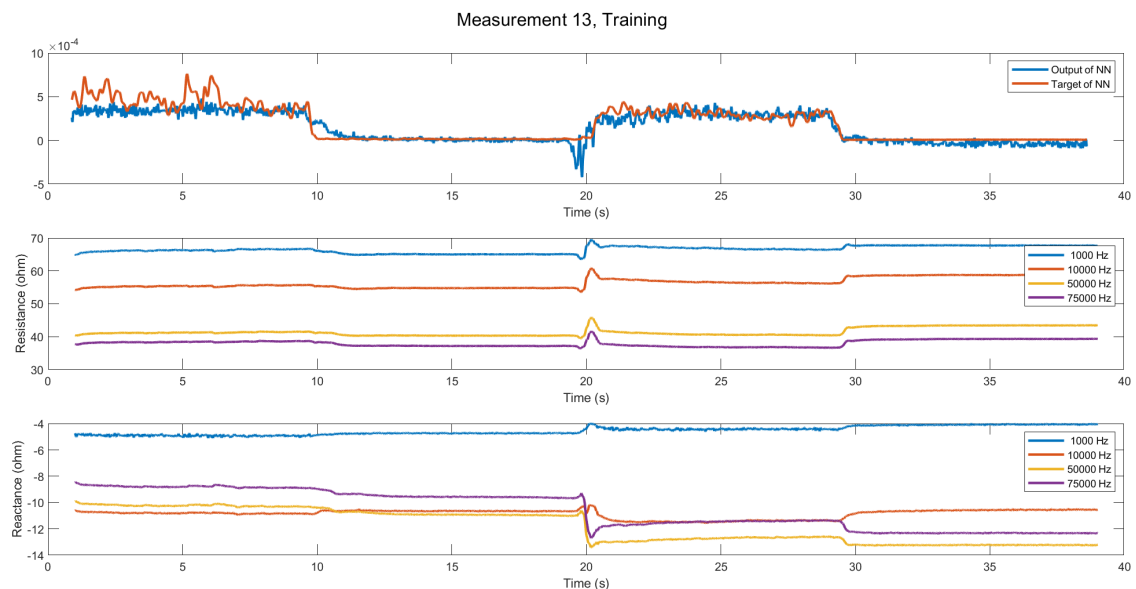


Figure F.14: Top figure: the target and the output of the time delay Neural network. The used Neural Network is given in Figure E.1. Middle figure: the 4 measured resistances, which are 4 of the 8 inputs for the NN. Bottom figure: the 4 measured reactances, which form the other 4 of 8 inputs for the NN.

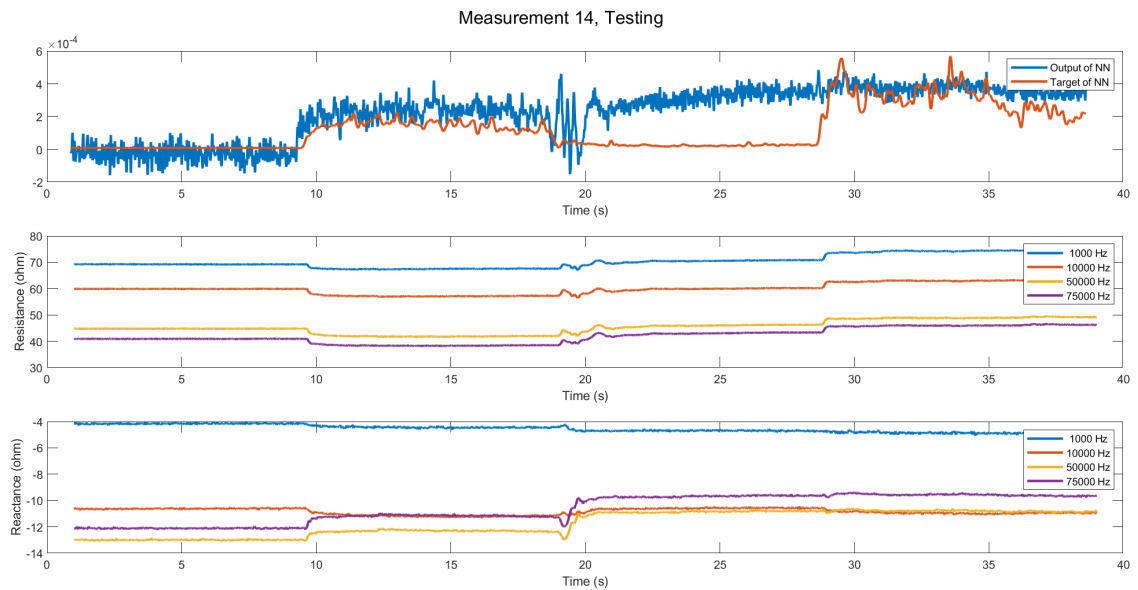


Figure F.15: Top figure: the target and the output of the time delay Neural network. The used Neural Network is given in Figure F.1. Middle figure: the 4 measured resistances, which are 4 of the 8 inputs for the NN. Bottom figure: the 4 measured reactances, which form the other 4 of 8 inputs for the NN.

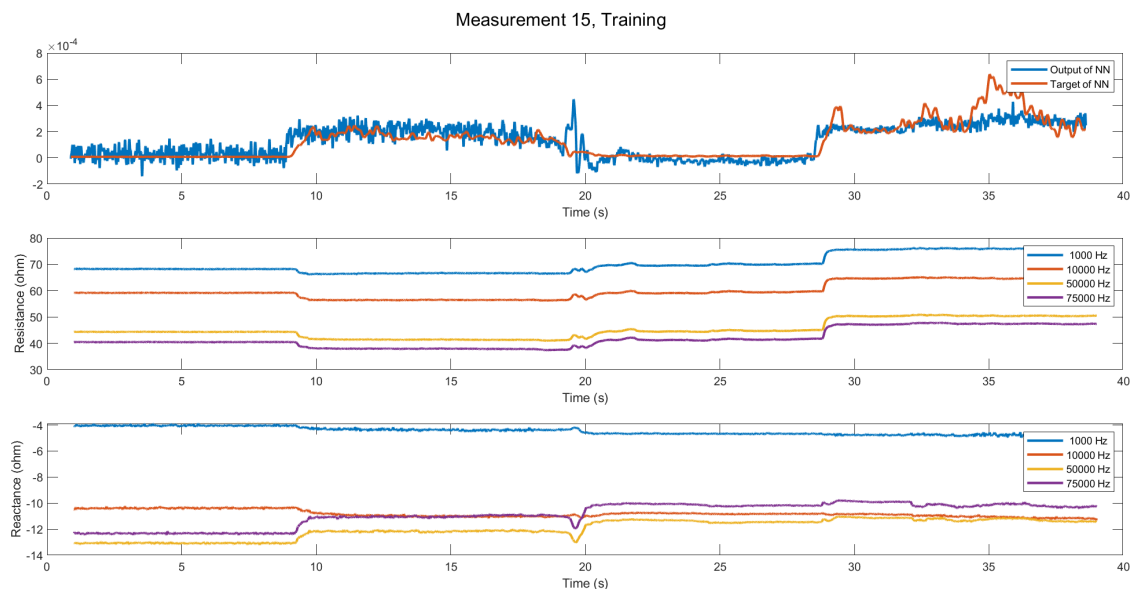


Figure F.16: Top figure: the target and the output of the time delay Neural network. The used Neural Network is given in Figure F.1. Middle figure: the 4 measured resistances, which are 4 of the 8 inputs for the NN. Bottom figure: the 4 measured reactances, which form the other 4 of 8 inputs for the NN.

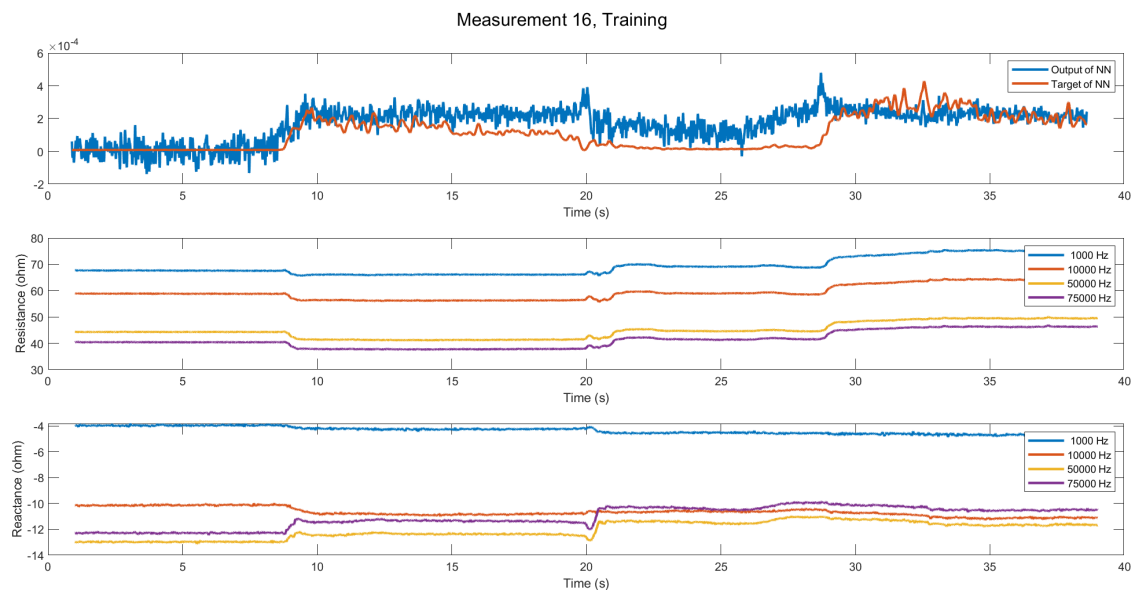


Figure F.17: Top figure: the target and the output of the time delay Neural network. The used Neural Network is given in Figure E.1. Middle figure: the 4 measured resistances, which are 4 of the 8 inputs for the NN. Bottom figure: the 4 measured reactances, which form the other 4 of 8 inputs for the NN.

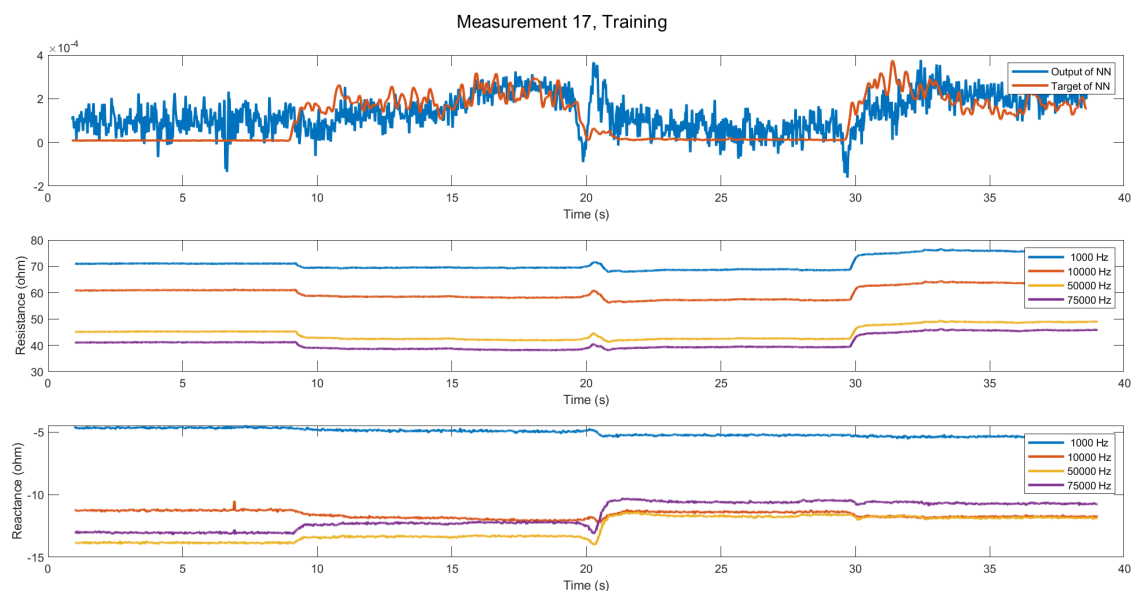


Figure F.18: Top figure: the target and the output of the time delay Neural network. The used Neural Network is given in Figure E.1. Middle figure: the 4 measured resistances, which are 4 of the 8 inputs for the NN. Bottom figure: the 4 measured reactances, which form the other 4 of 8 inputs for the NN.

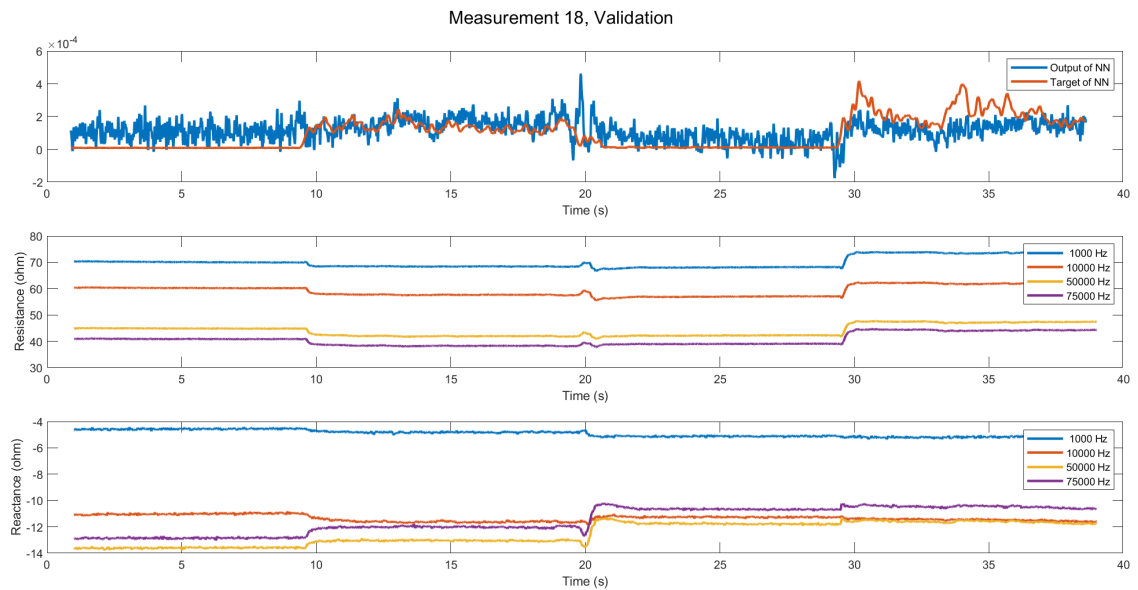


Figure F.19: Top figure: the target and the output of the time delay Neural network. The used Neural Network is given in Figure F.1. Middle figure: the 4 measured resistances, which are 4 of the 8 inputs for the NN. Bottom figure: the 4 measured reactances, which form the other 4 of 8 inputs for the NN.



Figure F.20: Top figure: the target and the output of the time delay Neural network. The used Neural Network is given in Figure F.1. Middle figure: the 4 measured resistances, which are 4 of the 8 inputs for the NN. Bottom figure: the 4 measured reactances, which form the other 4 of 8 inputs for the NN.

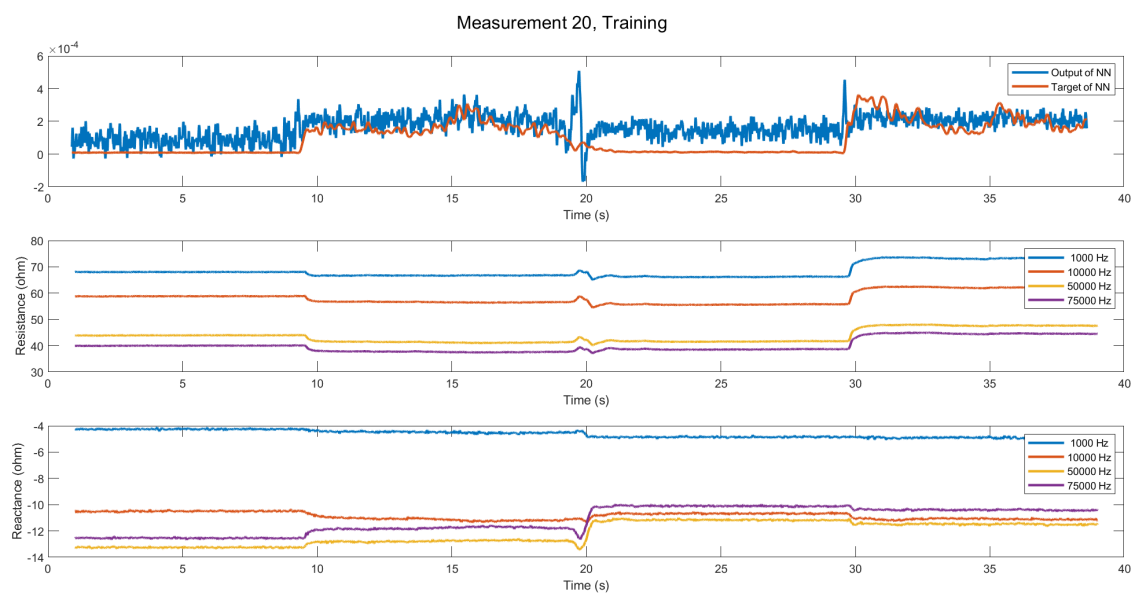


Figure E21: Top figure: the target and the output of the time delay Neural network. The used Neural Network is given in Figure E.1. Middle figure: the 4 measured resistances, which are 4 of the 8 inputs for the NN. Bottom figure: the 4 measured reactances, which form the other 4 of 8 inputs for the NN.

G Muscle contraction and movement data

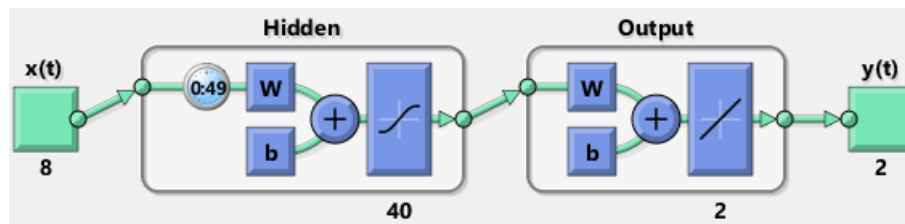


Figure G.1: The neural network used for the EMG and movement signals. The NN has 50 delays, 40 neurons, 8 inputs and 2 outputs.

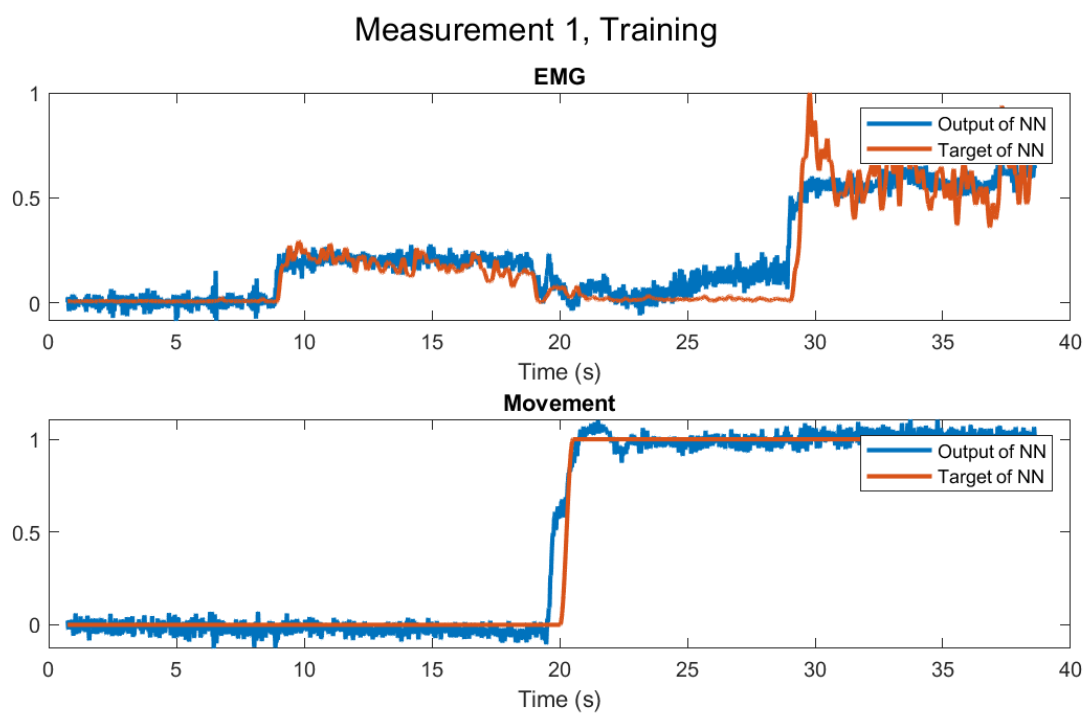


Figure G.2: Top figure: the first target and output of the NN. The target is the measured EMG which is down sampled and normalized between 0 and 1. Bottom figure: the second target and output of the NN. The target represents the arm position which is either 0 or 1. The switching point is based on the switching point in the reactance at 75 kHz around 20 s.

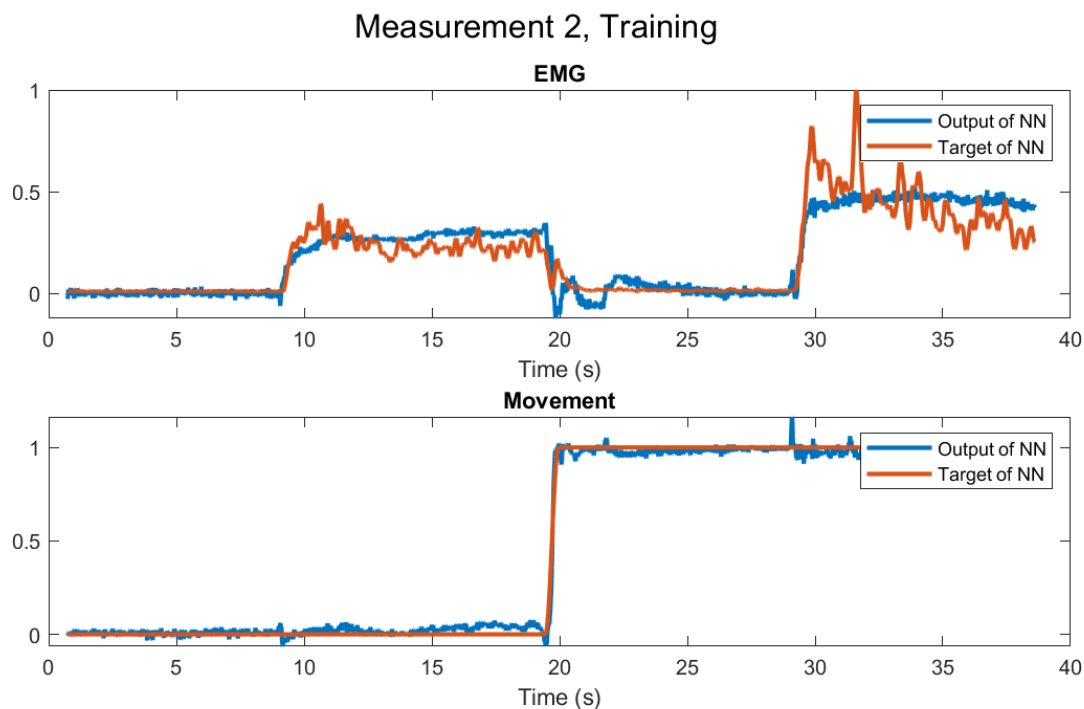


Figure G.3: Top figure: the first target and output of the NN. The target is the measured EMG which is down sampled and normalized between 0 and 1. Bottom figure: the second target and output of the NN. The target represents the arm position which is either 0 or 1. The switching point is based on the switching point in the reactance at 75 kHz around 20 s.

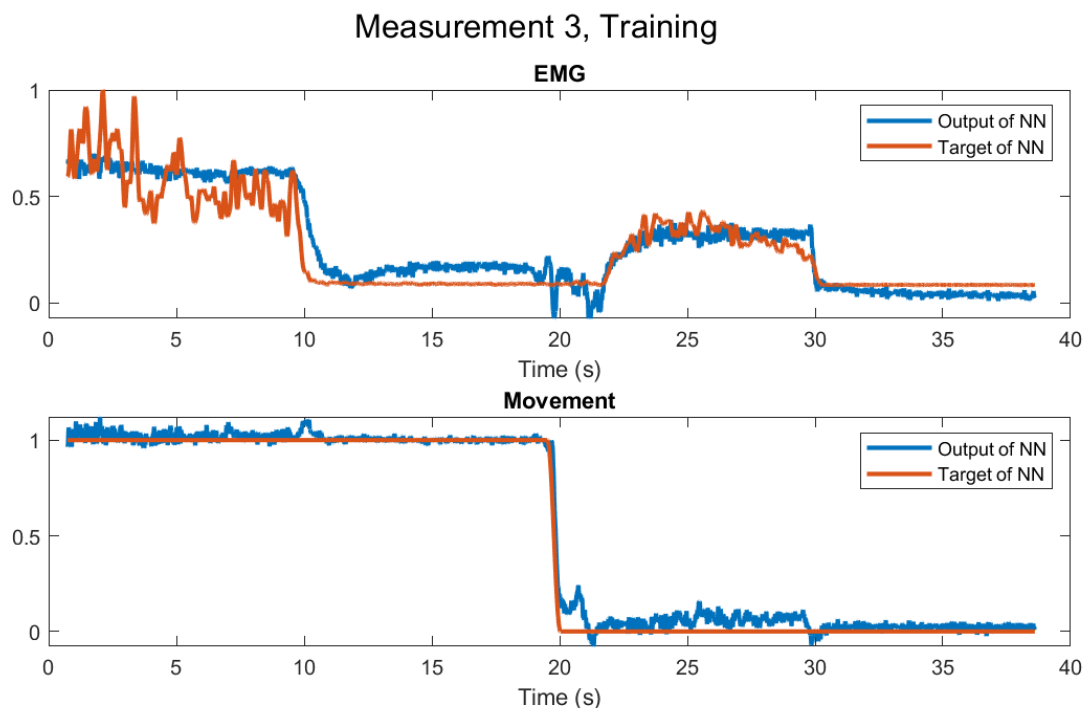


Figure G.4: Top figure: the first target and output of the NN. The target is the measured EMG which is down sampled and normalized between 0 and 1. Bottom figure: the second target and output of the NN. The target represents the arm position which is either 0 or 1. The switching point is based on the switching point in the reactance at 75 kHz around 20 s.

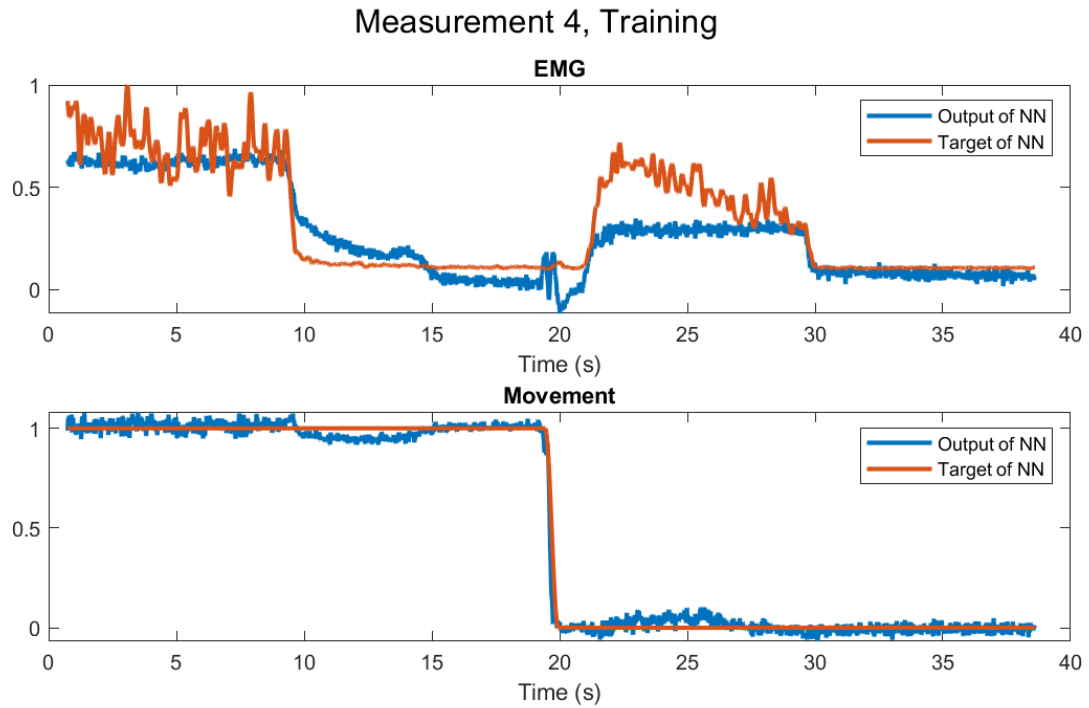


Figure G.5: Top figure: the first target and output of the NN. The target is the measured EMG which is down sampled and normalized between 0 and 1. Bottom figure: the second target and output of the NN. The target represents the arm position which is either 0 or 1. The switching point is based on the switching point in the reactance at 75 kHz around 20 s.

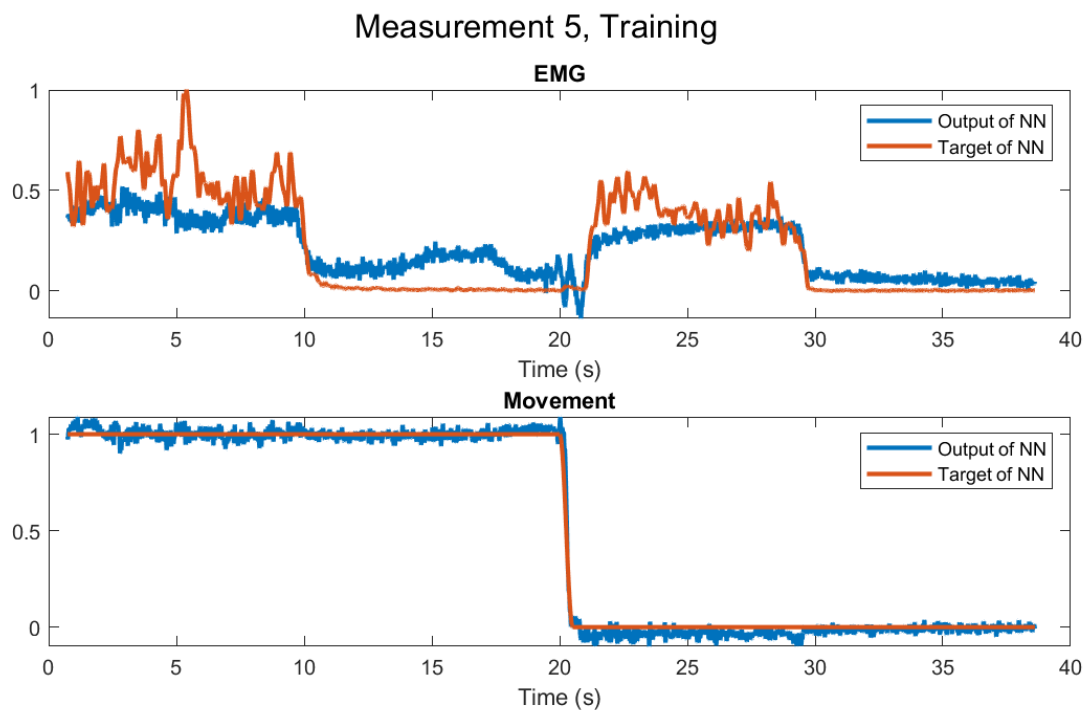


Figure G.6: Top figure: the first target and output of the NN. The target is the measured EMG which is down sampled and normalized between 0 and 1. Bottom figure: the second target and output of the NN. The target represents the arm position which is either 0 or 1. The switching point is based on the switching point in the reactance at 75 kHz around 20 s.

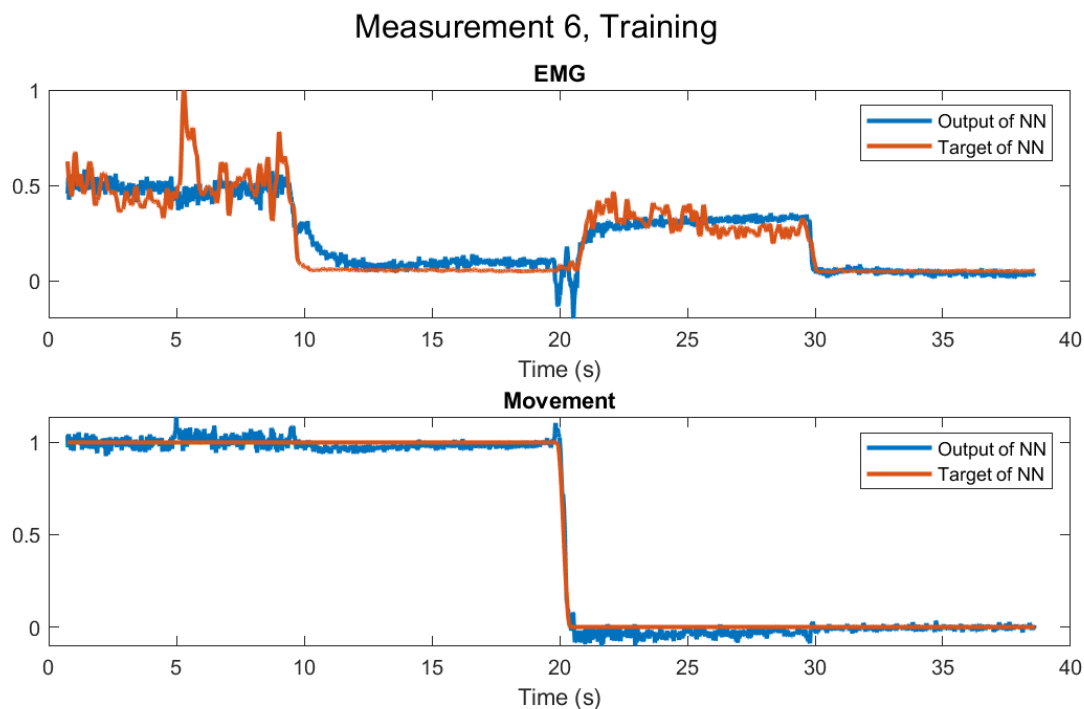


Figure G.7: Top figure: the first target and output of the NN. The target is the measured EMG which is down sampled and normalized between 0 and 1. Bottom figure: the second target and output of the NN. The target represents the arm position which is either 0 or 1. The switching point is based on the switching point in the reactance at 75 kHz around 20 s.

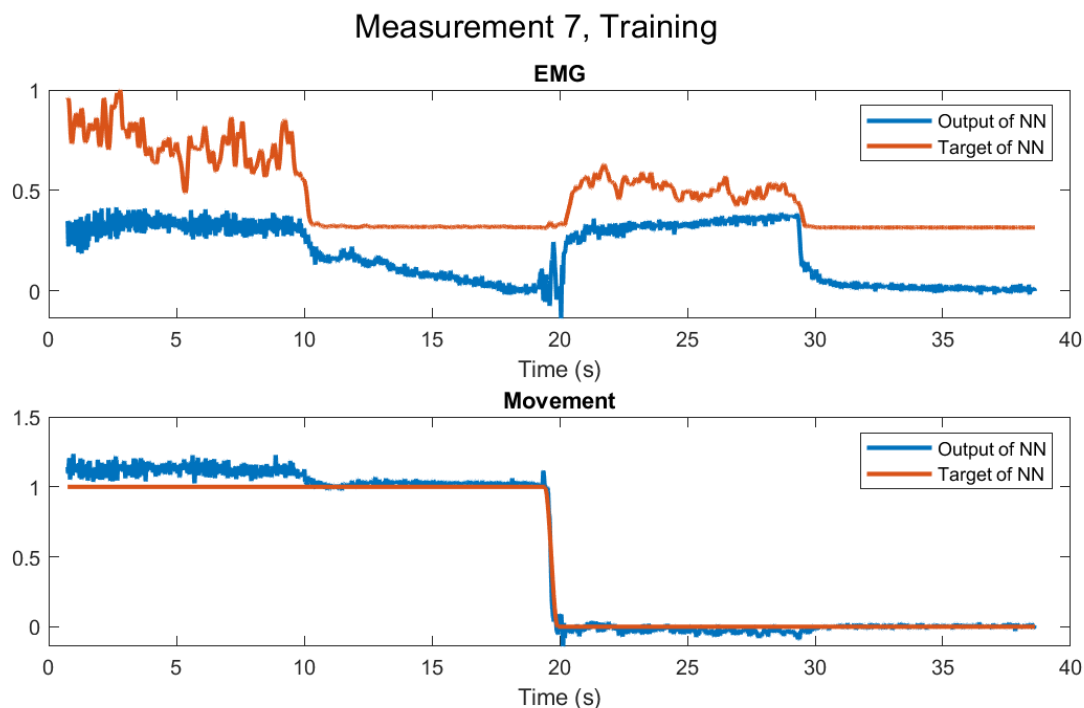


Figure G.8: Top figure: the first target and output of the NN. The target is the measured EMG which is down sampled and normalized between 0 and 1. Bottom figure: the second target and output of the NN. The target represents the arm position which is either 0 or 1. The switching point is based on the switching point in the reactance at 75 kHz around 20 s.

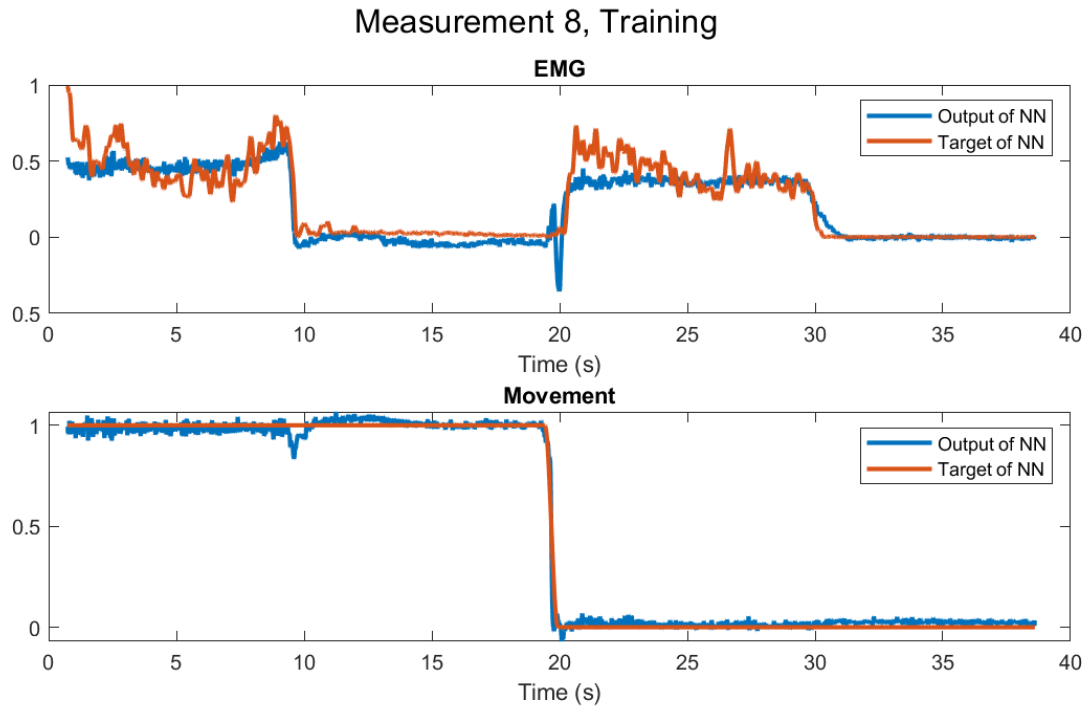


Figure G.9: Top figure: the first target and output of the NN. The target is the measured EMG which is down sampled and normalized between 0 and 1. Bottom figure: the second target and output of the NN. The target represents the arm position which is either 0 or 1. The switching point is based on the switching point in the reactance at 75 kHz around 20 s.

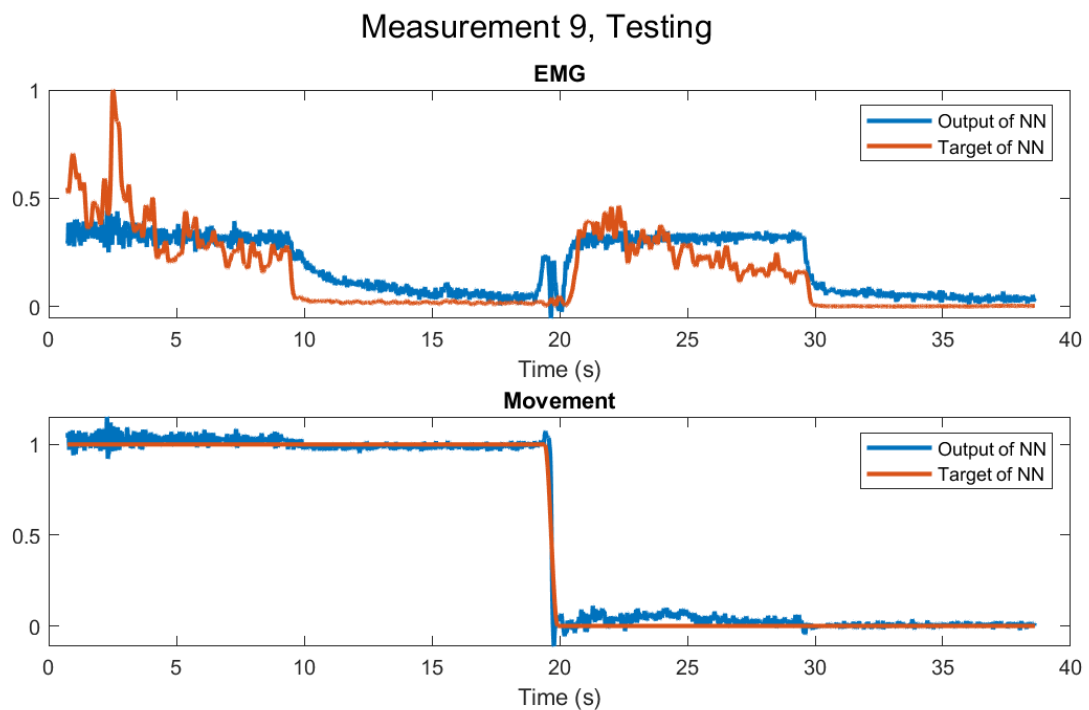


Figure G.10: Top figure: the first target and output of the NN. The target is the measured EMG which is down sampled and normalized between 0 and 1. Bottom figure: the second target and output of the NN. The target represents the arm position which is either 0 or 1. The switching point is based on the switching point in the reactance at 75 kHz around 20 s.

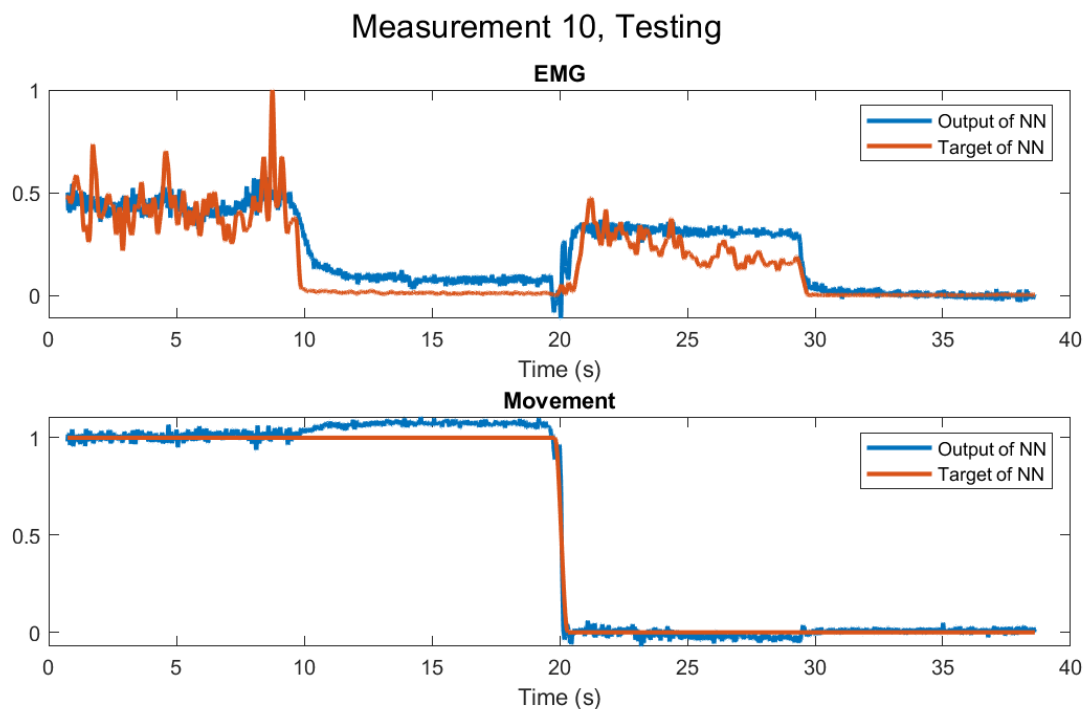


Figure G.11: Top figure: the first target and output of the NN. The target is the measured EMG which is down sampled and normalized between 0 and 1. Bottom figure: the second target and output of the NN. The target represents the arm position which is either 0 or 1. The switching point is based on the switching point in the reactance at 75 kHz around 20 s.

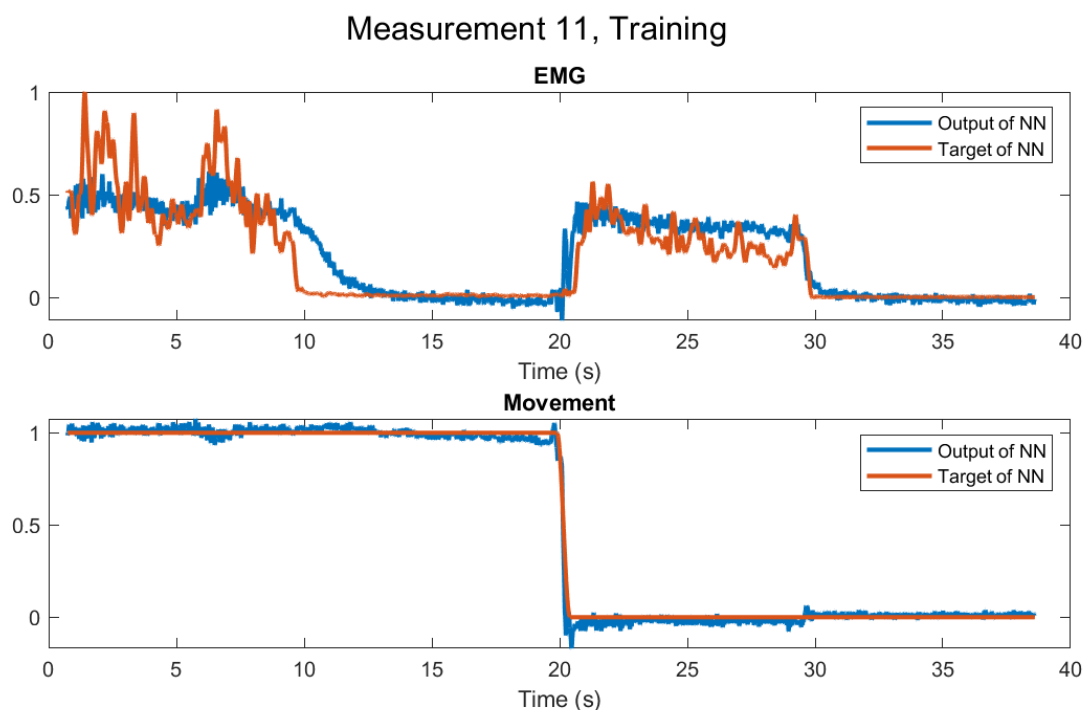


Figure G.12: Top figure: the first target and output of the NN. The target is the measured EMG which is down sampled and normalized between 0 and 1. Bottom figure: the second target and output of the NN. The target represents the arm position which is either 0 or 1. The switching point is based on the switching point in the reactance at 75 kHz around 20 s.

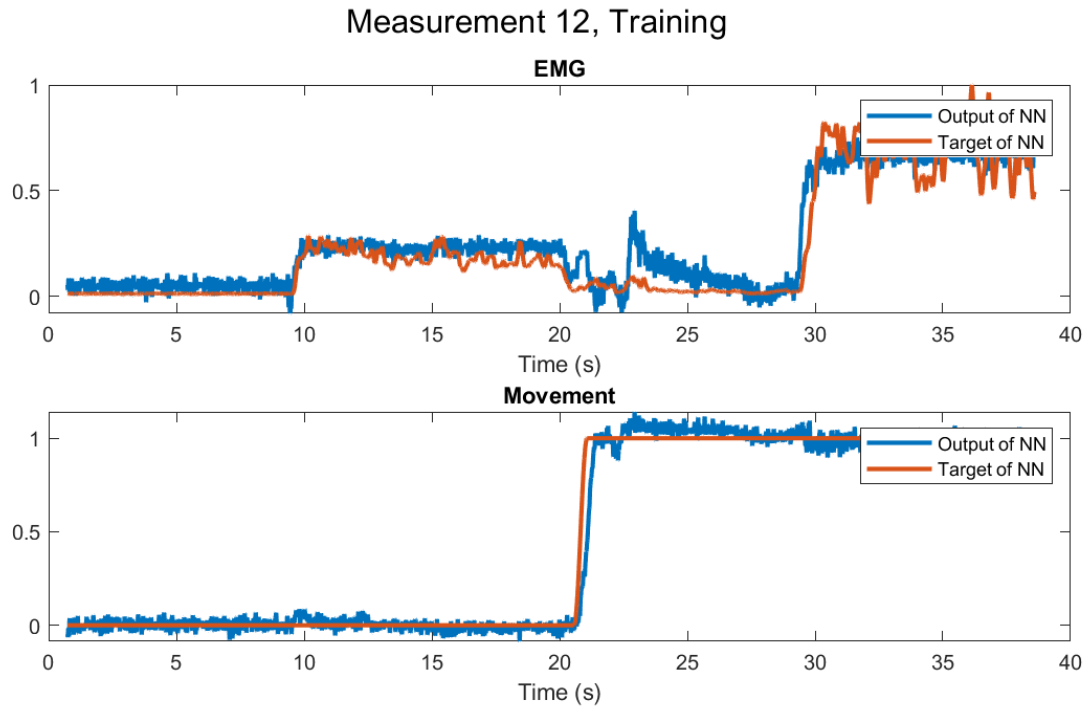


Figure G.13: Top figure: the first target and output of the NN. The target is the measured EMG which is down sampled and normalized between 0 and 1. Bottom figure: the second target and output of the NN. The target represents the arm position which is either 0 or 1. The switching point is based on the switching point in the reactance at 75 kHz around 20 s.

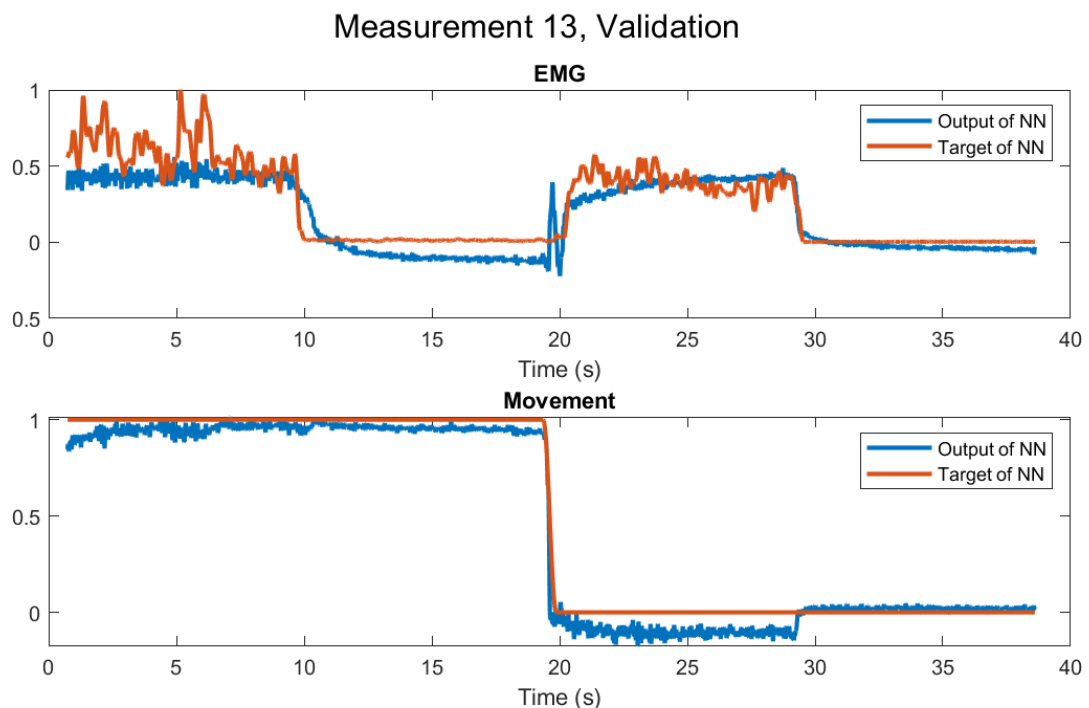


Figure G.14: Top figure: the first target and output of the NN. The target is the measured EMG which is down sampled and normalized between 0 and 1. Bottom figure: the second target and output of the NN. The target represents the arm position which is either 0 or 1. The switching point is based on the switching point in the reactance at 75 kHz around 20 s.

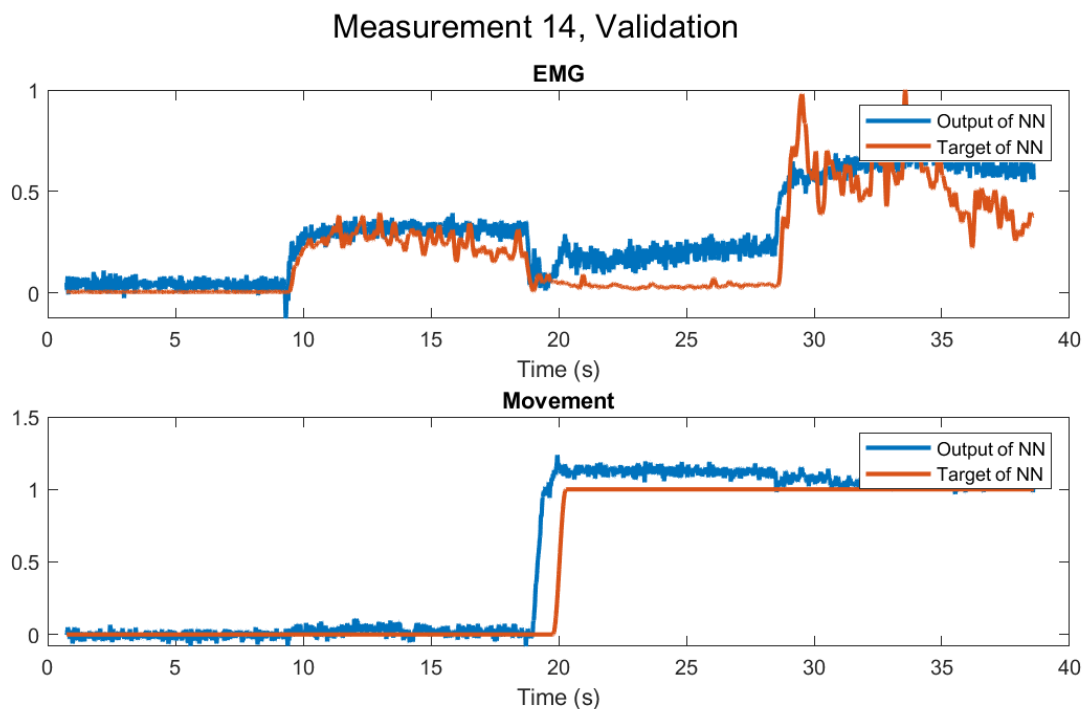


Figure G.15: Top figure: the first target and output of the NN. The target is the measured EMG which is down sampled and normalized between 0 and 1. Bottom figure: the second target and output of the NN. The target represents the arm position which is either 0 or 1. The switching point is based on the switching point in the reactance at 75 kHz around 20 s.

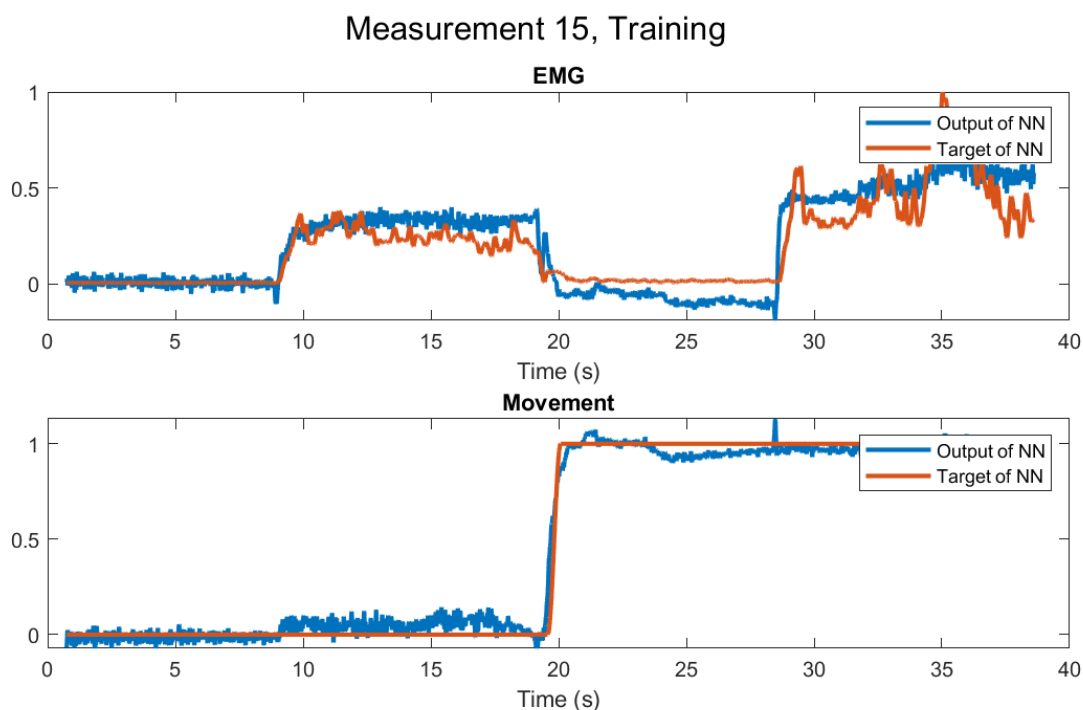


Figure G.16: Top figure: the first target and output of the NN. The target is the measured EMG which is down sampled and normalized between 0 and 1. Bottom figure: the second target and output of the NN. The target represents the arm position which is either 0 or 1. The switching point is based on the switching point in the reactance at 75 kHz around 20 s.

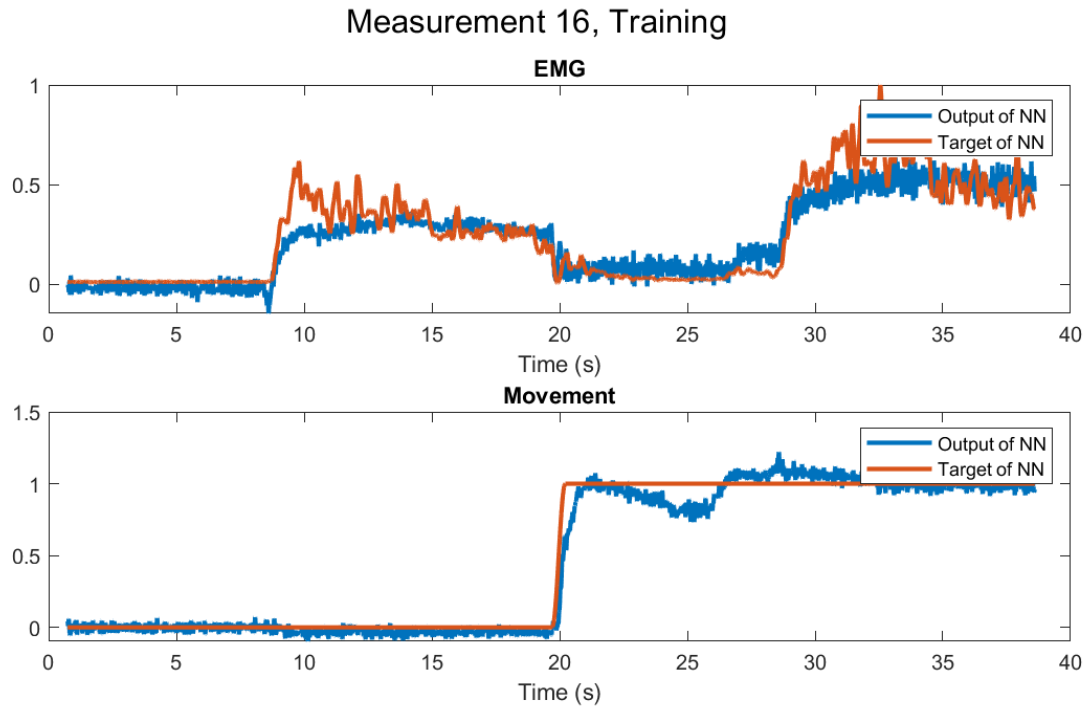


Figure G.17: Top figure: the first target and output of the NN. The target is the measured EMG which is down sampled and normalized between 0 and 1. Bottom figure: the second target and output of the NN. The target represents the arm position which is either 0 or 1. The switching point is based on the switching point in the reactance at 75 kHz around 20 s.

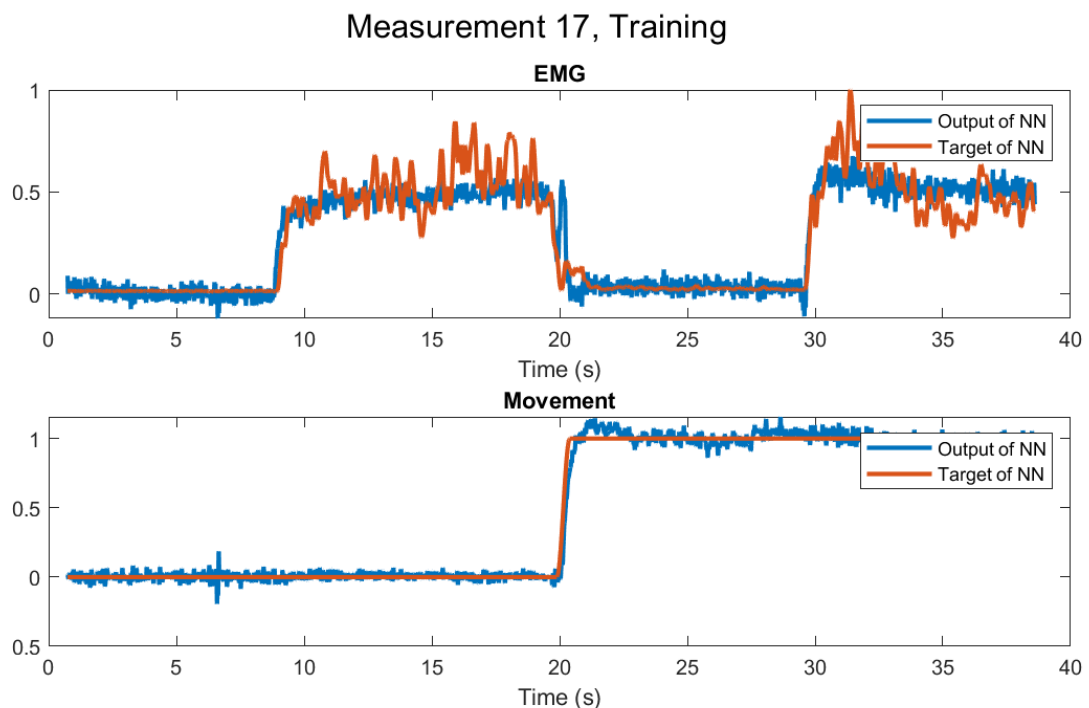


Figure G.18: Top figure: the first target and output of the NN. The target is the measured EMG which is down sampled and normalized between 0 and 1. Bottom figure: the second target and output of the NN. The target represents the arm position which is either 0 or 1. The switching point is based on the switching point in the reactance at 75 kHz around 20 s.

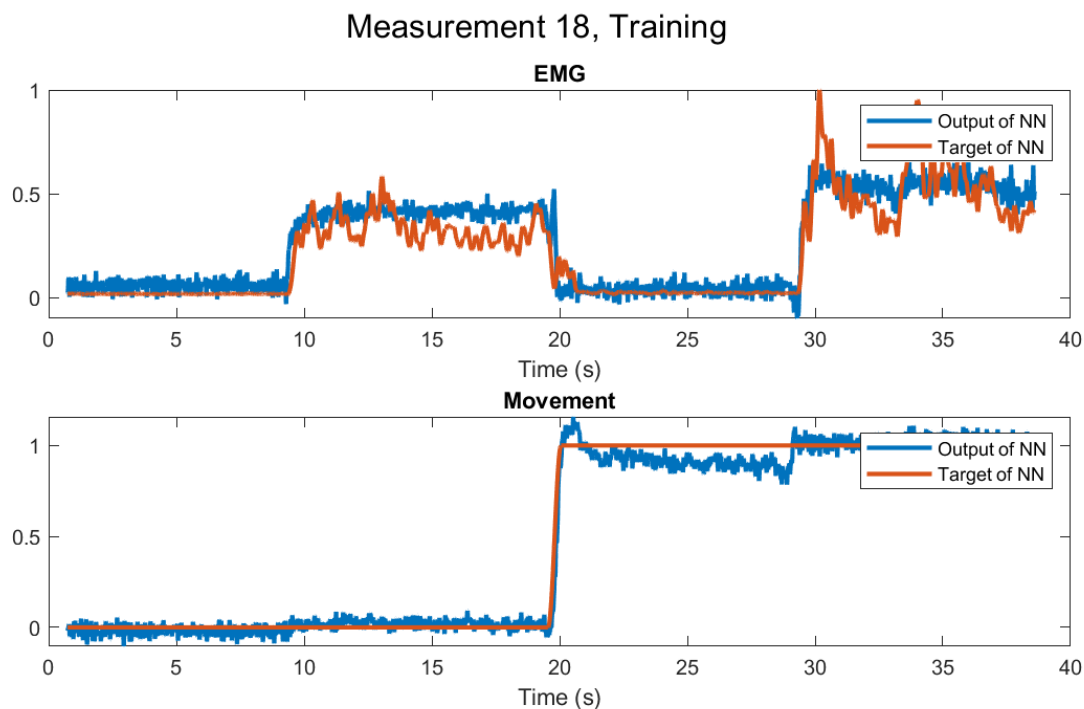


Figure G.19: Top figure: the first target and output of the NN. The target is the measured EMG which is down sampled and normalized between 0 and 1. Bottom figure: the second target and output of the NN. The target represents the arm position which is either 0 or 1. The switching point is based on the switching point in the reactance at 75 kHz around 20 s.

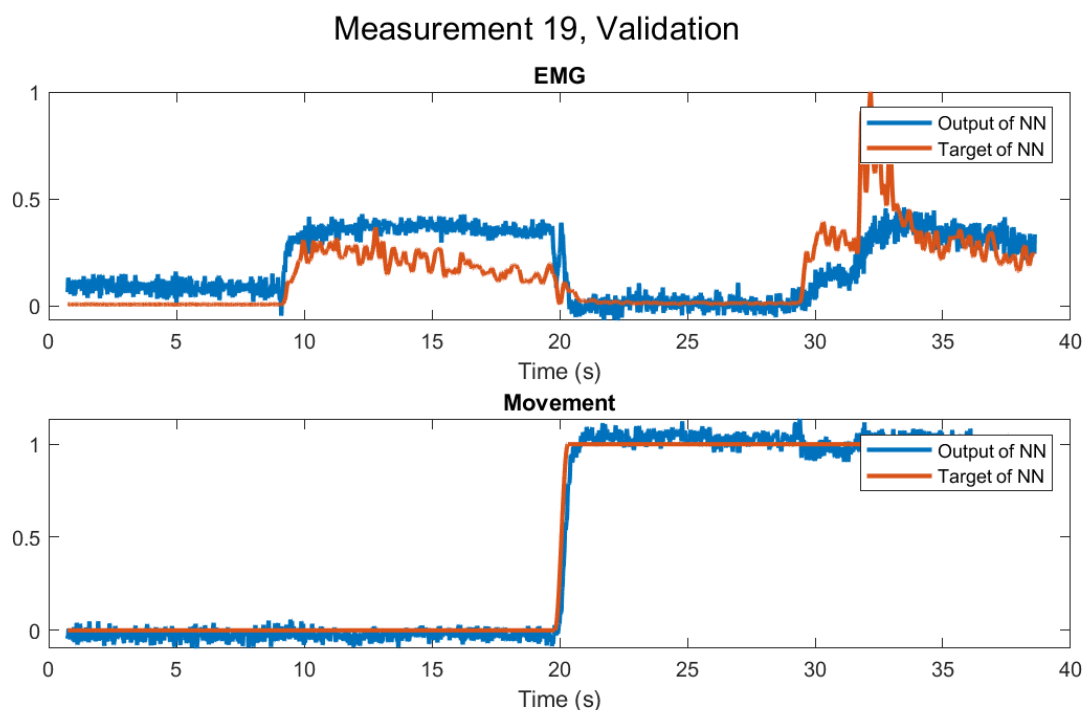


Figure G.20: Top figure: the first target and output of the NN. The target is the measured EMG which is down sampled and normalized between 0 and 1. Bottom figure: the second target and output of the NN. The target represents the arm position which is either 0 or 1. The switching point is based on the switching point in the reactance at 75 kHz around 20 s.

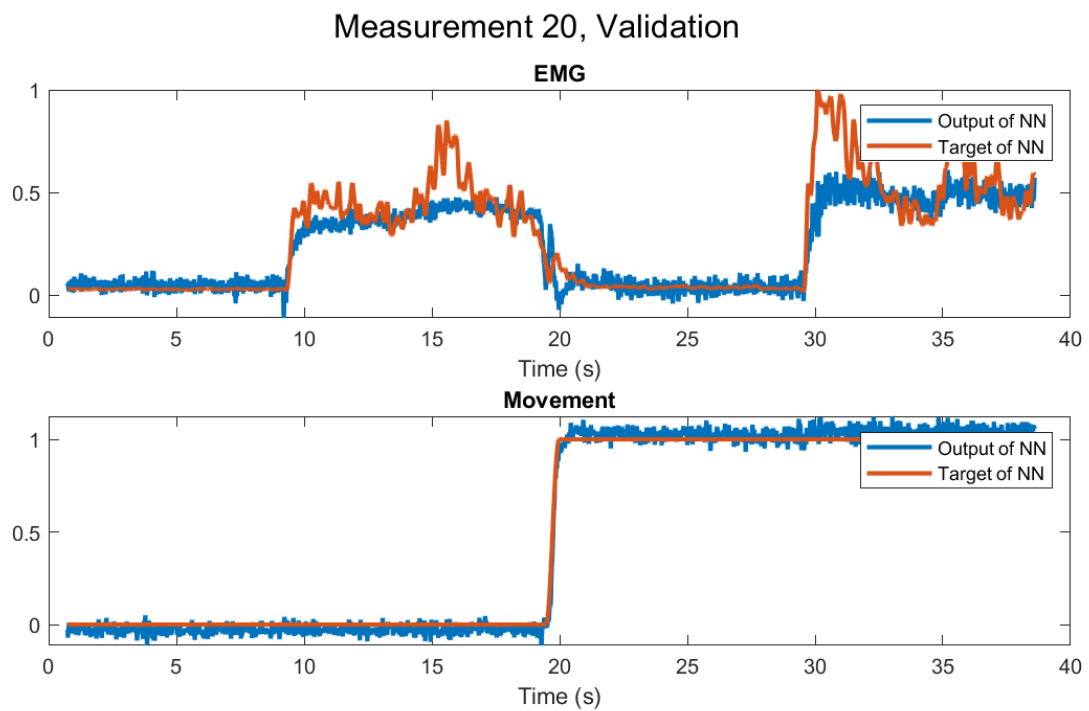


Figure G.21: Top figure: the first target and output of the NN. The target is the measured EMG which is down sampled and normalized between 0 and 1. Bottom figure: the second target and output of the NN. The target represents the arm position which is either 0 or 1. The switching point is based on the switching point in the reactance at 75 kHz around 20 s.

H Force measurements

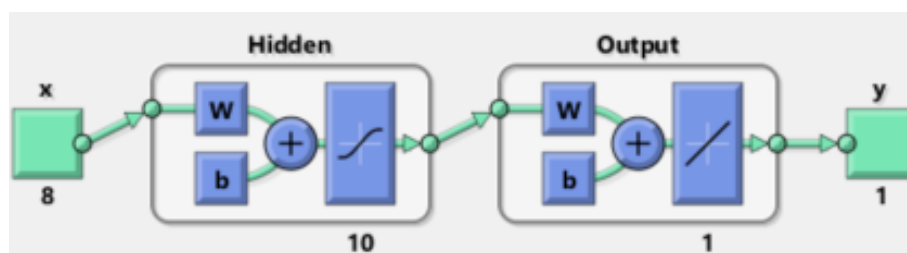


Figure H.1: The used neural network for the bio-impedance input signals. The EMG NN is exactly the same except that it has only one input instead of 8. No time delay is used because all signals are in the same state at the time of measurement. Only ten neurons are used because there is no movement within the contraction.

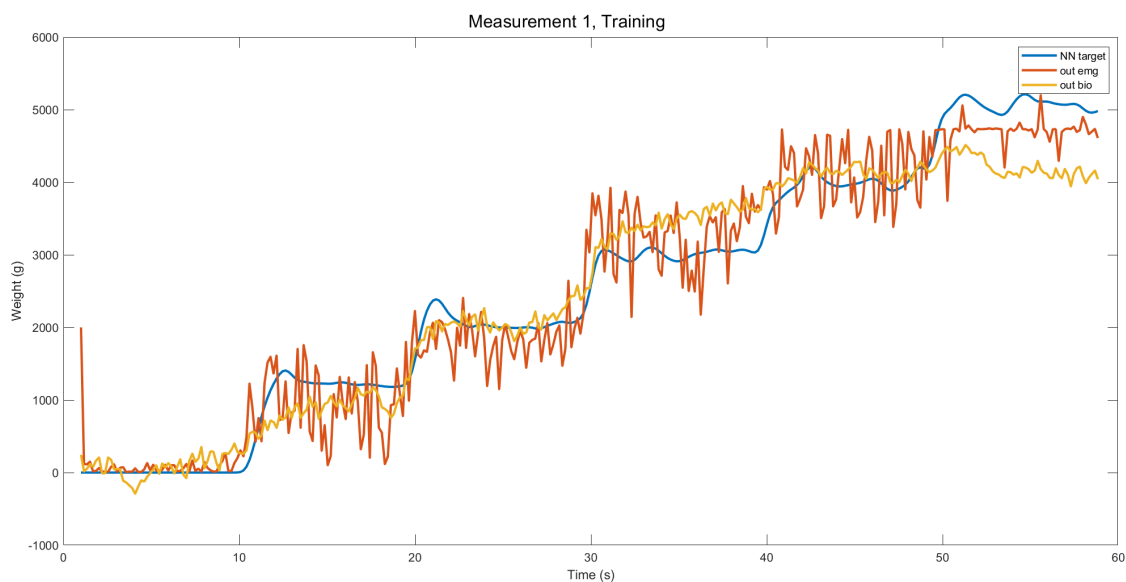


Figure H.2: The target, output of the bio-impedance NN and the output of the EMG NN of measurement number 1 of the force measurement as described in Section 3.4.2. The desired force is changed with 1 kg every 10 s.

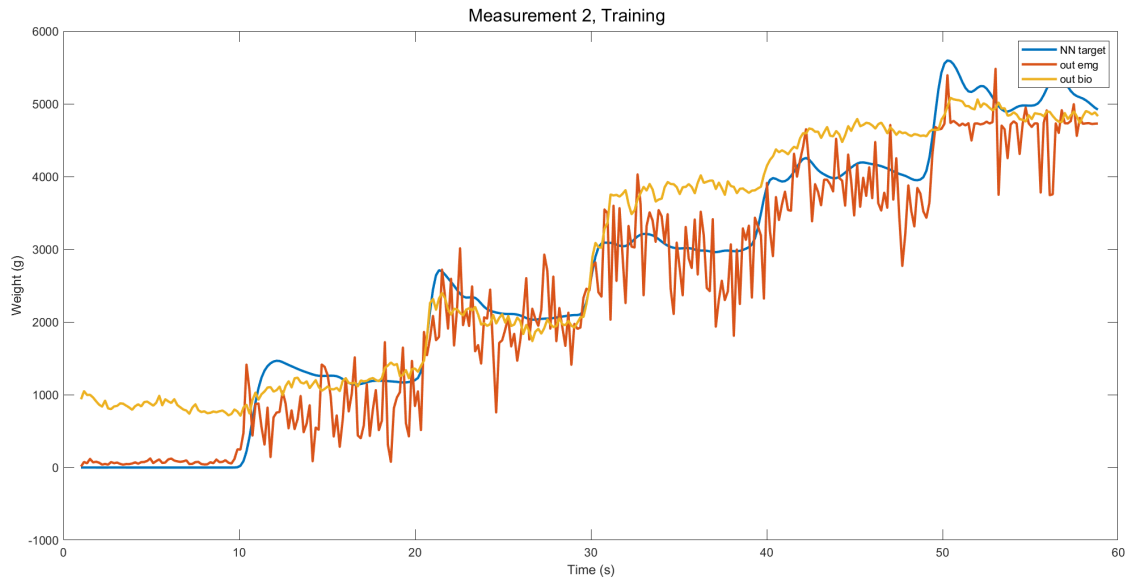


Figure H.3: The target, output of the bio-impedance NN and the output of the EMG NN of measurement number 2 of the force measurement as described in Section 3.4.2. The desired force is changed with 1 kg every 10 s.

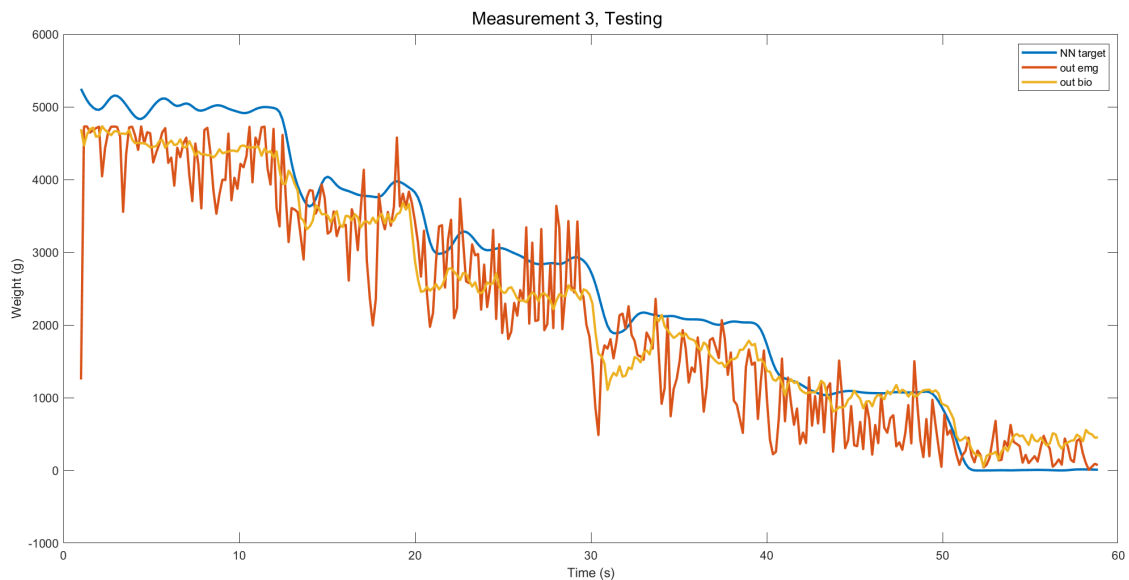


Figure H.4: The target, output of the bio-impedance NN and the output of the EMG NN of measurement number 3 of the force measurement as described in Section 3.4.2. The desired force is changed with 1 kg every 10 s.

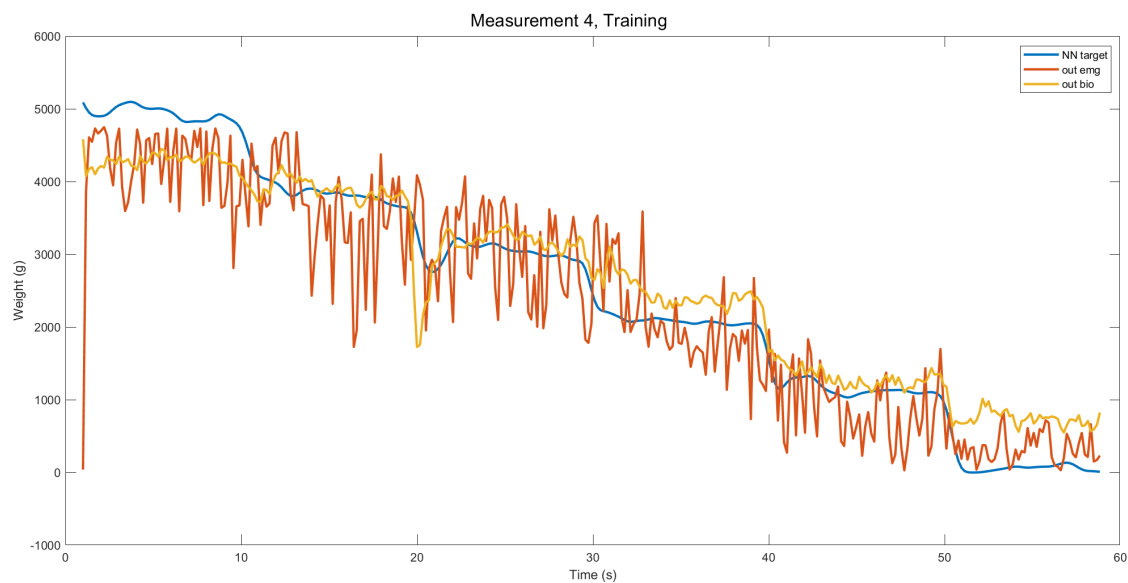


Figure H.5: The target, output of the bio-impedance NN and the output of the EMG NN of measurement number 4 of the force measurement as described in Section 3.4.2. The desired force is changed with 1 kg every 10 s.

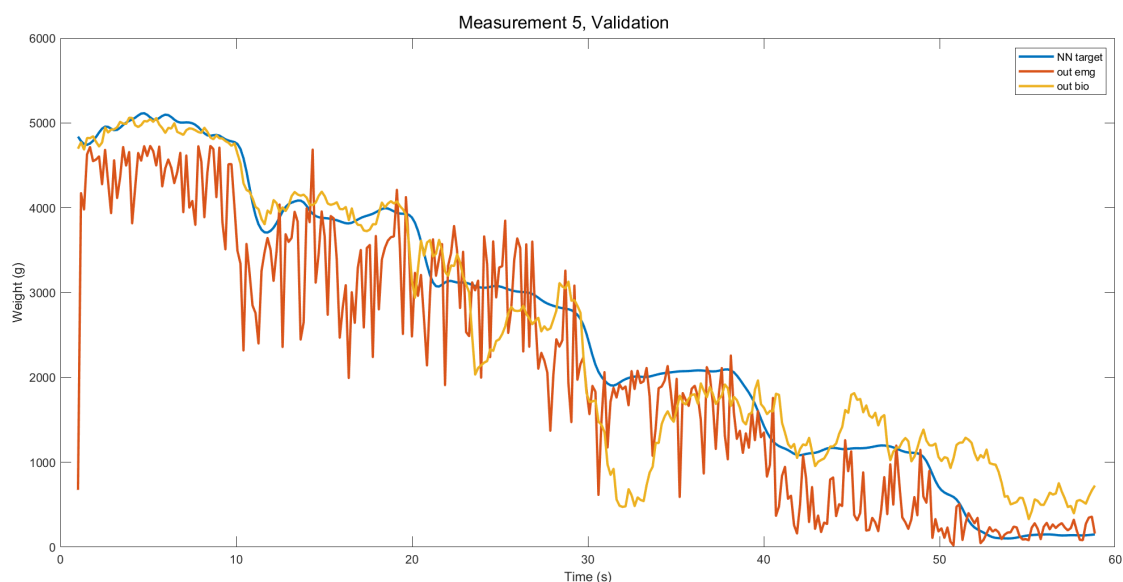


Figure H.6: The target, output of the bio-impedance NN and the output of the EMG NN of measurement number 5 of the force measurement as described in Section 3.4.2. The desired force is changed with 1 kg every 10 s.

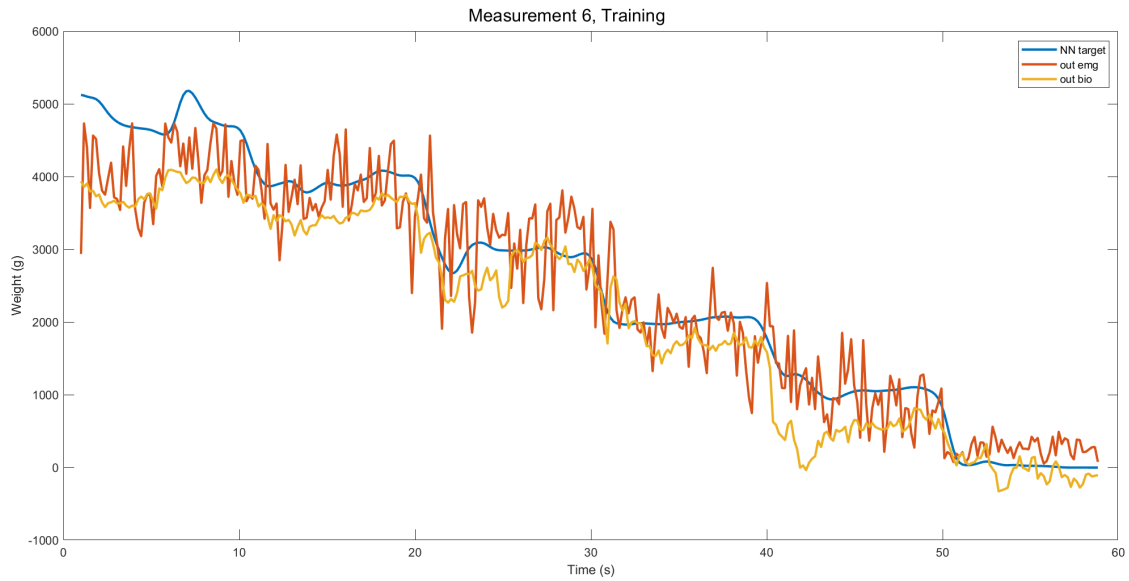


Figure H.7: The target, output of the bio-impedance NN and the output of the EMG NN of measurement number 6 of the force measurement as described in Section 3.4.2. The desired force is changed with 1 kg every 10 s.

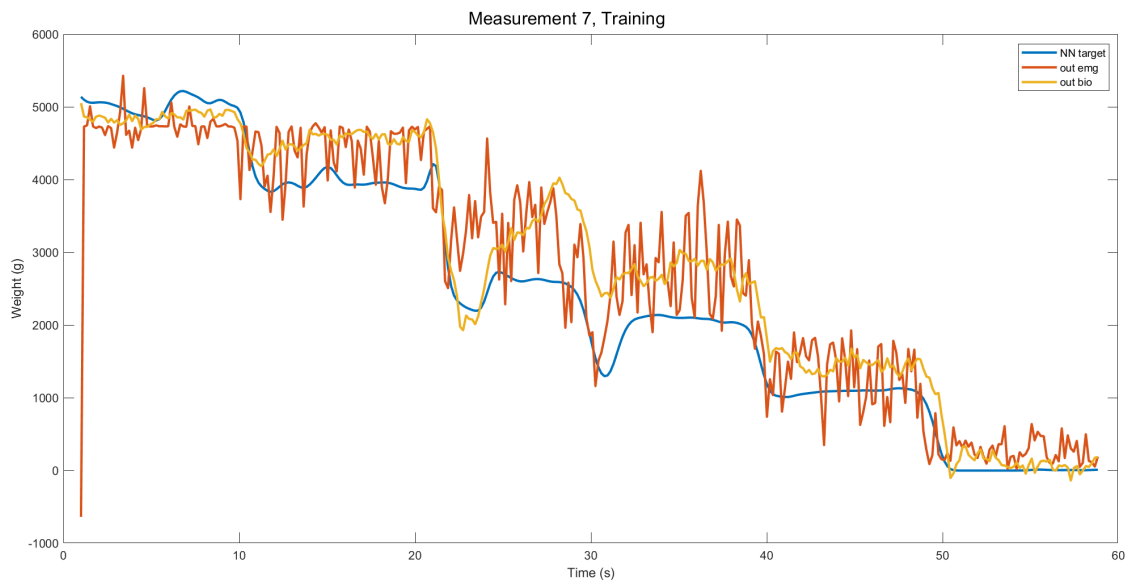


Figure H.8: The target, output of the bio-impedance NN and the output of the EMG NN of measurement number 7 of the force measurement as described in Section 3.4.2. The desired force is changed with 1 kg every 10 s.

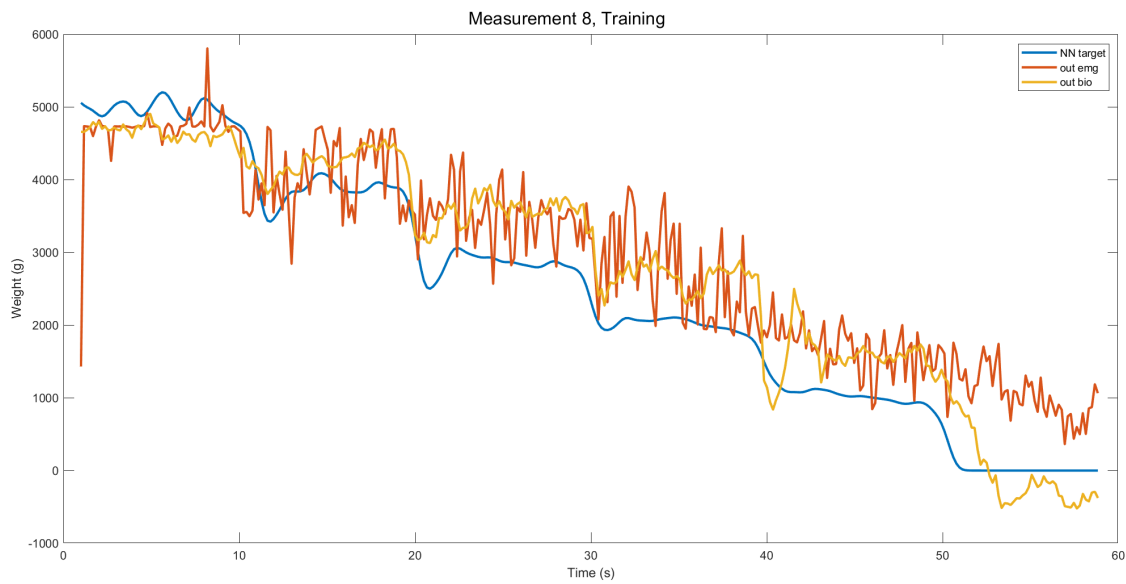


Figure H.9: The target, output of the bio-impedance NN and the output of the EMG NN of measurement number 8 of the force measurement as described in Section 3.4.2. The desired force is changed with 1 kg every 10 s.

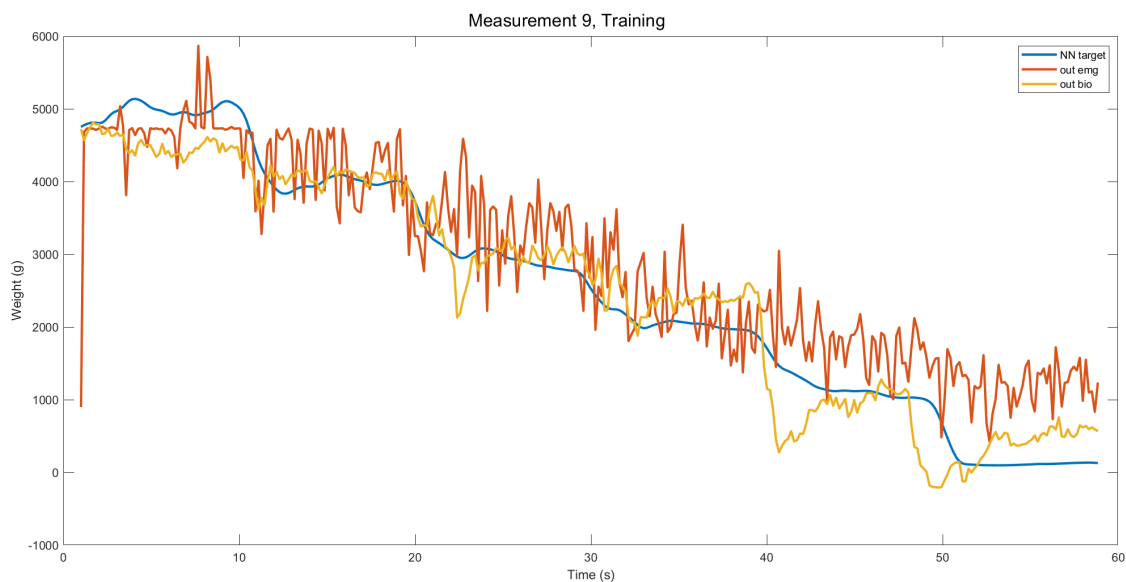


Figure H.10: The target, output of the bio-impedance NN and the output of the EMG NN of measurement number 9 of the force measurement as described in Section 3.4.2. The desired force is changed with 1 kg every 10 s.

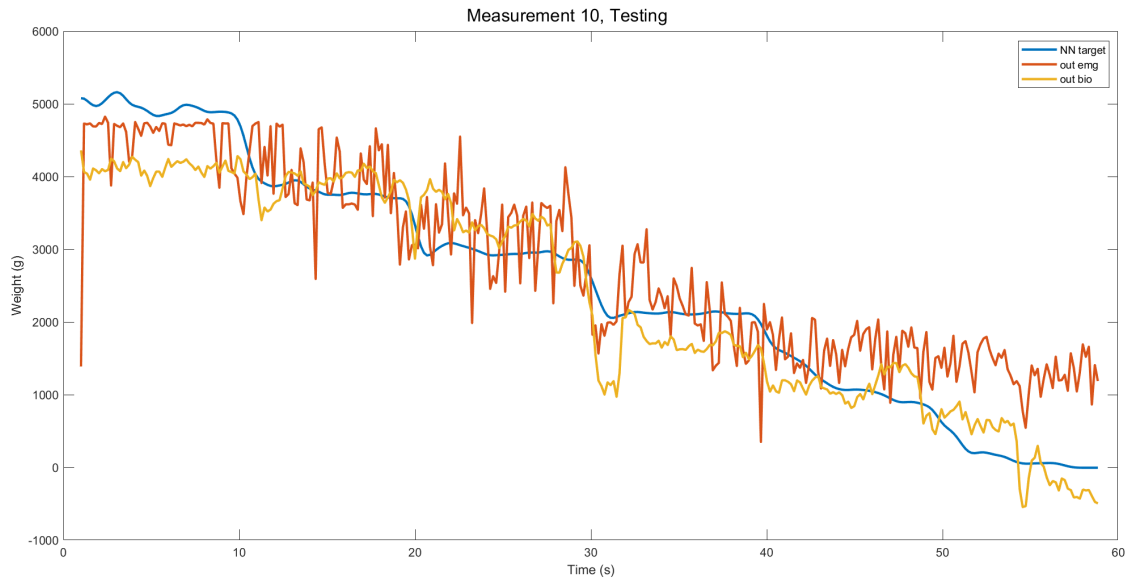


Figure H.11: The target, output of the bio-impedance NN and the output of the EMG NN of measurement number 10 of the force measurement as described in Section 3.4.2. The desired force is changed with 1 kg every 10 s.

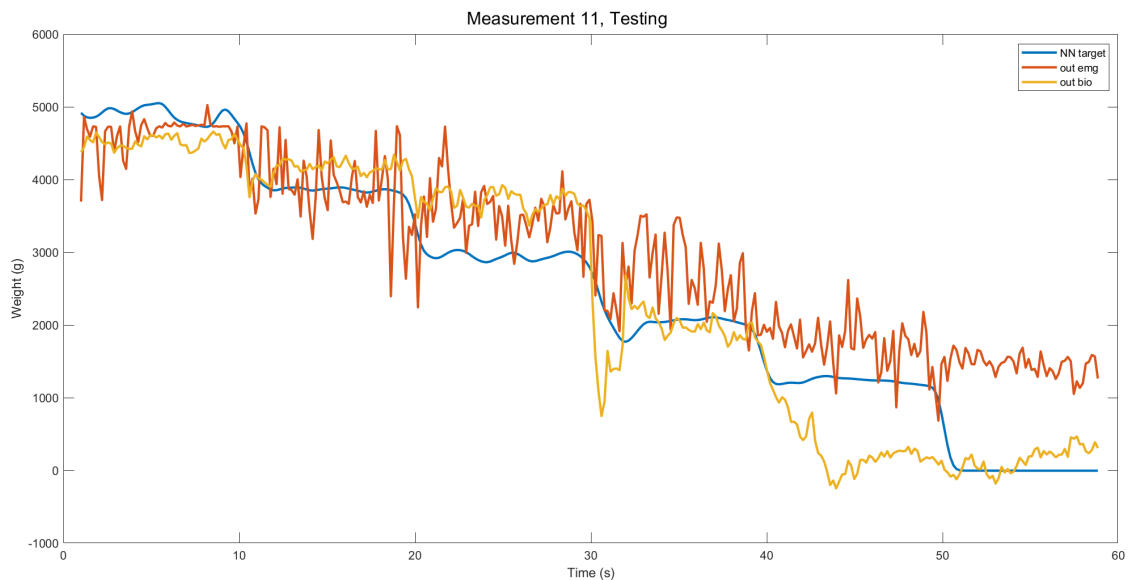


Figure H.12: The target, output of the bio-impedance NN and the output of the EMG NN of measurement number 11 of the force measurement as described in Section 3.4.2. The desired force is changed with 1 kg every 10 s.

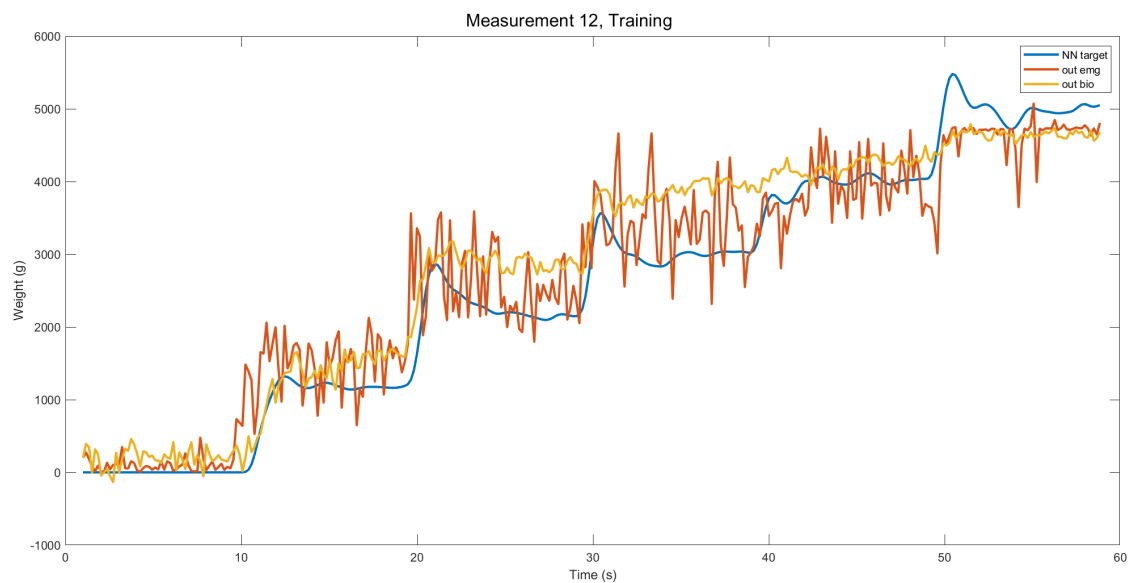


Figure H.13: The target, output of the bio-impedance NN and the output of the EMG NN of measurement number 12 of the force measurement as described in Section 3.4.2. The desired force is changed with 1 kg every 10 s.

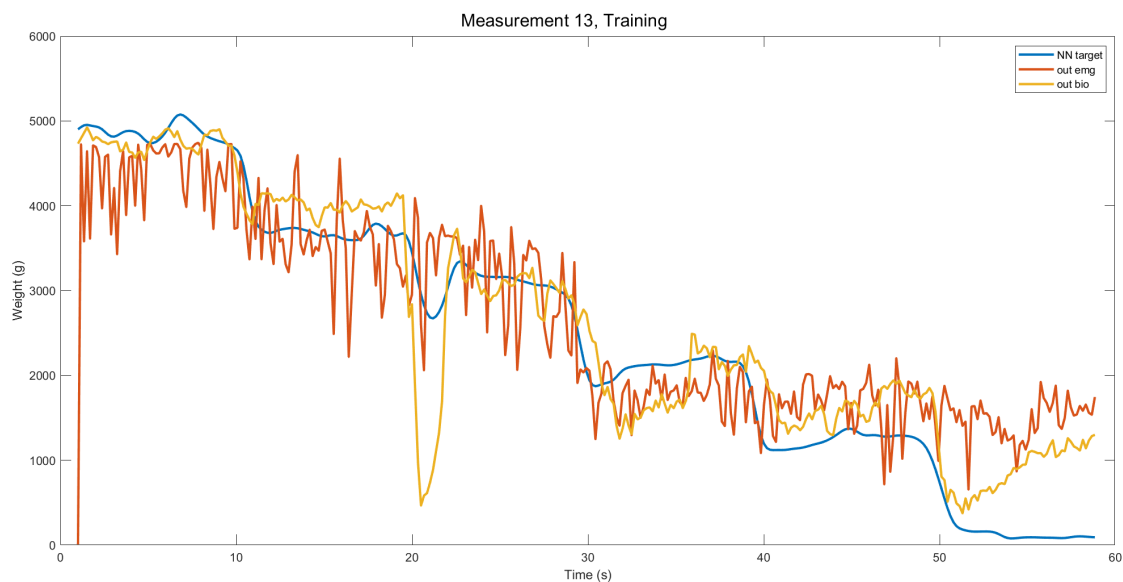


Figure H.14: The target, output of the bio-impedance NN and the output of the EMG NN of measurement number 13 of the force measurement as described in Section 3.4.2. The desired force is changed with 1 kg every 10 s.

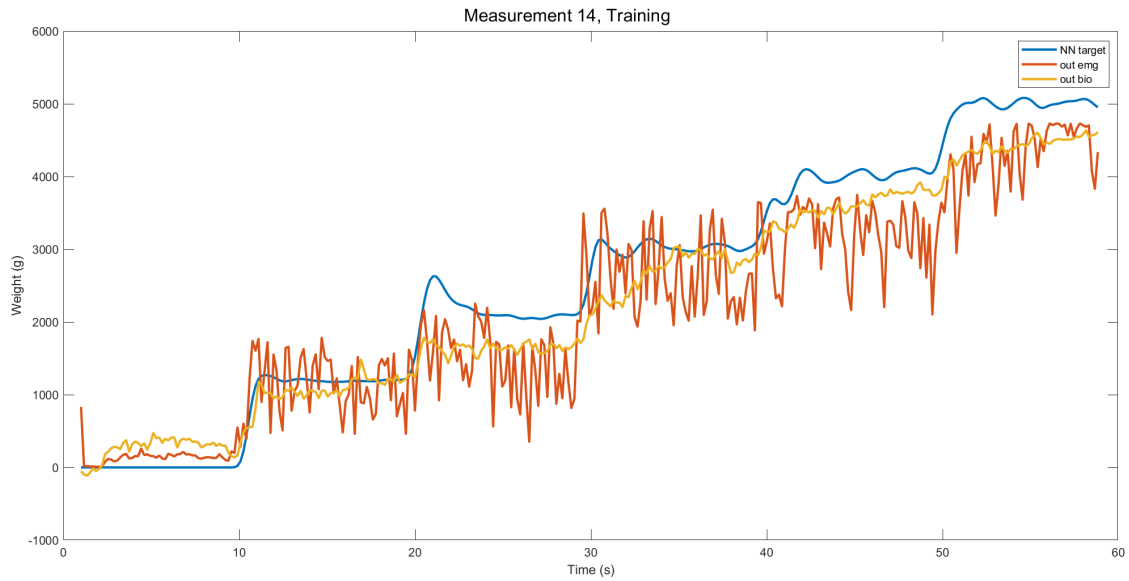


Figure H.15: The target, output of the bio-impedance NN and the output of the EMG NN of measurement number 14 of the force measurement as described in Section 3.4.2. The desired force is changed with 1 kg every 10 s.

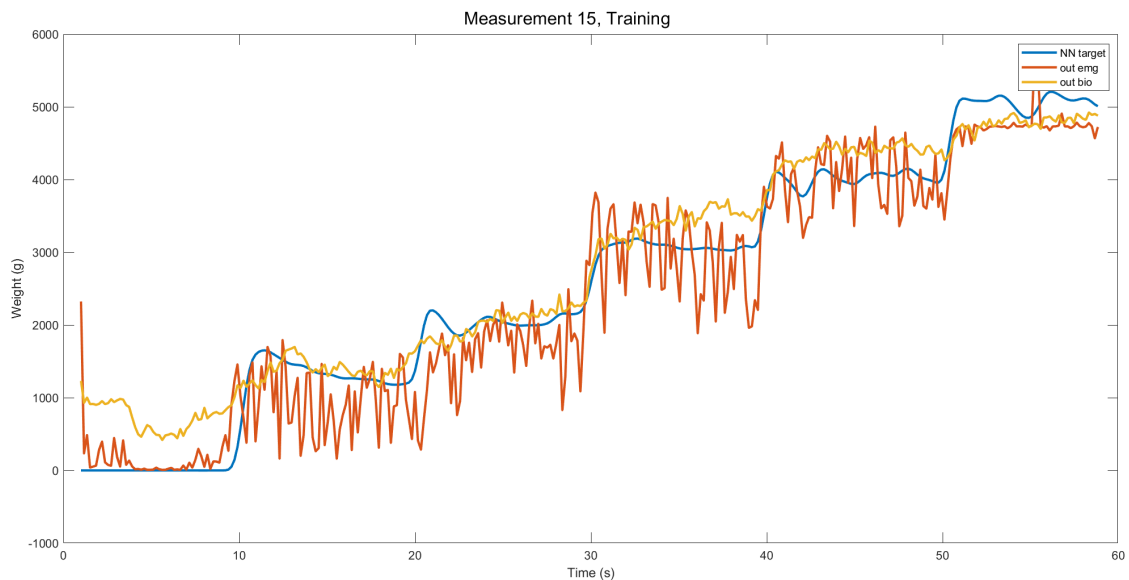


Figure H.16: The target, output of the bio-impedance NN and the output of the EMG NN of measurement number 15 of the force measurement as described in Section 3.4.2. The desired force is changed with 1 kg every 10 s.

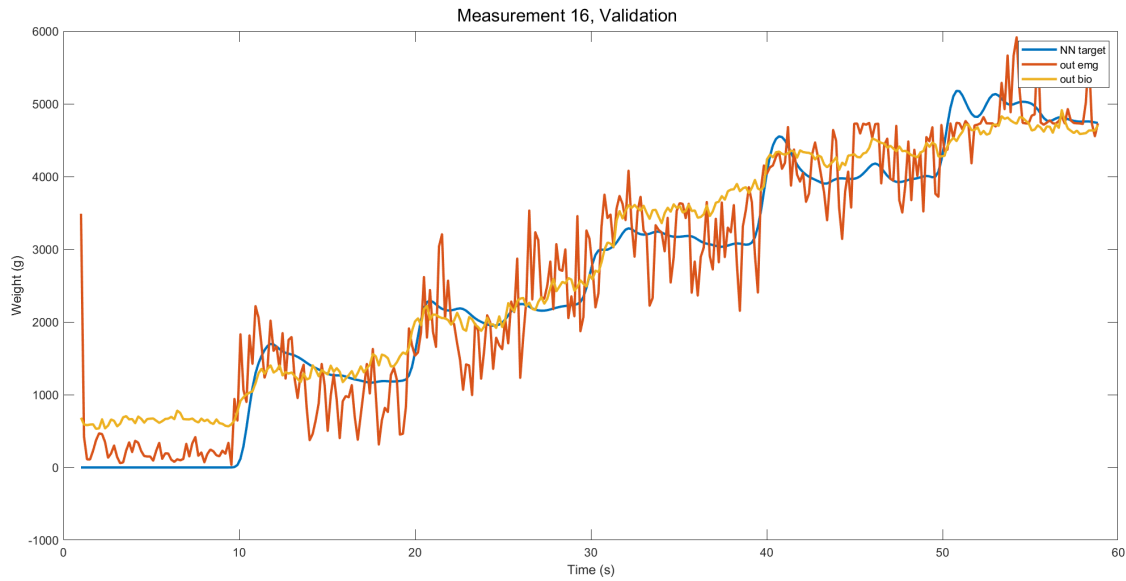


Figure H.17: The target, output of the bio-impedance NN and the output of the EMG NN of measurement number 16 of the force measurement as described in Section 3.4.2. The desired force is changed with 1 kg every 10 s.

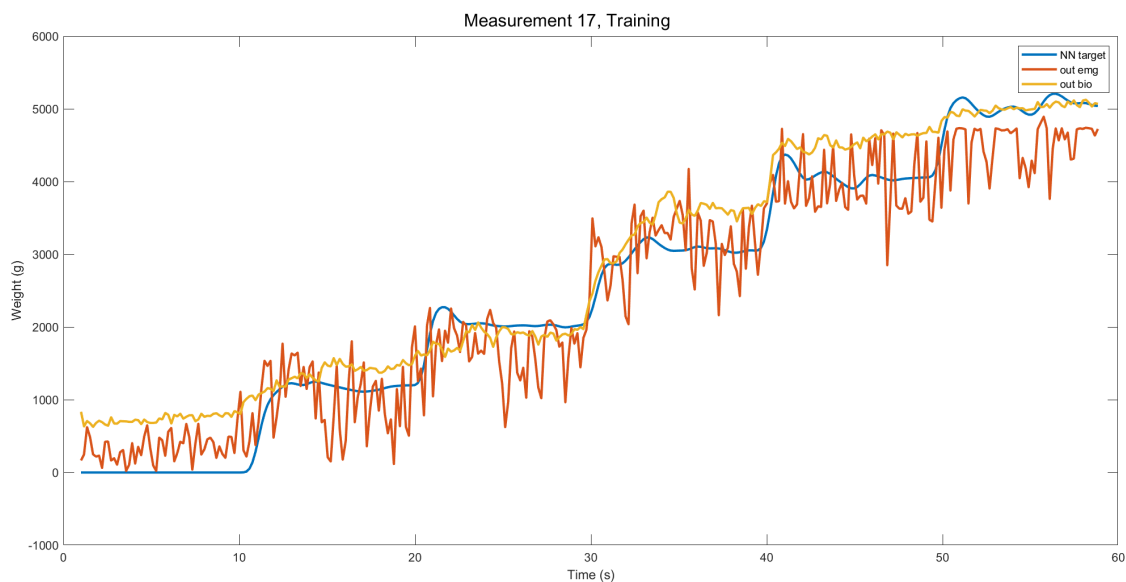


Figure H.18: The target, output of the bio-impedance NN and the output of the EMG NN of measurement number 17 of the force measurement as described in Section 3.4.2. The desired force is changed with 1 kg every 10 s.

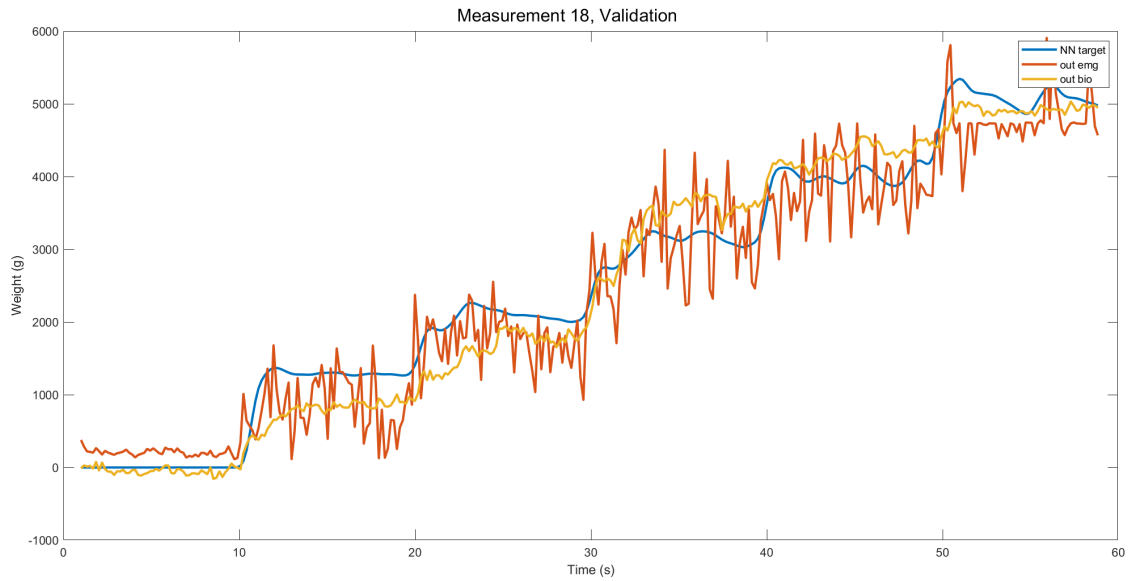


Figure H.19: The target, output of the bio-impedance NN and the output of the EMG NN of measurement number 18 of the force measurement as described in Section 3.4.2. The desired force is changed with 1 kg every 10 s.

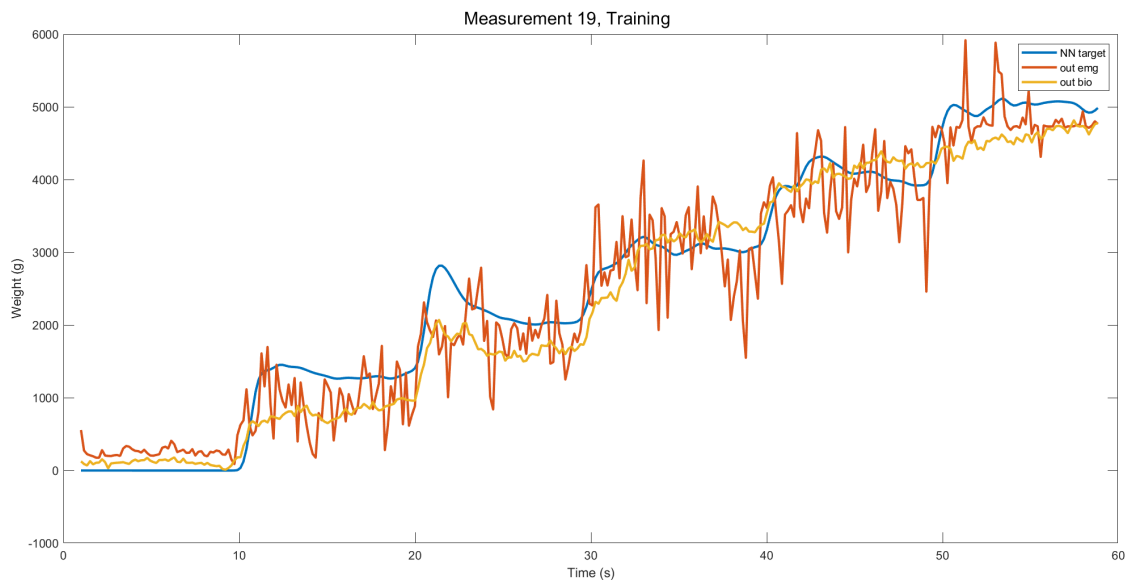


Figure H.20: The target, output of the bio-impedance NN and the output of the EMG NN of measurement number 19 of the force measurement as described in Section 3.4.2. The desired force is changed with 1 kg every 10 s.

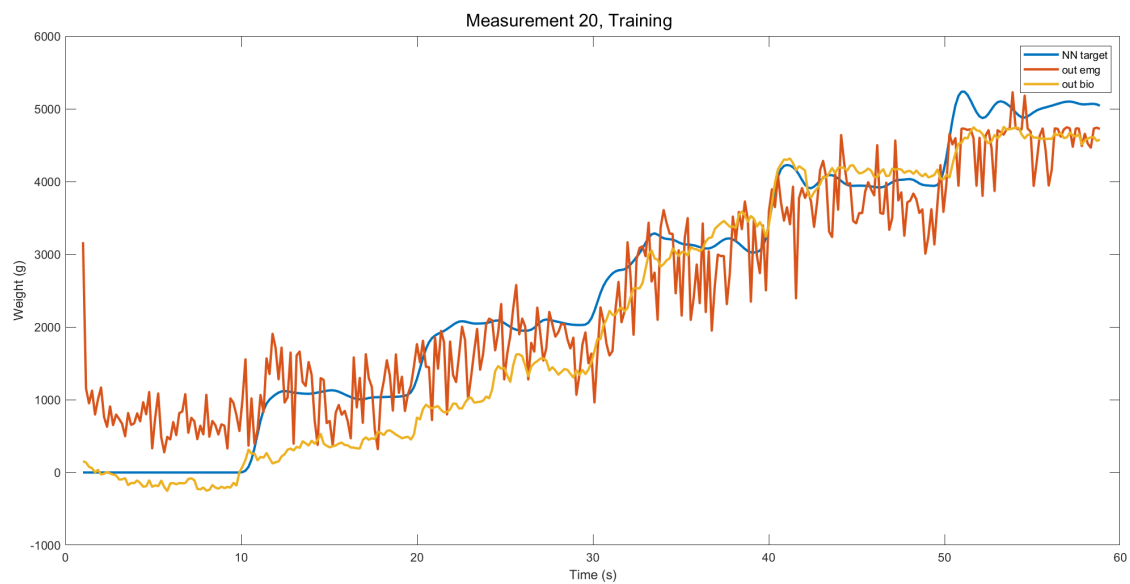


Figure H.21: The target, output of the bio-impedance NN and the output of the EMG NN of measurement number 20 of the force measurement as described in Section 3.4.2. The desired force is changed with 1 kg every 10 s.

I Time delay

The measurements as described in Section 5.7 are processed. The resulting figures of all 7 measurements are given below. Movement pattern 1 of Figure 3.8 is performed. Each second the subject switches between relaxing and contracting for 30 seconds assisted by a metronome beating at 60 beats per minute. All signals are normalized between 0 and 1. All of the resistance and some of the reactance signals are inverted such that the shape of these signals is the same as the EMG signal.

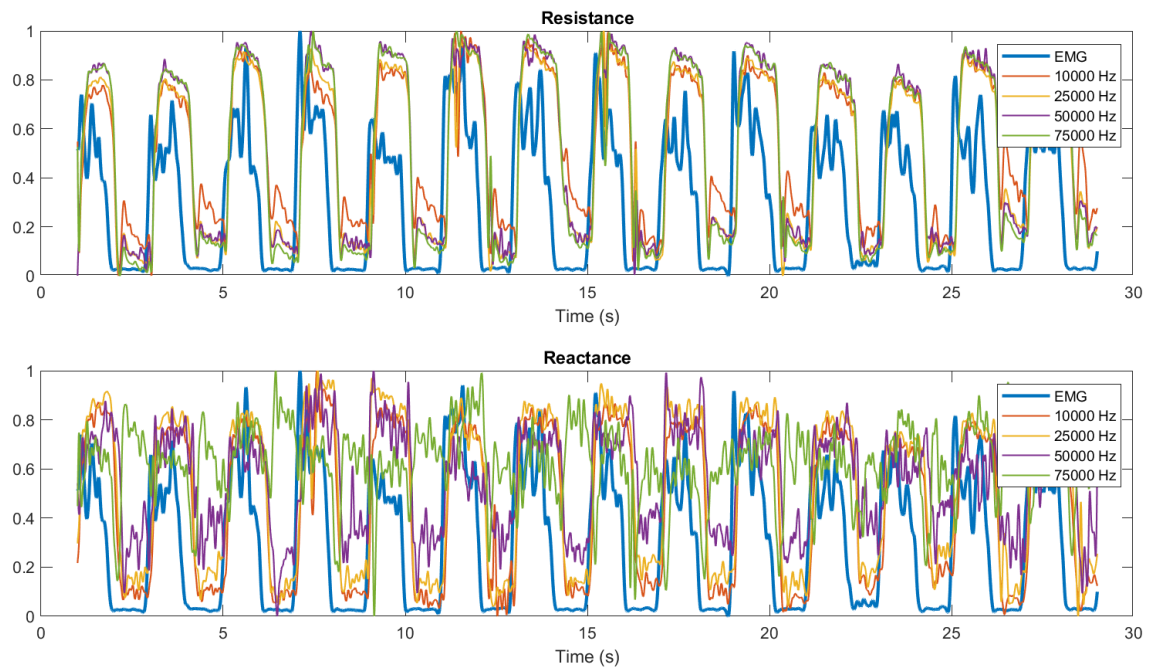


Figure I.1: The measured bio-impedance and EMG signal while movement pattern 1 (Figure 3.8) is performed. All of the resistance and some of the reactance signals are inverted such that the shape of these signals is the same as the EMG signal.

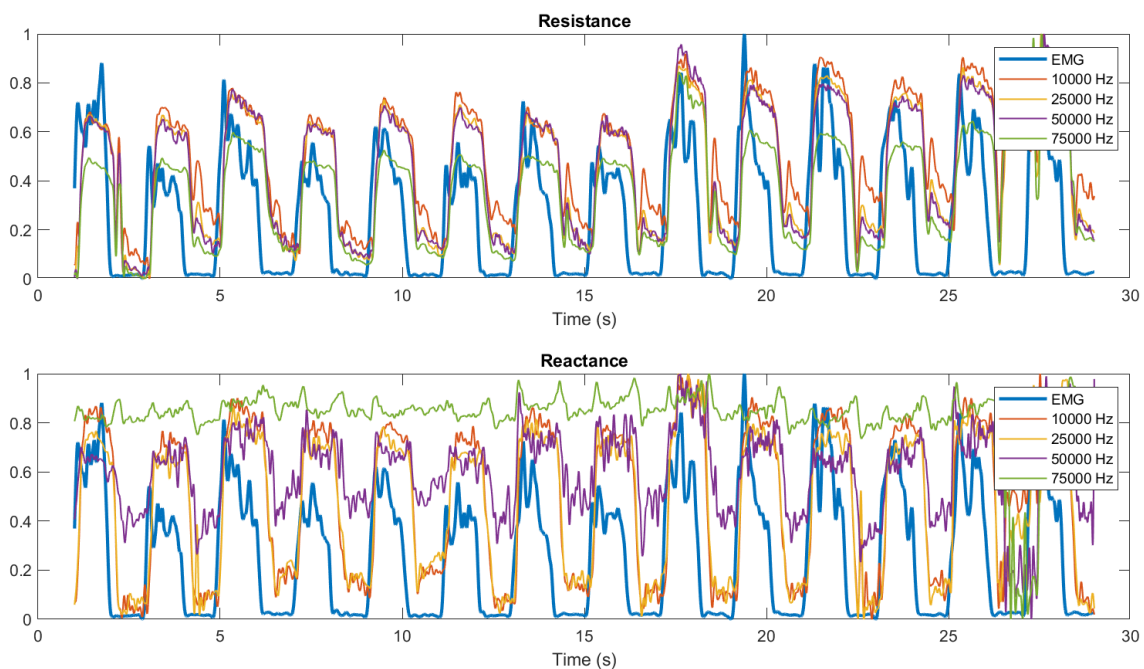


Figure I.2: The measured bio-impedance and EMG signal while movement pattern 1 (Figure 3.8) is performed. All of the resistance and some of the reactance signals are inverted such that the shape of these signals is the same as the EMG signal.

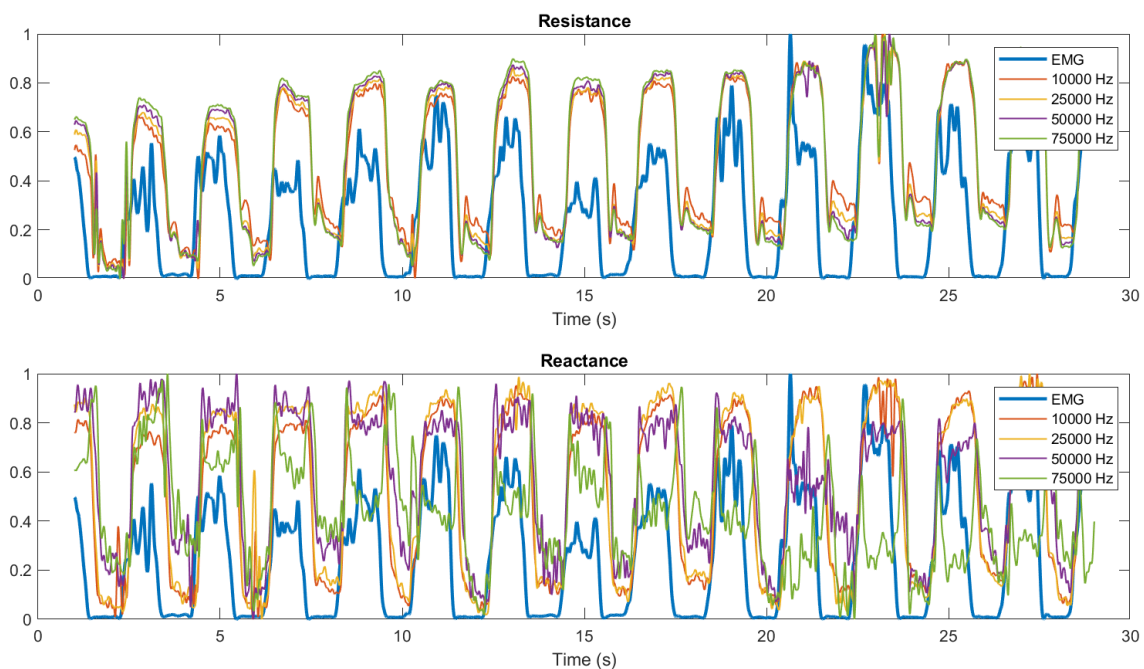


Figure I.3: The measured bio-impedance and EMG signal while movement pattern 1 (Figure 3.8) is performed. All of the resistance and some of the reactance signals are inverted such that the shape of these signals is the same as the EMG signal.

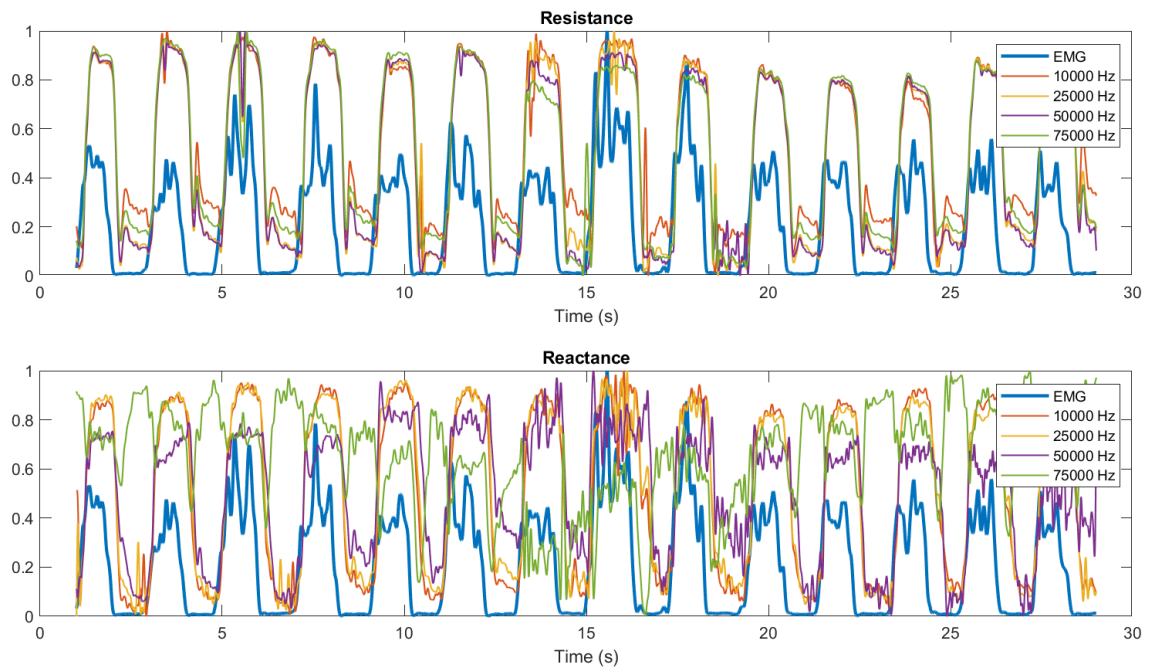


Figure I.4: The measured bio-impedance and EMG signal while movement pattern 1 (Figure 3.8) is performed. All of the resistance and some of the reactance signals are inverted such that the shape of these signals is the same as the EMG signal.

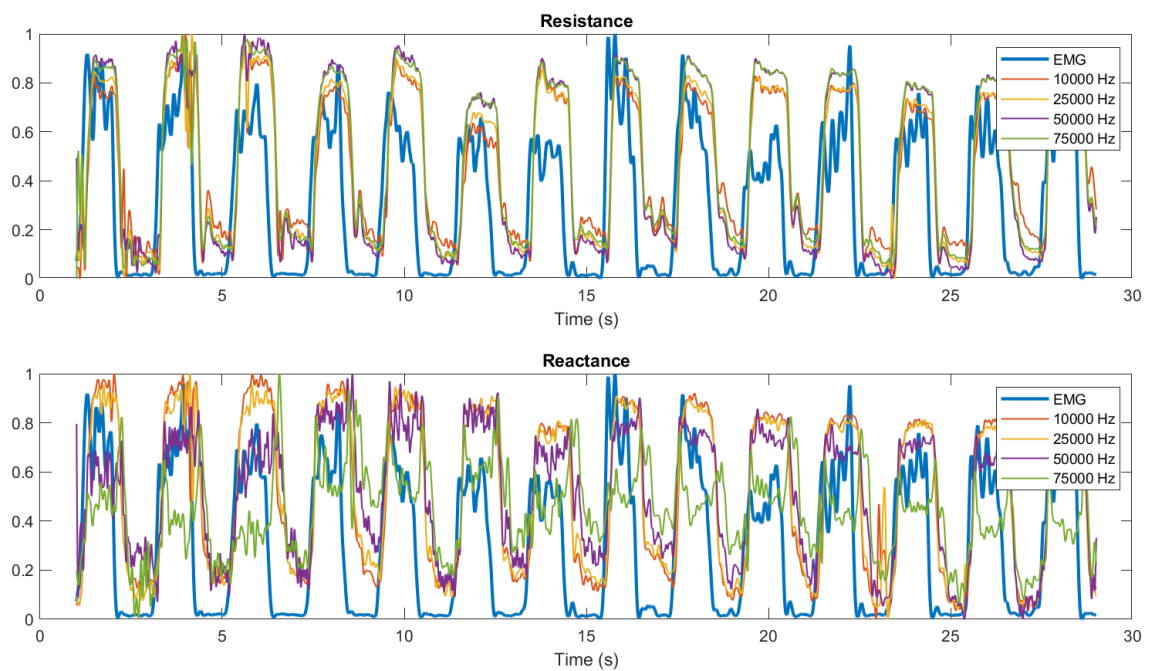


Figure I.5: The measured bio-impedance and EMG signal while movement pattern 1 (Figure 3.8) is performed. All of the resistance and some of the reactance signals are inverted such that the shape of these signals is the same as the EMG signal.

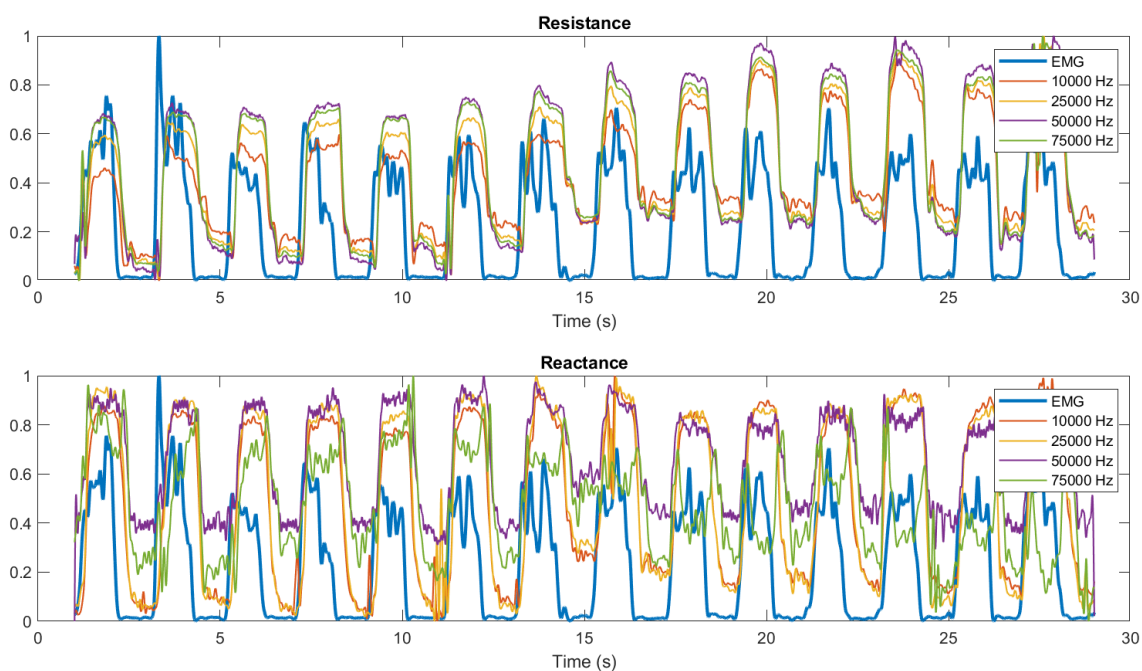


Figure I.6: The measured bio-impedance and EMG signal while movement pattern 1 (Figure 3.8) is performed. All of the resistance and some of the reactance signals are inverted such that the shape of these signals is the same as the EMG signal.

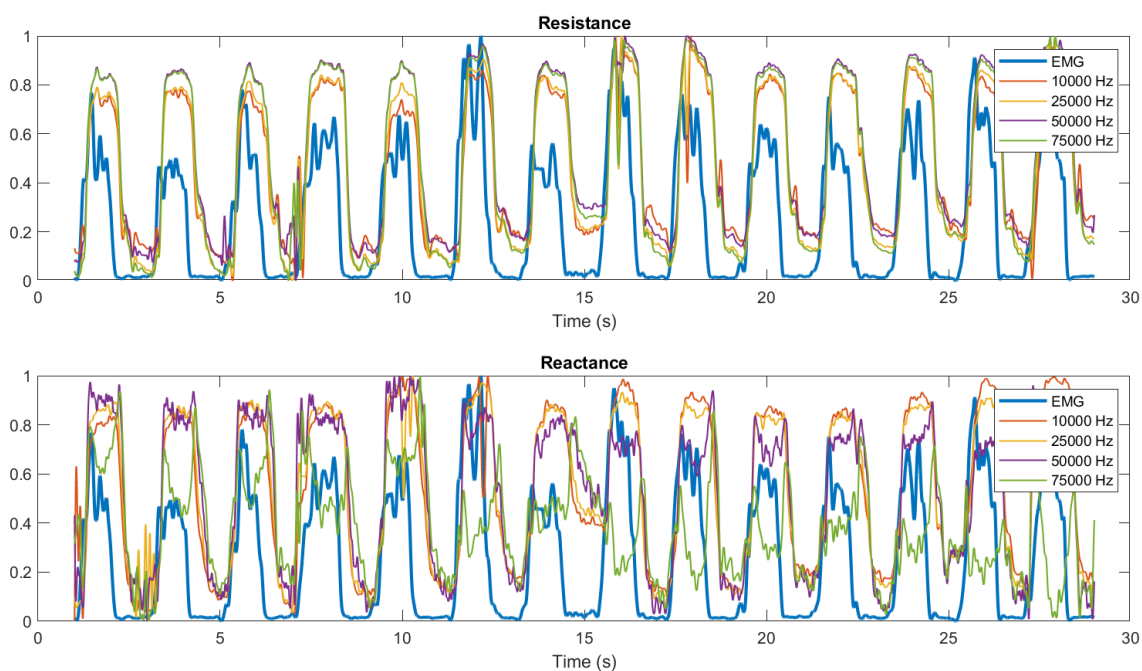


Figure I.7: The measured bio-impedance and EMG signal while movement pattern 1 (Figure 3.8) is performed. All of the resistance and some of the reactance signals are inverted such that the shape of these signals is the same as the EMG signal.

J System validation

The measurement system is validated on three points as mentioned in Section 3.2.3, accuracy and precision, the drift and the time delay. Three different resistor capacitor combinations are used. The first one is a 10 k Ω resistor with no capacitor, the second one is a 1 k Ω resistor with a 1 nF capacitor and the last one is a 100 Ω resistor with a 4.7 nF capacitor. The impedance is measured 6 times for each set. The first five measurements take 1 minute and the last ten minutes. The mean and standard error is calculated over each measurement. Figure J.1 shows the results of the measurement including the 10 k Ω resistor. At all frequencies the measured resistance is around 10 k Ω . The highest frequency of 1 MHz shows a lower resistance compared to the other measurement frequencies, therefore can it be expected that this measurement has a higher error than the others. The capacitance is close to zero when looking at the bottom graph of Figure J.1, this is as expected since no capacitor is placed. In Figure J.2 the second resistor and capacitor measurements are shown. Again are for the resistance the measurements at the lower frequencies the most precise. In this case it is logical for the higher frequencies to indicate a lower resistance, since the capacitor is placed in parallel. The capacitance on the other hand is the most precise for the high frequencies. The last combination is shown in Figure J.3. Again the resistance is lower for the higher frequencies while the capacitance measurement is better at high frequencies. Besides the precision is the accuracy of the 100 Hz measurement worse than the higher frequencies when looking at the capacitance.

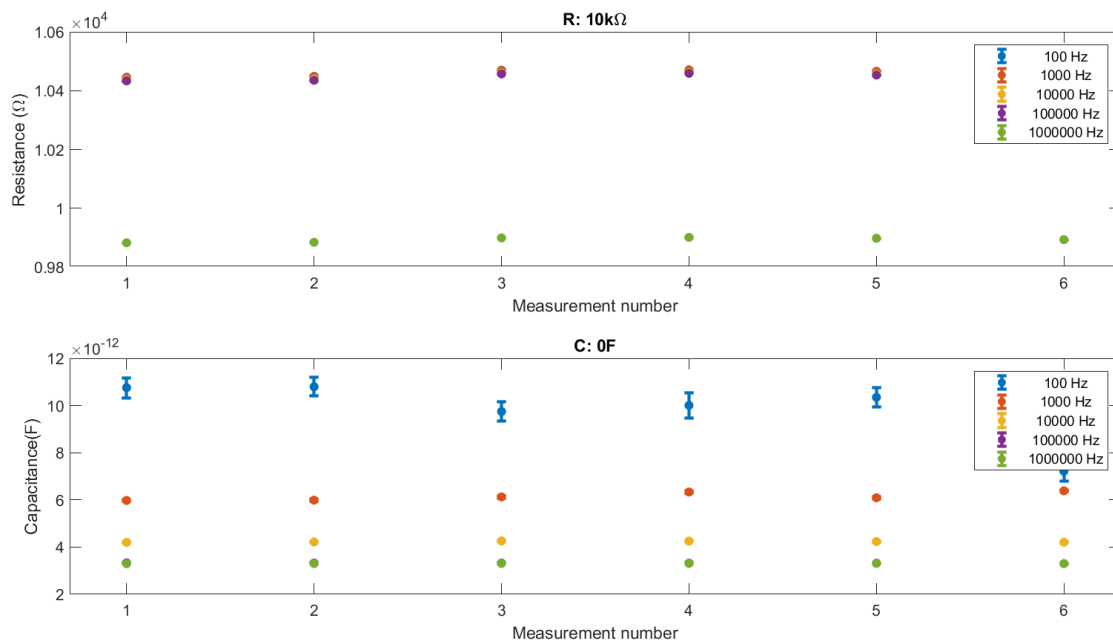


Figure J.1: The mean and standard error of 6 impedance measurements. A resistor of 10 k Ω is used and no capacitor was used.

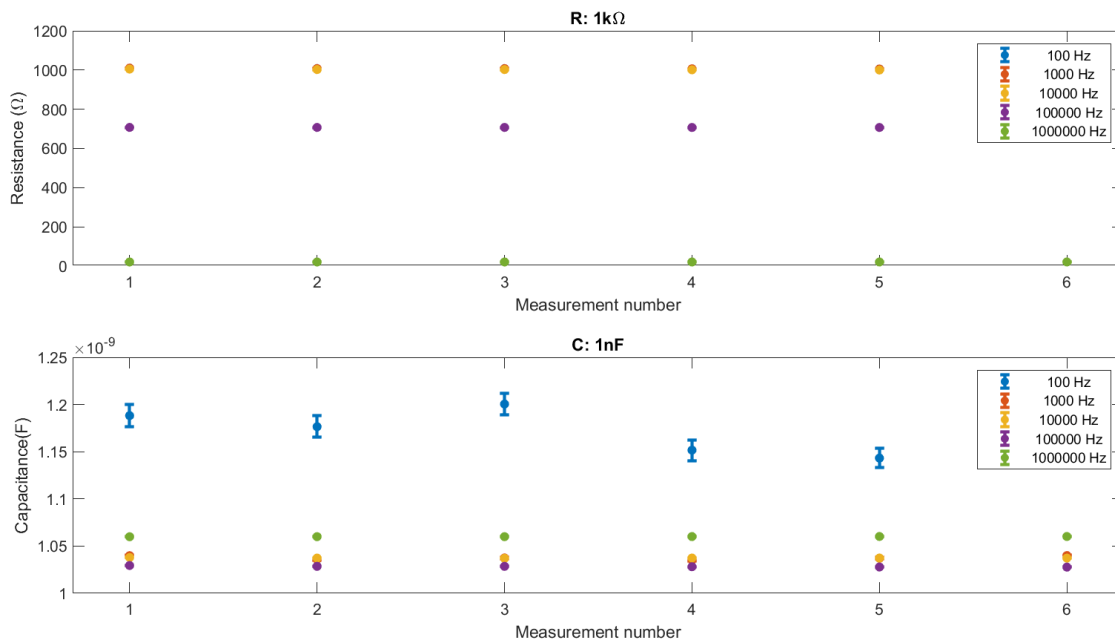


Figure J.2: The mean and standard error of 6 impedance measurements. A resistor of 1 kΩ is used and a capacitor of 1 nF is placed parallel to the resistor.

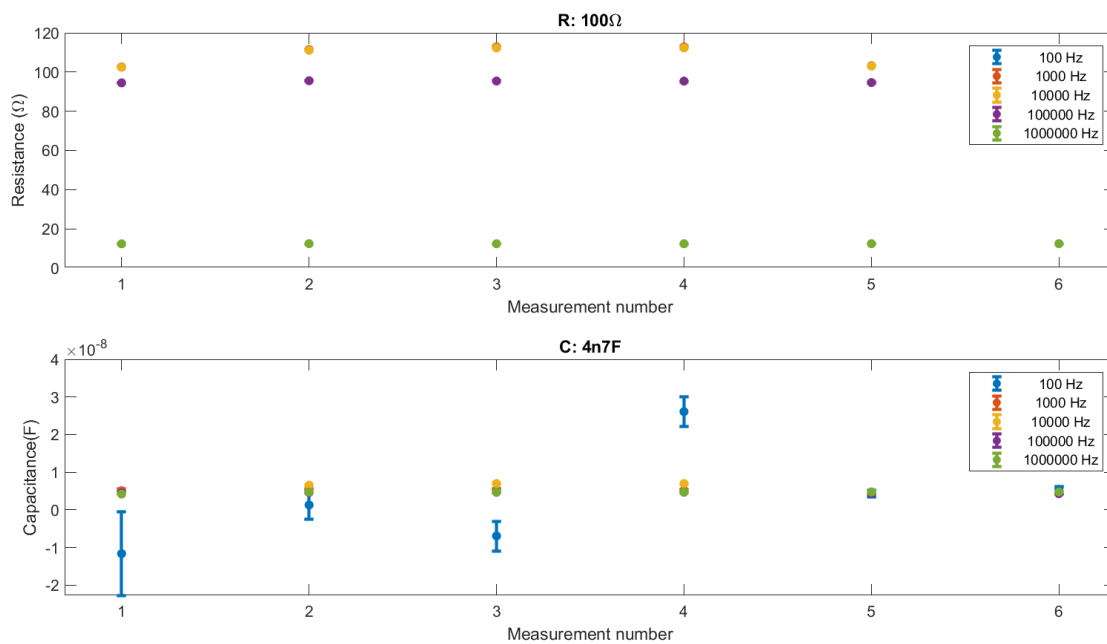


Figure J.3: The mean and standard error of 6 impedance measurements. The resistance of this measurement was 100 Ω and a capacitor of 4.7 nF is placed parallel to the resistor.

The 10 minutes measurements are given in Figure J.4, Figure J.5 and Figure J.6. Just by looking at the graphs no real drift can be discriminated. If drift is present in the system it is too low to notice over the time period of 10 minutes. Since every measurement will be a lot shorter than 10 minutes it can be assumed that the drift will not influence the measurements significantly.

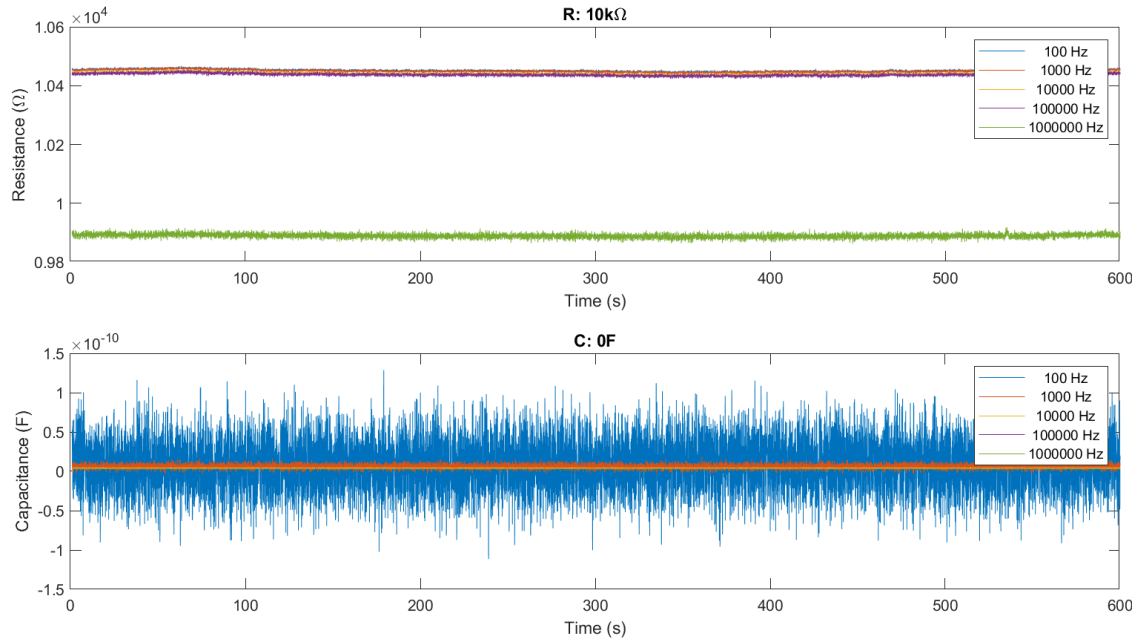


Figure J.4: A 10 minute measurement of a resistor of 10 kΩ.

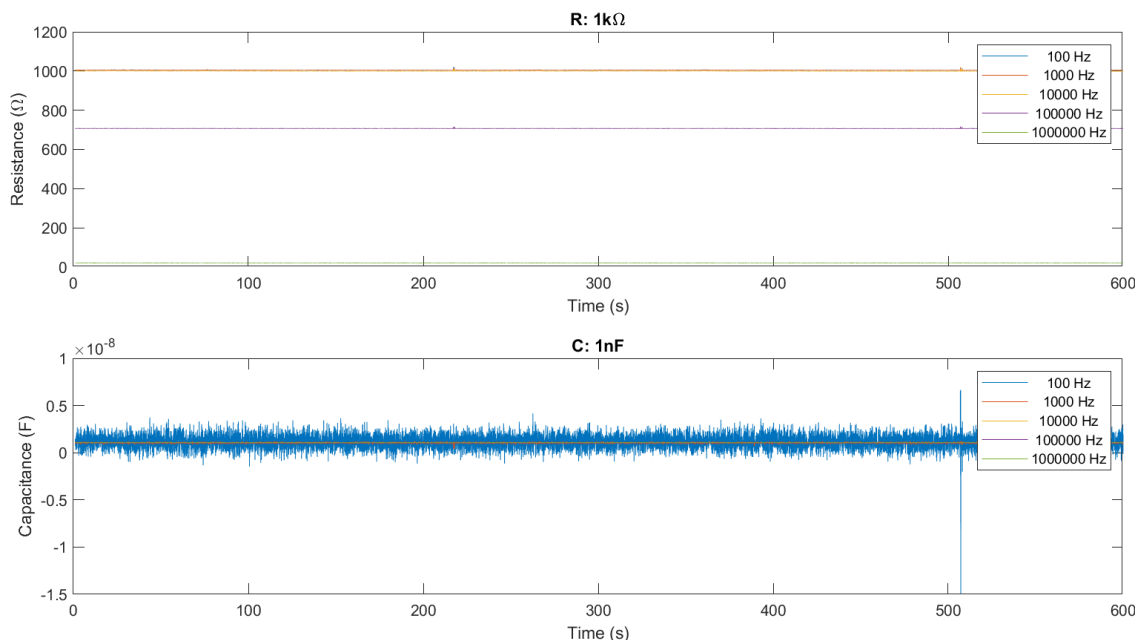


Figure J.5: A 10 minute measurement of a resistor of 1 kΩ and a capacitor of 1 nF

The time delay is measured by connecting a resistor and capacitor in parallel to the measurement setup. Every 5 s another resistor in parallel is connected or disconnected. This way the bio-impedance as well the signal offset used for the EMG creation change on the exact same time. If there is any delay present between the bio-impedance signal and the “EMG” signal this

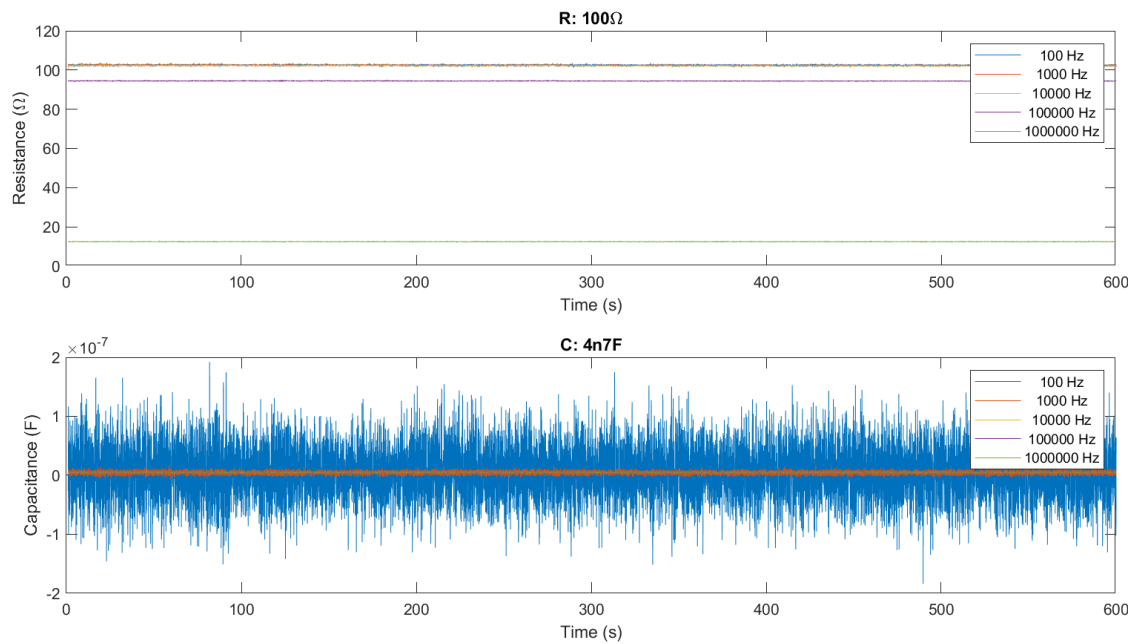


Figure J.6: A 10 minute measurement of a resistor of $100\ \Omega$ and a capacitor of $4.7\ \text{nF}$

is due to the measurement system or processing. The EMG signals has to be down sampled, which is done using a weighted interpolation algorithm. All signals are normalized between 0 and 1 before the cross-correlation is applied. The measured bio-impedance and “EMG” signals are given in the following figures. The cross-correlation is calculated between the EMG signal and the resistance and between the EMG signal and the reactance for all measurement frequencies and for all measurements. The measurement is performed 20 times each time using 4 measurement frequencies, this gives $20 \cdot 4 \cdot 2 = 160$ cross correlations and thus 160 time delay values. The mean and standard deviation of these values comes down to $0.0569\ \text{s}$ and $9.818 \times 10^{-4}\ \text{s}$ respectively. Which means there is a significant and constant time delay in the measurement system.

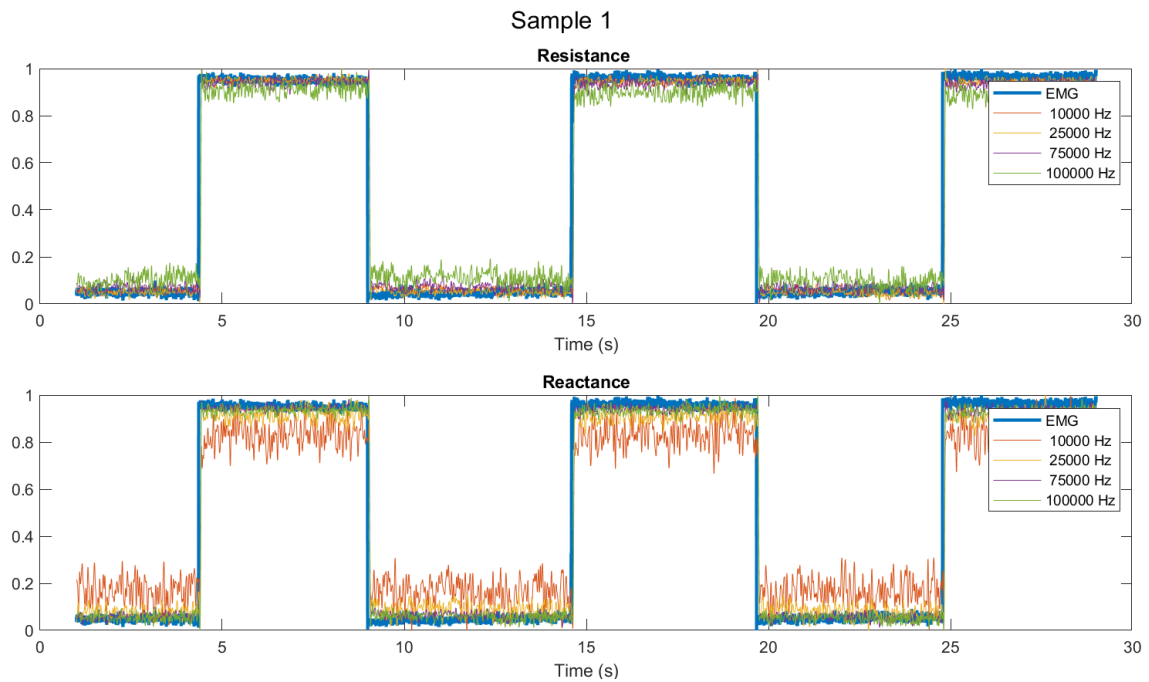


Figure J.7: Measurement number 1 of the impedance and “EMG” signals used for determining the time delay of the measurement system and signal processing. All signals are normalized between 0 and 1.

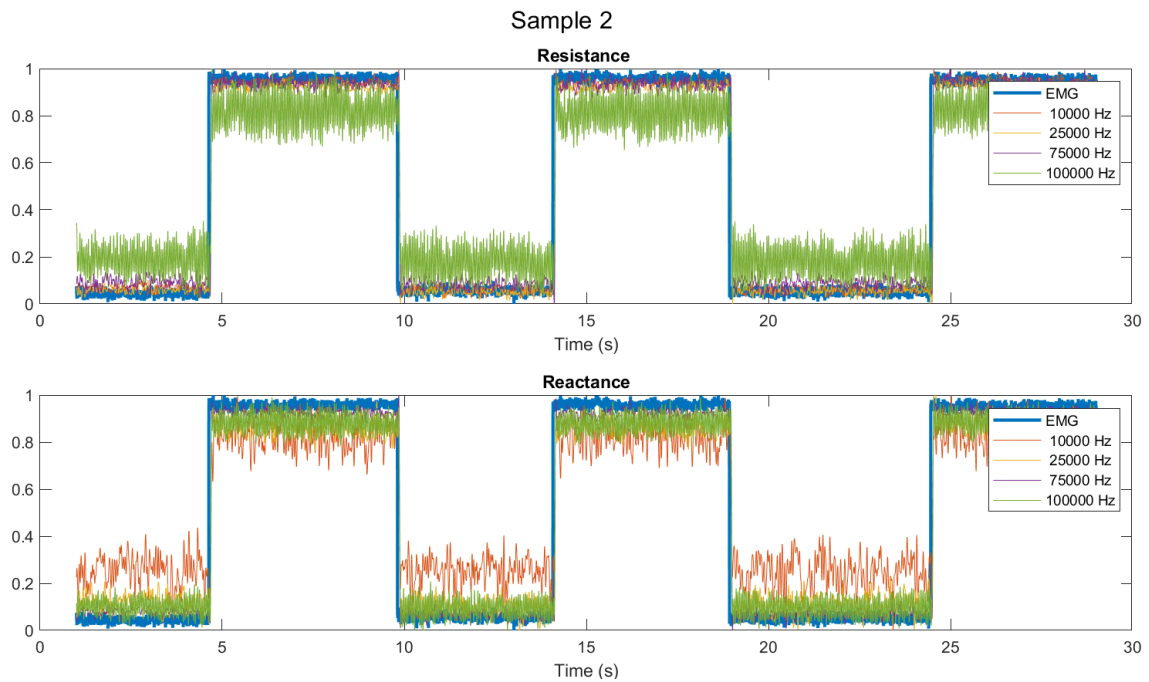


Figure J.8: Measurement number 2 of the impedance and “EMG” signals used for determining the time delay of the measurement system and signal processing. All signals are normalized between 0 and 1.

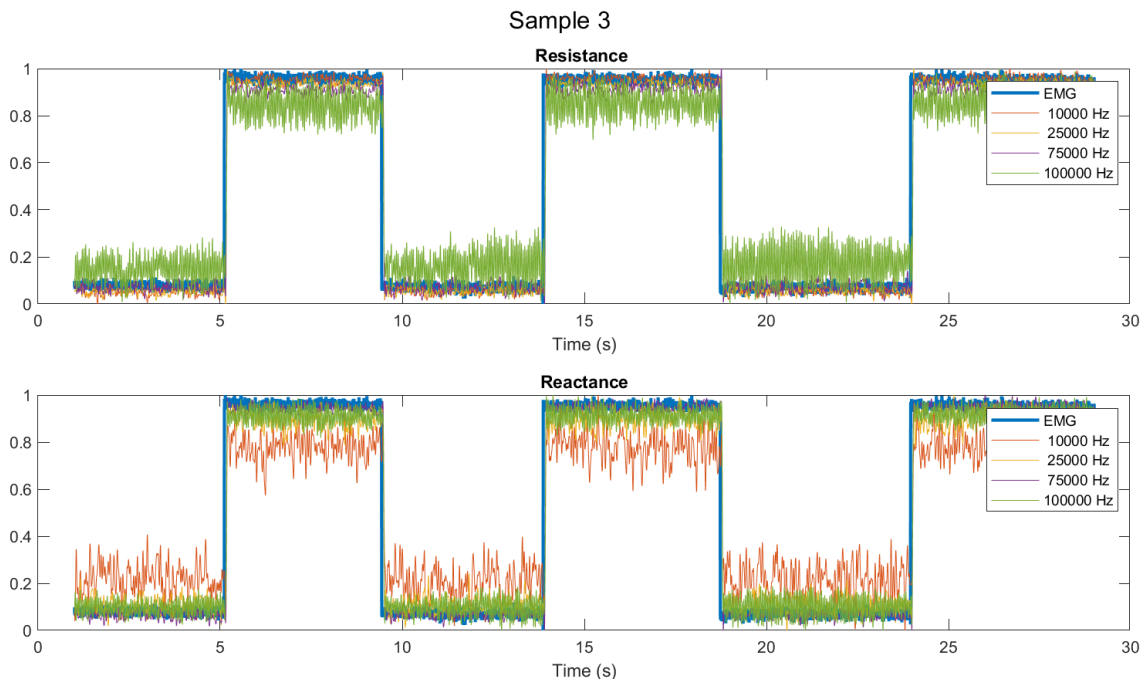


Figure J.9: Measurement number 3 of the impedance and “EMG” signals used for determining the time delay of the measurement system and signal processing. All signals are normalized between 0 and 1.

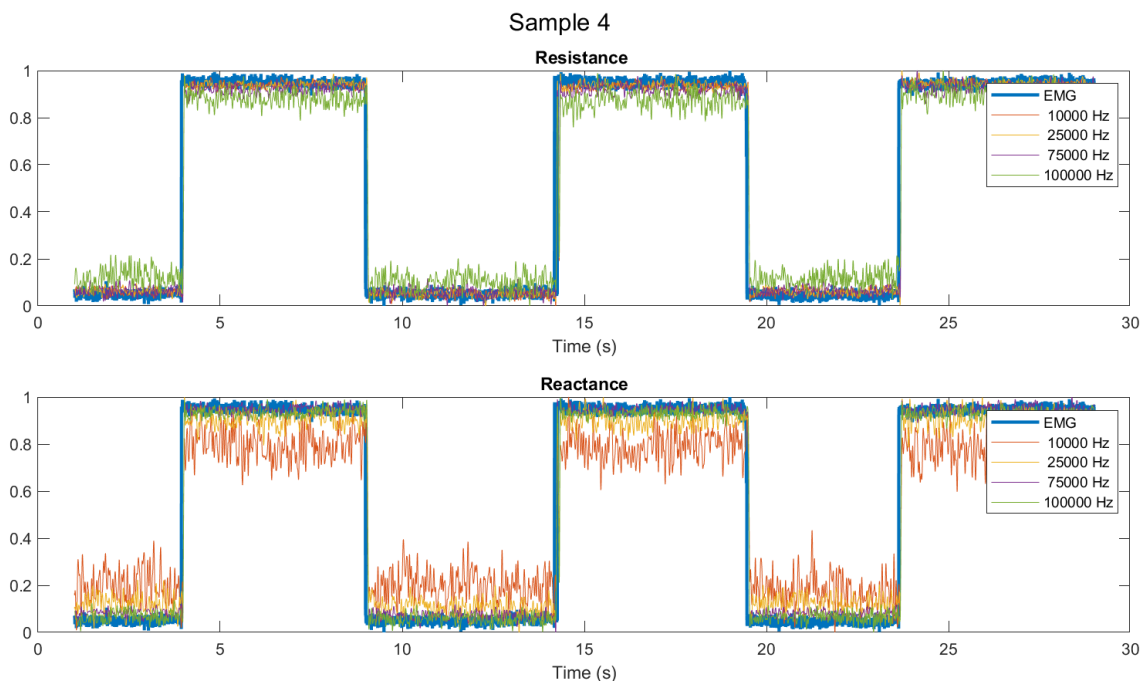


Figure J.10: Measurement number 4 of the impedance and “EMG” signals used for determining the time delay of the measurement system and signal processing. All signals are normalized between 0 and 1.

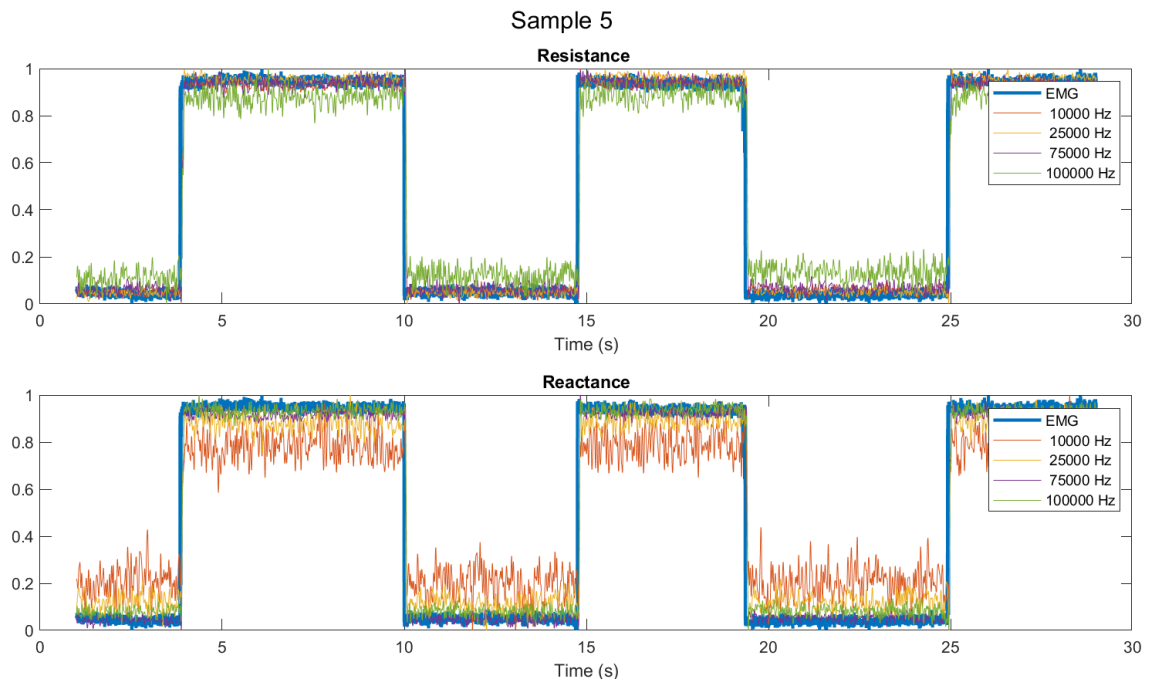


Figure J.11: Measurement number 5 of the impedance and “EMG” signals used for determining the time delay of the measurement system and signal processing. All signals are normalized between 0 and 1.

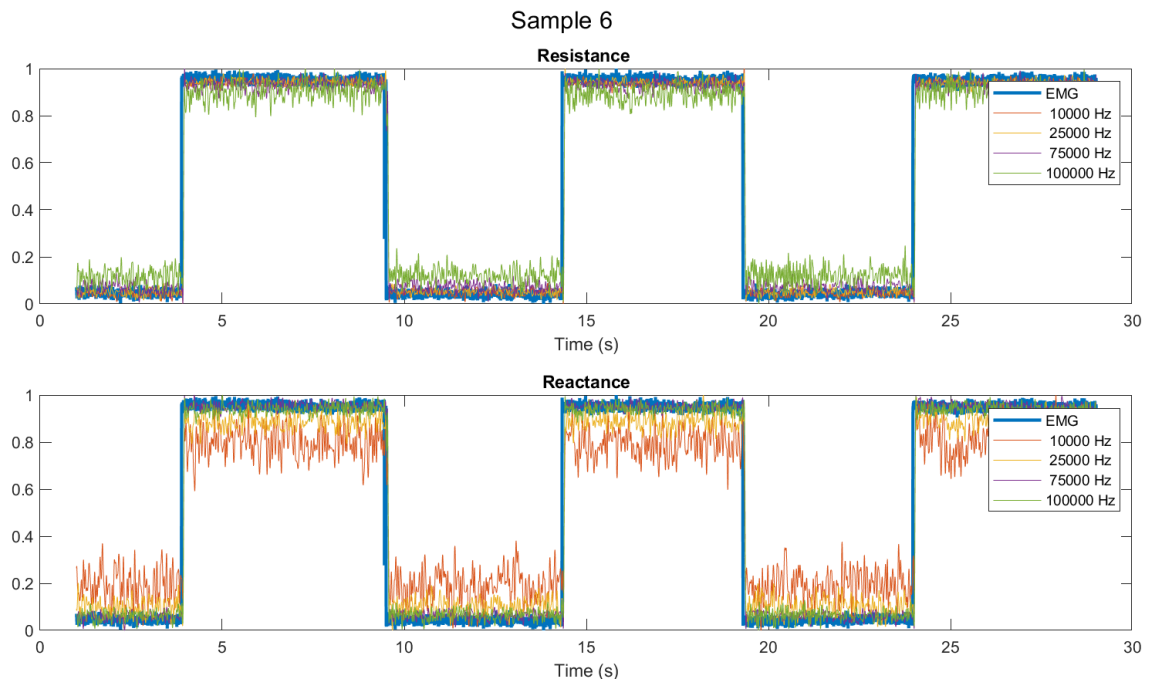


Figure J.12: Measurement number 6 of the impedance and “EMG” signals used for determining the time delay of the measurement system and signal processing. All signals are normalized between 0 and 1.

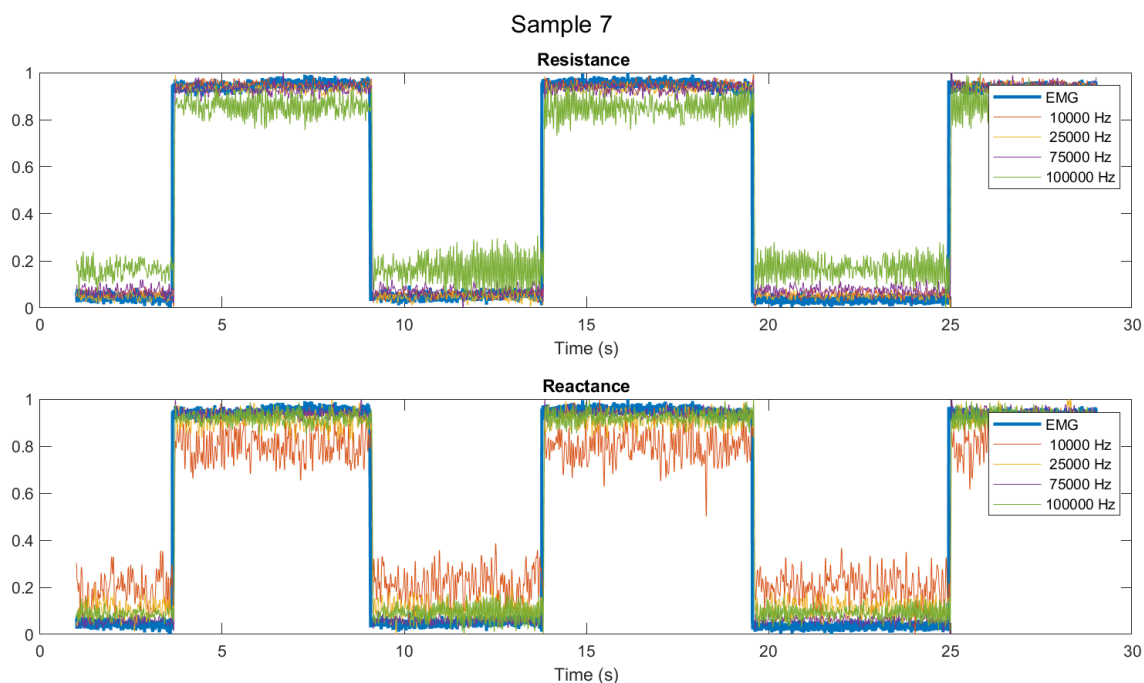


Figure J.13: Measurement number 7 of the impedance and “EMG” signals used for determining the time delay of the measurement system and signal processing. All signals are normalized between 0 and 1.

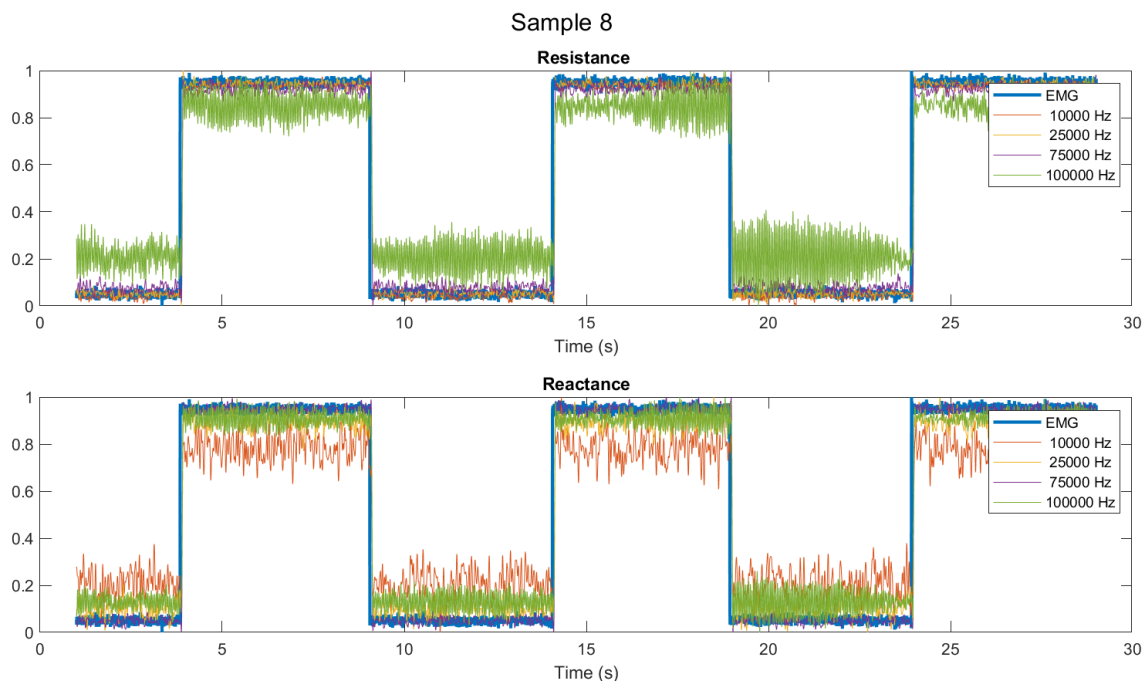


Figure J.14: Measurement number 8 of the impedance and “EMG” signals used for determining the time delay of the measurement system and signal processing. All signals are normalized between 0 and 1.

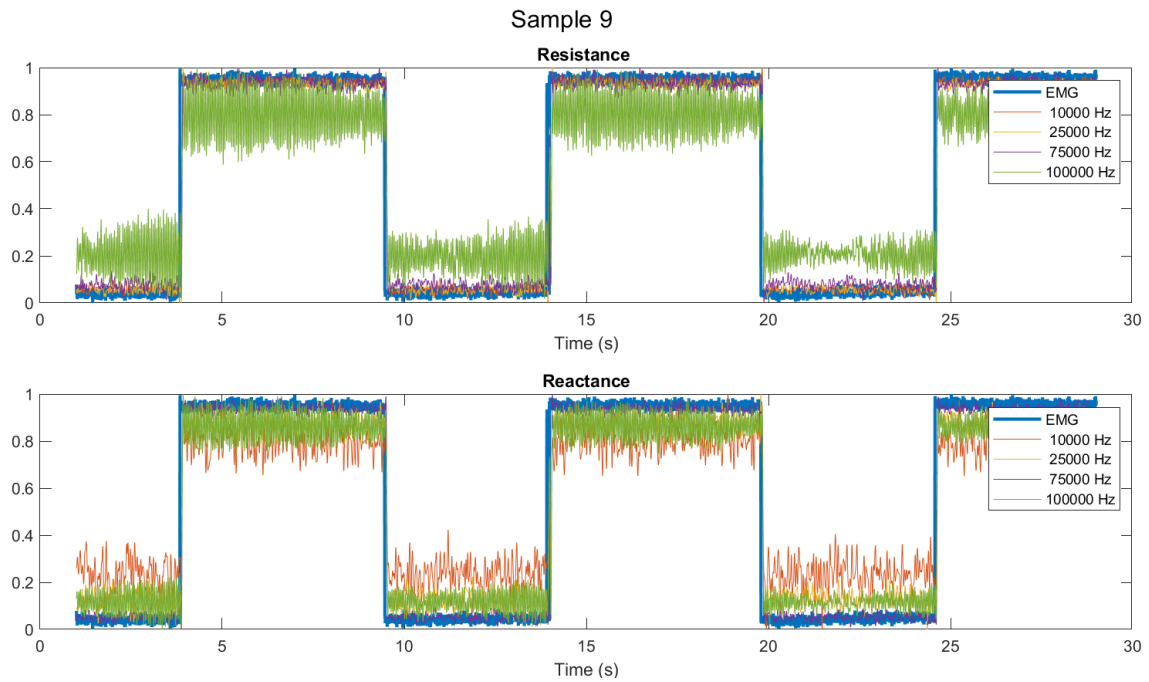


Figure J.15: Measurement number 9 of the impedance and “EMG” signals used for determining the time delay of the measurement system and signal processing. All signals are normalized between 0 and 1.

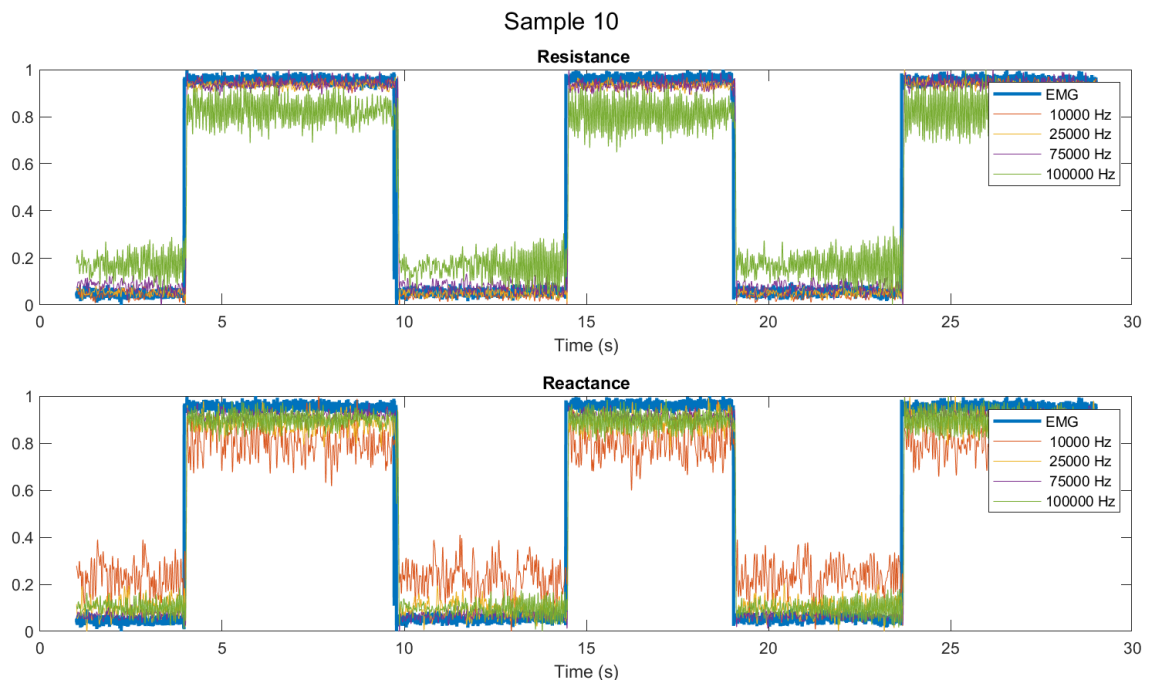


Figure J.16: Measurement number 10 of the impedance and “EMG” signals used for determining the time delay of the measurement system and signal processing. All signals are normalized between 0 and 1.

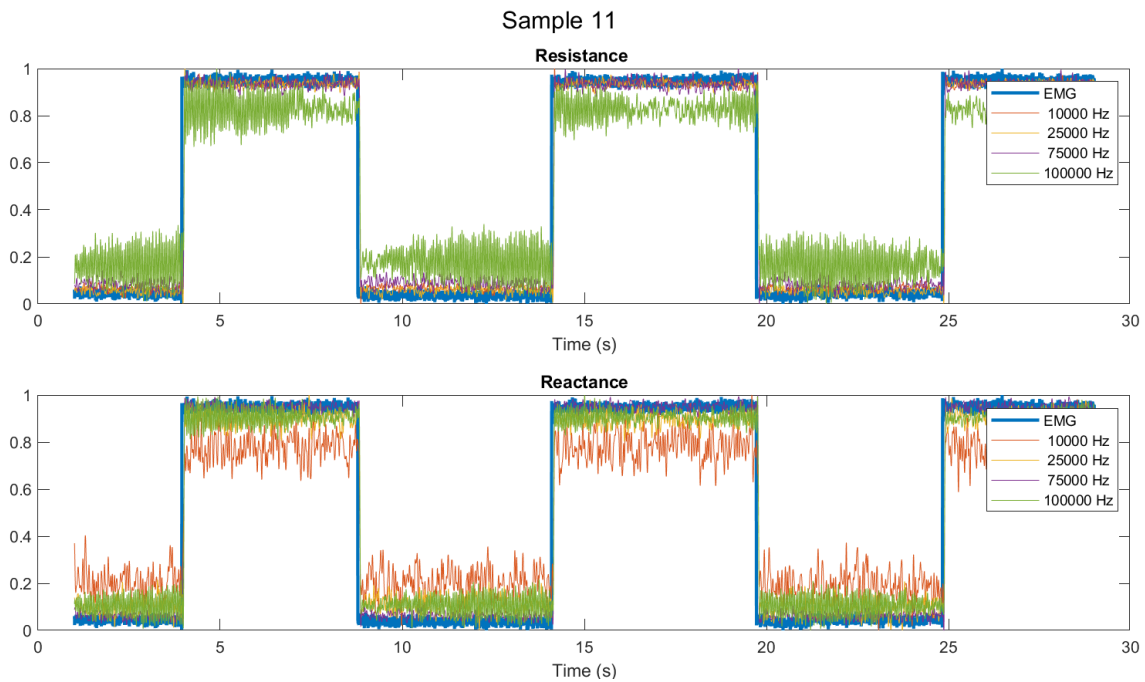


Figure J.17: Measurement number 11 of the impedance and “EMG” signals used for determining the time delay of the measurement system and signal processing. All signals are normalized between 0 and 1.

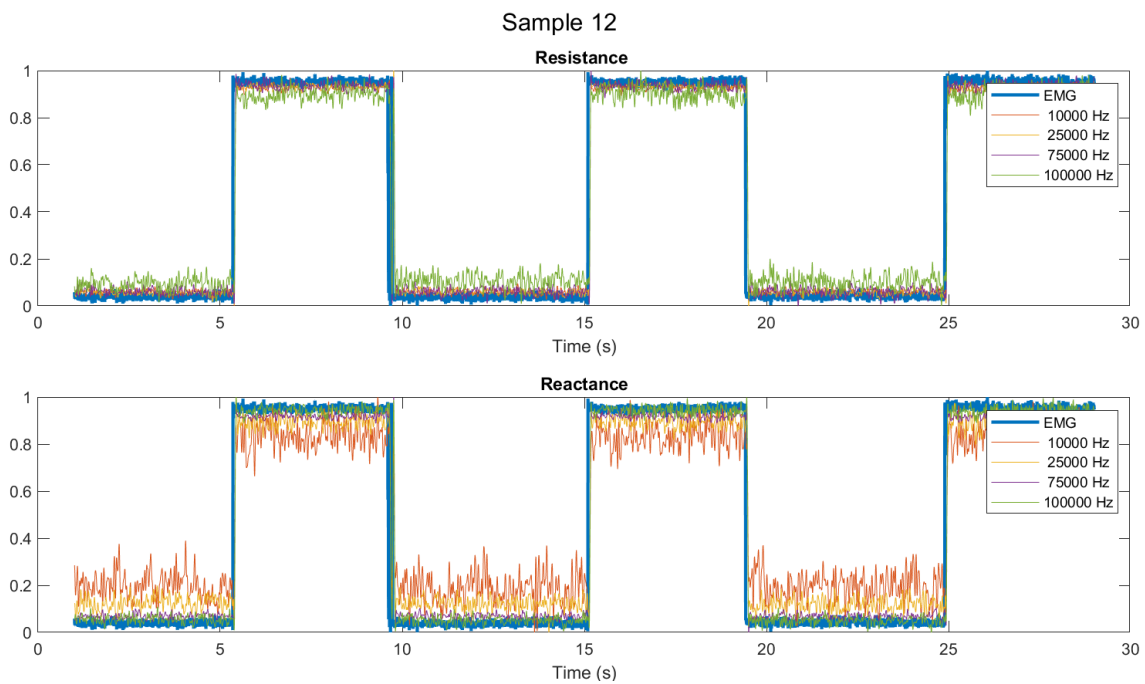


Figure J.18: Measurement number 12 of the impedance and “EMG” signals used for determining the time delay of the measurement system and signal processing. All signals are normalized between 0 and 1.

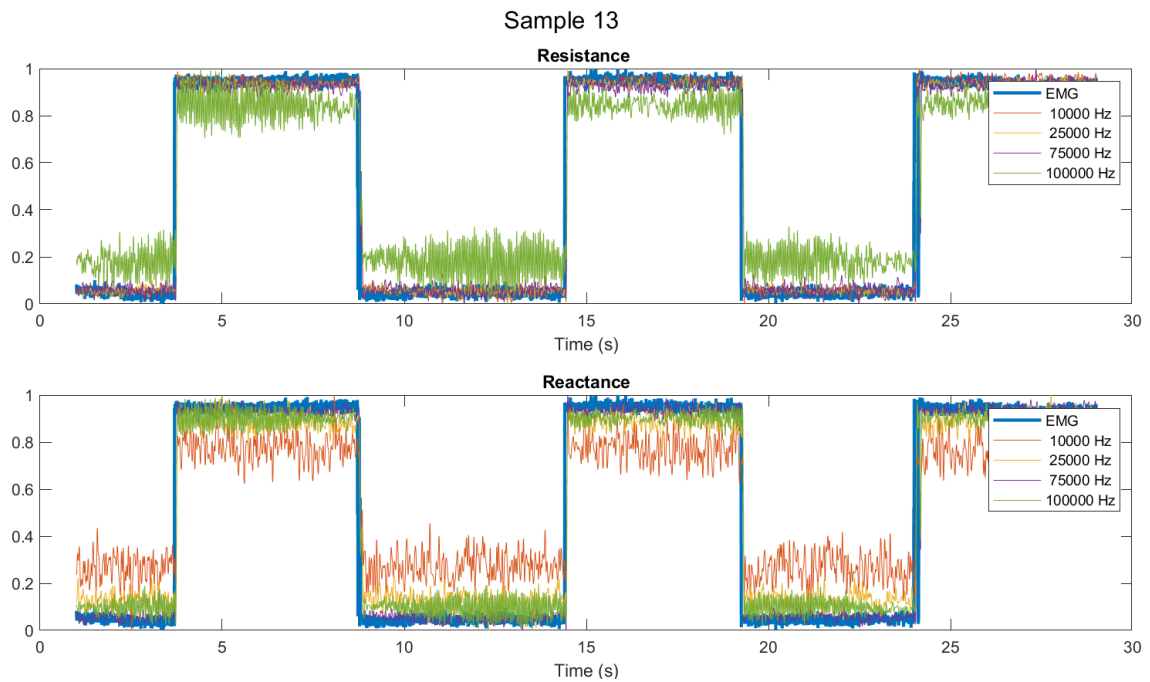


Figure J.19: Measurement number 13 of the impedance and “EMG” signals used for determining the time delay of the measurement system and signal processing. All signals are normalized between 0 and 1.

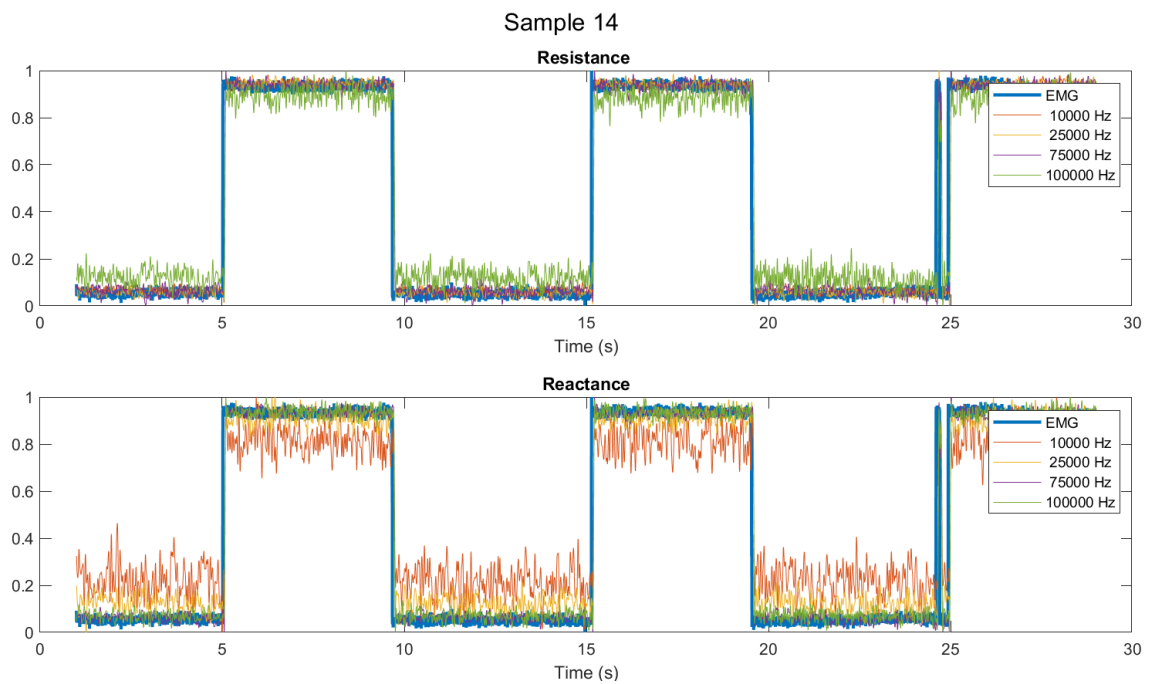


Figure J.20: Measurement number 14 of the impedance and “EMG” signals used for determining the time delay of the measurement system and signal processing. All signals are normalized between 0 and 1.

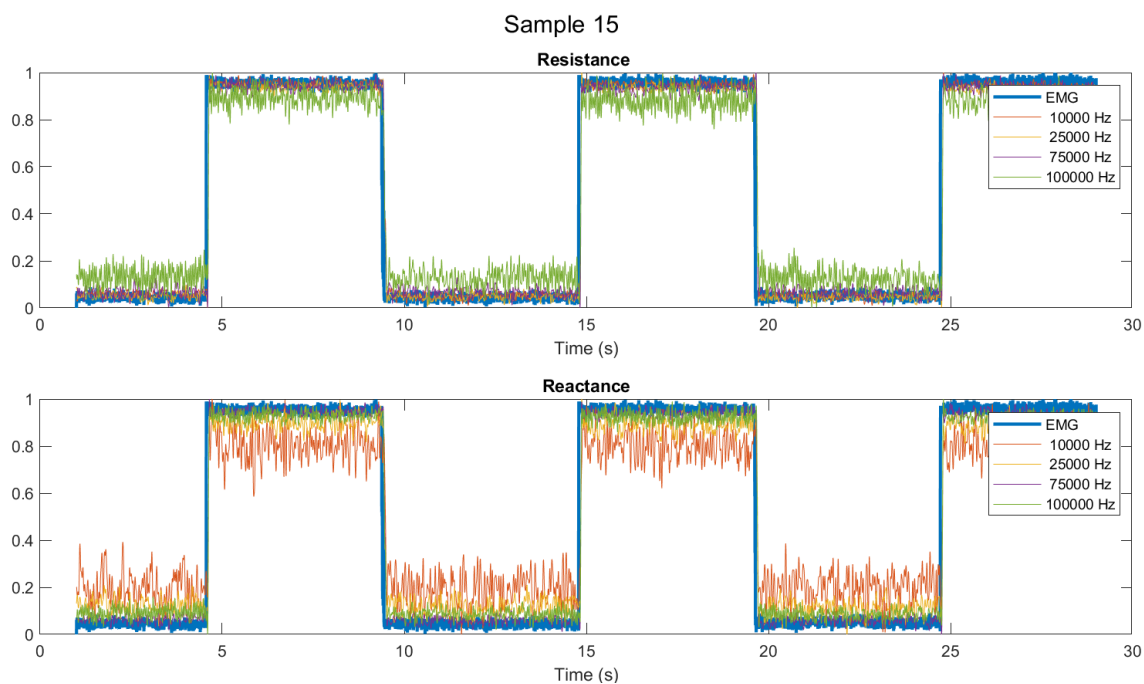


Figure J.21: Measurement number 15 of the impedance and “EMG” signals used for determining the time delay of the measurement system and signal processing. All signals are normalized between 0 and 1.

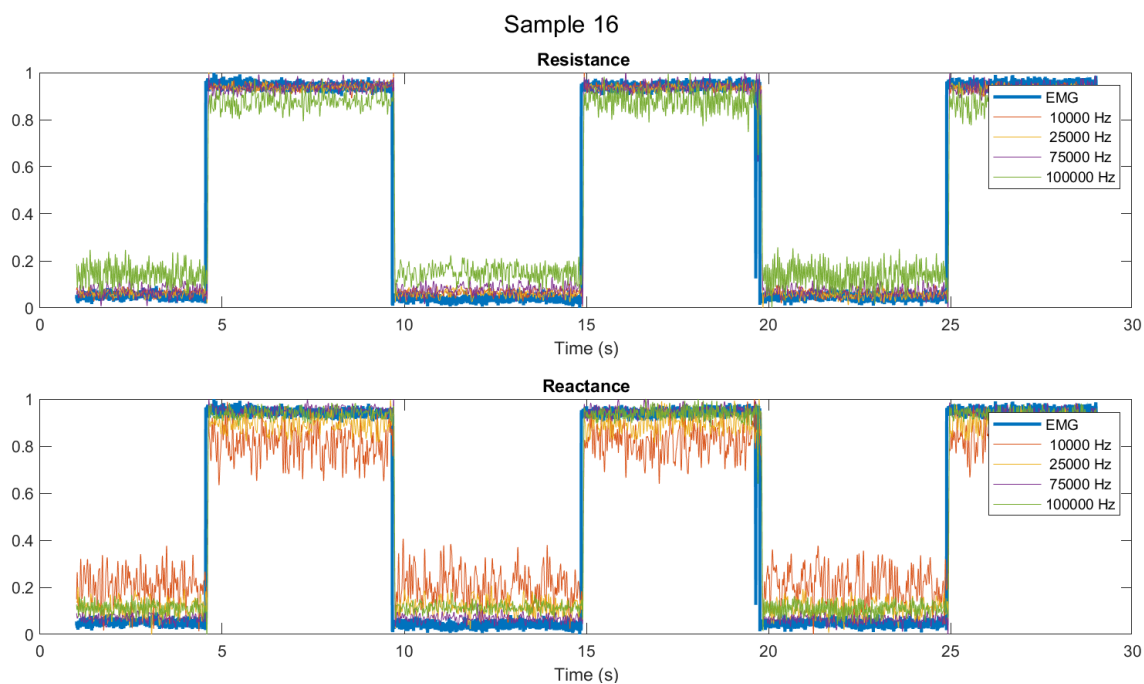


Figure J.22: Measurement number 16 of the impedance and “EMG” signals used for determining the time delay of the measurement system and signal processing. All signals are normalized between 0 and 1.

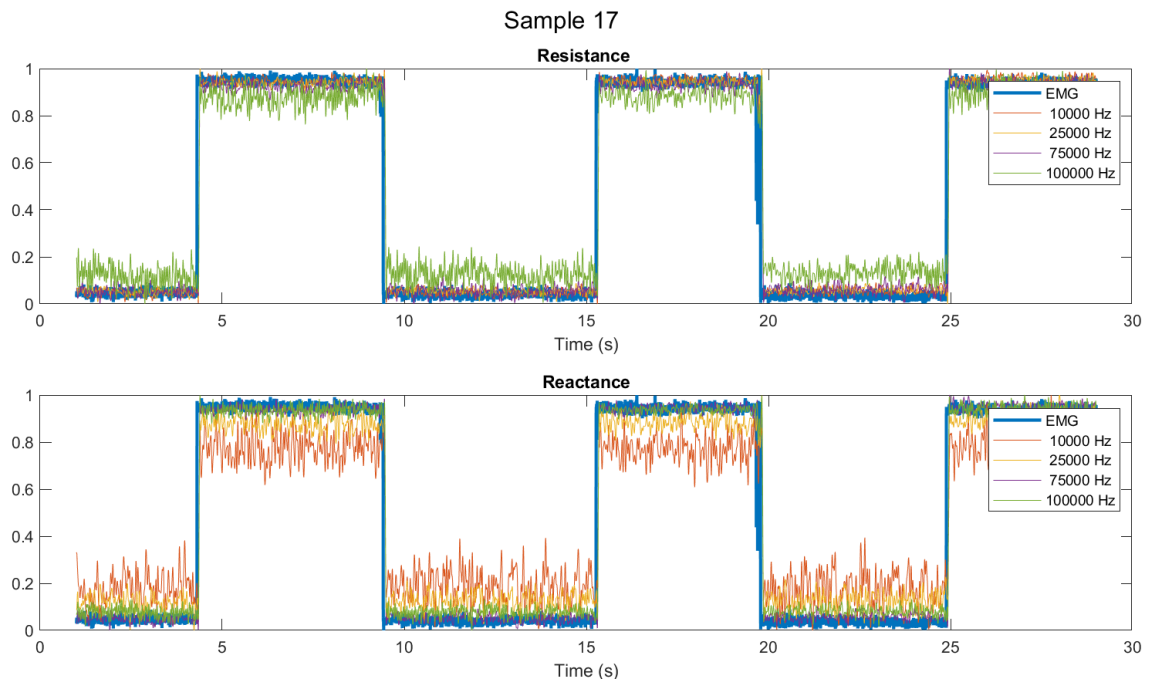


Figure J.23: Measurement number 17 of the impedance and “EMG” signals used for determining the time delay of the measurement system and signal processing. All signals are normalized between 0 and 1.

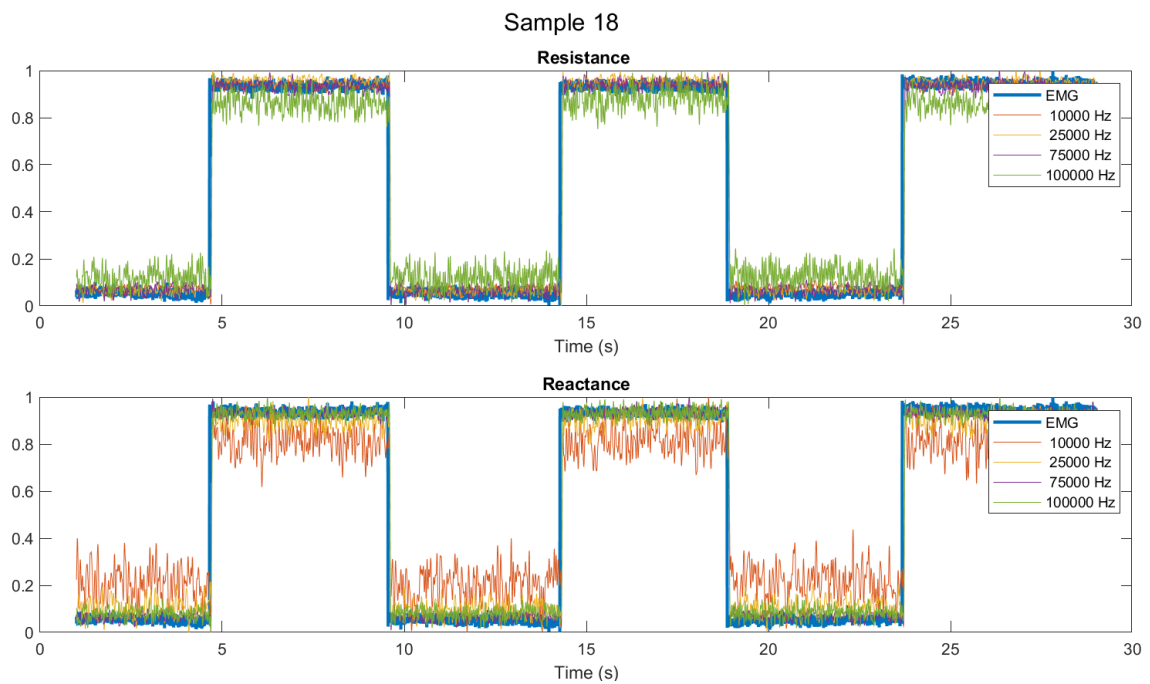


Figure J.24: Measurement number 18 of the impedance and “EMG” signals used for determining the time delay of the measurement system and signal processing. All signals are normalized between 0 and 1.

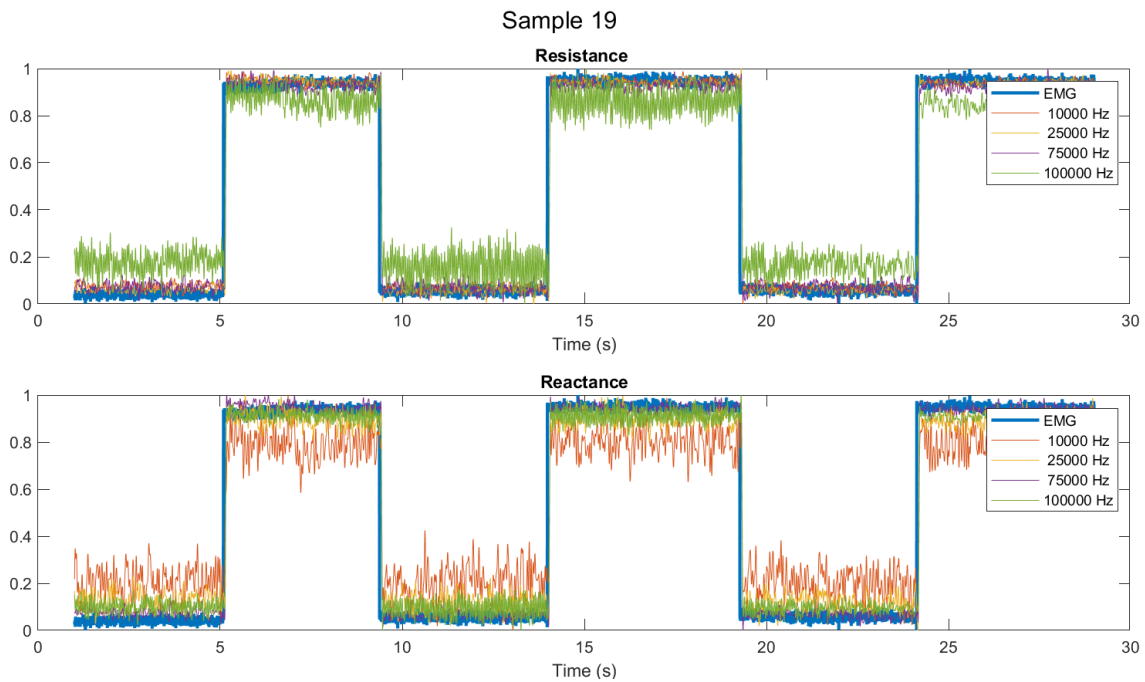


Figure J.25: Measurement number 19 of the impedance and “EMG” signals used for determining the time delay of the measurement system and signal processing. All signals are normalized between 0 and 1.

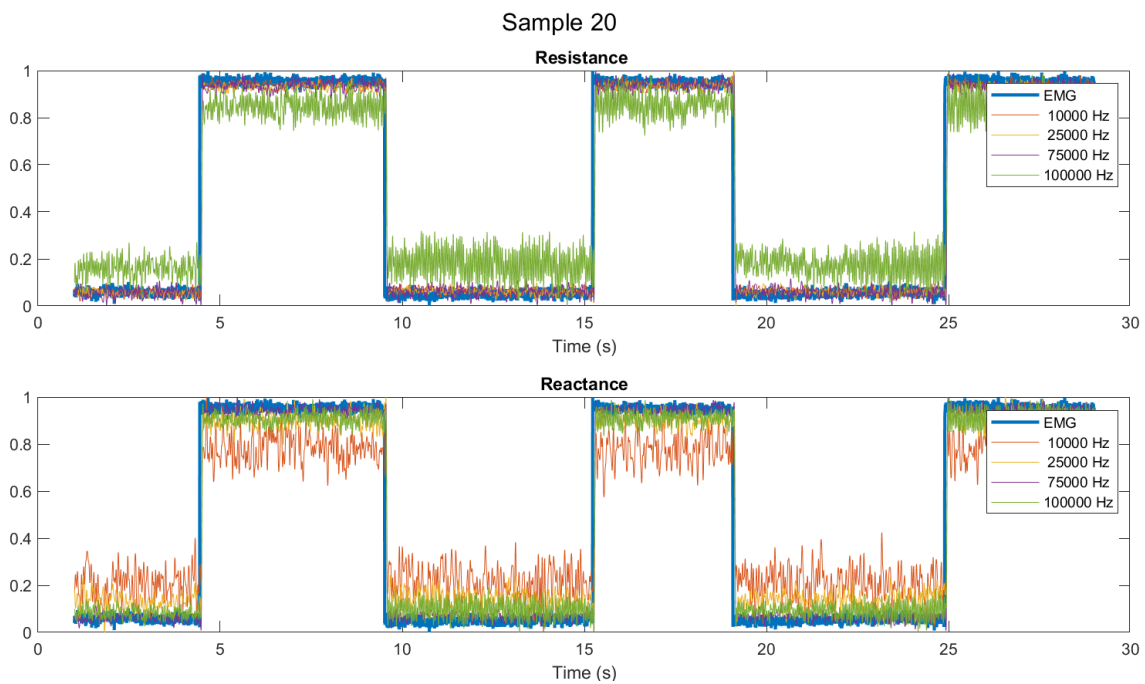


Figure J.26: Measurement number 20 of the impedance and “EMG” signals used for determining the time delay of the measurement system and signal processing. All signals are normalized between 0 and 1.